

10
I 29A
NO. 210
COPR

CIVIL ENGINEERING STUDIES
STRUCTURAL RESEARCH SERIES NO. 210



RESPONSE OF ARCHES UNDER DYNAMIC LOADS

Metz Reference Room
Civil Engineering Department
B106 C. E. Building
University of Illinois
Urbana, Illinois 61801

Civil Engineering Department
B106 C. E. Building
University of Illinois
Urbana, Illinois 61801

By
R. T. EPPINK
and
A. S. VELETSOS

Report to
RESEARCH DIRECTORATE
AIR FORCE SPECIAL WEAPONS CENTER
Air Research and Development Command
Kirtland Air Force Base, New Mexico
CONTRACT AF 29(601)-2591
PROJECT 1080

UNIVERSITY OF ILLINOIS
URBANA, ILLINOIS
DECEMBER 1960

AFSWC-TR-60-53

RESPONSE OF ARCHES UNDER DYNAMIC LOADS

by

R. T. Eppink
A. S. Veletsos

University of Illinois
Department of Civil Engineering

August 1960

Research Directorate
AIR FORCE SPECIAL WEAPONS CENTER
Air Research and Development Command
Kirtland Air Force Base, New Mexico

Approved:



PERRY L. HUIE
Colonel USAF
Chief, Structures Division

Project No. 1080

Contract No. AF 29(601)-2591



LEONARD A. EDDY
Colonel USAF
Director, Research Directorate

ABSTRACT

This report is concerned with a study of the response of arches subjected to the influence of transient forces.

A numerical procedure is presented for the computation of the dynamic response of arches for both the elastic and the inelastic ranges of deformation. The procedure is applicable to arches having any shape and any distribution of mass and stiffness. The distribution of the pressure along the arch and its timewise variation may be arbitrary.

The analysis is simplified by replacing the actual arch which has an infinite number of degrees of freedom by a discrete framework consisting of a series of rigid bars, flexible joints, and concentrated point masses. For the computation of the response in the inelastic range, the cross-sectional area of the arch is considered to consist of two concentrated flange areas connected by a thin rigid web. The equations of motion of the replacement system are solved by use of a step-by-step method of numerical integration.

Computer programs are described for the analysis of two general classes of problems: (a) circular elastic arches subjected to a uniform normal pressure of arbitrary timewise variation; and (b) arches of arbitrary shape subjected to a triangular moving pressure pulse. For the latter case it is possible to evaluate the response in the inelastic range of behavior.

Numerical solutions are presented for a wide range of the parameters involved, and the effects of the various parameters are discussed.

PUBLICATION REVIEW

This report has been reviewed and is approved.



CAREY L. O'BRYAN, JR.
Colonel USAF
Deputy Commander

TABLE OF CONTENTS

	<u>Page</u>
I. INTRODUCTION	1
1.1 Object and Scope	1
1.2 Notation	3
1.3 Acknowledgment	5
II. METHOD OF ANALYSIS	7
2.1 Characteristics of Replacement Structure	7
2.2 Designation of Joints and Bars	7
2.3 Equations of Motion in Terms of Forces	8
2.3.1 General	8
2.3.2 Components of Resisting Forces	10
2.3.3 Components of External Forces	10
2.4 Displacement-Deformation Relationships	11
2.5 Deformation-Force Relationships	12
2.5.1 Elastic Range of Behavior	12
2.5.2 Inelastic Range of Behavior	13
2.6 Method of Numerical Integration	16
III. COMPUTER PROGRAMS	19
3.1 General	19
3.2 Arch Subjected to a Uniform All-Around Pressure	19
3.2.1 Description of Programs	19
3.2.2 Outline of Programs	21
3.3 Arch Subjected to a Triangular Moving Pressure	24
3.3.1 Description of Programs	24
3.3.2 Outline of Programs	26
IV. NUMERICAL SOLUTIONS FOR ARCH SUBJECTED TO A UNIFORM PRESSURE PULSE	29
4.1 Problem Parameters	29
4.2 Presentation of Results	30
4.2.1 General	30
4.2.2 Typical Response Characteristics	30
4.2.3 Effect of Length of Time Interval of Integration and Number of Bars	32

TABLE OF CONTENTS (Continued)

4.2.4	Effect of Duration of Loading	35
4.2.5	Effect of Parameters Influencing Tendency for Buckling	37
4.2.6	Effect of Arch Dimensions	38
V.	NUMERICAL SOLUTIONS FOR ARCH SUBJECTED TO A TRIANGULAR MOVING PRESSURE	41
5.1	Problem Parameters	41
5.2	Presentation of Results	41
5.2.1	Typical Response Characteristics	41
5.2.2	Effects of Characteristics of Pressure Pulse	43
5.2.3	Effect of Arch Dimensions	46
5.2.4	Effect of Inelastic Action	47
VI.	SUMMARY	50
6.1	Summary	50
6.1.1	General	50
6.1.2	Solutions for Arches Subjected to a Uniform All- Around Pressure	50
6.1.3	Solutions for Arches Subjected to a Triangular Moving Pressure	51
	REFERENCES	53
	APPENDIX A "EXACT" DEFORMATION-FORCE RELATIONSHIPS FOR INELASTIC BEHAVIOR	54
	APPENDIX B EQUATIONS FOR CIRCULAR ARCHES IN POLAR COORDINATES	57
	B.1 Equations of Motion	57
	B.2 Displacement-Deformation Relationships	58
	APPENDIX C MODAL METHOD OF ANALYSIS	59

LIST OF TABLES

<u>Table No.</u>	<u>Page</u>
4.1 Natural Periods of a Two-Hinged Uniform Circular Arch	61
4.2 Modal Solution for a Two Hinged Circular Arch	62
4.3 Maximum Values of Response and Times of Occurrence for a Two-Hinged Uniform Circular Arch	63
4.4 Static Effects in a Two-Hinged Uniform Circular Arch for a Uniform All-Around Pressure	63
4.5 Effect of Time Interval of Integration on Maximum Values of Response and Times of Occurrence	64
4.6 Comparison of Solutions by Numerical Integration Procedure and Modal Method	66
4.7 Effect of Load Duration on Maximum Values of Response and Times of Occurrence	68
4.8 Comparison of Approximate and Exact Maximum Stresses	70
4.9 Effects of Peak Pressure and Initial Out-of-Roundness on Maximum Values of Response	71
4.10 Effect of Arch Dimensions on Maximum Values of Response and Times of Occurrence	72
C.1 Symmetrical Modes of Vibration for a Two-Hinged Uniform Circular Arch and Participation Factors for Modal Solution.	74

LIST OF FIGURES

<u>Figure No.</u>	<u>Page</u>
2.1 Model Considered in Analysis	75
2.2 Free Body Diagrams for a Typical Bar and Joint	76
2.3 Diagram Used in Determining Displacement-Deformation Relationships	76
2.4 Bilinear Stress-Deformation Relationship	77
2.5 Deformed Joint	77
3.1 Coordinate System for Circular Arch Model	78
3.2 Triangular-Shaped Moving Pressure Pulse	78
3.3 Flow Diagram of Computer Program for Circular Arch Subjected to a Uniform All-Around Pressure	79
3.4 Flow Diagram of Computer Program for Arch Subjected to a Triangular Moving Pressure	80
4.1 Triangular Pressure Pulse with Initial Peak	81
4.2 Natural Modes of Vibration for a Two-Hinged Uniform Circular Arch	82
4.3 Typical Response Curves for an Arch Under a Uniform All-Around Pressure Pulse	84
4.4 Response Curves of Bending Moment in an Arch for a Uniform All-Around Pressure Pulse	86
4.5 Effect of Number of Bars on Response	88
4.6 Response Curves for an Arch Under a Uniform All-Around Pressure Pulse-- $t_d/T_0 = 0.25$	90
4.7 Response Curves for an Arch Under a Uniform All-Around Pressure Pulse-- $t_d/T_0 = 0.50$	92
4.8 Response Curves for an Arch Under a Uniform All-Around Pressure Pulse-- $t_d/T_0 = 0.75$	94
4.9 Response Curves for an Arch Under a Uniform All-Around Pressure Pulse-- $t_d/T_0 = 1.0$	96

LIST OF FIGURES (Continued)

	<u>Page</u>
4.10 Response Curves for an Arch Under a Uniform All-Around Pressure Pulse-- $t_d/T_o = 1.5$	98
4.11 Response Curves for an Arch Under a Uniform All-Around Pressure Pulse-- $t_d/T_o = 4.0$	100
4.12 Response Spectra for an Arch Under a Uniform All-Around Pressure Pulse	102
4.13 Effect of Peak Pressure on Response for a Uniform All-Around Pressure Pulse	104
4.14 Effect of Initial out-of-Roundness on Response for a Uniform All-Around Pressure Pulse	106
4.15 Response Curves for an Arch Under a Uniform All-Around Pressure Pulse-- $L_o/r = 50$	108
4.16 Response Curves for an Arch Under a Uniform All-Around Pressure Pulse-- $L_o/r = 200$	110
4.17 Response Curves for an Arch Under a Uniform All-Around Pressure Pulse-- $f/L_o = 0.1$	112
4.18 Response Curves for an Arch Under a Uniform All-Around Pressure Pulse-- $f/L_o = 0.5$	114
5.1 Typical Response Curves for an Arch Subjected to a Triangular Moving Pressure	116
5.2 Response Curves of Bending Moment in an Arch for a Triangular Moving Pressure	118
5.3 Response Curves for an Arch Subjected to a Triangular Moving Pressure-- $t_d/t_t = 0.5$	121
5.4 Response Curves for an Arch Subjected to a Triangular Moving Pressure-- $t_d/t_t = 2.0$	123
5.5 Response Spectra for an Arch Subjected to a Triangular Moving Pressure	126
5.6 Response Curves for an Arch Subjected to a Triangular Moving Pressure-- $p_o/p_{cr} = 0.001$	127
5.7 Response Curves for an Arch Subjected to a Triangular Moving Pressure-- $p_o/p_{cr} = 2.0$	130

LIST OF FIGURES (Continued)

	<u>Page</u>
5.8 Response Curves for an Arch Subjected to a Triangular Moving Pressure-- $t_t/T_o = 2.0$	132
5.9 Response Curves for an Arch Subjected to a Triangular Moving Pressure-- $t_t/T_o = 0.5$	135
5.10 Response Curves for an Arch Subjected to a Triangular Moving Pressure-- $L_o/r = 50$	137
5.11 Response Curves for an Arch Subjected to a Triangular Moving Pressure-- $L_o/r = 200$	139
5.12 Response Curves for an Arch Subjected to a Triangular Moving Pressure-- $f/L_o = 0.1$	141
5.13 Response Curves for an Arch Subjected to a Triangular Moving Pressure-- $f/L_o = 0.5$	143
5.14 Curves for Inelastic Response of an Arch Subjected to a Triangular Moving Pressure-- $\epsilon_y = 1.0 p_o R/AE$	145
5.15 Curves for Inelastic Response of an Arch Subjected to a Triangular Moving Pressure-- $\epsilon_y = 0.5 p_o R/AE$	147

RESPONSE OF ARCHES UNDER DYNAMIC LOADS

I. INTRODUCTION

1.1 Object and Scope

The objectives of this study were: (a) to develop a method for the computation of the response of arches deflecting in their own plane under the influence of transient forces, and (b) with the aid of this method, to obtain numerical solutions for a range of the parameters involved in order to gain insight into the dynamic behavior of this structural type. The ultimate purpose of this investigation is the development of a rational method of design for arches subjected to dynamic loads of the type arising from bomb blasts.

Although of an exploratory nature, the numerical data presented in this report provide information on the effects of the major variables that enter into the problem. Furthermore, they may be used to evaluate the adequacy of existing methods of design for arches under dynamic loads. [4][6]*

The method is applicable to arches having any shape and any distribution of mass and stiffness. The distribution of the forces along the arch and their timewise variation may be arbitrary. The response of the structure for both the elastic and the inelastic ranges of deformation may be investigated.

The problem is analyzed approximately by replacing the continuous arch, which has an infinite number of degrees of freedom, by a discrete framework consisting of a series of rigid bars and flexible joints. The actual distributed mass of the structure is lumped into a series of point masses at the joints. For the computation of the response in the inelastic range, the cross-sectional area of the arch is approximated by two flanges connected by a thin rigid web. The resistance of each flange is represented by a bilinear stress-strain diagram. The equations of motion for the analogous framework are solved by use of a step-by-step method of numerical integration.

Mathematically, the replacement of the original continuous system by a discrete system is analogous to the solution of the governing differential equation by means of difference equations. The major advantage of a physical

* Unless otherwise identified, numbers in brackets refer to the corresponding items in the list of References given at the end of the text.

analogue is that it attaches physical significance to the various assumptions and approximations introduced in the analysis. This is particularly true for the inelastic range of deformation for which the problem becomes considerably more involved. In several respects, the present analysis is similar to one reported previously by J. A. Brooks [1].

The method has been programmed for the ILLIAC, the high-speed electronic digital computer of the University of Illinois. Programs have been prepared for two general classes of problems: (a) circular elastic arches subjected to a uniform all-around pressure having any timewise variation, and (b) arches of arbitrary shape subjected to a triangular moving pressure pulse. The latter program can be used to evaluate the response in both the elastic and post-elastic ranges of behavior. There are no restrictions as to the distribution of mass or stiffness along the arch, and the arch supports may be either hinged or fixed. For a moving pressure, it is also possible to consider the effects of partial fixity at the supports. In addition, a specialized program has been prepared which accounts for the effect of an initial out-of-roundness. This program is restricted to uniform circular arches subjected to a uniform pressure.

The computer programs have been used to obtain numerical solutions for the response of two-hinged circular arches. Results were obtained (a) for a uniform all-around pressure with a timewise variation represented by a triangle with an initial peak, and (b) for a triangular moving pressure pulse. While most of the results are for the elastic range of behavior, a few solutions have also been obtained to investigate the response into the post-elastic range of deformation. In these solutions the cross-sectional area and the mass per unit of length of the arch were considered to be constant. Although limited in number, the numerical solutions cover a wide range of load and arch parameters. The load parameters include the duration of the pressure pulse, the magnitude of the peak pressure as compared to the critical buckling pressure, and, for the moving pressure solutions, the velocity of propagation of the pressure front. The arch parameters include the geometric and physical properties of the arch. The effect of an initial out-of-roundness was investigated by considering a pressure pulse uniformly distributed around the arch.

The characteristics of the analogous framework used in the analysis are described in Chapter II. Also included in this chapter are the derivations of the equations necessary for dynamic response calculations and an outline of the procedure for their solution for both the elastic and inelastic ranges of behavior. The capabilities and the general organization of the computer programs are described in Chapter III. In Chapters IV and V, the numerical results are presented and the effects of the various variables are discussed briefly. Chapter IV is devoted to the uniform all-around pressure solutions, and Chapter V to the triangular moving pressure solutions. A summary of the more important results is given in Chapter VI.

1.2 Notation

The letter symbols used in this report are defined where they are first introduced in the text. The most important of these are summarized below in alphabetical order.

A_j	= area of the cross-section at joint j
A_j^t, A_j^b	= areas of the top and bottom flanges at joint j
b	= instantaneous set
c_j^t, c_j^b	= distance from the centroidal axis of the cross-section at joint j to the centers of the top and bottom flanges, respectively.
d_j	= distance between the centers of flanges at joint j
E_j	= modulus of elasticity of material at joint j
f	= rise of arch
F_j	= concentrated external force acting at joint j
I_j	= moment of inertia of the cross-section of the arch at joint j
L_o	= span length of arch
L_j	= length of bar j
m_j	= mass at joint j
M_j	= moment at center of joint j
M_j^l, M_j^r	= moments immediately to the left and right of joint j

N_j = axial force in bar j

N_j^{lt}, N_j^{rt}
 N_j^{lb}, N_j^{rb} } = axial forces in the top and bottom flanges to the left and right of joint j

p = intensity of external pressure

p_0 = peak value of external pressure

$p_{cr} = \left[\frac{4\pi^2}{\phi_0^2} - 1 \right] \frac{EI}{R^3}$ = critical buckling pressure for a hinged arch subjected to a uniform static pressure. The corresponding deflection configuration is antisymmetrical.

P_j^l, P_j^r = components of F_j immediately to the left and right of joint j and normal to the respective bars

Q_j = transverse shearing force in bar j

r = radius of gyration of cross-section

R = radius of circular arch

t_d = duration of pressure pulse

t_t = time of transit of pressure front across the arch

T_0 = fundamental period of vibration of complete ring, the breathing period

v_j = tangential component of displacement of joint j

V_j = x-component of internal forces at joint j

w_j = radial component of displacement at joint j

\bar{w}_m = amplitude of initial out-of-roundness

W_j = y-component of internal forces at joint j

x_j = x-coordinate of joint j in undeformed position

X_j = x-component of external forces at joint j

y_j = y-coordinate of joint in undeformed position

Y_j = y-component of external forces at joint j

- z = number of bars in arch model
 α_j = angle between the y-axis and the line of action of F_j when first applied, positive when clockwise
 β_j = direction angle of bar j with positive x-axis
 δ_j = total change in distance between joints $j-1$ and j
 δ_j^l, δ_j^r = portions of the total deformation of joint j to the left and right of the joint
 $\left. \begin{array}{l} \delta_j^{lt}, \delta_j^{rt} \\ \delta_j^{lb}, \delta_j^{rb} \end{array} \right\}$ = deformations of the top and bottom flanges to the left and right of joint j , respectively
 η_j = component of displacement of joint j in y-direction
 θ_j = angle between the line of action of F_j when first applied to the arch and its line of action after deformation
 μ = mass per unit of length of the arch
 ξ_j = component of displacement of joint j in x-direction
 σ_j = stress at joint j
 $\left. \begin{array}{l} \sigma_j^{lt}, \sigma_j^{rt} \\ \sigma_j^{lb}, \sigma_j^{rb} \end{array} \right\}$ = stresses in the top and bottom flanges to the left and right of joint j , respectively
 ϕ_0 = total angle of opening of circular arch
 χ_j = angle change at joint j
 χ_j^l, χ_j^r = angle changes to the left and right of joint j
 ψ_j = rotation of bar j

1.3 Acknowledgment

This study was performed as part of an investigation conducted in the Civil Engineering Department of the University of Illinois under contracts

AF 29(601)-464 and AF 29(601)-2591 with the Air Force Special Weapons Center, Albuquerque, New Mexico. This report is based on Dr. Eppink's doctoral dissertation. It was prepared under the general direction of Dr. N. M. Newmark, Head of the Department of Civil Engineering, and the immediate supervision of Dr. A. S. Veletsos, Professor of Civil Engineering. Appreciation is expressed to the Air Force for the support that has made this study possible.

II. METHOD OF ANALYSIS

2.1 Characteristics of Replacement Structure

A schematic drawing of the substitute framework is shown in Fig. 2.1. It consists of a number of flexible joints connected by rigid bars, which, for convenience, are assumed to be straight. Inasmuch as the flexibility of the structure is assumed to be concentrated at the joints, all axial and angular deformations take place at the joints. The individual bars are considered to be massless, and the actual distributed mass of the structure is lumped into a series of point masses at the joints. The characteristics at a joint of the substitute framework are determined from the characteristics of the section of the true arch included between the midpoints of the adjoining segments. For a non-uniform arch the flexibilities of the joints and the magnitudes of the concentrated masses will vary from one joint to the next.

This system is in some respects similar to a physical system used by Clough [2] in an experimental investigation of buckling of arches.

In considering the behavior of the structure in the inelastic range, it is further assumed that the cross-sectional area of the arch is made up of two flanges connected by a thin web which is rigid in shear. It is assumed that the web resists no direct forces. A cross-section of this type is an idealization of a steel I-beam or wide-flange beam. It also approximates a section of a cylindrical shell consisting of an I-beam with a concrete cover. The resistance of each of the flanges is given by a bilinear stress-deformation diagram. The areas of the top and bottom flanges may be different at any one joint, and the total areas of the sections may vary from one joint to the next. The physical properties of the top and bottom flanges may differ, but a variation in these properties from joint to joint is not considered in the equations presented here.

2.2 Designation of Joints and Bars

The joints of the analogous framework are numbered consecutively starting with zero at the left end and terminating with z at the right end. The bars are numbered in the same order from 1 to z . Bar j is the bar connecting joints $j-1$ and j .

As shown in Fig. 2.1, the configuration of the undeformed arch is specified by the rectangular coordinates, x_j and y_j , of the joints. The configuration of the deformed structure is defined by the displacements of the joints, measured from the undeformed position of the structure. The components of displacement of joint j in the positive x and y directions are designated by ξ_j and η_j , respectively.

2.3 Equations of Motion in Terms of Forces

2.3.1 General. The forces acting at the ends of a representative bar and joint are shown in Fig. 2.2. They include the axial thrust, N , the transverse shearing force, Q , and the bending moment, M . An axial thrust is positive when it produces tension. A shearing force is positive when it tends to rotate an element of the arch in a clockwise direction. A bending moment is positive when it produces compression in the exterior fiber of the arch. The concentrated external force at joint j is denoted by F_j , and the angle between its line of action and the y axis, measured in a clockwise direction, is denoted by α_j . The x and y components of the external force are considered to be positive when they act in the positive x and y directions. In Fig. 2.2 all forces are shown in their positive directions.

Referring to Fig. 2.2a and considering the equilibrium of bar j , one finds that both N_j and Q_j are constant along the length of the bar and that Q_j is related to the moments acting at the ends by the equation,

$$Q_j = \frac{M_j^l - M_{j-1}^r}{L_j} \quad (2.1)$$

where L_j is the length of bar j . The superscripts l and r designate, respectively, values of the moment to the left and to the right of the joint. The total change in the distance between joints $j-1$ and j is denoted by δ_j . Also, δ_j^l and δ_{j-1}^r designate the components of the total deformation occurring at joints j and $j-1$, respectively. Thus,

$$\delta_j = \delta_{j-1}^r + \delta_j^l \quad (2.2)$$

The quantities δ_j , δ_j^l , and δ_j^r are measured along a reference axis which passes through the centroid of the cross-sectional area of the analogous framework.

If the cross-section consists of more than one material, the centroid is determined from the transformed cross-section.

Consideration is next given to the equilibrium of moments at the joint about an axis normal to the plane of the framework. Referring to Fig. 2.2b and defining M_j to be the moment at the center of joint j , one finds that M_j^l and M_j^r are given by the equations,

$$M_j^l = M_j - Q_j \delta_j^l$$

$$M_j^r = M_j + Q_{j+1} \delta_j^r .$$

The last term in each of these equations represents the moment produced by the shears as a result of the deformations at the joint. These terms are likely to be important only for large axial deformations. Substituting these expressions into Eq. 2.1 and making use of Eq. 2.2, one obtains,

$$Q_j = \frac{M_j - M_{j-1}}{L_j + \delta_j} . \quad (2.3)$$

From the preceding discussion it follows that the axial thrusts and shearing forces are essentially defined at the centers of the bars, whereas the bending moments are defined at the centers of the joints.

The equations of motion for mass m_j in the x and y directions are

$$m_j \ddot{\xi}_j = V_j + X_j \quad (2.4)$$

$$m_j \ddot{\eta}_j = W_j + Y_j \quad (2.5)$$

where V_j represents the component of all internal forces acting at joint j in the positive x direction, and X_j represents the corresponding component of the external forces. Similarly, W_j designates the component of all internal forces acting at joint j in the positive y direction, and Y_j designates the corresponding component of the external forces. A dot superscript denotes differentiation with respect to time. Thus, $\ddot{\xi}_j$ and $\ddot{\eta}_j$ denote the accelerations in the x and y directions of the j^{th} mass.

2.3.2 Components of Resisting Forces. In the following derivations, the effects of the deformation of the structure are taken into account. Referring to Fig. 2.2b and summing the components of all internal forces in the x direction, one obtains the following expression for V_j :

$$\begin{aligned} V_j = & -N_j \cos(\beta_j - \psi_j) + N_{j+1} \cos(\beta_{j+1} - \psi_{j+1}) \\ & -Q_j \sin(\beta_j - \psi_j) + Q_{j+1} \sin(\beta_{j+1} - \psi_{j+1}) \end{aligned} \quad (2.6)$$

where ψ , with the appropriate subscript, denotes the rotation of a bar and is positive in the clockwise direction. The direction angle of bar j with the positive x-axis for the undeformed arch is denoted by β_j .

In a similar manner, summation of the components of all internal forces in the y-direction leads to the following equation for W_j :

$$\begin{aligned} W_j = & -N_j \sin(\beta_j - \psi_j) + N_{j+1} \sin(\beta_{j+1} - \psi_{j+1}) \\ & +Q_j \cos(\beta_j - \psi_j) - Q_{j+1} \cos(\beta_{j+1} - \psi_{j+1}) \end{aligned} \quad (2.7)$$

It may be recalled that the shearing forces Q_j and Q_{j+1} in the above equations are related to the bending moments M_{j-1} , M_j , and M_{j+1} by Eq. 2.3.

2.3.3 Components of External Forces. In order to express X_j and Y_j in terms of the total force F_j , it is necessary to know or assume the line of action of F_j as the structure deforms. For example, if in the process of deformation, F_j remains parallel to its original direction, then,

$$X_j = F_j \sin \alpha_j \quad (2.8)$$

$$Y_j = F_j \cos \alpha_j \quad (2.9)$$

To obtain general expressions, let θ_j represent the angle between the line of action of F_j when first applied to the structure and its line of action after deformation, as shown in Fig. 2.2b. Then,

$$X_j = F_j \sin(\alpha_j + \theta_j) \quad (2.10)$$

$$Y_j = F_j \cos(\alpha_j + \theta_j) \quad (2.11)$$

An important practical case is one in which the structure is subjected to a pressure which remains normal to the surface. In this case, it is convenient to express the concentrated force F_j in terms of a component P_j^l which is normal to the bar j immediately to the left of joint j , and a component P_j^r which is normal to the bar $j+1$ immediately to the right of the joint. These components, considered to be positive in the outward direction, can readily be evaluated in terms of the normal pressure. Then,

$$X_j = -P_j^l \sin(\beta_j - \psi_j) - P_j^r \sin(\beta_{j+1} - \psi_{j+1}) \quad (2.12)$$

$$Y_j = P_j^l \cos(\beta_j - \psi_j) + P_j^r \cos(\beta_{j+1} - \psi_{j+1}) \quad (2.13)$$

2.4 Displacement-Deformation Relationships

In Fig. 2.3, ab and $a'b'$ represent, respectively, the positions of bar j and joints $j-1$ and j before and after deformation of the arch. Let the projection $a'c'$ of the deformed system on the undeformed system be designated by $L_j + \bar{\delta}_j$; then $\bar{\delta}_j$ can be expressed in terms of the displacements of joint $j-1$ and j as follows:

$$\bar{\delta}_j = (\xi_j - \xi_{j-1})\cos \beta_j + (\eta_j - \eta_{j-1})\sin \beta_j \quad (2.14a)$$

Similarly, let the projection $c'b'$ of the deformed system in a direction normal to the undeformed system be denoted by $L_j \bar{\psi}_j$; then,

$$\bar{\psi}_j = \frac{1}{L_j} [(\xi_j - \xi_{j-1})\sin \beta_j + (\eta_j - \eta_{j-1})\cos \beta_j] \quad (2.15a)$$

In terms of δ_j the length $a'b'$ can be expressed as,

$$L_j + \delta_j = L_j \sqrt{\bar{\psi}_j^2 + (1 + \bar{\delta}_j/L_j)^2}$$

whence

$$\delta_j = L_j \left[-1 + \sqrt{\bar{\psi}_j^2 + (1 + \bar{\delta}_j/L_j)^2} \right] \approx \bar{\delta}_j + \frac{1}{2} L_j \bar{\psi}_j^2 \quad (2.14b)$$

The rotation of the bar, ψ_j , can likewise be expressed in terms of δ_j and $\bar{\psi}_j$ as follows:

$$\psi_j = \tan^{-1} \frac{\bar{\psi}_j}{1 + \bar{\delta}_j/L_j} \approx \bar{\psi}_j (1 - \bar{\delta}_j/L_j) \quad (2.15b)$$

It is noted that the quantities $\bar{\delta}_j$ and $\bar{\psi}_j$ represent the first order approximations to the change in distance δ_j and to the rotation ψ_j .

Referring to Fig. 2.3 one also finds that:

$$\cos \beta_j = \frac{x_j - x_{j-1}}{L_j} \quad (2.16)$$

$$\sin \beta_j = \frac{y_j - y_{j-1}}{L_j}$$

and that

$$\begin{aligned} \cos(\beta_j - \psi_j) &= \frac{(x_j + \xi_j) - (x_{j-1} + \xi_{j-1})}{L_j + \delta_j} \\ \sin(\beta_j - \psi_j) &= \frac{(y_j + \eta_j) - (y_{j-1} + \eta_{j-1})}{L_j + \delta_j} \end{aligned} \quad (2.17)$$

The angle change at joint j , denoted by X_j , is given by the expression,

$$X_j = \psi_{j+1} - \psi_j \quad (2.18)$$

2.5 Deformation-Force Relationships

The equilibrium equations and the geometrical relationships developed in the preceding sections are valid irrespective of the properties of the material composing the structure. However, in the formulation of the deformation-force relationships, a distinction must be made between the expressions applicable to the elastic and inelastic ranges of behavior.

2.5.1 Elastic Range of Behavior. The deformations to the left and to the right of joint j are given by the following equations:

$$\delta_j^l = \frac{L_j}{2} \frac{N_j}{E_j A_j} \quad (2.19a)$$

$$\delta_j^r = \frac{L_{j+1}}{2} \frac{N_{j+1}}{E_j A_j} \quad (2.19b)$$

The symbols E_j and A_j represent the modulus of elasticity of the material and the cross-sectional area at joint j . If the cross-section consists of more than one material, the values of these quantities are those of the transformed cross-section. Combining Eqs. 2.19 by use of Eq. 2.2 and solving for N_j , one obtains the expression,

$$N_j = \frac{2 E_j A_j \frac{\delta_j}{L_j}}{1 + \frac{E_j A_j}{E_{j-1} A_{j-1}}} \quad (2.20)$$

For a uniform arch the coefficient 2 cancels with the terms in the denominator.

The bending moment, M_j , may be evaluated from the equation,

$$M_j = - \frac{2 E_j I_j}{L_j + L_{j+1}} \chi_j \quad (2.21)$$

where I_j represents the moment of inertia of the cross-section at joint j . The bending moment produced by a uniform extension of the arch axis is not taken into account in Eq. 2.21.

2.5.2 Inelastic Range of Behavior. As already discussed in Section 2.1, the analysis for the inelastic range of behavior is restricted to cross-sections which can be approximated by a thin rigid web and two flanges, *as*. The relationship between the stress and the deformation for each flange is considered to be represented by the bilinear diagram shown in Fig. 2.4. The curve is shown in dimensionless form such that the slope of the elastic resistance line is unity and yielding occurs for δ/δ_y equal to one. The slope of the second line which represents the inelastic resistance is \bar{E}/E , the ratio of the stiffness of the material in the post-elastic range to that in the elastic range. For an elasto-plastic stress-deformation relationship, \bar{E} is equal to zero. Unloading is considered to take place along a line parallel to the initial elastic line, such as line AB in Fig. 2.4. The intercept of this line on the δ/δ_y -axis is the instantaneous set, b/δ_y , expressed in dimensionless form. Unloading will continue along this line until a new "elastic" limit is reached at B. The total change in deformation between points A and B is $2\delta_y$. Further unloading will occur along a line having a slope equal to \bar{E}/E . In the figure, a possible path for a loading and unloading cycle is represented by OABCD.

Whereas for elastic response the axial force, N_j , and the moment, M_j , can be determined directly from δ_j and X_j , the same procedure cannot be used if inelastic behavior is to be considered. In this case it is first necessary to compute the deformations of the flanges. The forces in the flanges at each of the joints can then be determined from the stress-deformation relationships. Once these have been evaluated, N_j and M_j can readily be determined.

For the analogous system considered, an "exact" determination of the flange deformations can be made; however, the procedure is extremely time-consuming even in terms of the time required on a high-speed computer. (The details of this analysis are included in Appendix A.) It is therefore desirable to introduce a further approximation. Fig. 2.5 shows schematically a deformed joint. As before, δ_j^l and δ_j^r denote the deformations to the left and right of joint j . The superscripts t and b have been added to these symbols to identify the deformations in the top and bottom flanges, respectively. For example, δ_j^{rt} denotes the deformation in the top flange on the right side of joint j .

If it is assumed that the angle change at a joint is distributed to each side of the joint according to the lengths of the bars adjacent to the joint (i.e., according to the relative stiffnesses of the adjacent bars) and the total change in length between adjacent joints is proportioned to the two joints inversely according to the areas of their cross-sections, then the deformations are given by the following equations:

$$\begin{aligned}
 \delta_j^{lb} &= \frac{A_{j-1}}{A_j + A_{j-1}} \delta_j - \frac{L_j}{L_j + L_{j+1}} c_j^b X_j \\
 \delta_j^{lt} &= \frac{A_{j-1}}{A_j + A_{j-1}} \delta_j + \frac{L_j}{L_j + L_{j+1}} c_j^t X_j \\
 \delta_j^{rb} &= \frac{A_{j+1}}{A_j + A_{j+1}} \delta_{j+1} - \frac{L_j}{L_j + L_{j+1}} c_j^b X_j \\
 \delta_j^{rt} &= \frac{A_{j+1}}{A_j + A_{j+1}} \delta_{j+1} + \frac{L_j}{L_j + L_{j+1}} c_j^t X_j
 \end{aligned} \tag{2.22}$$

The symbols c_j^t and c_j^b denote the distances from the centroidal axis to the top

and bottom flanges, respectively. These equations yield exact results when all flange deformations remain within the elastic range.

At the supports, these equations must be specialized to account for the appropriate boundary conditions. For example, for joint 0 the expressions are:

For a hinged boundary,

$$\delta_o^{rb} = \delta_o^{rt} = \frac{A_1}{A_o + A_1} \delta_1 \quad (2.23)$$

For a fixed boundary,

$$\delta_o^{rb} = \frac{A_1}{A_o + A_1} \delta_1 - c_o^b \psi_1 \quad (2.24a)$$

$$\delta_o^{rt} = \frac{A_1}{A_o + A_1} \delta_1 + c_o^t \psi_1 \quad (2.24b)$$

If the ends of the arch are elastically restrained by moment-resisting springs, the expressions for the flange deformations at the supports can be generalized further. For a spring of stiffness $k \frac{EI}{L_o}$, the resisting moment is given by the expression,

$$M = k \frac{EI}{L_o} \theta \quad (2.25)$$

where

θ = the rotation at the support

E = the modulus of elasticity of the arch material for a reference section

I = the moment of inertia of the cross-section at the reference section

k = stiffness coefficient for the spring.

For an elastically restrained boundary at joint 0, the expressions for the flange deformations are:

$$\delta_o^{rb} = \frac{A_1}{A_o + A_1} \delta_1 - \frac{L_1}{2 \frac{I_o}{kI} L_o + L_1} c_o^b \psi_1 \quad (2.26a)$$

$$\delta_o^{rt} = \frac{A_1}{A_o + A_1} \delta_1 + \frac{L_1}{2 \frac{I_o}{kI} L_o + L_1} c_o^t \psi_1 \quad (2.26b)$$

where I_o is the moment of inertia of the cross-section at joint 0. For hinged ends, k is equal to zero, and for fixed ends, k is equal to infinity. Substitution of these values into Eqs. 2.26 leads to Eqs. 2.23 and 2.24, respectively.

When the deformations of the individual flanges are determined from Eqs. 2.22 and the appropriate expressions for the boundary conditions, the moments on each side of the joints and the axial forces at each end of the bars will not be equal as required for equilibrium. This difficulty is overcome by evaluating these quantities by the following averaging procedure,

$$N_j = \frac{1}{2} (N_{j-1}^{rb} + N_{j-1}^{rt} + N_j^{lb} + N_j^{lt}) \quad (2.27)$$

$$M_j = \frac{1}{2} (N_j^{lb} c_j^b - N_j^{lt} c_j^t + N_j^{rb} c_j^b - N_j^{rt} c_j^t) \quad (2.28)$$

2.6 Method of Numerical Integration

The problem of determining the dynamic response of the structure considered herein is essentially one of satisfying the two equations of motion, Eqs. 2.4 and 2.5, for joints 1 through $z-1$. With the aid of the relationships established in the preceding sections, it is possible to express these equations in terms of displacements and to solve the resulting equations numerically using a step-by-step method of integration. In passing, it may be of interest to note that the resulting equations constitute a system of $2(z-1)$ simultaneous, nonlinear differential equations of the second order.

In this method of solution, the time during which the response of the system is to be determined is divided into a number of small time intervals, Δt , and for each interval the equations are solved by means of an iterative scheme. The procedure is described by assuming that at some time t_n the values of the displacements, velocities, and accelerations of all joints are known, and that it is desired to determine the corresponding quantities for a time t_{n+1} , which differs from t_n by the interval Δt .

1. The solution is started by assuming the values of the accelerations in the x- and y-directions for each joint at the end of the time interval considered. These values can be taken equal to those for the beginning of the interval, or they can be estimated on some other basis.

2. An assumption is then made regarding the manner in which the accelerations vary during the small time interval, and the values of the velocities and displacements at the ends of the interval are evaluated in terms of the assumed accelerations and the known accelerations, velocities, and displacements at the beginning of the interval. The following equations due to N. M. Newmark [5] were used:

$$\dot{x}_{n+1} = \dot{x}_n + \frac{1}{2} (\Delta t) \ddot{x}_n + \frac{1}{2} (\Delta t) \ddot{x}_{n+1} \quad (2.29a)$$

$$x_{n+1} = x_n + (\Delta t) \dot{x}_n + \left(\frac{1}{2} - \beta\right) (\Delta t)^2 \ddot{x}_n + \beta (\Delta t)^2 \ddot{x}_{n+1} \quad (2.29b)$$

In these expressions x may be interpreted as the component of displacement of joint j either in the x-direction, ξ_j , or in the y-direction, η_j . As before, a dot superscript denotes differentiation with respect to time. The subscripts n and $n+1$ refer to times t_n and t_{n+1} , respectively. The dimensionless parameter β depends on the assumption made regarding the variation of the acceleration within the interval Δt . For a linear variation, $\beta = 1/6$.

3. From the values of the displacements at the end of the interval, the changes of length and rotations of the bars and the angle changes of the joints are evaluated using Eqs. 2.14, 2.15, and 2.18.

4. For each joint the forces X_j and Y_j are then evaluated by use of Eqs. 2.12 and 2.13 (It is assumed that the load on the arch arises from a normal pressure). Next the axial forces, bending moments, shears, and the forces V_j and W_j are determined. For an elastic arch this is accomplished by use of Eqs. 2.20, 2.21, 2.3, 2.6 and 2.7, respectively. When inelastic behavior is to be considered, it is first necessary to determine the deformations of the flange elements at each joint. This is accomplished approximately by use of Eqs. 2.22 and 2.26. Having evaluated the deformations at time t_{n+1} , one computes the forces in the flanges by use of the appropriate stress-deformation

curves. Finally, N_j and M_j are calculated from Eqs. 2.27 and 2.28. The shears and the forces V_j and W_j are found from Eqs. 2.3, 2.6, and 2.7 as before.

5. The resulting values of W_j , V_j , X_j , and Y_j are then substituted into Eqs. 2.4 and 2.5, and a new set of accelerations is determined. The accelerations in the x-direction are obtained from Eq. 2.4, and those in the y-direction are obtained from Eq. 2.5.

6. The derived accelerations are finally compared with the assumed values. If the agreement is not satisfactory, the process is repeated with the derived accelerations taken as the new assumed accelerations. When a satisfactory degree of agreement is reached between assumed and derived values, one proceeds to the next time interval and repeats the procedure.

III. COMPUTER PROGRAMS

3.1 General

Computer programs have been prepared for two classes of problems:
 (a) circular elastic arches subjected to a uniform all-around pressure, and
 (b) arches of arbitrary shape subjected to a moving pressure pulse.

For the circular arches considered under (a), the equations used in the analysis were formulated in terms of polar coordinates. A schematic drawing of a circular arch model is shown in Fig. 3.1. In this case the arch is divided into bars of equal length; each bar subtends a central angle ϕ . The displacement of joint j is expressed in terms of its radial component, w_j , and its tangential component, v_j . The component w_j acts along a radius through joint j and is positive when outward. The component v_j acts along an axis perpendicular to the radius through joint j and is positive in a clockwise direction. The equations pertaining to this analysis have been presented in Reference [3]. For convenience, a summary of these equations for a normal pressure is given in Appendix B. These equations parallel those presented in Chapter II.

For this class of problems it is also possible to consider the effect of an initial out-of-roundness. The out-of-roundness is defined in terms of the deviations of the unstressed arch from a perfectly circular shape.

For the second class of problems, the loading is an initially peaked triangular pressure pulse moving across the arch at a constant velocity as illustrated in Fig. 3.2. The pressure is considered to act normal to the arch at all times. There is no restriction as to the shape of the arch that may be considered, and the response of the system may be investigated for both the elastic and inelastic ranges of deformation.

3.2 Arch Subjected to a Uniform All-Around Pressure

3.2.1 Description of Programs. Rather than developing a single general program for the analysis of arches under a uniform pressure, it was found desirable to prepare a separate program for the solution of problems in which an initial out-of-roundness is to be specified. The pressure-time

relationship may be arbitrary, but it must be approximated by a series of straight-line segments. Both programs have been coded to solve either hinged or fixed-ended arches. The program which was prepared specifically to handle an initial out-of-roundness is restricted to uniform arches; however, the other program is completely general in this respect, and it is possible to obtain solutions for arches with varying cross-sections.

The quantities evaluated include N_j , M_j , w_j , and v_j . In addition, for a uniform arch the extreme fiber stresses in the cross-section may be calculated. These results are printed in dimensionless form at specified intervals of time together with the maximum values of these quantities and the times at which they occur. For cross-sections which are symmetrical about the arch axis, the maximum stress in the section at each joint may be evaluated for two values of c/r , where c is the distance from the center of gravity of the cross-section to the extreme fiber and r is the radius of gyration of the cross-section. The quantity c/r depends on the shape of the cross-section; for a rectangular section it is equal to $\sqrt{3}$, and for a section consisting of two concentrated flanges, it is equal to 1. For sections which are not symmetrical about the arch axis, the program evaluates the stresses in both the top and bottom fibers of the cross-section.

In their present forms, the programs utilize the entire Williams (fast) memory of the ILLIAC but only a part of the magnetic drum (slow) memory. The computer time required to obtain a solution depends obviously on the number of segments into which the arch is divided, the length of the time interval used in the integration procedure, the number of time intervals for which the problem is to run, and to a certain extent on the arch dimensions. For a perfectly circular arch the average computer time required for each of the twelve-bar solutions presented herein was about twenty minutes. The time required when an initial out-of-roundness is specified is approximately twice that amount.

The problem parameters which must be specified in using these programs include the geometric and physical characteristics of the arch. These are specified in terms of the angle of opening, Φ_0 , and the quantity L_0/r , which represents the ratio of the span length of the arch to the radius of gyration of a reference cross-section. Throughout the remaining parts of this report,

the quantity L_0/r will be referred to as the "slenderness ratio". Parameters which describe the variation in cross-section and mass from joint to joint must also be given. An initial out-of-roundness is defined in terms of the radial and tangential components of the deviation of each joint from a perfectly circular configuration. The timewise variation of pressure is specified in terms of the coordinates of the end points of each straight-line segment. The magnitude of the pressure at any time is defined in terms of the dimensionless parameter, pR^3/EI , where p is the intensity of pressure and R is the radius of the arch. Other parameters which must be designated are the number of bars, z , the time interval of integration, Δt , the total number of time intervals the problem is to run, and the number of time intervals between print-out of results. If stresses are to be calculated, the values of c/r must be specified.

In the use of these programs, limitations must be placed on the values of these parameters. The maximum number of segments into which the arch can be divided is twelve when it is desired to solve a problem in which an initial out-of-roundness is to be introduced. For a perfectly circular arch, it is possible to consider up to twenty bars in the analogous framework. The largest value that can be input for the pressure parameter, pR^3/EI , is 100. The maximum value of L_0/r which can be considered is 1000, that of ϕ_0 is 180° . Limitations also exist with regard to the minimum values of these quantities; however, the lower limits are not so well defined because they are a result of the scaling of the intermediate quantities. Enough solutions have not been obtained to define accurately these limits. It is believed that the range of these parameters is sufficiently large to include all practical cases.

3.2.2 Outline of Programs. In this section a general description is given of the computer programs for the uniform all-around pressure. A more detailed description of these programs and of those described in Section 3.3, including copies of the codes, have been placed in the Library of the Structural Research Group of the Civil Engineering Department at the University of Illinois.

The complete program is divided into several subroutines each of which performs a specific function. A flow chart of the program indicating

the sequence of orders executed is presented in Fig. 3.3. The roles of the individual subroutines are also indicated in the flow chart.

The program is started by transferring control to the first instruction of the main input routine (M1) which reads in the problem parameters from the data tape, sets the quantities necessary to begin a solution, and prints a heading which identifies the specific problem to be solved.

The integration procedure is started after control is transferred to routine (21). Except for the initial cycle corresponding to $t = 0$ when a special technique is required, trial values are first assumed for the radial and tangential components of the accelerations of the joints for the end of the time interval considered. These values are taken equal to those at the beginning of the interval. Next the velocities and displacements are evaluated by use of Eqs. 2.29 with β taken equal to $1/6$.

The quantities required to determine improved values for the accelerations are calculated by routines (12), (10), and (11). Since the velocities and displacements are known initially, the accelerations for $t = 0$ are calculated by entering these routines directly after leaving (M1). Routine (12) evaluates the uniform pressure coefficient, pR^3/EI . This is determined for the end of the time interval under consideration. Routine (10) calculates the quantities δ_j/L , ψ_j , $\sin(\phi/2 \pm \psi_j)$, $\cos(\phi/2 \pm \psi_j)$, and $1/(1 + \delta_j/L)$. In the calculation of δ_j/L and ψ_j , the second order approximations given in Eqs. 2.14b and 2.15b are used. The quantities $\bar{\delta}_j$ and $\bar{\psi}_j$ are determined by use of Eqs. B.2.14 and B.2.15 in Appendix B. The sine and cosine terms are evaluated by use of the trigonometric identities for the sum and difference of two angles, with the terms $\sin \psi_j$ and $\cos \psi_j$ determined from the second order approximations

$$\sin \psi_j \approx \bar{\psi}_j (1 - \bar{\delta}_j/L)$$

$$\cos \psi_j \approx 1 - \frac{1}{2} \bar{\psi}_j^2$$

Similarly, the following second order expression is used in the calculation of the remaining quantity:

$$\frac{1}{1 + \delta_j/L} \approx 1 - \frac{\delta_j}{L} + \left(\frac{\delta_j}{L}\right)^2 .$$

Routine (11) calculates the angle changes χ_j , by use of Eq. 2.18, and the axial forces, N_j , and moments, M_j , by use of Eqs. 2.20 and 2.21, respectively. Routine (01) serves as the control for routines (10), (11), and (12).

The improved accelerations are computed by routine (20) which evaluates Eqs. B.2.4 and B.2.5. The terms on the right-hand side of these equations are evaluated from Eqs. B.2.6, B.2.7, B.2.12, and B.2.13, wherein the shearing forces have been expressed in terms of the bending moments by use of Eq. 2.3. These accelerations are compared with the assumed accelerations, and the procedure is repeated if the difference between the derived and assumed accelerations exceeds a specified tolerance. It has been found convenient to make this comparison after calculating the velocities and displacements from the derived accelerations.

When convergence is accomplished, control is transferred to the output routine (M2) which first calculates the deformations corresponding to the final displacements. Following this, a test is made to determine whether or not the extreme fiber stresses are to be calculated. If the stresses are desired, they are determined from the following equation which is applicable to uniform arches* :

$$\sigma_j = \frac{1}{A} \left[\frac{N_j + N_{j+1}}{2} + \frac{M_j}{r} \left(\frac{c}{r} \right) \right] .$$

The maximum values of the various quantities are then evaluated by comparing the results at the end of each time interval against the previously stored

* For non-uniform arches the corresponding expression is

$$\sigma_j = \frac{1}{A_j} \left[\frac{N_j + N_{j+1}}{2} + \frac{M_j}{r_j} \frac{c_j}{r_j} \right] .$$

This expressions has not been included in the programs.

maxima. Finally, the routine prints the values of the various quantities in tabular form at specified intervals of time.

Subroutine (MP) is used to print the absolute maximum values of the response. It is entered at the end of each problem and also at the instant the pressure pulse terminates if the termination of the pulse occurs in the interval of time for which the response is evaluated. A test is provided in routine (12) which detects the end of the pulse and transfers control to routine (MP). After these maxima have been printed, the memory locations in which they are stored are set equal to zero. Consequently, in this case, the maximum values printed at the end of the problem are for the era of free vibration.

The basic features of the program which allows consideration of an initial out-of-roundness are the same as for the program applicable to a perfectly circular arch. However, in the latter case account is taken of symmetry, and only one-half of the arch is considered, while the former requires consideration of the entire arch. Another difference concerns the manner in which the deformations are computed. For a perfectly circular arch, the deformations are calculated directly from the displacements measured with reference to the undeformed configuration of the structure. However, for an arch with an initial out-of-roundness, the deformations are calculated in two steps: First, a fictitious set of deformations is determined in terms of displacements measured not from the undeformed configuration of the arch but from the perfectly circular configuration. Second, the actual deformations are determined by subtracting from these fictitious deformations the "deformations" corresponding to the initial out-of-roundness. The first step is accomplished by use of routine (10). Subroutine (13), not shown in the flow chart, has been added immediately after routine (10) to perform the subtractions of the second step. The "deformations" corresponding to the initial out-of-roundness are calculated and permanently stored with the aid of subroutine (10), which is entered from routine (M1) during the initial stages of the solution.

3.3 Arch Subjected to a Triangular Moving Pressure

3.3.1 Description of Programs. Two separate programs have been prepared for the solution of an arch subjected to a triangular-shaped moving

pressure. Because the computation of the response of arches in the post-elastic range of behavior is very time-consuming, it was found desirable to prepare a specialized program for the solution of elastic arches.

The quantities evaluated by both programs include the forces N_j and M_j and the displacements ξ_j and η_j . In addition, the "inelastic program" determines the average strains at each joint in the top and bottom flanges. All of these results are printed in dimensionless form at specified intervals of time.

Non-uniform arches having either hinged or fixed boundaries can be considered by both programs. In addition, the "inelastic program" can be used to study the effects of partial fixity at the supports.

The programs make use of the complete Williams memory and part of the magnetic drum memory of the ILLIAC. The time required for a solution depends on the same factors which have been enumerated in Section 3.2.1. For each of the elastic solutions presented herein, the computer time averaged about forty-five minutes. For the inelastic solutions, the average time was roughly twice that for a corresponding elastic solution.

The problem parameters which must be specified in using the programs can be classified into four groups. The first group determines the shape of the arch and includes the rectangular coordinates of the joints of the arch. For circular and parabolic arches, subroutines have been prepared for calculating these coordinates within the machine so that it is not necessary to input the coordinates of the individual joints directly. The second group of parameters describes the physical properties of the arch and includes the slenderness ratio, L_0/r , the variations in cross-section and mass from joint to joint, the characteristics of the bilinear stress-deformation relationships for the top and bottom flanges, and the boundary conditions of the arch. The third group of parameters defines the characteristics of the moving pressure pulse and includes the peak value of the pressure and parameters related to the duration and speed of the pressure wave. Finally, the time interval, Δt , the number of bars, z , the total number of time intervals the problem is to run, and the number of time intervals between print-out of results must also be specified.

The maximum number of bars that can be considered in the analogous arch is eighteen for an elastic solution, and fourteen when use is made of the "inelastic program". The largest value of the peak pressure which can be considered corresponds to a value of $p_0 L_0^3 / EI$ equal to 1000. Other limitations exist with regard to some of the other parameters; however, there is sufficient latitude to permit consideration of most problems of practical interest.

3.3.2 Outline of Programs. A general description of the computer programs is included in this section. A flow chart of the program indicating the functions of the various subroutines, is shown in Figure 3.4. The principal features of these programs are the same as those of the programs described in Section 3.2.2. The significant differences lie in the determination of the external forces at the joints and in the additional subroutines necessary to determine the axial forces and moments for the "inelastic program" since these cannot be calculated directly from the total deformations and rotations of the bars.

The program begins when control is transferred to the input routine (M1) which, in conjunction with subroutines (M1.2) and M1.3), reads in the problem parameters from the data tape, sets the quantities necessary to begin a solution, and prints a heading used to identify each problem. The specific function of subroutine (M1.2) is to set the rectangular coordinates of the joints into their proper locations in the memory. Several versions of routine (M1.2) have been developed. One of these is applicable to arches of arbitrary shape; in this case, the coordinates x_j and y_j are specified on the input tape. The subroutine, then, merely reads these values and places them in their correct locations in the machine. Another version applies to circular arches for the case in which the geometry is specified by the rise-span ratio, f/L_0 . Using this parameter, the subroutine evaluates the coordinates of the joints and then stores them. A similar routine has also been developed for parabolic arches; other shapes can be evaluated in a similar manner by simply replacing this subroutine with a proper substitute.

The integration procedure is accomplished by routine (-21). As in the case of the programs for a uniform all-around pressure, the initial trial values of the accelerations at the end of each time interval are taken equal

to those at the beginning of the interval except for the special case when $t = 0$. The velocities and displacements then are determined by use of Eqs. 2.29 with $\beta = 1/6$.

Improved values of accelerations are determined using quantities evaluated in routines (11), (12), (13) and (-44), and (14). Using the displacements derived from the assumed accelerations, routine (11) calculates the quantities δ_j/L_j , ψ_j , $\cos(\beta_j - \psi_j)$, $\sin(\beta_j - \psi_j)$ and $\frac{1}{1 + \delta_j/L_j}$. The quantities δ_j/L_j and ψ_j are determined by use of the second order approximations given in Eqs. 2.14b and 2.15b, where $\bar{\delta}_j$ and $\bar{\psi}_j$ are given by Eqs. 2.14a and 2.15a. The sine and cosine terms are evaluated by use of Eqs. 2.17, where $1/(L_j + \delta_j)$ is determined by use of the second order approximation,

$$\frac{1}{L_j + \delta_j} = \frac{1}{L_j} \left[1 - \frac{\delta_j}{L_j} + \left(\frac{\bar{\delta}_j}{L_j} \right)^2 \right].$$

In the "inelastic program", the deformations of the flanges, δ_j^{lt} , etc., are determined by routine (12) using Eqs. 2.22 and 2.26. In routines (13) and (-44) the corresponding stresses are found by use of the bilinear stress-deformation relationship described in Section 2.5.2. The axial forces, N_j , and moments, M_j , are then calculated in routine (14) by use of Eqs. 2.27 and 2.28. For an elastic arch, routines (12) and (13) are omitted, and a different routine (14) is used which calculates N_j and M_j directly by use of Eqs. 2.20 and 2.21. Routine (01) serves as the control for routines (11), (12), (13), and (14).

The external forces at each joint, P_j^l and P_j^r , are determined in subroutine (21) which is controlled from routine (22). These quantities are calculated by determining the instantaneous static reactions at the ends of the bars; the bars are assumed to be simply supported. It may be noted that these reactions are different for each time interval, since the pressure distribution changes as the load moves across the arch. Routine (22) calculates the improved accelerations by evaluating the equations of motion, Eqs. 2.4 and 2.5. The terms on the right-hand side of these equations are calculated by use of Eqs. 2.6, 2.7, 2.12, and 2.13. In Eqs. 2.6 and 2.7 the shearing forces have been expressed in terms of the moments by use of Eq. 2.3. These

accelerations are compared with the assumed accelerations, and, if satisfactory agreement is not attained, the integration procedure is repeated.

At the end of each time interval, control is transferred to routine (M2) which evaluates the final deformations and stresses by use of subroutines (11), (12), and (13). At the times when the results are to be printed, the final values of the moments and axial forces are calculated by use of subroutine (14). Then the results are printed in tabular form.

IV. NUMERICAL SOLUTIONS FOR ARCH SUBJECTED TO A UNIFORM PRESSURE PULSE

4.1 Problem Parameters

In this chapter numerical solutions are presented for the elastic response of two-hinged circular arches subjected to a uniform all-around pressure pulse. The cross-section and mass per unit of length of the arch are considered to be constant. The pressure-time relationship is represented by a triangle with an initial peak as shown in Fig. 4.1.

For the benefit of the reader who may have bypassed Chapter III, the parameters used to define the problem are summarized below. The dimensions of the structure are expressed in terms of the rise-span ratio, f/L_0 , and the slenderness ratio, L_0/r . (Note that $\tan(\varphi_0/4) = 2f/L_0$, where φ_0 is the central angle of opening of the arch.) The characteristics of the pressure pulse are expressed in terms of the ratios p_0/p_{cr} and t_d/T_0 . The quantity p_0 is the peak value of the pressure; p_{cr} represents the critical buckling pressure corresponding to an antisymmetrical mode of deformation and is given by the equation,

$$p_{cr} = \left[\frac{4\pi^2}{\varphi_0^2} - 1 \right] \frac{EI}{R^3},$$

where R is the radius of the arch. The symbols E and I represent the modulus of elasticity of the material and the moment of inertia of the cross-section of the arch, respectively. The quantity t_d denotes the duration of loading, and T_0 , the fundamental period of vibration of a complete ring. The latter quantity is given by the equation,

$$T_0 = 2\pi \sqrt{\frac{\mu R^2}{EA}} = 2\pi \frac{R}{C}$$

where C is the speed of sound in the material of the arch, A is the cross-sectional area, and μ is the mass per unit of length of the arch.

The initial out-of-roundness considered in some of the solutions to be presented is taken in the form of a complete sine wave with nodes at the supports and at the crown. The magnitude of the out-of-roundness is expressed in terms of \bar{w}_m/L_0 , where \bar{w}_m is the amplitude of the deviation.

4.2 Presentation of Results

4.2.1 General. The majority of the solutions presented are for a perfectly circular two-hinged arch of uniform cross-section having the following dimensions,

$$f/L_0 = 0.20 \quad (\text{corresponds to } \phi_0 = 87.21^\circ)$$

$$L_0/r = 100 \quad (\text{corresponds to } R/r = 72.5)$$

Except where otherwise indicated, these solutions were obtained by considering twelve bars of equal length in the analogous framework. The natural frequencies and modes of vibration for this structure have been reported in Reference [3]. For convenience, the natural periods are summarized in Table 4.1, and the first three antisymmetrical and symmetrical modes of vibration are given in Fig. 4.2.

4.2.2 Typical Response Characteristics. In Figs. 4.3a through 4.3d are plots of the response of the arch analogue referred to above when subjected to a loading defined by the parameters $t_d/T_0 = 2$ and $p_0/p_{cr} = 1$. Included are the deflection configurations at a few selected times and time histories of the radial displacement, axial force, and bending moment. The radial displacements and bending moments are plotted for the crown and quarter point, and the axial force, for the crown. No tangential displacements are presented because they are generally small compared to the radial displacements. The displacement configurations are shown to an exaggerated scale.

The axial forces are expressed in terms of $p_0 R$, and the displacements, in terms of $p_0 R^2/AE$. These quantities represent, respectively, the axial force and the radial displacement caused by a uniform pressure p_0 acting statically on a complete ring. The bending moments are expressed in terms of $p_0 Rr$. For a section consisting of two concentrated flange areas, c/r is equal to one and, consequently, the stress at the extreme fiber of a section is proportional to the sum of the ordinates of the axial force curve and the corresponding moment curve.

The response curves presented in Figs. 4.3 are generally smooth and regular. The period of the oscillations in the curve for the axial force is

approximately equal to that of the second symmetrical mode of vibration of the arch. The period of this mode, which is predominantly extensional, is close to T_0 , the "breathing" period of a complete ring. The periods of the oscillations in the curves for bending moment are not directly identifiable with any of the natural periods of the arch, and, in fact, those for moment at the crown and quarter point are between the periods of the second and third modes. The principal oscillations in the response curves for radial displacement at the quarter point have a period equal to that of the second symmetrical mode; however, oscillations of a period equal to that of the first and third natural modes are also noticeable in the response curves for displacement at the crown. The contributions of these three modes can also be seen by comparing the displacement configurations in Fig. 4.3a with the natural modes given in Fig. 4.2b.

The participation of the various modes can be determined more readily by a modal method of analysis. Such a solution was obtained primarily for the purpose of checking the results of the computer calculations. The basic equations used for this analysis are given in Appendix C. The results of this modal solution are presented in Table 4.2 where the contributions of each mode to the values of displacement, axial force, and moment are listed. The function $f_r(t)$ represents the dynamic amplification factor for the r^{th} mode and depends on the shape of the pressure pulse. The structure considered in this solution is the same twelve-bar framework, and the load is a step-pulse of infinite duration. The solution applies only to values of p_0 which are small in comparison to the critical buckling load. From an examination of the results presented in this table, it can be seen that the major part of the response arises from the participation of the first three symmetrical modes of vibration. This is consistent with the observations made above on the basis of the response curves.

The results show that at any time the distribution of the axial force, N , is essentially uniform throughout the arch. Consequently, the curve in Fig. 4.3c may be interpreted as representing the time variation of N for any point on the arch. This result also holds for the solutions presented in the following sections of this chapter. The distribution of bending moment across the arch can best be seen from Figs. 4.4 which show the variation of the moment at each joint. It can be seen that the bending moment reaches a maximum first

near the supports and that the absolute maximum moment occurs at the crown. In Fig. 4.3 it is of interest to note that the maximum displacement at the quarter point is larger than that at the crown. It may also be noted that the absolute maximum value corresponds to the first maximum for both the displacements and axial forces.

In Table 4.3 are listed the maximum values of the radial displacement, axial force, and bending moment and the times at which these maxima occur. Displacements and moments are given for each joint of the analogous framework and axial forces are given for each bar. Also included in this table are values of the maximum stresses at each joint for cross-sections with $c/r = 1$ and $c/r = 2$. The corresponding static values are given in Table 4.4. For convenience, the maximum dynamic effects for the quarter point and crown are compared with the corresponding static values in the following table.

	$\frac{w}{p_o R^2/AE}$		$\frac{N}{p_o R}$		$\frac{M}{p_o Rr}$	
	1/4 point	crown	1/4 point*	crown*	1/4 point	crown
Static	-1.110	-1.578	-0.994	-0.994	0.063	0.086
Max. Dynamic	-2.385	-1.875	-1.684	-1.679	0.934	-1.137

The displacement at the crown increases only 19 percent over the static value, whereas that at the quarter point increases 115 percent. The increase in the axial force due to the dynamic load is 69 percent. Because of the small static bending moments in the arch, the dynamic amplification of moment is quite large. It should be noticed that the maximum bending stresses are of the same order of magnitude as those due to the axial forces.

4.2.3 Effect of Length of Time Interval of Integration and Number of Bars. For the solution presented in the preceding section the arch was replaced by a framework of twelve bars and the time interval of integration was taken as $\Delta t = 0.01 T_o$. The purpose of this section is to discuss how the solution is influenced by the choice of the time interval and the number of segments used in the replacement system.

* The axial forces are defined for the bars to the immediate left of the points indicated.

The interval of integration should be small enough such that successive cycles of iteration converge and the resulting solutions are stable and accurate. In general, the smaller the time interval of integration, the more accurate will be the solution; however, the time required to obtain the solution will be correspondingly longer. In the integration procedure used in this analysis, the acceleration was assumed to vary linearly during each time interval. For a linear problem, it has been shown [5] that the procedure is convergent and leads to a stable solution when

$$\Delta t = 0.389 T,$$

where T is the smallest natural period of the structure. While not strictly applicable to the present non-linear problem, this relation may be used as a guide in the selection of the time interval of integration, with the quantity T interpreted as the smallest natural period of the unloaded arch. For the particular twelve-bar system considered, this corresponds to

$$\Delta t = 0.026 T_0$$

and for a sixteen-bar system, to

$$\Delta t = 0.019 T_0.$$

Comparisons were made of the results obtained for (a) a twelve-bar system using time intervals of $0.005 T_0$, $0.01 T_0$, and $0.02 T_0$ and (b) a sixteen-bar system using time intervals of $0.005 T_0$ and $0.01 T_0$. The maximum values for these solutions are presented in Tables 4.3 and 4.5. It can be seen that, for all practical purposes, the results for the same number of bars are identical. In other words, the accuracy of the solution does not appear to be sensitive to the choice of time interval, provided the convergence and stability requirements are satisfied.

As an indication of how the time required for solution is influenced by the choice of time interval, the number of iterations required in the solution of the problems mentioned in the preceding paragraph are listed in the following table. In this table are given the number of iterations required in the computation of the response for an interval of time equal to T_0 and the average number of iterations for each step of integration, Δt .

Number of Bars	$\frac{\Delta t}{T_0}$	Iterations per T_0	Iterations per Δt
12	0.005	583	2.91
	0.01	402	4.02
	0.02	755	15.11
16	0.005	600	3.00
	0.01	571	5.71

It is noted that the larger the time interval, the larger is the number of iterations required for convergence per time interval. However, the number of iterations per T_0 and, consequently, the time required to obtain a solution decreases with increasing $\Delta t/T_0$ until values close to the convergence limit are reached. The results of these solutions suggest that the optimum time interval, which leads to the minimum time for a solution, is of the order of one-third to one-half the convergence limit. It is found that for this time interval convergence is accomplished in approximately four or five iterations. These conclusions have also been verified by a few additional solutions which are not included here.

The effect of increasing the number of bars in the analogous framework was investigated to determine the adequacy of the twelve-bar solution in depicting the response of the continuous structure. Results were obtained for arches with 10, 12, 16 and 20 bars. Time histories of the radial displacements at the 1/4 point and crown are compared in Figs. 4.5a and 4.5b, and the axial forces and bending moments are shown in Figs. 4.5c and 4.5d. It is assumed that the significant characteristics of the response of the continuous arch are present in the 20-bar solution.

The results for the axial force and the radial displacement at the quarter point are in good agreement, except for a slight phase shift. The agreement is not as good for bending moment or displacement at the crown. For values of t/T_0 larger than 2.0, which correspond to the free vibration era, there are differences in the detailed characteristics of the curves shown in Fig. 4.5d in addition to the phase shift. The phase differences are attributed to the fact that the natural frequencies of the modes which contribute to the response are not the same for the different systems compared. The differences in the

response characteristics of the curves in Fig. 4.5d for the larger times can be explained on the basis that the structures with the higher number of bars can account better for the participation of the higher modes. However, it is important to note that there are no major differences in the values of the maximum effects or in the over-all characteristics of the various solutions.

The times required for solution of the 12-bar and 20-bar problems were approximately 20 and 40 minutes, respectively. For the purpose of the present exploratory study, it was felt that the twelve-bar system would provide results of sufficient accuracy, and it was used to obtain the remainder of the solutions.

In order to determine the reliability of the solutions obtained from the digital computer, an independent check of the arch problem was provided by obtaining comparative solutions by a modal method of analysis for an arch subjected to a step-pulse loading of infinite duration. This solution was obtained on a desk calculator. The system considered was the twelve-bar analogous framework described in Section 4.2. Since the modal method is applicable only to structures which deflect in a linearly elastic manner, it yields results only for "small" values of p_o/p_{cr} . The computer solution used in the comparison was obtained for a value of $p_o/p_{cr} = 0.01$.

The results of these solutions are compared in Table 4.6. Radial displacements, axial forces, and bending moments are tabulated at corresponding times for both methods of solution. The agreement between the two sets of solutions is quite satisfactory.

4.2.4 Effect of Duration of Loading. In Figs. 4.6a through 4.11d are presented response curves for an arch subjected to a triangular pressure pulse for durations represented by values of t_d/T_o up to 4. The arch is the same as that considered in Section 4.2.1, and $p_o/p_{cr} = 1$ for all solutions. The absolute maximum values for the various effects are summarized in Table 4.7.

The general features of these curves are similar to those presented in Fig. 4.3. As before, the period of the predominant oscillations in the curves for displacement and axial force is the period of the second symmetrical mode of vibration (close to the period T_o of the "breathing" mode for a complete

ring). The period of the oscillations in the curves for bending moment are not identifiable with any of the natural periods of the arch. The axial force is found to be relatively uniform throughout the arch, whereas the distribution of bending moment is non-uniform, with the maximum effect occurring at the crown. The value of the maximum displacement at the quarter point is found to be consistently larger than that at the crown.

In Figs. 4.12a through 4.12d are presented spectrum curves of radial displacements, stresses, axial forces, and bending moments. These are plots of the absolute values of the maximum effects versus the duration of loading, t_d/T_0 . The stress at a joint of the substitute framework is determined from the moment at that joint and the average value of the axial forces in the adjoining bars. The spectrum curves for stress have been calculated for $c/r = 1$. Within the range of load durations considered, the maximum displacement is 2.58 times the corresponding static value for a complete ring under uniform pressure. The maximum stress reaches a value 2.43 times the static value for a ring. The maximum axial force is $1.83 p_0 R$, and the maximum moment is $1.47 p_0 Rr$.

To indicate the relative importance of the bending effects, in the following table are listed the ratios of the true maximum stresses to the maximum stresses determined by disregarding the component due to bending. Results are tabulated for the quarter-point and the crown for different values of t_d/T_0 , and for $c/r = 1$ (two concentrated flange areas) and $\sqrt{3}$ (a rectangular cross-section).

Ratio of true σ_{\max} to σ_{\max} disregarding bending				
t_d/T_0	$c/r = 1$		$c/r = \sqrt{3}$	
	1/4 point	crown	1/4 point	crown
0.25	1.79	1.86	2.55	2.68
0.50	1.78	1.94	2.53	2.80
0.75	1.58	1.82	2.22	2.63
1.00	1.32	1.45	1.75	2.09
1.50	1.32	1.15	1.57	1.67
2.00	1.32	1.23	1.56	1.72
4.00	1.32	1.35	1.65	1.80

It may be noted that this ratio varies from 1.15 to 1.94 for $c/r = 1$ and from 1.56 to 2.80 for $c/r = \sqrt{3}$, and that there is a tendency for the ratios to

increase with decreasing values of t_d/T_0 . Obviously, the bending effects are more important for the cross-section having the larger c/r ratio.

The absolute maximum displacement occurs on the first maximum for the longer durations of load, and on the third or a later maximum for the shorter durations. It follows that the effect of damping in reducing the magnitude of the maximum values will be more pronounced for the shorter durations of loading. The absolute maximum value of the axial force occurs on the first maximum, whereas that for bending moment occurs on the third maximum.

Since the maximum axial force and maximum moment do not occur at the same time, and since the stress calculation is dependent on the ratio c/r , it is desirable to have an approximate method for calculating the maximum stresses. In Table 4.8 the exact maximum stresses are compared with those computed by use of the following equations:

$$\sigma_{\max} \leq \frac{1}{A} \left\{ |N_{\max}| + \left| \frac{M_{\max}}{r} \right| \frac{c}{r} \right\} \quad (a)$$

$$\sigma_{\max} \approx \frac{1}{A} \sqrt{(N_{\max})^2 + \left(\frac{M_{\max}}{r} \right)^2 \left(\frac{c}{r} \right)^2} \quad (b)$$

Comparisons are made for two values of c/r . It can be seen that Eq. (a) overestimates the maximum stress by a maximum of 49 percent and a minimum of 9 percent. The results obtained from Eq. (b) are, for the most part, too low. The maximum error is -20 percent.

4.2.5 Effect of Parameters Influencing Tendency for Buckling. The factors which govern the tendency of a circular arch to buckle under dynamic loading include the magnitude of the peak pressure, the duration of the loading, and the amount of initial out-of-roundness. Solutions are presented in this section for a perfectly circular arch and an arch with an initial out-of-roundness for different values of p_0/p_{cr} . The characteristics of the arch are considered to be the same as before, and the duration of loading, t_d , is taken equal to $2T_0$.

The effect of an increase in the peak pressure is indicated in Figs. 4.13 where the results for p_0/p_{cr} equal to 0.5 and 2.0 are compared. It can be seen that the peak values of the response are affected only slightly by

changes in the value of p_o/p_{cr} . The features of the response are also very similar except for a small decrease in frequency with an increase in pressure. This change is attributed to the reduction in stiffness of the arch due to the increased axial thrust. The curves presented in Figs. 4.3 for $p_o/p_{cr} = 1.0$ fall between those for $p_o/p_{cr} = 0.5$ and $p_o/p_{cr} = 2.0$.

In Figs. 4.14 are shown response curves for an arch having an initial out-of-roundness in the form of a complete sine wave and an amplitude

$$\bar{w}_m = 0.001 L_o .$$

For the value of $p_o/p_{cr} = 1$ considered, this corresponds to

$$\bar{w}_m = 0.452 p_o R^2 / AE .$$

Comparing these results with those presented in Figs. 4.3 for a perfectly circular arch, one may observe that the response curves at the 1/4 point (or 3/4 point) for the circular arch lie between the corresponding curves for the arch with the initial out-of-roundness, and that the differences in the values of the maximum effects are small. The maximum values for these solutions are compared in Table 4.9. Also included in this table are the results for the different values of p_o/p_{cr} discussed above and one additional solution for an arch with an initial out-of-roundness. These results indicate that for load durations less than $t_d/T_o = 2$, the effect of the magnitude of the peak pressure or of a small initial out-of-roundness is small. However, it is expected that for longer durations of loading the buckling tendency may become more important. Of equal importance, however, may be the effect of damping which was neglected in these solutions.

4.2.6 Effect of Arch Dimensions. The influence of the dimensions of the arch on the response was investigated by obtaining a few solutions for different values of the slenderness ratio, L_o/r , and the rise-span ratio, f/L_o . The values of L_o/r considered were 50, 100 and 200 for a value of f/L_o equal to 0.2. In addition, rise-span ratios of 0.1 ($\varphi_o = 45.24^\circ$), 0.2 ($\varphi_o = 97.21^\circ$), and 0.5 ($\varphi_o = 180^\circ$) were considered for L_o/r equal to 100. In each of these solutions, the load parameters were taken as $p_o/p_{cr} = 1.0$ and $t_d/T_o = 2.0$.

The results for L_0/r equal to 50 and 200 are given in Figs. 4.15 and 4.16. The maximum values are summarized in Table 4.10. From an examination of these results and those presented in Figs. 4.3 for $L_0/r = 100$, it can be seen that the detailed characteristics of these curves are, in general, different. However, insofar as the axial forces are concerned, the period of the principal oscillations in the response curves are approximately equal to T_0 , and the magnitude of the maximum forces are essentially the same. The maximum values range from $1.71 p_0 R$ to $1.74 p_0 R$.

As might be expected, the effect of changing L_0/r is most pronounced on the response curves for moment and displacement. It can be seen that the moment builds up more rapidly for the stiffer arches. There does not appear to be an appreciable difference in the maximum values of the dimensionless bending moment, $M/p_0 Rr$, for $L_0/r = 100$ and 200; however, for $L_0/r = 50$, the value is appreciably larger. This is also true for the radial displacements. For convenience, these results, in addition to those for the absolute maximum stresses, are summarized in the following table. The values presented represent the absolute maximum effects for the entire arch.

Absolute Maximum Values				
L_0/r	$\frac{w_{\max}}{p_0 R^2/AE}$	$\frac{M_{\max}}{p_0 Rr}$	$\frac{\sigma_{\max}}{p_0 R/A}$	$\frac{\sigma_{\max}}{p_0 R/A}$
			($c/r=1$)	($c/r= 3$)
50	2.84	1.65	2.30	3.16
100	2.39	1.14	2.22	2.88
200	2.44	1.19	2.13	2.69

It should be noted that the maximum stresses are not as sensitive to changes in L_0/r as are the moments.

Response curves corresponding to different values of the rise-span ratio are presented in Figs. 4.17 and 4.18, and the maximum values of the response are given in Table 4.10. These results together with those presented in Figs. 4.3 and Table 4.3 indicate that an increase in f/L_0 has the same general effect as an increase in L_0/r . A comparison of Figs. 4.17 and 4.15 shows a striking similarity between the corresponding time history curves. Comparing Figs. 4.18 and 4.16 one may notice the same tendencies in the response

curves even though the correspondence is not as pronounced in this case as in the previous comparison. It appears that an empirical relationship might be developed which combines the rise-span ratio and the slenderness ratio into a single parameter. On the basis of the meager data presented here, a possible choice for this parameter is

$$\frac{f}{L_0} \frac{L_0}{r} = \frac{f}{r} .$$

Additional solutions are necessary to determine both the adequacy and range of applicability of this parameter.

V. NUMERICAL SOLUTIONS FOR ARCH SUBJECTED TO A TRIANGULAR MOVING PRESSURE

5.1 Problem Parameters

Numerical solutions are presented in this chapter for two-hinged circular arches of uniform cross-section subjected to a triangular-shaped moving pressure as shown in Fig. 3.2. The characteristics of this type of loading are defined by the parameters p_o/p_{cr} , t_t/T_o , and t_d/t_t . The parameter p_o/p_{cr} describes the peak value of the pressure wave, p_o , in terms of the buckling pressure, p_{cr} . The quantity t_t represents the transit time, which is the time required for the front of the wave to move from one support of the arch to the other; t_d represents the duration of the pulse, i.e., the time required for the entire pressure pulse to pass over a fixed point on the arch. As before, T_o is the "breathing" period of vibration of a complete ring. Constant values of the parameter t_d/t_t represent pressure waves having the same physical length. The total length of time the pressure wave acts on the arch is given by the sum of t_t and t_d . As in the preceding chapter, the arch dimensions are expressed in terms of f/L_o and L_o/r .

The yield strain for the arch, ϵ_y , is expressed in the dimensionless form

$$\frac{\epsilon_y}{p_o R/AE}$$

A static uniform pressure of intensity p_o will initiate yielding in a complete ring when the value of the above parameter is equal to unity. The yield deformation for a flange is equal to the product of ϵ_y and half the length of the bar adjacent to the flange. For example,

$$(\delta_j^{lt})_y = \epsilon_y \frac{L_j}{2}$$

$$(\delta_j^{rt})_y = \epsilon_y \frac{L_{j+1}}{2}$$

Similar expressions for the bottom flanges are obtained by replacing the superscript t with b .

5.2 Presentation of Results

5.2.1 Typical Response Characteristics. Most of the solutions presented in this chapter are for the arch described in Section 4.2.1. Except

for the results discussed in Section 5.2.4, the response is restricted to the elastic range of behavior. The response curves for a loading characterized by the parameters $p_o/p_{cr} = 1$, $t_t/T_o = 1$ and $t_d/t_t = 1$ are presented in Figs. 5.1. In these figures are shown representative displacement configurations and time histories of the radial and tangential displacements, axial forces, and bending moments for the 1/4 point, crown, and 3/4 point. The curves for axial force are actually for the bars of the analogous framework just to the left of the designated points. All of these quantities are expressed in the same terms described in Section 4.2.2.

As might be expected, a major contribution to the response arises from the participation of the first antisymmetrical mode of vibration. This can be seen clearly from the displacement configurations shown in Fig. 5.1a which have the same general shape as the first antisymmetrical mode of vibration illustrated in Fig. 4.2a. The same observations can be made from the displacement curves for the 1/4 point and 3/4 point for which the period of the major oscillations seem to be equal to that of the first antisymmetrical mode.

Although the most critical section of the arch is away from the crown, the effects at the crown are also appreciable. The maximum radial displacement at the crown is about 59 percent of that at the 1/4 point, and the maximum moment at the crown is about 63 percent of that at the 3/4 point. It is of interest to note that the period of the predominant oscillations in the curves for radial displacement and moment at the crown appears to correspond to that of the first symmetrical mode of vibration. Response in the symmetrical modes is apparent also in the curves for axial force for which the principal period of oscillation is approximately equal to the second symmetrical, or extensional, mode of vibration.

It is of interest to note that for all of the curves for moment and axial force, higher frequency oscillations appear prominently. This may be contrasted to the very smooth and regular response curves for the uniform all-around pressure discussed in the preceding chapter.

The time histories for the axial force reveal that N does not vary appreciably throughout the arch. This result is in agreement with the results obtained for a uniform all-around pressure. The distribution of bending

moment across the arch can be seen from Fig. 5.2, in which are plotted the time histories of the moment for each joint. As might be expected for a moving pressure, the moment builds up progressively from the near support to the far support as the pressure wave moves across the arch. The maximum moment occurs at the $3/4$ point at a time when approximately one-half of the load is off the arch.

For the solution discussed in this section the pressure acts on the structure for a total time of $2 T_0$. Although it is conceivable that the maximum values of response beyond the time considered in the solution may be larger than those obtained, this does not appear to be the case. In this connection, it should be emphasized that the effect of damping will be to reduce the later maxima.

The maximum values for a uniform all-around pressure with a duration equal to $2 T_0$ are given in Table 4.3. Comparing the maximum values for the two types of loading, one may observe that the larger displacements result from the moving pressure. For the particular case considered, the largest radial displacement for the moving pressure is approximately $5 p_0 R^2/AE$, while for the uniform all-around pressure it is $2.4 p_0 R^2/AE$. The maximum bending moment is $1.63 p_0 Rr$ for the moving pressure and $1.14 p_0 Rr$ for the uniform pressure. The maximum axial force, on the other hand, is larger for the uniform-pressure solution, being equal to $1.71 p_0 R$ as compared to a value of $0.71 p_0 R$ for the moving-pressure solution.

5.2.2 Effects of Characteristics of Pressure Pulse. The influence of the duration, velocity, and magnitude of the pressure wave on the response of arches is discussed in this section. In Figs. 5.3 and 5.4 are presented response curves for two load durations represented by values of t_d/t_t equal to 0.5 and 2.0 respectively. For both solutions, the arch is the same as that considered before, and the characteristics of the pressure pulse are defined by the parameters $t_t/T_0 = 1$ and $p_0/p_{cr} = 1$.

In Fig. 5.5, the values of the first major maxima for moment, axial force, and radial displacement at selected points on the arch are plotted versus the duration of loading. In addition, the absolute maximum tangential displacement, which occurs at the crown, is shown. It can be seen that in general the maximum effects increase with increasing t_d/t_t . For $t_d/t_t = 2$,

the largest duration considered, the maximum radial displacement at the 1/4 point is equal to $8.77 p_o R^2 / AE$. The absolute maximum moment at the 3/4 point is $2.17 p_o Rr$, and the maximum axial force at the crown is $0.80 p_o R$. Except for the axial force, these effects are appreciably larger than the values computed for a uniform all-around pressure. Consequently, the bending effects, as indicated by a comparison of the values of the maximum moments and axial forces, are more important for the triangular moving pressures.

In order to study the effect of the magnitude of the pressure, a few solutions were obtained for different values of the parameter, p_o / p_{cr} . In Fig. 5.6 are shown the response curves obtained for $p_o / p_{cr} = 0.001$ with $t_t / T_o = 1$ and $t_d / t_t = 2$. For a small pressure of this magnitude, the large deflection effects are negligible and the response is essentially linear. An indication of the buckling tendency which occurs for the larger magnitudes of pressure may be obtained by comparing these results with those given in Fig. 5.4 which is for $p_o / p_{cr} = 1$. It can be seen that the larger pressure causes an over-all magnification in the amplitude of the response curves as well as a decrease in their frequencies. Maximum values for these solutions are compared in the following table. Also included in this table is a comparison of the maximum values for two pressures of larger magnitude acting on the arch for a shorter duration of time. For these solutions peak pressures of $p_o / p_{cr} = 1$ and 2 were considered with t_d / t_t and t_t / T_o both equal to unity. (The time histories for these solutions are presented in Figs. 5.1 and 5.7, respectively.) For this comparison it was necessary to consider only the first maxima since the second and later maxima were not attained in most of the solutions.

Quantity	Location	$t_d / t_t = 1.0$		$t_d / t_t = 2.0$	
		$p_o / p_{cr} = 1.0$	$p_o / p_{cr} = 2.0$	$p_o / p_{cr} = 0.001$	$p_o / p_{cr} = 1.0$
$\frac{w}{p_o R^2 / AE}$	1/4 point	-4.90	-6.01	-5.75	-8.77
	crown	-2.90	-3.46	-3.03	-4.13
	3/4 point	4.87	5.22	5.89	7.25
$\frac{M}{p_o Rr}$	1/4 point	1.02	1.19	1.08	1.52
	crown	1.03	1.02	0.93	0.98
	3/4 point	-1.63	-1.77	-1.75	-2.18
$\frac{N}{p_o R}$	1/4 point	-0.61	-0.60	-0.76	-0.76
	crown	-0.64	-0.62	-0.81	-0.80
	3/4 point	-0.66	-0.63	-0.91	-0.86

For the longer duration it can be seen that a change in p_o/p_{cr} from 0.001 to 1.0 causes an increase in the absolute maximum displacement from $5.89 p_o R^2/AE$ to $8.77 p_o R^2/AE$ or about 49 percent. The maximum moment at the 3/4 point increases from $1.75 p_o Rr$ to $2.18 p_o Rr$, or about 24 percent. These changes are appreciably larger than corresponding increases for a uniform all-around pressure as reported in Chapter IV. The increases will obviously be even larger for longer durations of load or higher pressures. For the shorter duration, a change in pressure from $p_o/p_{cr} = 1$ to 2 produces an increase in maximum displacement of about 23 percent and an increase in maximum moment of only 8 percent. It may be inferred that the effect of an increase in pressure is not as significant for short durations of load even for fairly large values of p_o/p_{cr} .

The influence of the velocity of the pressure pulse was studied by comparing solutions for pressure waves having the same physical length (same value of t_d/t_t), but different velocities (different values of t_t/T_o). In Fig. 5.8 are presented solutions for $t_d/t_t = 0.5$, which corresponds to a pressure wave having a length equal to one-half the span of the arch, and t_t/T_o equal to 2. As before, $p_o/p_{cr} = 1$. These curves can be compared with those given in Fig. 5.3 for $t_t/T_o = 1$. In Fig. 5.9 are presented solutions for $t_d/t_t = 2$ (length of pressure wave equals $2L_o$) and $t_t/T_o = 0.5$ with $p_o/p_{cr} = 1$. These results are comparable to those shown in Fig. 5.4 for $t_t/T_o = 1$. The most prominent difference between the corresponding curves is the reduction in magnitude of the response with an increase in velocity, i.e., with a decrease in t_t/T_o . The absolute maximum values for these solutions are listed in the following table.

Quantity	Location	$t_d/t_t = 0.5$		$t_d/t_t = 2.0$	
		(1)	(2)	(3)	(4)
		$t_t/T_o = 2.0$	$t_t/T_o = 1.0$	$t_t/T_o = 1.0$	$t_t/T_o = 0.5$
$\frac{w}{p_o R^2/AE}$	1/4 point	-7.33	-2.70	-8.77	-3.82
	crown	-7.13	-1.70	-4.13	1.62
	3/4 point	6.41	2.74	7.25	3.79
$\frac{M}{p_o Rr}$	1/4 point	1.21	0.69	1.52	0.87
	crown	-2.39	0.70	-1.01	0.83
	3/4 point	-2.72	-1.08	-2.18	-1.21
$\frac{N}{p_o R}$	1/4 point	-1.03	-0.39	-0.76	-1.18
	crown	-0.96	-0.42	-0.80	-1.16
	3/4 point	-0.97	-0.41	-0.86	-1.16

The influence of the velocity may also be studied by comparing solutions for which the velocities of the pulse differ but the total time that the pressure acts on the arch is constant. In the above table this amounts to comparing column (1) with column (3) and column (2) with column (4). In the first comparison the time that the pressure acts is $3.0 T_0$, and in the second, it is $1.5 T_0$.

On the basis of only four solutions, it is not clear which of these methods of comparison is more desirable or whether a comparison on some other basis might not prove to be superior.

5.2.3 Effect of Arch Dimensions. The effects of a variation in the dimensions of the arch for a triangular moving pressure were investigated in the same manner as for a uniform all-around pressure. Solutions were obtained for slenderness ratios, L_0/r , equal to 50, 100 and 200 for a value of f/L_0 equal to 0.2, and rise-span ratios of 0.1, 0.2, and 0.5 were considered for $L_0/r = 100$. The load parameters considered for each of these solutions were:

$$p_0/p_{cr} = 1, \quad t_t/T_0 = 1, \quad t_d/t_t = 1.$$

The results for L_0/r equal to 50 and 200 are presented in Figs. 5.10 and 5.11; for $L_0/r = 100$, the response curves are given in Fig. 5.1. A comparison of these curves reveals no basic similarities in the response characteristics. In the following table are listed the absolute maximum radial displacements, axial forces, and moments for these solutions.

Absolute Maximum Values			
$\frac{L_0}{r}$	$\frac{w_{max}}{p_0 R^2 / AE}$	$\frac{N_{max}}{p_0 R}$	$\frac{M_{max}}{p_0 Rr}$
50	4.51	1.35	2.42
100	4.90	0.71	1.63
200	6.07	0.69	1.60

It can be seen that the maximum displacements increase with increasing values of L_0/r . A substantial decrease in the maximum axial force and maximum moment occurs for an increase in L_0/r from 50 to 100, but very little change is noticeable for slenderness ratios of 100 and 200. This large variation in

moment for the smaller values of L_0/r was also noticeable for the uniform all-around pressure results. However, it will be recalled that for the uniform pressure solutions there was no change in the maximum axial force with changes in L_0/r .

The response curves for values of f/L_0 equal to 0.1 and 0.5 are presented in Figs. 5.12 and 5.13, and those for $f/L_0 = 0.2$ are given in Fig. 5.1. The effect of an increase in the value of the rise-span ratio appears to be the same as for an increase in the value of slenderness ratio. This is the same result which was found to be valid for the uniform all-around pressure solutions. A similarity can be noticed in the response features of the two solutions shown in Figs. 5.10 and 5.12 for which the parameter f/r is equal to 10. This similarity is not as pronounced as for the uniform pressure; nevertheless, it is quite apparent. Also, there is some resemblance in the trends observable in the solutions shown in Figs. 5.11 and 5.13 for which f/r is equal to 40 and 50, respectively. These results appear to substantiate the observation made in Section 4.2.6 to the effect that the two parameters f/L_0 and L_0/r may be replaced by the single parameter, f/r .

5.2.4 Effect of Inelastic Action. To illustrate the effect of inelastic action, two solutions were obtained using an elasto-plastic stress-deformation relationship for the flange areas. Two different yield levels were considered. The arch dimensions and loading are the same as for the elastic solution presented in Section 5.2.1. For this elastic solution, the maximum stress developed in the arch is equal to $1.97 p_0 R/A$ and the corresponding strain is equal to $1.97 p_0 R/AE$. The maximum radial displacement is $4.90 p_0 R^2/AE$.

In Fig. 5.14 are presented response curves for a yield level prescribed by the parameter

$$\frac{\epsilon_y}{p_0 R/AE} = 1.0 .$$

This corresponds to a yield stress in the flanges, σ_y , equal to $1.0 p_0 R/A$ or approximately one-half the maximum stress obtained for the elastic case. Included in this figure are the radial displacements, axial forces, moments, and average strains for the 1/4 point, crown, and 3/4 point. The strain is shown only for the flange for which the maximum value is largest. At the 1/4 point the largest strains occur in the top flange, whereas, at the crown and

3/4 point, they occur in the bottom flange. In Figs. 5.14a and b are shown also the curves for the corresponding elastic solution. These results cover an interval of time of only $1.4 T_0$ because of the large amount of computer time required to obtain the solution. This particular problem was run on the ILLIAC for a total of one hour and forty minutes before the solution was discontinued.

The second "inelastic" solution was obtained for a yield level given by

$$\frac{\epsilon_y}{p_0 R/AE} = 0.5 .$$

This corresponds to a yield stress equal to approximately one-fourth the maximum stress obtained for the elastic system. The results are summarized graphically in Fig. 5.15.

Of major interest is a comparison of the maximum values of the two "inelastic" solutions with the corresponding elastic solution. The absolute maximum values for all three solutions are listed in the following table:

Absolute Maximum Values						
$\frac{\epsilon_y}{p_0 R/AE}$	$\frac{\epsilon_{max}}{p_0 R/AE}$	$\frac{\sigma_{max}}{p_0 R/A}$	$\frac{w_{max}}{p_0 R^2/AE}$	$\frac{v_{max}}{p_0 R^2/AE}$	$\frac{N_{max}}{p_0 R}$	$\frac{M_{max}}{p_0 Rr}$
Elastic	1.97	1.97	4.90	2.32	0.71	1.63
1.0	2.91	1.00	6.23	2.44	0.64	0.78
0.5	8.56	0.50	14.82	3.51	0.50	0.47

For $\epsilon_y = 1.0 p_0 R/AE$ it can be seen that the maximum strain is 48 percent larger than the corresponding strain in the elastic system. The maximum inelastic strain is 1.91 times the limiting elastic strain. Of course, the maximum stress is equal to the yield stress, $\sigma_y = 1.0 p_0 R/A$. It is of interest to note that the maximum radial displacement is only 27 percent larger than that for the elastic solution. For $\epsilon_y = 0.5 p_0 R/AE$, the maximum inelastic strain is 16.1 times the limiting elastic strain, whereas the maximum radial displacement is 3.0 times the corresponding displacement for the elastic system.

The values of the maximum strain at each of the joints of the analogous arch are tabulated below for both inelastic solutions. These results

are expressed in the form $\epsilon_{\max}/\epsilon_y$. The values in parentheses do not represent true maxima; they are the largest computed values for the interval investigated.

Maximum Strains, $\epsilon_{\max}/\epsilon_y$				
Joint	$\frac{\epsilon_y}{p_o R/AE} = 1.0$		$\frac{\epsilon_y}{p_o R/AE} = 0.5$	
	top flange	bottom flange	top flange	bottom flange
0	-0.60	-0.60	-4.71	-4.71
1	-0.99	-0.77	-6.66	-5.41
2	-2.20	-0.50	(-14.33)	-1.90
3	-2.91	-0.36	-17.13	-1.36
4	-2.44	-0.63	-6.77	-4.00
5	(-1.81)	-0.88	-1.23	-3.39
6	(-0.76)	-1.14	-1.32	-4.16
7	-0.55	-1.26	1.22	-3.42
8	-0.54	(-1.68)	-1.79	-1.96
9	(0.66)	-2.84	-3.59	-3.71
10	-0.38	-2.17	-2.72	(-9.47)
11	-0.56	-1.28	-5.20	-9.83
12	-0.70	-0.70	-8.70	-8.70

It can be seen that for $\epsilon_y = 0.5 p_o R/AE$ yielding extends over the complete arch; even for $\epsilon_y = 1.0 p_o R/AE$ yielding covers all of the arch except for sections close to the supports. For both solutions the maximum strains occur at the quarter point. It may be noted that the strains in the top and bottom flanges are unequal over a major portion of the arch indicating the importance of the bending effects.

VI. SUMMARY

6.1 Summary

6.1.1 General. This investigation was concerned with the computation of the response of arches subjected to time-dependent forces. A method of analysis has been developed which is applicable to both the elastic and post-elastic ranges of deformation. In this analysis the continuous arch is approximated by a discrete framework consisting of a series of rigid bars and flexible joints. For the computation of the response in the inelastic range, the cross-sectional area of the arch is considered to consist of two concentrated flange areas connected by a thin rigid web. The stress-deformation relationship for each flange is represented by a bilinear diagram. The equations of motion for the analogous framework are solved by use of a step-by-step method of numerical integration.

Computer programs have been prepared for obtaining numerical solutions on the ILLIAC, the high-speed digital computer of the University of Illinois. These programs are applicable to two general classes of problems: (a) circular elastic arches subjected to a uniform all-around pressure having any timewise variation, and (b) arches of arbitrary shape subjected to a triangular moving pressure pulse. For the latter case response into the post-elastic range of behavior may be evaluated. The effect of an initial out-of-roundness may also be considered in the case of the uniform all-around pressure.

Numerical solutions were obtained for two-hinged circular arches of uniform cross-section subjected to a uniform all-around pressure having a pressure-time relationship represented by a triangle with an initial peak and also to a triangular-shaped moving pressure. Observations based on these results are summarized below. Unless otherwise indicated, these comments refer to response in the elastic range of behavior.

6.1.2 Solutions for Arches Subjected to a Uniform All-Around Pressure.

The major aspects of the response for arches subjected to a uniform all-around pressure can be explained in terms of the participation of the first three symmetrical modes of vibration. The mode which participates most significantly is the extensional mode of vibration for which the period is close to the "breathing" period of a complete ring. The predominance of this mode can be

seen most clearly in the history curves of the axial force. This force is essentially uniform throughout the arch.

In spite of the predominance of the extensional mode, the bending effects are significant, particularly for the smaller durations of loading. For durations, t_d , less than about 0.75 times the "breathing" period, T_0 , of a complete ring, bending contributes roughly 40 percent of the total maximum stress for a cross-section composed of two concentrated flange areas, i.e. for $c/r = 1$, and about 60 percent of the total stress for a rectangular cross-section for which $c/r = \sqrt{3}$. For load durations of the order of $t_d/T_0 = 2$ or 4, the contribution of bending is about 25 percent for $c/r = 1$ and about 40 percent for $c/r = \sqrt{3}$.

As may be expected, the absolute maximum axial force increases with an increase in the duration of the pressure pulse. The same is generally true of the maximum values of stress and displacement, although the increase is not continuous as in the case of the axial force. For values of t_d/T_0 in the range between 2 to 4, the maximum value of the radial displacement is of the order of 2.5 to 3.0 times the static deflection produced in a complete ring by a uniform pressure having a magnitude equal to the peak dynamic pressure. The maximum axial force is approximately 1.8 times the static value in a complete ring, and the absolute maximum stress is of the order of 2 or 2.5 times the static value for $c/r = 1$, and 3 times the static value for $c/r = \sqrt{3}$.

For the range of parameters considered, the maximum effects were not significantly affected by variations in the magnitude of the peak pressure and by initial imperfections in the arch of the order of $\bar{w}_m/L_0 = 0.001$. This observation may not be valid for longer durations of loading.

The effects of variations in the slenderness ratio, L_0/r , or the rise-span ratio, f/L_0 , on the maximum effects were not large for the limited number of cases studied. An increase in the value of L_0/r has essentially the same effect as an increase in f/L_0 . It appears that the parameters f/L_0 and L_0/r can be incorporated into the single parameter $(f/L_0)(L_0/r) = f/r$.

6.1.3 Solutions for Arches Subjected to a Triangular Moving Pressure.

For the case of an arch subjected to a triangular moving pressure, the major contribution to the response appears to be due to the participation of the first antisymmetrical mode of vibration.

Although the absolute maximum effects in the arch occur at sections away from the crown, the effects at the crown are also appreciable. For the solutions presented, it was found that the maximum radial displacements and bending moments at the crown are from 30 percent to 90 percent of the corresponding absolute maximum values of these quantities. The axial force remains relatively uniform for all sections along the arch.

A comparison of the maximum effects for a moving pressure and a uniform all-around pressure both of which have the same magnitude and duration shows that the largest displacements and moments occur for the moving pressure, whereas the maximum axial force occurs for the uniform pressure. For pressures which act on the arch for a total time of from 2 to 3 T_0 , the maximum displacements for a moving pressure are of the order of 2 to 3 times those for a uniform pressure, and the maximum moments are of the order of 1.5 to 2 times the corresponding values for a uniform pressure. On the other hand, the maximum axial forces for the moving pressure are about one-half the corresponding maxima for a uniform pressure. It follows from these results that the bending effects due to a moving pressure are more significant than for a uniform all-around pressure pulse.

For durations of load t_d of the order of 2 T_0 , it was found that the buckling tendencies are appreciable for high magnitudes of pressure. For a value of $p_0/p_{cr} = 1$, the maximum displacements were found to be about 50 percent larger, and the maximum moments about 25 percent larger than would have been the case had the buckling tendency been neglected. For shorter durations, however, the maximum effects are not influenced significantly by changes in the magnitude of the pressure even for large values of p_0/p_{cr} .

The effects of changes in the values of the slenderness ratio, L_0/r , were found to be the same as corresponding changes in values of the rise-span ratio, f/L_0 . Since this relationship between the slenderness ratio and the rise-span ratio is the same as that observed from the results for a uniform all-around pressure, it offers additional assurance that the significant structural parameter may be f/r .

Because of the limited number of solutions obtained, it was not possible to make any definite observations concerning the effects of the velocity of the pressure pulse or the effects of inelastic action. However, a few example solutions have been presented which illustrate, to a certain extent, the influence of these variables.

REFERENCES

1. Brooks, J. A., "Solution of Structural Mechanics Problems on High Speed Digital Computing Machines", Ph.D. Dissertation, University of Illinois, 1955.
2. Clough, R. W., "Elastic Stability of Arch Ribs", Thesis for Doctor of Science Degree, Massachusetts Institute of Technology, 1949.
3. Eppink, R. T., and Veletsos, A. S., "Analysis and Design of Domes, Arches, and Shells, Volume II: Analysis of Circular Arches", AFSWC-TR-59-9, Air Force Special Weapons Center, Kirtland Air Force Base, New Mexico, July, 1959.
4. Newmark, N. M., "Vulnerability of Arches - Preliminary Notes", Department of Civil Engineering, University of Illinois, 21 May 1956 (Unpublished manuscript).
5. Newmark, N. M., "A Method of Computation for Structural Dynamics", Journal of the Engineering Mechanics Division, Proceedings of the American Society of Civil Engineers, Vol. 85, no. EM 3, July 1959, pp. 67-94.
6. Manuals-Corps of Engineers, U. S. Army, "Engineering and Design; Design of Structures to Resist the Effects of Atomic Weapons - Arches and Domes", EM 1110-345-420, January 15, 1960.

APPENDIX A. "EXACT" DEFORMATION-FORCE RELATIONSHIPS FOR INELASTIC BEHAVIOR

The purpose of this section is to formulate the equations for determining the actual deformations of the individual flanges in terms of δ_j and χ_j .

From the geometry of the deformed joint j shown in Fig. 2.5, it can be seen that

$$\delta_j^l = \frac{c_j^t}{d_j} \delta_j^{lb} + \frac{c_j^b}{d_j} \delta_j^{lt}$$

$$\delta_j^r = \frac{c_j^t}{d_j} \delta_j^{rb} + \frac{c_j^b}{d_j} \delta_j^{rt}$$

where d_j denotes the distance between flanges. Application of Eq. 2.2 yields the following relationship:

$$\frac{c_{j-1}^t}{d_{j-1}} \delta_{j-1}^{rb} + \frac{c_{j-1}^b}{d_{j-1}} \delta_{j-1}^{rt} + \frac{c_j^t}{d_j} \delta_j^{lb} + \frac{c_j^b}{d_j} \delta_j^{lt} = \delta_j \quad (A.1)$$

An analogous procedure is followed to relate the flange deformations to χ_j . With χ_j^l and χ_j^r denoting the angle changes to the left and right of joint j , respectively, the following expressions are obtained:

$$\chi_j^l = \frac{1}{d_j} (-\delta_j^{lb} + \delta_j^{lt})$$

$$\chi_j^r = \frac{1}{d_j} (-\delta_j^{rb} + \delta_j^{rt})$$

Since,

$$\chi_j = \chi_j^l + \chi_j^r$$

it follows that

$$\frac{1}{d_j} (-\delta_j^{lb} + \delta_j^{lt} - \delta_j^{rb} + \delta_j^{rt}) = \chi_j \quad (A.2)$$

Two additional relationships are obtained by considering the equilibrium of the j^{th} bar and the j^{th} joint. The forces in the flanges are indicated

in a manner similar to that used to identify deformations. Thus, N_j^{rt} denotes the force in the top right flange at joint j . Considering the equilibrium of bar j , one obtains the equation,

$$N_{j-1}^{rb} + N_{j-1}^{rt} = N_j^{lb} + N_j^{lt} \quad (A.3)$$

If the small moments $Q\delta$ produced by the shearing forces on either side of a joint are assumed to be negligible, the following equilibrium equation is obtained for the j^{th} joint:

$$N_j^{lb} c_j^b - N_j^{lt} c_j^t = N_j^{rb} c_j^b - N_j^{rt} c_j^t \quad (A.4)$$

It is important to notice that the forces appearing in Eqs. (A.3) and (A.4) are actually functions of the deformations δ_j^{rb} , δ_b^{rt} , etc., which are to be evaluated. These forces are related to the deformations through the stress-deformation relationships and the following equations:

$$\begin{aligned} N_j^{lb} &= \sigma_j^{lb} A_j^b \\ N_j^{lt} &= \sigma_j^{lt} A_j^t \\ N_j^{rb} &= \sigma_j^{rb} A_j^b \\ N_j^{rt} &= \sigma_j^{rt} A_j^t \end{aligned} \quad (A.5)$$

However, in order to express them in terms of the corresponding deformations, it is necessary to know the region of the stress-deformation curve in which the deformation is located. In general this region is determined from a knowledge of the past history of the deformations.

For a structure with z bars, there is a total of $4z$ unknown flange deformations, four at each intermediate joint and two at each of the end joints. By application of Eqs. (A.2) and (A.4) to each joint and Eqs. (A.1) and (A.3) to each bar, one obtains $4z-2$ equations. The boundary condition equations are specialized forms of Eqs. (A.2) and (A.4). For example, with a hinge at joint 0, M_0 is equal to zero, and Eq. (A.4) becomes,

$$N_0^{rb} c_0^b - N_0^{rt} c_0^t = 0.$$

If joint 0 is fixed, Eq. (A.2) becomes

$$\frac{1}{d_0} (-\delta_0^{rb} + \delta_0^{rt}) = \psi_1 .$$

Thus one obtains $4z$ equations which relate the $4z$ unknown deformations to δ_j and χ_j . The solution of these equations results in a complete determination of the changes in length of the flanges.

Once the flange deformations have been calculated, the corresponding forces can be computed by use of the stress-deformation diagrams. The total axial force, N_j , is found from the expression on either the left or right side of Eq. (A.3), and the moment M_j is determined by use of the left or right side of Eq. (A.4).

As stated above, the computation of N_j and M_j from the quantities δ_j and χ_j involves the solution of a set of simultaneous equations. The computer time required for just one such solution may amount to several minutes. For a dynamic response analysis, these steps are repeated several hundreds of times. Consequently, the time required to effect a complete solution of the problem makes this "exact" method entirely impractical on present-day digital computers such as the ILLIAC.

APPENDIX B. EQUATIONS FOR CIRCULAR ARCHES IN POLAR COORDINATES

The equations presented in this section are for the coordinate system shown in Fig. 3.1. They are derived in a manner analogous to that used in the main body of the report, and they are numbered so as to correspond to the equations given in Chapter II.

B.1 Equations of Motion

The equations of motion for mass m_j in the radial and tangential directions are

$$m_j \ddot{w}_j = \bar{Z}_j + \bar{W}_j \quad (\text{B.2.4})$$

$$m_j \ddot{v}_j = \bar{Y}_j + \bar{V}_j \quad (\text{B.2.5})$$

The quantities \bar{Z}_j and \bar{Y}_j represent the components of all internal forces at joint j acting in the positive w_j and v_j directions, respectively; \bar{W}_j and \bar{V}_j represent the components of the external forces at joint j acting in the positive radial and tangential directions, respectively. The quantities \ddot{w}_j and \ddot{v}_j denote the radial and tangential accelerations of the j^{th} mass.

By considering the equilibrium of joint j and by summing the components of all internal forces first in the radial direction and then in the tangential direction, one obtains the following two equations:

$$\begin{aligned} \bar{Z}_j = & -N_j \sin\left(\frac{\Phi}{2} - \psi_j\right) - N_{j+1} \sin\left(\frac{\Phi}{2} + \psi_{j+1}\right) \\ & + Q_j \cos\left(\frac{\Phi}{2} - \psi_j\right) - Q_{j+1} \cos\left(\frac{\Phi}{2} + \psi_{j+1}\right) \end{aligned} \quad (\text{B.2.6})$$

$$\begin{aligned} \bar{Y}_j = & -N_j \cos\left(\frac{\Phi}{2} - \psi_j\right) + N_{j+1} \cos\left(\frac{\Phi}{2} + \psi_{j+1}\right) \\ & - Q_j \sin\left(\frac{\Phi}{2} - \psi_j\right) - Q_{j+1} \sin\left(\frac{\Phi}{2} + \psi_{j+1}\right) \end{aligned} \quad (\text{B.2.7})$$

For the case in which the analogous arch is subjected to a pressure which remains normal to the surface, the components of the external forces acting in the radial and tangential directions are given by the equations,

$$\bar{w}_j = P_j^l \cos\left(\frac{\Phi}{2} - \psi_j\right) + P_j^r \cos\left(\frac{\Phi}{2} + \psi_{j+1}\right) \quad (\text{B.2.12})$$

$$\bar{v}_j = -P_j^l \sin\left(\frac{\Phi}{2} - \psi_j\right) + P_j^r \sin\left(\frac{\Phi}{2} + \psi_{j+1}\right) \quad (\text{B.2.13})$$

For a uniform all-around pressure p ,

$$P_j^l = P_j^r = -0.5 pL.$$

B.2 Displacement-Deformation Relationships

In terms of the radial and tangential displacements, the quantities $\bar{\delta}_j$ and $\bar{\psi}_j$ are expressed as follows:

$$\bar{\delta}_j = (v_j - v_{j-1}) \cos \frac{\Phi}{2} + (w_j + w_{j-1}) \sin \frac{\Phi}{2} \quad (\text{B.2.14})$$

$$\bar{\psi}_j = (v_j + v_{j-1}) \sin \frac{\Phi}{2} - (w_j - w_{j-1}) \cos \frac{\Phi}{2} \quad (\text{B.2.15})$$

The expressions for the quantities given by Eqs. (2.14b) and 2.15b) are the same for both coordinate systems. In addition, one finds that

$$\sin \psi_j = \frac{\bar{\psi}_j}{\sqrt{\bar{\psi}_j^2 + (1 - \bar{\delta}_j/L)^2}} \cong \bar{\psi}_j (1 - \bar{\delta}_j/L)$$

$$\cos \psi_j = \frac{1 + \bar{\delta}_j/L}{\sqrt{\bar{\psi}_j^2 + (1 + \bar{\delta}_j/L)^2}} \cong 1 - \frac{1}{2} \bar{\psi}_j^2$$

APPENDIX C. MODAL METHOD OF ANALYSIS

In the modal method of analysis, the radial and tangential displacements of the arch analogue are expressed by the following equations:

$$w_j = \sum_{r=1}^n c^{(r)} \bar{w}_j^{(r)} f_r(t) \quad (C.1)$$

$$v_j = \sum_{r=1}^n c^{(r)} \bar{v}_j^{(r)} f_r(t)$$

where $\bar{w}_j^{(r)}$ = radial displacement of joint j for the r^{th} mode of vibration
 $\bar{v}_j^{(r)}$ = tangential displacement of joint j for the r^{th} mode of vibration
 $f_r(t)$ = dynamic amplification factor for the r^{th} mode
 $c^{(r)}$ = participation factor for the r^{th} mode
 n = number of degrees of freedom of the system.

The participation factors are given by the equation,

$$c^{(r)} = \frac{\sum_{j=1}^{z-1} [\bar{W}_j \bar{w}_j^{(r)} + \bar{V}_j \bar{v}_j^{(r)}]}{(\omega_r)^2 \sum_{j=1}^{z-1} m_j \left\{ [\bar{w}_j^{(r)}]^2 + [\bar{v}_j^{(r)}]^2 \right\}} \quad (C.2)$$

where ω_r is the circular natural frequency corresponding to the r^{th} mode, m_j is the concentrated mass at joint j , and \bar{W}_j and \bar{V}_j are as defined in Appendix B. For a uniform all-around external pressure of intensity p , \bar{V}_j is equal to zero and \bar{W}_j is equal to $-pL \cos \frac{\theta}{2}$. The amplification factor $f_r(t)$ is a time function which depends on the nature of the forcing function. For a step pulse of infinite duration,

$$f_r(t) = (1 - \cos \omega_r t) = \left(1 - \cos 2\pi \frac{t}{T_r}\right) \quad (C.3)$$

The bending moments, M_j , and the axial forces, N_j , are determined in an analogous manner by use of the following equations:

$$\begin{aligned} N_j &= \sum_{r=1}^n c^{(r)} \bar{N}_j^{(r)} f_r(t) \\ M_j &= \sum_{r=1}^n c^{(r)} \bar{M}_j^{(r)} f_r(t) \end{aligned} \tag{C.4}$$

where $\bar{N}_j^{(r)}$ is the axial force in bar j for the r^{th} natural mode of vibration and $\bar{M}_j^{(r)}$ is the corresponding bending moment.

The values of the symmetrical modes of vibration and the corresponding natural periods for the arch described in Section 4.2.1 are listed in Table C.1. These values were determined from the equations given in reference [3]. Also included in this table are the values of the participation factors, $c^{(r)}$, for the particular modal solution mentioned in Section 4.2.2. The modal response coefficients presented in Table 4.2 for w_j , N_j , and M_j are the products of the participation factors and the corresponding values of $\bar{w}_j^{(r)}$, $\bar{N}_j^{(r)}$, or $\bar{M}_j^{(r)}$, respectively.

TABLE 4.1 NATURAL PERIODS OF A TWO-HINGED UNIFORM CIRCULAR ARCH

$$f/L_0 = 0.2, L_0/r = 100, z = 12$$

Tabulated values represent the ratio T_r/T_0 , where T_r is the r th natural period and T_0 is given by the expression

$$T_0 = 2\pi \sqrt{\frac{\mu R^2}{EA}} = 0.04555 \sqrt{\frac{\mu L_0^4}{EI}}$$

Order of Period	Antisymmetrical Modes	Symmetrical Modes
1	4.996	2.225
2	1.204	1.066
3	0.592	0.784
4	0.444	0.465
5	0.389	0.342
6	0.313	0.297
7	0.164	0.240
8	0.104	0.126
9	0.080	0.090
10	0.069	0.073
11	0.064	0.066

TABLE 4.2 MODAL SOLUTION FOR A TWO-HINGED UNIFORM CIRCULAR ARCH
Uniform All-Around Rectangular Pressure Pulse of Infinite Duration

$$f/L_0 = 0.2, L_0/r = 100, z = 12$$

$$\begin{bmatrix} W \\ W \\ W \\ W \\ W \\ W \\ W \\ 0 \end{bmatrix} \left(\frac{1}{p_0 R^2 / AE} \right) = \begin{bmatrix} 0.3568 \\ 0.4601 \\ 0.2270 \\ -0.2270 \\ -0.6588 \\ -0.8346 \end{bmatrix} f_1(t) + \begin{bmatrix} -0.4113 \\ -1.1729 \\ -1.5008 \\ -1.3086 \\ -0.7406 \\ -0.4385 \end{bmatrix} f_2(t) + \begin{bmatrix} -0.3045 \\ -0.1949 \\ 0.1483 \\ 0.2020 \\ -0.1176 \\ -0.3310 \end{bmatrix} f_3(t) + \begin{bmatrix} -0.0344 \\ 0.0170 \\ 0.0242 \\ -0.0313 \\ -0.0100 \\ 0.0343 \end{bmatrix} f_4(t) + \begin{bmatrix} -0.0065 \\ 0.0093 \\ -0.0066 \\ -0.0001 \\ 0.0065 \\ -0.0094 \end{bmatrix} f_5(t) + \begin{bmatrix} -0.0006 \\ 0.0011 \\ -0.0015 \\ 0.0019 \\ -0.0021 \\ 0.0022 \end{bmatrix} f_6(t) + \dots$$

$$\begin{bmatrix} N \\ N \\ N \\ N \\ N \\ N \\ N \\ 0 \end{bmatrix} \left(\frac{1}{p_0 R} \right) = \begin{bmatrix} -0.0494 \\ -0.0506 \\ -0.0482 \\ -0.0426 \\ -0.0362 \\ -0.0320 \end{bmatrix} f_1(t) + \begin{bmatrix} -0.8955 \\ -0.8843 \\ -0.8674 \\ -0.8607 \\ -0.8678 \\ -0.8776 \end{bmatrix} f_2(t) + \begin{bmatrix} -0.0613 \\ -0.0623 \\ -0.0737 \\ -0.0833 \\ -0.0802 \\ -0.0714 \end{bmatrix} f_3(t) + \begin{bmatrix} 0.0000 \\ -0.0015 \\ -0.0042 \\ -0.0035 \\ -0.0029 \\ -0.0052 \end{bmatrix} f_4(t) + \begin{bmatrix} 0.0006 \\ -0.0001 \\ -0.0004 \\ -0.0003 \\ -0.0011 \\ -0.0008 \end{bmatrix} f_5(t) + \begin{bmatrix} 0.0001 \\ 0.0000 \\ 0.0000 \\ -0.0001 \\ -0.0001 \\ -0.0001 \end{bmatrix} f_6(t) + \dots$$

$$\begin{bmatrix} M \\ M \\ M \\ M \\ M \\ M \\ M \\ 0 \end{bmatrix} \left(\frac{1}{p_0 R r} \right) = \begin{bmatrix} -0.2125 \\ -0.2824 \\ -0.1862 \\ 0.0165 \\ 0.2117 \\ 0.2914 \end{bmatrix} f_1(t) + \begin{bmatrix} -0.2087 \\ 0.1983 \\ 0.5248 \\ 0.3171 \\ -0.2270 \\ -0.5137 \end{bmatrix} f_2(t) + \begin{bmatrix} 0.3530 \\ 0.1991 \\ -0.2459 \\ -0.3173 \\ 0.0907 \\ 0.3637 \end{bmatrix} f_3(t) + \begin{bmatrix} 0.0733 \\ -0.0378 \\ -0.0536 \\ 0.0657 \\ 0.0197 \\ -0.0757 \end{bmatrix} f_4(t) + \begin{bmatrix} 0.0191 \\ -0.0271 \\ 0.0192 \\ -0.0000 \\ -0.0192 \\ 0.0272 \end{bmatrix} f_5(t) + \begin{bmatrix} 0.0019 \\ -0.0036 \\ 0.0052 \\ -0.0063 \\ 0.0071 \\ -0.0073 \end{bmatrix} f_6(t) + \dots$$

$f_r(t)$ = amplification factor for r^{th} mode, a function of the pulse shape

TABLE 4.3 MAXIMUM VALUES OF RESPONSE AND TIMES OF OCCURRENCE FOR A TWO-HINGED UNIFORM CIRCULAR ARCH
Uniform All-Around Triangular Pressure Pulse With Initial Peak

$$f/L_0 = 0.2, L_0/r = 100, p_0/p_{cr} = 1.0, t_d/T_0 = 2.0, z = 12, \Delta t/T_0 = 0.01$$

Joint or Bar j	$\frac{w}{p_0 R^2/AE}$	$\frac{t}{T_0}$	$\frac{N}{p_0 R}$	$\frac{t}{T_0}$	$\frac{M}{p_0 Rr}$	$\frac{t}{T_0}$	$\frac{\sigma}{p_0 R/A}$ c/r = 1	$\frac{t}{T_0}$	$\frac{\sigma}{p_0 R/A}$ c/r = 2	$\frac{t}{T_0}$
	1	-1.076	0.41	-1.712	0.50	0.762	2.08	-1.814	0.44	-2.401
2	-1.959	0.47	-1.700	0.50	0.585	2.77	-2.180	0.47	-2.703	0.45
3	-2.384	0.53	-1.684	0.50	0.934	1.61	-2.222	0.54	-2.813	1.60
4	-2.277	0.58	-1.678	0.50	0.856	1.64	-1.890	0.61	-2.635	1.63
5	-1.936	0.52	-1.679	0.50	0.457	1.12	-1.852	0.52	-2.030	0.53
6	-1.874	0.49	-1.679	0.51	-1.136	1.66	-2.068	1.64	-3.197	1.65

TABLE 4.4 STATIC EFFECTS IN A TWO-HINGED UNIFORM CIRCULAR ARCH FOR A UNIFORM ALL-AROUND PRESSURE

$$f/L_0 = 0.2, L_0/r = 100, z = 12$$

Joint or Bar j	$\frac{w}{p_0 R^2/AE}$	$\frac{v}{p_0 R^2/AE}$	$\frac{N}{p_0 R}$	$\frac{M}{p_0 Rr}$
1	-0.400	-0.101	-0.995	0.025
2	-0.780	-0.152	-0.994	0.047
3	-1.110	-0.159	-0.994	0.063
4	-1.363	-0.128	-0.994	0.076
5	-1.523	-0.071	-0.994	0.083
6	-1.578	0.000	-0.994	0.086

TABLE 4.5 EFFECT OF TIME INTERVAL OF INTEGRATION ON MAXIMUM VALUES OF RESPONSE AND TIMES OF OCCURRENCE
Two-Hinged Uniform Circular Arch; Uniform All-Around Triangular Pressure Pulse With Initial Peak

$$f/L_0 = 0.2, L_0/r = 100, p_0/p_{cr} = 1.0, t_d/T_0 = 2.0$$

Joint or Bar j	$\frac{w}{p_0 R^2/AE}$	$\frac{t}{T_0}$	$\frac{N}{p_0 R}$	$\frac{t}{T_0}$	$\frac{M}{p_0 Rr}$	$\frac{t}{T_0}$	$\frac{\sigma}{p_0 R/A}$	$\frac{t}{T_0}$	$\frac{\sigma}{p_0 R/A}$	$\frac{t}{T_0}$
							c/r = 1	c/r = 2		
(a) $z = 10, \Delta t/T_0 = 0.005$										
1	-1.311	0.42	-1.720	0.50	-0.884	1.69	-1.946	0.44	-2.615	1.67
2	-2.211	0.50	-1.701	0.50	0.565	0.52	-2.258	0.51	-2.822	0.51
3	-2.326	0.56	-1.686	0.50	1.072	0.69	-1.965	0.58	-2.948	1.66
4	-1.999	0.52	-1.683	0.50	0.228	0.94	-1.802	0.52	-1.924	0.52
5	-1.914	0.50	-1.683	0.52	-1.149	2.57	-1.865	1.66	-2.893	1.68
(b) $z = 12, \Delta t/T_0 = 0.005$										
1	-1.076	0.42	-1.713	0.50	0.763	2.08	-1.814	0.44	-2.401	1.59
2	-1.959	0.47	-1.699	0.50	0.586	2.77	-2.181	0.46	-2.702	0.45
3	-2.385	0.54	-1.684	0.50	0.934	1.61	-2.222	0.54	-2.812	1.60
4	-2.278	0.58	-1.678	0.50	0.857	1.64	-1.891	0.60	-2.636	1.62
5	-1.936	0.52	-1.679	0.50	0.457	1.12	-1.852	0.52	-2.031	0.53
6	-1.875	0.48	-1.679	0.51	-1.137	1.66	-2.070	1.64	-3.200	1.64
(c) $z = 12, \Delta t/T_0 = 0.02$										
1	-1.076	0.42	-1.713	0.50	0.761	2.08	-1.814	0.44	-2.212*	1.58
2	-1.957	0.48	-1.699	0.50	0.581	2.78	-2.181	0.46	-2.561*	0.46
3	-2.384	0.54	-1.684	0.50	0.934	1.62	-2.221	0.54	-2.631	0.54
4	-2.277	0.58	-1.679	0.50	0.856	1.64	-1.890	0.60	-2.406	1.62
5	-1.937	0.52	-1.679	0.50	0.458	1.12	-1.851	0.52	-1.979	0.54
6	-1.874	0.48	-1.677	0.52	-1.133	1.66	-2.062	1.64	-2.883	1.64

* Stress values in this column are for $c/r = \sqrt{3}$.

TABLE 4.5 (Continued)

Joint or Bar j	$\frac{w}{p_o R^2/AE}$	$\frac{t}{T_o}$	$\frac{N}{p_o R}$	$\frac{t}{T_o}$	$\frac{M}{p_o Rr}$	$\frac{t}{T_o}$	$\frac{\sigma}{p_o R/A}$		$\frac{\sigma}{p_o R/A}$	
							$c/r = 1$	$\frac{t}{T_o}$	$c/r = 2$	$\frac{t}{T_o}$
(d) $z = 16, t/T_o = 0.005$										
1	-0.802	2.66	-1.709	0.50	-0.546	1.59	-1.840	0.56	-2.141	1.60
2	-1.537	0.44	-1.701	0.50	0.610	1.94	-1.994	0.44	-2.393	0.40
3	-2.090	0.48	-1.687	0.50	0.560	2.59	-2.208	0.48	-2.745	0.47
4	-2.374	0.53	-1.677	0.50	-0.912	1.10	-2.199	0.52	-2.767	1.59
5	-2.391	0.57	-1.674	0.50	0.923	1.54	-2.087	0.60	-2.814	1.54
6	-2.144	0.56	-1.675	0.50	0.296	1.48	-1.791	0.44	-1.964	0.43
7	-1.863	0.50	-1.675	0.50	0.723	1.12	-1.894	0.54	-2.200	1.56
8	-1.810	0.46	-1.675	0.50	1.020	1.14	-2.148	0.58	-2.927	1.58
(e) $z = 16, t/T_o = 0.01$										
1	-0.801	0.40	-1.709	0.50	0.547	1.94	-1.840	0.56	-2.135	1.60
2	-1.537	0.44	-1.700	0.50	0.609	1.94	-1.994	0.44	-2.393	0.41
3	-2.090	0.48	-1.687	0.50	0.561	2.59	-2.208	0.48	-2.745	0.47
4	-2.374	0.53	-1.678	0.50	-0.912	1.10	-2.198	0.53	-2.766	1.59
5	-2.391	0.57	-1.674	0.50	0.924	1.54	-2.086	0.61	-2.817	1.55
6	-2.144	0.56	-1.674	0.50	0.296	1.47	-1.791	0.44	-1.964	0.43
7	-1.863	0.50	-1.675	0.50	0.723	1.12	-1.893	0.54	-2.205	1.56
8	-1.810	0.46	-1.676	0.50	1.018	1.13	-2.149	0.58	-2.919	1.58
(f) $z = 20, t/T_o = 0.005$										
1	-0.638	0.40	-1.708	0.50	-0.549	1.51	-1.849	0.54	-1.986*	0.56
2	-1.250	0.42	-1.703	0.50	-0.596	1.52	-1.864	0.44	-2.075	0.40
3	-1.775	0.46	-1.692	0.50	0.638	2.56	-2.089	0.46	-2.418	0.44
4	-2.158	0.49	-1.682	0.50	0.555	0.46	-2.220	0.48	-2.623	0.48
5	-2.366	0.53	-1.675	0.50	-0.884	1.08	-2.161	0.52	-2.573	0.60
6	-2.435	0.56	-1.673	0.50	-0.838	1.10	-2.185	0.58	-2.653	0.60
7	-2.288	0.56	-1.671	0.50	0.532	1.49	-1.944	0.57	-2.226	0.60
8	-2.010	0.54	-1.672	0.50	0.340	1.02	-1.754	0.46	-1.855	0.42
9	-1.810	0.48	-1.673	0.50	0.857	1.12	-2.007	0.55	-2.298	0.59
10	-1.759	0.46	-1.674	0.50	1.152	1.12	-1.379	0.60	2.176	1.12

*Stress values in this column are for $c/r = \sqrt{3}$.

TABLE 4.6 COMPARISON OF SOLUTIONS BY NUMERICAL INTEGRATION PROCEDURE AND MODAL METHOD
Two-Hinged Uniform Circular Arch; Uniform All-Around Rectangular Pressure Pulse of Infinite Duration

$$f/L_0 = 0.2, L_0/r = 100, z = 12$$

t/T ₀	$\frac{w}{p_0 R^2/AE}$				$\frac{N}{p_0 R}$		$\frac{M}{p_0 Rr}$			
	1/4-point		crown		crown		1/4-point		crown	
	Numerical Method	Modal Method	Numerical Method	Modal Method	Numerical Method	Modal Method	Numerical Method	Modal Method	Numerical Method	Modal Method
0.1	-0.191	-0.191	-0.190	-0.191	-0.190	-0.190	-0.004	-0.003	0.000	-0.001
0.2	-0.708	-0.708	-0.692	-0.692	-0.633	-0.634	-0.017	-0.017	-0.001	-0.001
0.3	-1.424	-1.424	-1.331	-1.331	-1.200	-1.200	0.056	0.056	0.003	0.003
0.4	-2.135	-2.135	-1.878	-1.878	-1.675	-1.675	0.296	0.297	-0.009	-0.009
0.5	-2.552	-2.551	-2.128	-2.128	-1.888	-1.888	0.518	0.518	-0.138	-0.139
0.6	-2.476	-2.473	-2.046	-2.046	-1.811	-1.810	0.532	0.530	-0.399	-0.400
0.7	-1.940	-1.935	-1.842	-1.845	-1.433	-1.430	0.406	0.404	-0.477	-0.475
0.8	-1.110	-1.105	-1.770	-1.775	-0.946	-0.944	0.191	0.188	-0.097	-0.090
0.9	-0.201	-0.195	-1.858	-1.864	-0.485	-0.482	-0.176	-0.181	0.487	0.493
1.0	0.507	0.511	-2.024	-2.029	-0.216	-0.217	-0.618	-0.622	0.911	0.914
1.1	0.726	0.727	-2.226	-2.230	-0.232	-0.235	-0.876	-0.877	1.120	1.122
1.2	0.330	0.326	-2.383	-2.411	-0.472	-0.474	-0.762	-0.759	1.055	1.053
1.3	-0.552	-0.558	-2.402	-2.400	-0.899	-0.901	-0.320	-0.316	0.643	0.638
1.4	-1.586	-1.592	-2.276	-2.273	-1.332	-1.334	0.231	0.235	0.058	0.054
1.5	-2.392	-2.395	-2.061	-2.057	-1.680	-1.682	0.646	-0.646	-0.480	-0.483
1.6	-2.693	-2.691	-1.832	-1.829	-1.817	-1.816	0.756	0.753	-0.786	-0.786
1.7	-2.426	-2.421	-1.678	-1.677	-1.677	-1.675	0.588	0.584	-0.619	-0.611
1.8	-1.731	-1.724	-1.564	-1.562	-1.340	-1.334	0.290	0.287	-0.054	-0.045
1.9	-0.843	-0.835	-1.320	-1.311	-0.853	-0.848	-0.078	-0.082	-0.423	0.423
2.0	-0.072	-0.068	-0.902	-0.890	-0.415	-0.415	-0.420	-0.421	-0.531	0.524

TABLE 4.6 (Continued)

t/T ₀	$\frac{w}{p_0 R^2 / AE}$				$\frac{N}{p_0 R}$		$\frac{M}{p_0 R r}$			
	1/4-point		crown		crown		1/4-point		crown	
	Numerical Method	Modal Method	Numerical Method	Modal Method	Numerical Method	Modal Method	Numerical Method	Modal Method	Numerical Method	Modal Method
2.1	0.248	0.246	-0.477	-0.466	-0.136	-0.134	-0.459	-0.453	0.392	0.385
2.2	-0.006	-0.014	-0.233	-0.226	-0.127	-0.128	-0.140	-0.131	0.152	0.146
2.3	-0.667	-0.675	-0.253	-0.253	-0.419	-0.421	0.237	0.240	-0.173	-0.177
2.4	-1.466	-1.473	-0.547	-0.554	-0.894	-0.902	0.469	0.467	-0.493	-0.493
2.5	-2.161	-2.164	-1.075	-1.088	-1.446	-1.454	0.561	0.557	-0.603	-0.597
2.6	-2.541	-2.539	-1.678	-1.692	-1.820	-1.821	0.516	0.511	-0.435	-0.425
2.7	-2.497	-2.490	-2.124	-2.134	-1.912	-1.909	0.389	0.386	-0.137	-0.129
2.8	-2.042	-2.031	-2.248	-2.251	-1.677	-1.668	0.249	0.248	0.123	0.126
2.9	-1.280	-1.267	-2.044	-2.043	-1.184	-1.179	0.050	0.045	0.238	0.235
3.0	-0.438	-0.426	-1.698	-1.697	-0.647	-0.642	-0.190	-0.193	0.222	0.218

TABLE 4.7 EFFECT OF LOAD DURATION ON MAXIMUM VALUES OF RESPONSE AND TIMES OF OCCURRENCE
Two-Hinged Uniform Circular Arch; Uniform All-Around Triangular Pressure Pulse With Initial Peak

$$f/L_0 = 0.2, L_0/r = 100, p_0/p_{cr} = 1.0, z = 12, \Delta t/T_0 = 0.01$$

Joint or Bar j	$\frac{w}{p_0 R^2/AE}$	$\frac{t}{T_0}$	$\frac{N}{p_0 R}$	$\frac{t}{T_0}$	$\frac{M}{p_0 Rr}$	$\frac{t}{T_0}$	$\frac{\sigma}{p_0 R/A}$	$\frac{t}{T_0}$	$\frac{\sigma}{p_0 R/A}$	$\frac{t}{T_0}$
							$c/r = 1$	$c/r = \sqrt{3}$		
(a) $t_d/T_0 = 0.25$										
1	(0.623)	3.00	-0.675	0.34	-0.480	1.41	1.038	1.93	1.374	1.92
2	(1.069)	3.00	-0.670	0.34	-0.447	2.98	(1.083)	3.00	1.406	2.99
3	-1.296	1.42	-0.669	0.33	0.700	1.43	-1.196	1.42	-1.707	1.42
4	1.127	1.91	-0.672	0.34	-0.552	1.87	1.051	1.90	1.445	1.89
5	-0.791	2.54	-0.674	0.34	-0.342	1.47	-0.831	1.44	-1.078	1.45
6	-0.820	2.61	-0.672	0.35	-0.757	1.47	-1.248	1.44	-1.799	1.45
(b) $t_d/T_0 = 0.5$										
1	(0.958)	3.00	-1.128	0.42	0.783	1.95	1.725	2.00	2.277	1.99
2	(1.587)	3.00	-1.119	0.42	(-0.655)	3.00	-1.513	0.40	(1.972)	3.00
3	-2.195	1.51	-1.111	0.42	1.150	1.51	-1.975	1.50	-2.815	1.50
4	1.818	2.00	-1.110	0.42	0.795	1.55	1.607	1.99	-2.181	1.53
5	-1.444	2.63	-1.112	0.41	-0.597	1.52	-1.437	1.51	-1.873	1.51
6	-1.534	2.69	-1.110	0.41	-1.320	1.56	-2.149	1.53	-3.110	1.54
(c) $t_d/T_0 = 0.75$										
1	-0.880	0.37	-1.360	0.46	0.853	2.01	1.887	2.06	2.486	2.05
2	-1.612	1.59	-1.347	0.46	(-0.658)	3.00	-1.778	0.43	-2.112	0.42
3	-2.390	1.57	-1.337	0.45	1.183	1.56	-2.106	1.57	-2.972	1.57
4	1.930	2.07	-1.336	0.45	0.841	1.59	-1.764	1.58	-2.378	1.58
5	-1.682	2.71	-1.332	0.45	-0.629	1.57	-1.578	1.56	-2.038	1.57
6	-1.816	2.75	-1.326	0.45	-1.472	1.61	-2.415	1.59	-3.489	1.60

Values in parentheses do not represent a true maximum. They are the largest computed values for interval investigated.

TABLE 4.7 (Continued)

Joint or Bar j	$\frac{w}{p_o R^2/AE}$	$\frac{t}{T_o}$	$\frac{N}{p_o R}$	$\frac{t}{T_o}$	$\frac{M}{p_o Rr}$	$\frac{t}{T_o}$	$\frac{\sigma}{p_o R/A}$	$\frac{t}{T_o}$	$\frac{\phi}{p_o R/A}$	$\frac{t}{T_o}$
							$c/r = 1$		$c/r = \sqrt{3}$	
	(d) $t_d/T_o = 1$									
1	-0.953	0.39	-1.492	0.48	0.749	2.02	1.607	2.09	2.116	2.08
2	-1.720	0.44	-1.480	0.48	(-0.572)	3.00	-1.929	0.44	-2.281	0.43
3	-2.062	0.50	-1.466	0.47	1.018	1.58	-1.932	0.51	-2.559	1.59
4	-1.935	0.54	-1.463	0.47	0.735	1.60	-1.580	0.57	-2.077	1.60
5	-1.679	0.48	-1.461	0.47	-0.534	1.59	-1.601	0.49	-1.744	1.60
6	-1.645	0.46	-1.455	0.48	-1.277	1.63	-2.109	1.62	-3.043	1.62
	(e) $t_d/T_o = 1.5$									
1	-1.033	0.41	-1.636	0.49	0.813	2.04	-1.736	0.43	2.185	2.07
2	-1.876	0.46	-1.623	0.49	0.532	0.40	-2.093	0.46	-2.463	0.44
3	-2.272	0.52	-1.608	0.49	0.920	1.59	-2.121	0.53	-2.517	0.54
4	-2.157	0.56	-1.602	0.49	0.799	1.62	-1.782	0.59	-2.085	0.64
5	-1.846	0.51	-1.603	0.49	0.451	1.11	-1.765	0.51	-1.889	0.52
6	-1.795	0.48	-1.601	0.50	-1.150	1.64	-1.843	1.62	-2.680	1.63
	(f) $t_d/T_o = 4$									
1	-1.145	0.43	-1.833	0.52	0.831	2.13	-2.164	1.63	-2.745	1.63
2	-2.091	0.48	-1.819	0.52	0.574	0.42	-2.320	0.48	-2.715	0.47
3	-2.564	0.55	-1.804	0.52	0.957	1.64	-2.381	0.55	-2.984	1.63
4	-2.576	1.64	-1.800	0.52	0.952	1.67	-2.253	1.65	-2.945	1.66
5	-2.079	0.54	-1.801	0.52	0.464	1.14	-1.989	0.54	-2.129	0.54
6	-1.999	0.50	-1.802	0.52	-1.117	1.69	-2.426	1.67	-3.239	1.67

TABLE 4.8 COMPARISON OF APPROXIMATE AND EXACT MAXIMUM STRESSES
 Two-Hinged Uniform Circular Arch; Uniform All-Around Triangular Pressure Pulse With Initial Peak
 $f/L_0 = 0.2$, $L_0/r = 100$, $p_0/p_{cr} = 1.0$, $z = 12$

$\frac{t_d}{T_0}$	Location	$c/r = 1$					$c/r = \sqrt{3}$				
		$\frac{\sigma_{max}}{p_0 R/A}$	$\frac{\sigma_{max}}{p_0 R/A}$ Eq. (a)	% Error	$\frac{\sigma_{max}}{p_0 R/A}$ Eq. (b)	% Error	$\frac{\sigma_{max}}{p_0 R/A}$	$\frac{\sigma_{max}}{p_0 R/A}$ Eq. (a)	% Error	$\frac{\sigma_{max}}{p_0 R/A}$ Eq. (b)	% Error
0.25	1/4 point crown	-1.196	1.372	14.7	0.970	-18.9	-1.707	1.884	10.3	1.386	-18.8
		-1.248	1.429	14.5	1.012	-18.9	-1.799	1.983	10.2	1.473	-18.1
0.50	1/4 point crown	-1.975	2.260	14.4	1.598	-19.1	-2.815	3.102	10.2	2.280	-19.0
		-2.149	2.430	13.1	1.725	-19.7	-3.110	3.396	9.2	2.542	-18.3
0.75	1/4 point crown	-2.106	2.509	19.1	1.777	-15.6	-2.972	3.375	13.6	2.441	-17.9
		-2.415	2.798	15.9	1.981	-18.0	-3.489	3.386	11.1	2.874	-17.6
1.00	1/4 point crown	-1.932	2.473	28.0	1.776	-8.1	-2.559	3.218	25.8	2.502	-2.2
		-2.109	2.732	29.5	1.936	-8.2	-3.043	3.667	20.5	2.647	-13.0
1.50	1/4 point crown	-2.121	2.521	18.9	1.847	-12.9	-2.517	3.194	26.9	2.259	-10.3
		-1.843	2.751	49.3	1.971	6.9	-2.680	3.593	34.1	2.556	-4.6
2.00	1/4 point crown	-2.222	2.613	17.6	1.921	-13.5	-2.631	3.295	25.2	2.330	-11.4
		-2.070	2.816	36.0	2.028	-2.0	-2.883	3.639	26.2	2.581	-10.5
4.00	1/4 point crown	-2.381	2.759	15.9	2.040	-14.3	-2.984	3.460	16.0	2.448	-18.0
		-2.426	2.919	20.3	2.120	-12.6	-3.239	3.737	15.4	2.644	-18.4

TABLE 4.9 EFFECTS OF PEAK PRESSURE AND INITIAL OUT-OF-ROUNDNESS
ON MAXIMUM VALUES OF RESPONSE

Two-Hinged Circular Arch; Uniform All-Around
Triangular Pressure Pulse With Initial Peak

$$f/L_0 = 0.2, L_0/r = 100, t_a/T_0 = 2.0, z = 12$$

Quantity	Joint or Bar j	$p_0/p_{cr} = 0.5$	$p_0/p_{cr} = 1$		$p_0/p_{cr} = 2$	
		$\bar{w}_m/L_0 = 0$	$\bar{w}_m/L_0 = 0$	$\bar{w}_m/L_0 = 0.001$	$\bar{w}_m/L_0 = 0$	$\bar{w}_m/L_0 = 0.001$
$\frac{w_j}{p_0 R^2/AE}$	1	-1.040	-1.076	-1.136	-1.235	-1.508
	2	-1.892	-1.959	-2.003	-2.131	-2.337
	3	-2.323	-2.385	-2.613	-2.535	-2.913
	4	-2.270	-2.278	-2.469	-2.277	-2.720
	5	-1.948	-1.936	-1.971	-1.917	-1.950
	6	-1.873	-1.875	-1.874	-1.881	-1.881
$\frac{N_j}{p_0 R}$	1	-1.698	-1.713	-1.726	-1.743	-1.756
	2	-1.685	-1.699	-1.713	-1.729	-1.742
	3	-1.669	-1.684	-1.696	-1.714	-1.725
	4	-1.664	-1.678	-1.687	-1.707	-1.716
	5	-1.666	-1.679	-1.685	-1.703	-1.708
	6	-1.668	-1.679	-1.681	-1.699	-1.700
$\frac{M_j}{p_0 Rr}$	1	0.743	0.763	0.832	0.957	1.018
	2	0.539	0.586	0.667	0.832	0.936
	3	-0.893	0.934	1.060	1.123	1.278
	4	0.777	0.857	0.967	1.005	1.148
	5	0.525	0.457	0.495	-0.454	-0.528
	6	1.065	-1.137	-1.135	-1.329	-1.326
$\frac{\sigma_j}{p_0 R/A}$ c/r = 1	1	-1.780	-1.814	-1.832	-1.896	-1.914
	2	-2.128	-2.181	-2.205	-2.310	-2.337
	3	-2.181	-2.222	-2.250	-2.317	-2.349
	4	-1.894	-1.891	-1.917	-1.852	-1.968
	5	-1.822	-1.852	-1.855	-1.921	-1.925
	6	-1.993	-2.070	-2.066	-2.167	-2.164
$\frac{\sigma_j}{p_0 R/A}$ c/r = $\sqrt{3}$	1	2.336*	-2.212	-2.336	-2.449	-2.593
	2	-2.620	-2.561	-2.592	-2.751	-2.786
	3	-2.711	-2.631	-2.783	-2.794	-3.058
	4	-2.527	-2.406	-2.599	-2.553	-2.807
	5	-1.979	-1.979	-1.991	-2.095	-2.107
	6	-3.003	-2.883	-2.890	-3.139	-3.134

* Stress values in this column are for c/r = 2.

TABLE 4.10 EFFECT OF ARCH DIMENSIONS ON MAXIMUM VALUES OF RESPONSE AND TIMES OF OCCURRENCE
Two-Hinged Uniform Circular Arch; Uniform All-Around Triangular Pressure Pulse With Initial Peak

$$p_o/p_{cr} = 1.0, t_d/T_o = 2.0, z = -12$$

Joint or Bar j	$\frac{w}{p_o R^2/AE}$		$\frac{N}{p_o R}$		$\frac{M}{p_o Rr}$		$\frac{\sigma}{p_o R/A}$ c/r = 1		$\frac{\sigma}{p_o R/A}$ c/r = $\sqrt{3}$	
	$\frac{t}{T_o}$	$\frac{t}{T_o}$	$\frac{t}{T_o}$	$\frac{t}{T_o}$	$\frac{t}{T_o}$	$\frac{t}{T_o}$	$\frac{t}{T_o}$	$\frac{t}{T_o}$	$\frac{t}{T_o}$	$\frac{t}{T_o}$
(a) $f/L_o = 0.2, L_o/r = 50, \Delta t/T_o = 0.01$										
1	-1.234	1.45	-1.730	0.54	1.166	1.45	-1.780	0.54	-2.270	1.47
2	-1.791	1.45	-1.712	0.54	1.646	1.44	-2.133	0.50	-3.077	1.45
3	-2.209	0.49	-1.695	0.55	1.138	1.44	-2.296	0.48	-2.788	0.47
4	-2.452	0.55	-1.686	0.55	0.403	0.44	-2.042	0.53	-2.312	0.50
5	-2.673	0.64	-1.684	0.55	1.091	1.94	-1.948	0.65	2.314	1.94
6	-2.841	0.69	-1.687	0.54	1.569	1.94	-2.041	0.68	3.163	1.94
(b) $f/L_o = 0.2, L_o/r = 200, \Delta t/T_o = 0.01$										
1	-1.453	0.43	-1.736	0.49	-0.891	2.73	-2.044	0.45	-2.316	0.43
2	-2.169	0.51	-1.726	0.49	0.749	2.72	-2.126	0.52	-2.438	0.54
3	-2.064	0.53	-1.717	0.49	0.622	2.70	-1.720	0.52	-1.819	2.66
4	-1.916	0.50	-1.710	0.49	0.893	2.23	-1.763	0.51	-2.338	1.63
5	-1.909	0.50	-1.705	0.50	0.269	1.39	-1.710	0.50	-1.715	0.50
6	-2.443	1.63	-1.703	0.50	1.185	1.73	-1.898	1.64	-2.687	1.67
(c) $f/L_o = 0.1, L_o/r = 100, \Delta t/T_o = 0.004$										
1	-1.160	1.42	-1.734	0.54	1.225	1.41	-1.817	0.54	-2.280	1.43
2	-1.670	0.48	-1.731	0.55	1.665	1.40	-2.149	0.49	-2.964	1.41
3	-2.226	0.50	-1.729	0.55	1.091	1.41	-2.291	0.48	-2.764	0.46
4	-2.529	0.56	-1.729	0.55	0.393	0.43	-2.100	0.55	-2.372	0.54
5	-2.823	0.66	-1.729	0.55	1.198	1.89	-2.059	0.66	-2.478	0.70
6	-3.013	0.70	-1.731	0.55	1.701	1.88	-2.171	0.70	3.105	1.88

TABLE 4.10 (Continued)

Joint or Bar j	$\frac{w}{p_o R^2/AE}$		$\frac{N}{p_o R}$		$\frac{M}{p_o Rr}$		$\frac{\sigma}{p_o R/A}$		$\frac{\sigma}{p_o R/A}$	
		$\frac{t}{T_o}$		$\frac{t}{T_o}$		$\frac{t}{T_o}$	$c/r = 1$	$\frac{t}{T_o}$	$c/r = \sqrt{3}$	$\frac{t}{T_o}$
	(d) $f/L_o = 0.5, L_o/r = 100, \Delta t/T_o = 0.02$									
1	-1.686	0.46	-1.799	0.50	0.605	2.48	-2.148	0.48	-2.434	0.46
2	-2.127	0.52	-1.755	0.50	0.539	2.80	-1.931	0.52	-2.090	0.54
3	-1.926	0.50	-1.718	0.48	-0.802	2.74	-1.739	0.50	-2.068	2.68
4	-1.863	1.52	-1.682	0.50	-0.461	2.12	-1.692	0.50	-1.823	1.52
5	-1.838	0.50	-1.659	0.50	0.538	2.86	-1.664	0.50	-1.669	0.50
6	-1.833	0.50	-1.656	0.50	0.759	2.28	-1.663	0.50	1.857	2.18

TABLE C.1 SYMMETRICAL MODES OF VIBRATION FOR A TWO-HINGED UNIFORM CIRCULAR ARCH AND PARTICIPATION FACTORS FOR MODAL SOLUTION

$$f/L_0 = 0.2, L_0/r = 100, z = 12$$

	r = 1		r = 2		r = 3		r = 4	
T_r/T_0	2.225		1.066		0.784		0.465	
j	\bar{w}_j	\bar{v}_j	\bar{w}_j	\bar{v}_j	\bar{w}_j	\bar{v}_j	\bar{w}_j	\bar{v}_j
1	-1.179	0.096	-0.630	-0.134	-2.212	0.084	-2.098	0.133
2	-1.520	0.288	-1.643	-0.162	-1.415	0.257	1.041	0.188
3	-0.750	0.453	-2.299	-0.080	1.077	0.210	1.479	-0.004
4	0.750	0.470	-2.004	0.026	1.467	-0.028	-1.913	-0.004
5	2.176	0.300	-1.134	0.056	-0.854	-0.141	-0.614	0.134
6	2.757	0.000	-0.672	0.000	-2.404	0.000	2.092	0.000
$\frac{c(r)}{p_0 R^2/AE}$	-0.3027		0.6528		0.1377		0.0164	

	r = 5		r = 6		r = 7		r = 8	
T_r/T_0	0.342		0.297		0.240		0.126	
j	\bar{w}_j	\bar{v}_j	\bar{w}_j	\bar{v}_j	\bar{w}_j	\bar{v}_j	\bar{w}_j	\bar{v}_j
1	-1.517	0.114	0.551	-0.048	-0.512	-1.070	0.132	1.865
2	2.152	0.071	-1.078	-0.015	-0.197	-1.826	-0.126	1.853
3	-1.540	0.019	1.528	0.045	-0.015	-2.101	-0.241	-0.007
4	-0.017	0.108	-1.862	-0.014	0.261	-1.815	-0.120	-1.860
5	1.500	-0.019	2.094	-0.018	0.432	-1.047	0.121	-1.857
6	-2.182	0.000	-2.149	0.000	0.505	0.000	0.242	0.000
$\frac{c(r)}{p_0 R^2/AE}$	0.0043		-0.0010		-0.00091		0.00013	

	r = 9		r = 10		r = 11	
T_r/T_0	0.090		0.073		0.066	
j	\bar{w}_j	\bar{v}_j	\bar{w}_j	\bar{v}_j	\bar{w}_j	\bar{v}_j
1	-0.005	-2.154	-0.040	1.865	-0.034	1.077
2	0.144	0.006	-0.043	-1.870	0.020	-1.868
3	0.000	2.154	0.085	0.003	0.000	2.158
4	-0.143	-0.003	-0.043	1.867	-0.020	-1.869
5	0.000	-2.154	-0.042	-1.868	0.035	1.079
6	0.143	0.000	0.085	0.000	-0.040	0.000
$\frac{c(r)}{p_0 R^2/AE}$	-0.000039		0.000015		0.000006	

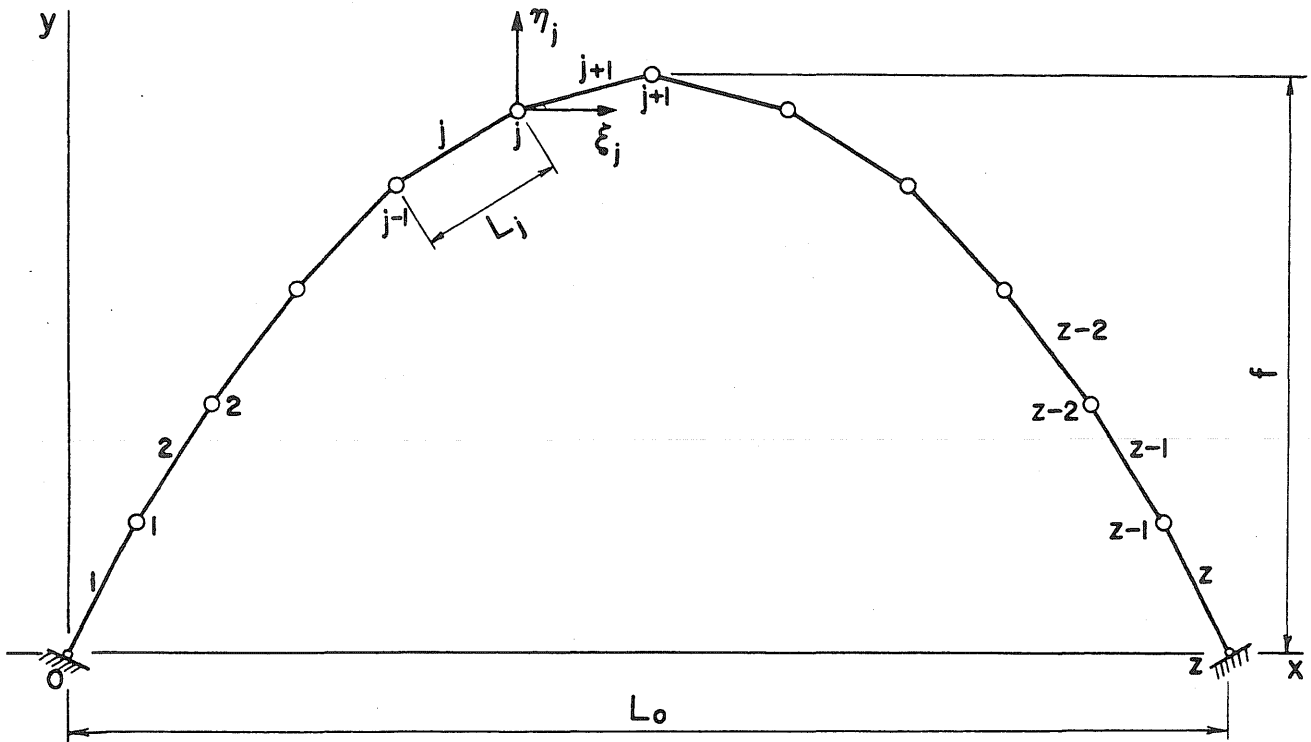


FIG. 2.1 MODEL CONSIDERED IN ANALYSIS

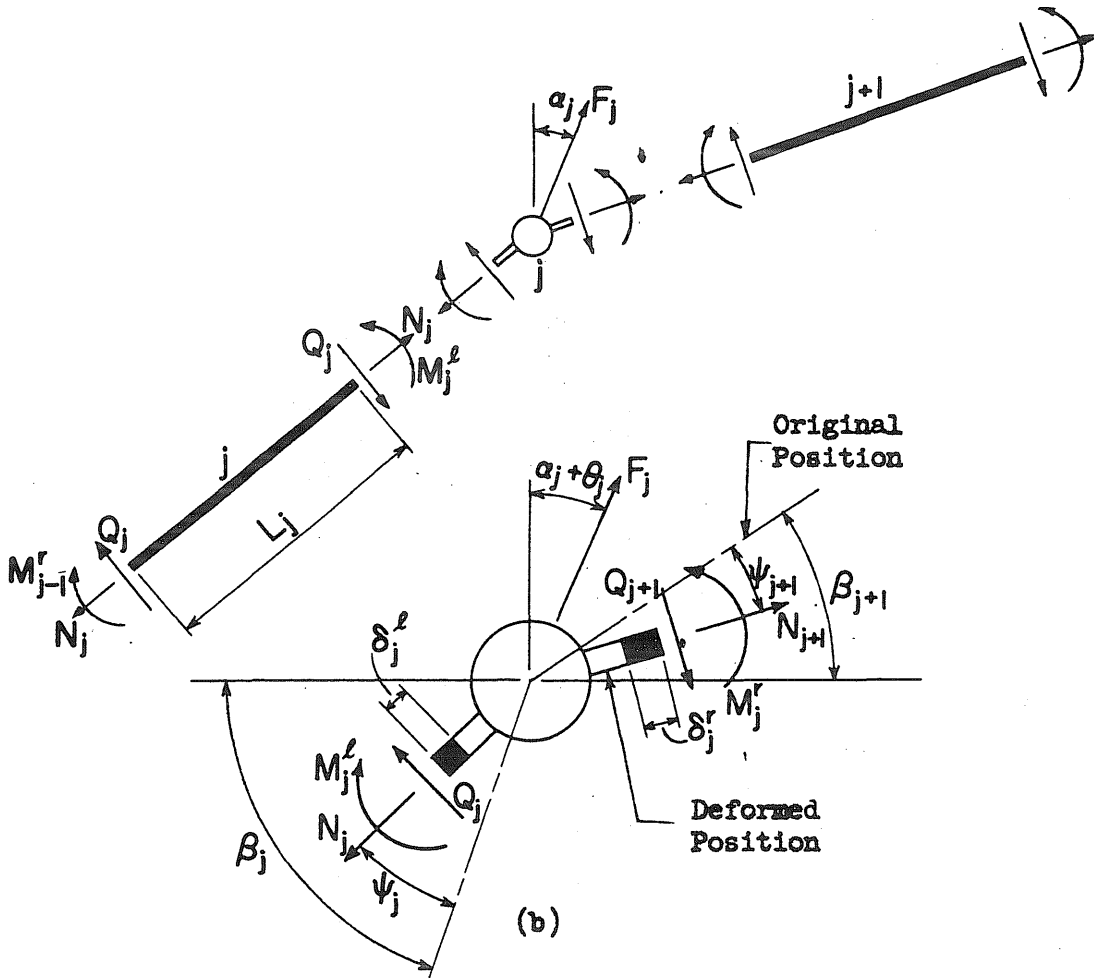


FIG. 2.2 FREE BODY DIAGRAMS FOR A TYPICAL BAR AND JOINT

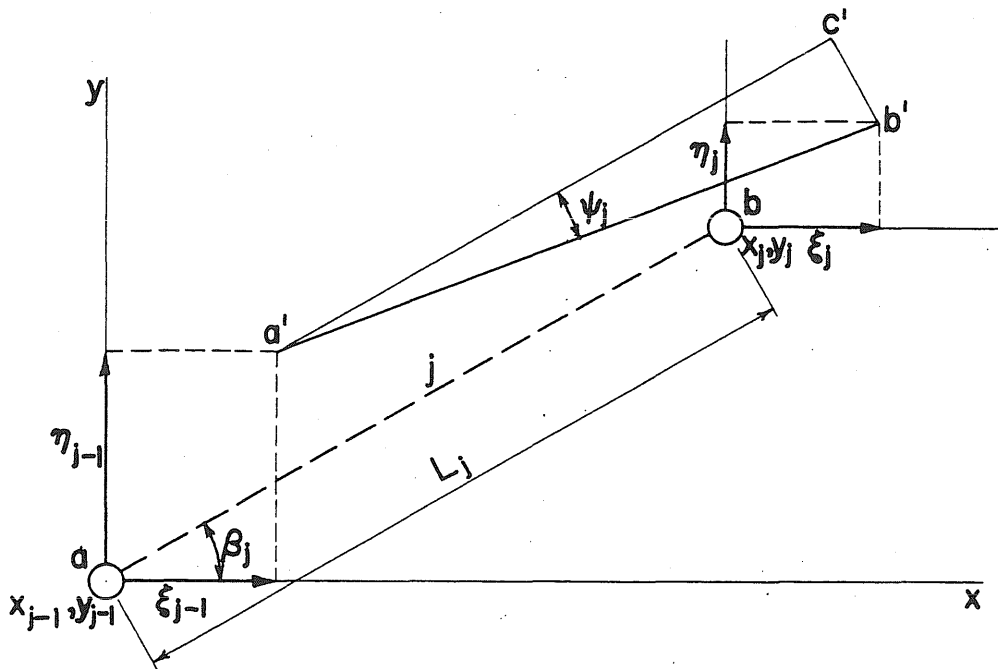


FIG. 2.3 DIAGRAM USED IN DETERMINING DISPLACEMENT-DEFORMATION RELATIONSHIPS

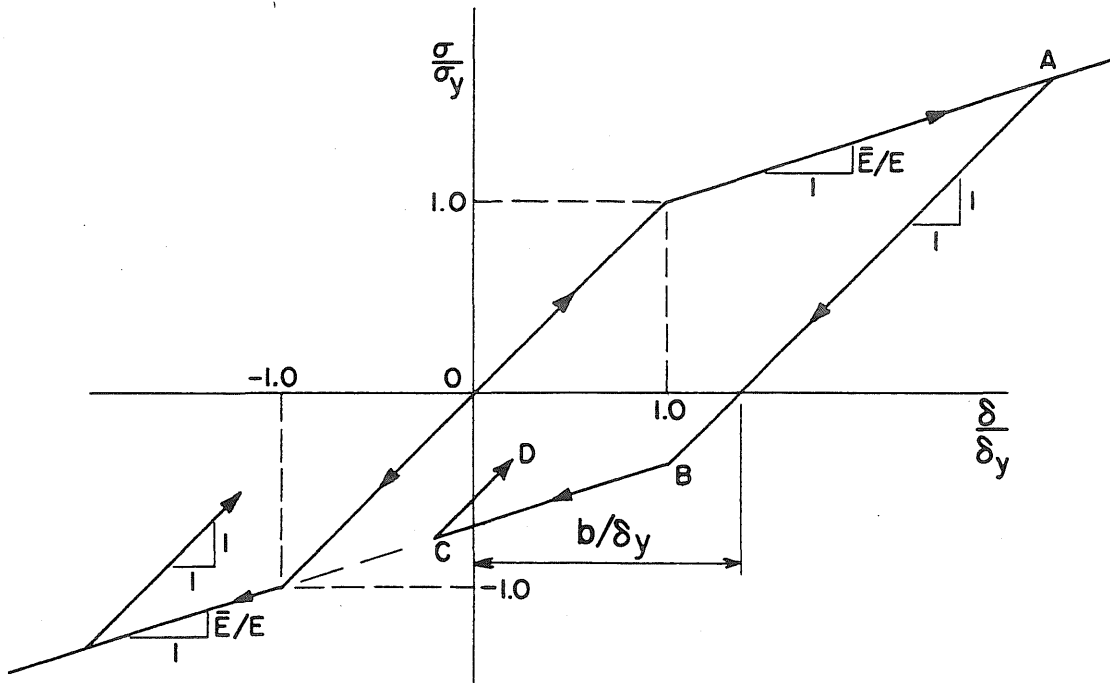


FIG. 2.4 BILINEAR STRESS-DEFORMATION RELATIONSHIP

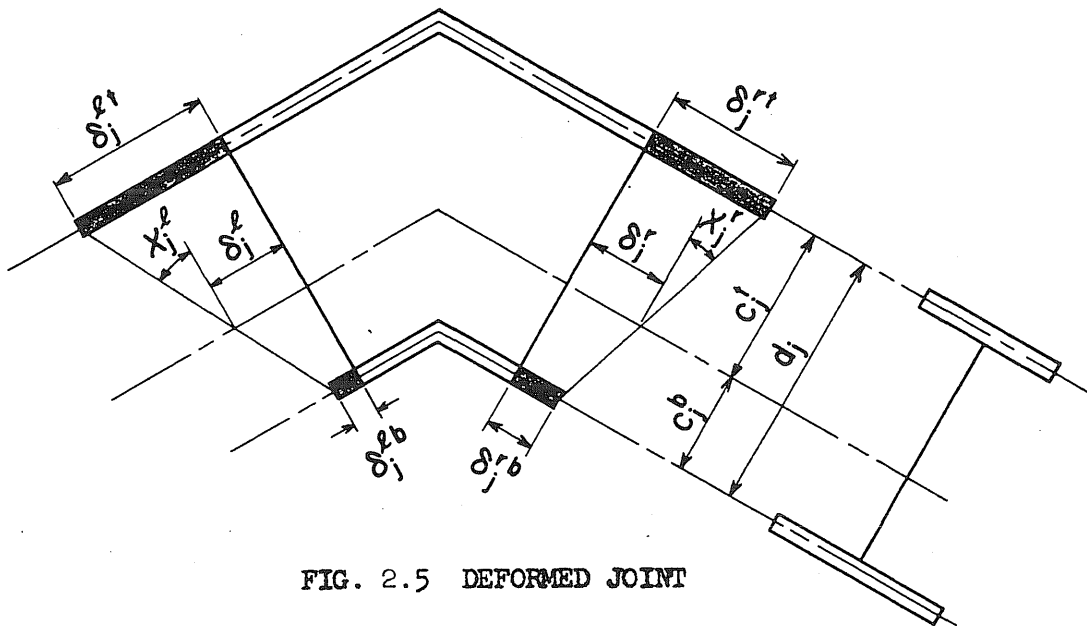


FIG. 2.5 DEFORMED JOINT

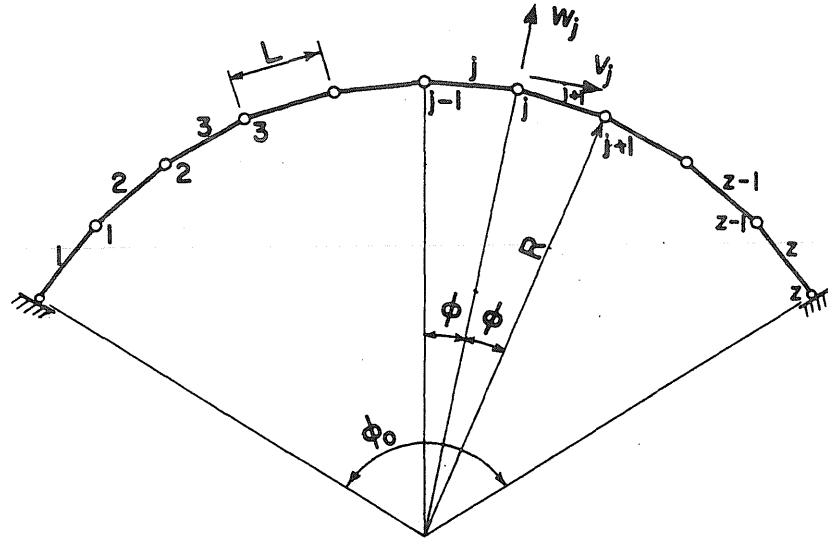


FIG. 3.1 COORDINATE SYSTEM FOR CIRCULAR ARCH MODEL

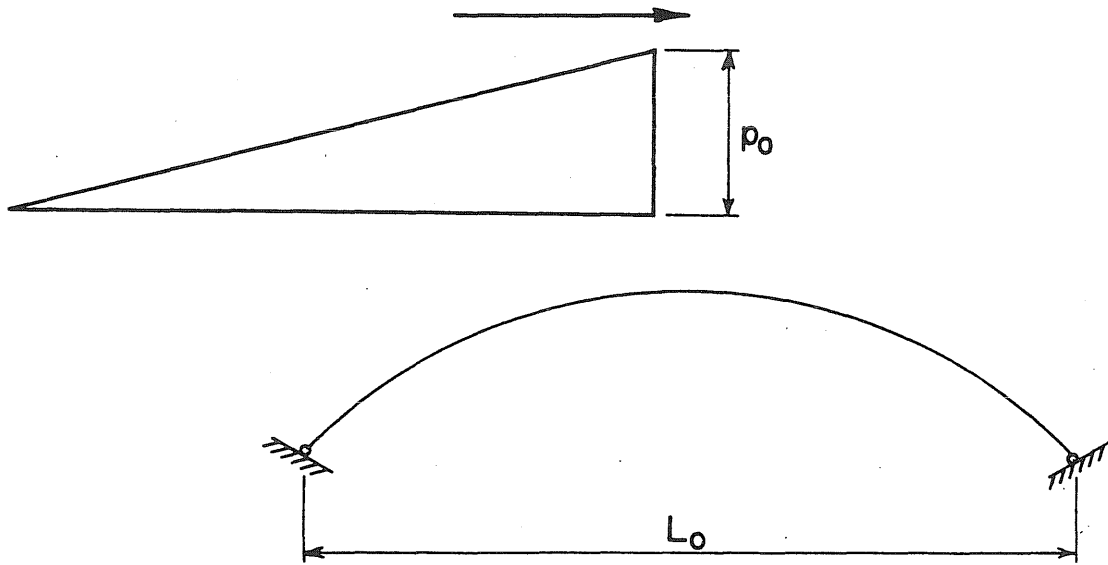


FIG. 3.2 TRIANGULAR-SHAPED MOVING PRESSURE PULSE

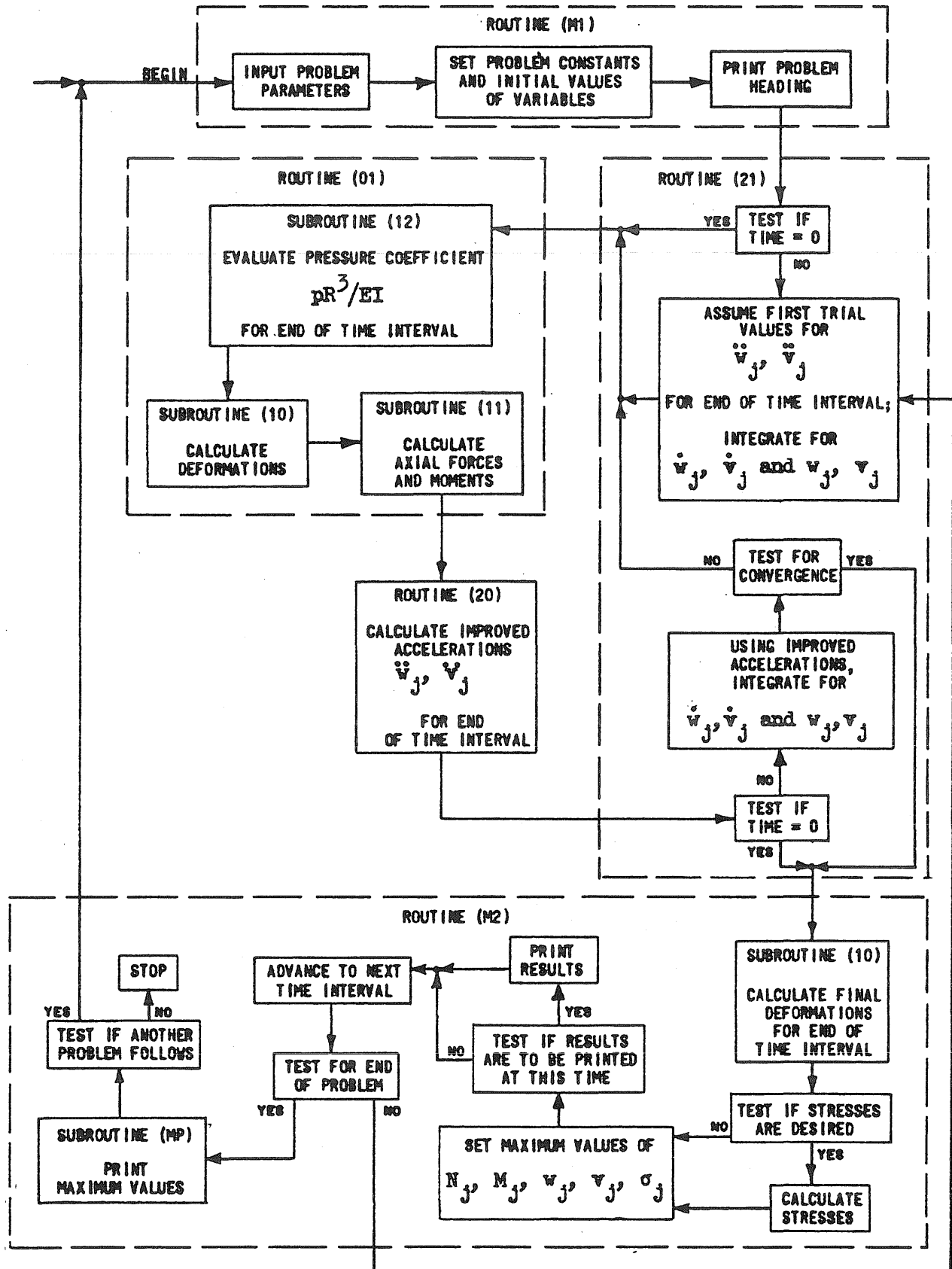


FIG. 3.3 FLOW DIAGRAM OF COMPUTER PROGRAM FOR CIRCULAR ARCH SUBJECTED TO A UNIFORM ALL-AROUND PRESSURE

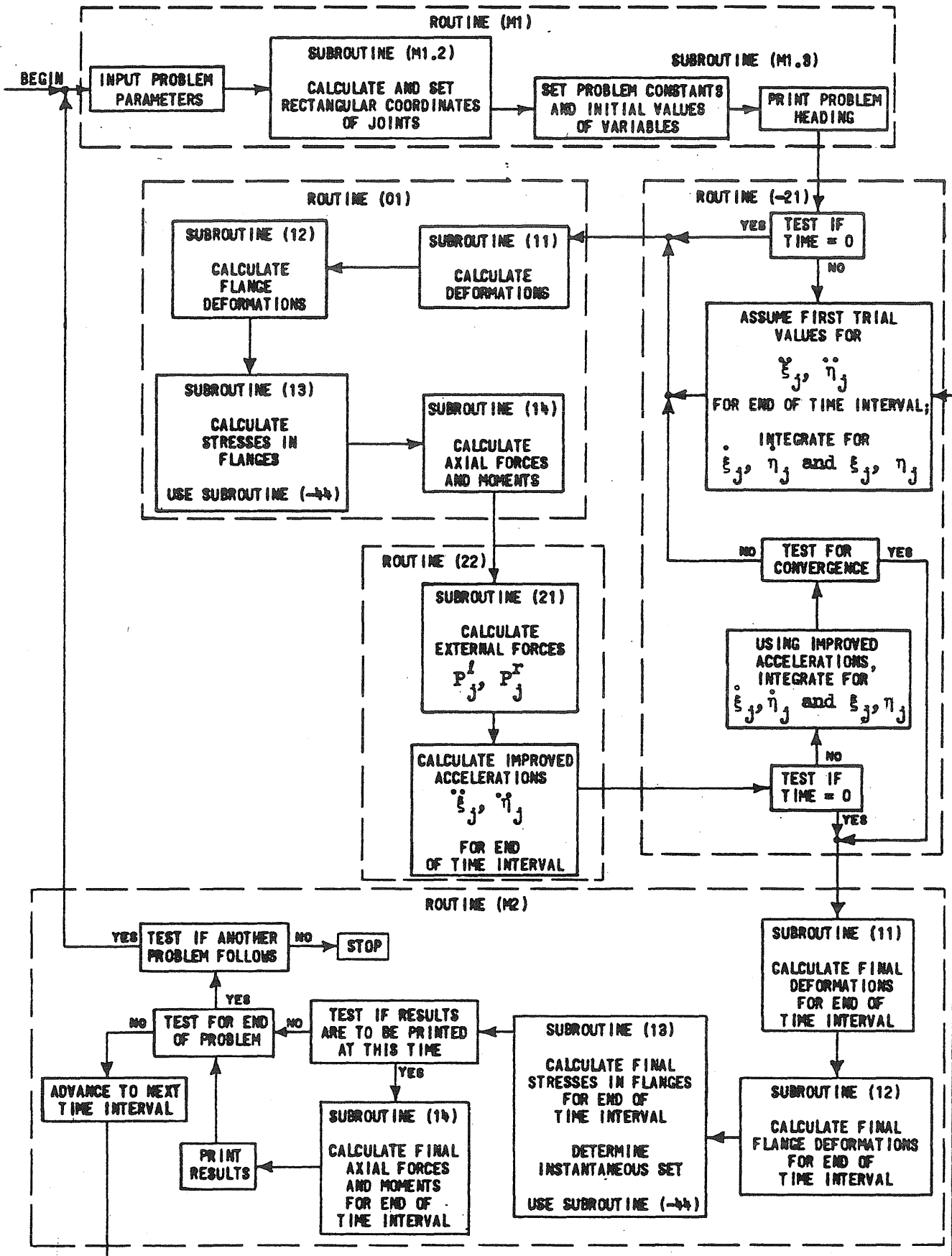


FIG. 3.4 FLOW DIAGRAM OF COMPUTER PROGRAM FOR ARCH SUBJECTED TO A TRIANGULAR MOVING PRESSURE

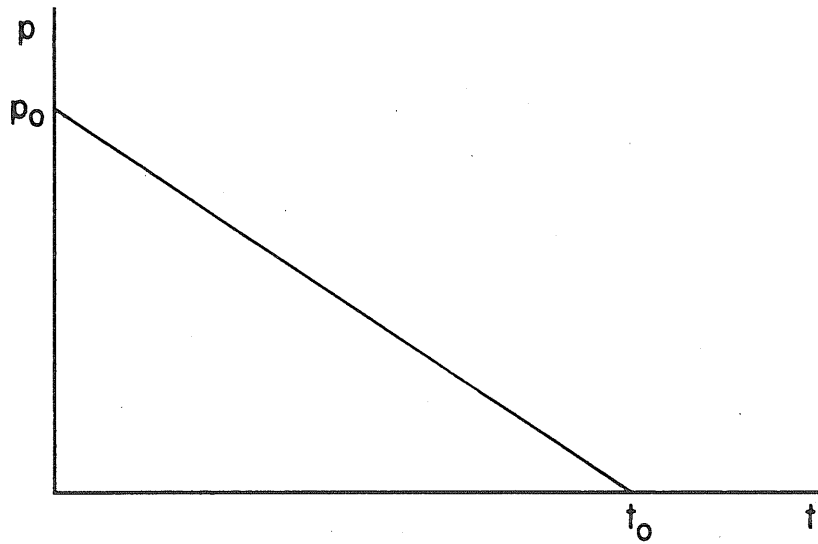
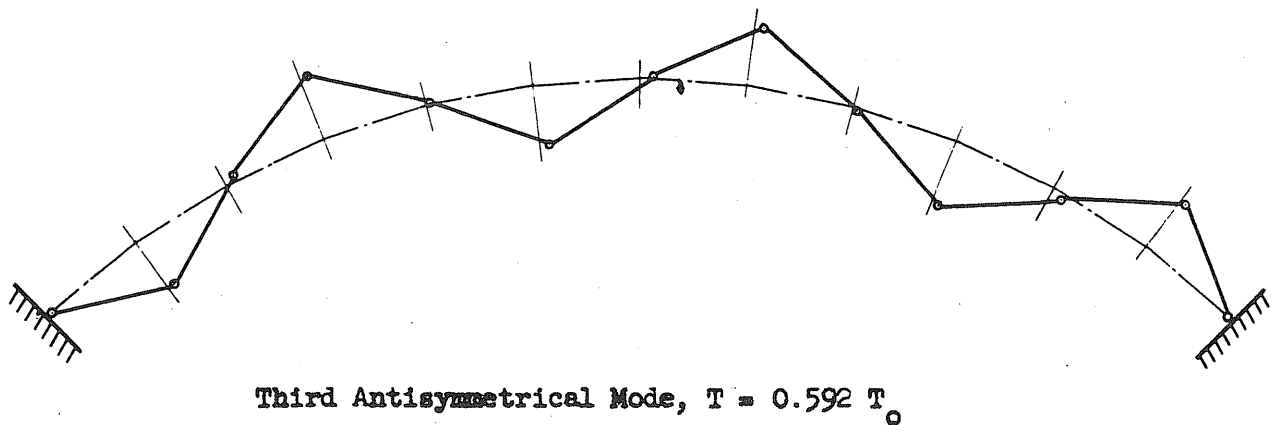
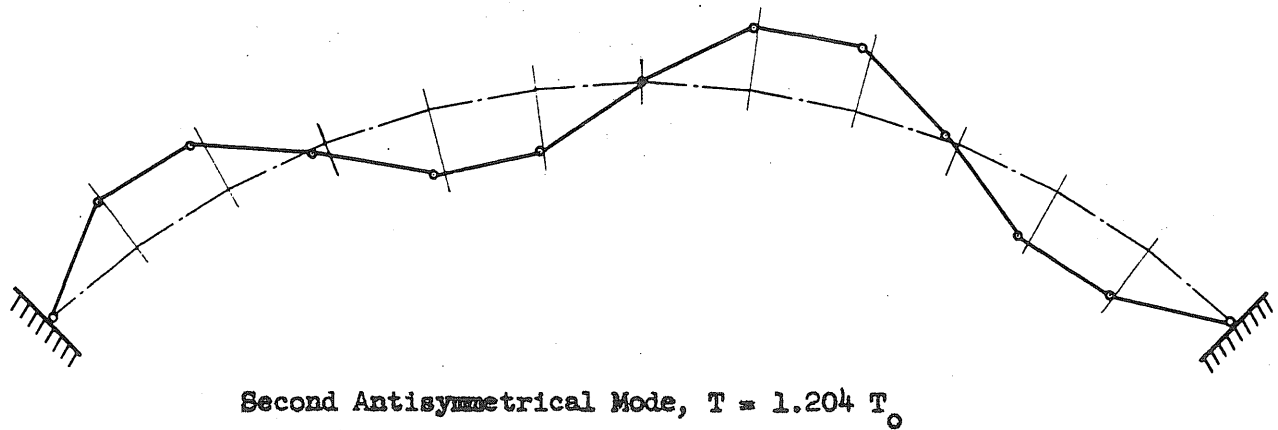
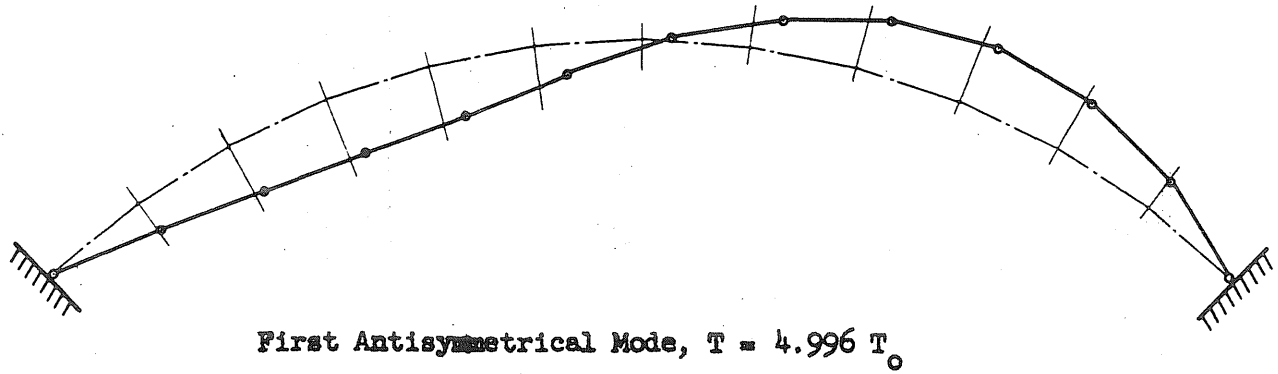
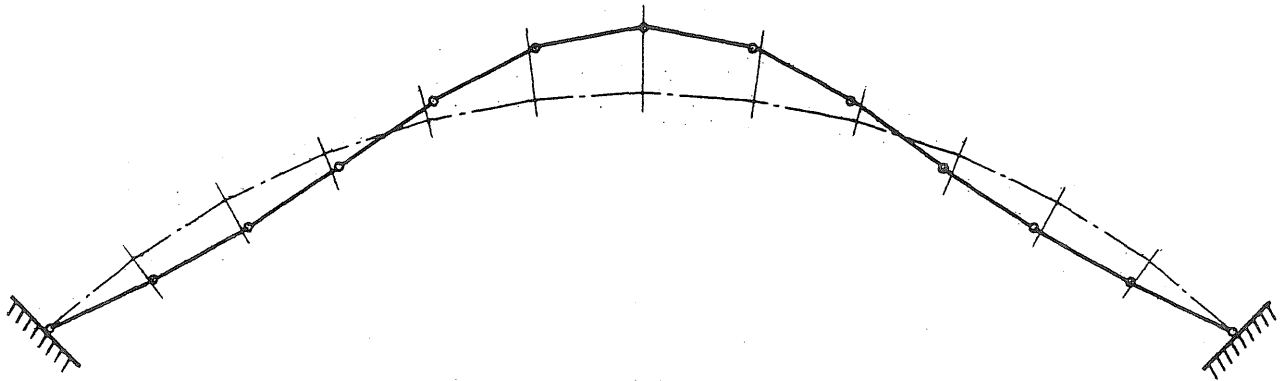


FIG. 4.1 TRIANGULAR PRESSURE PULSE WITH INITIAL PEAK

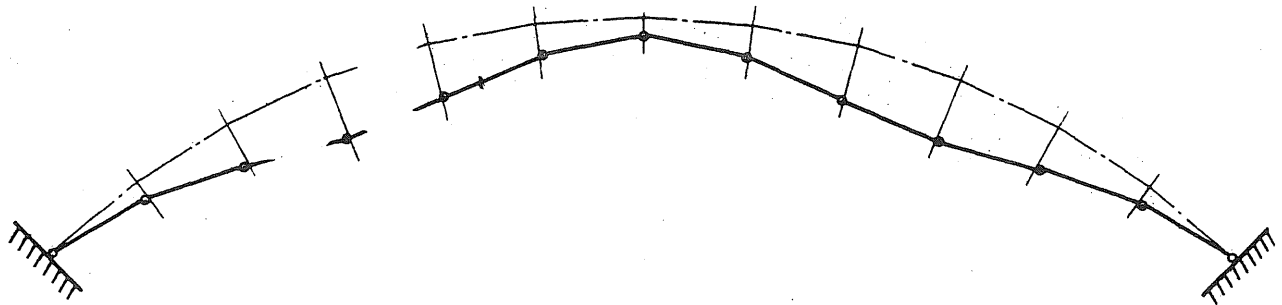


(a) Antisymmetrical Modes

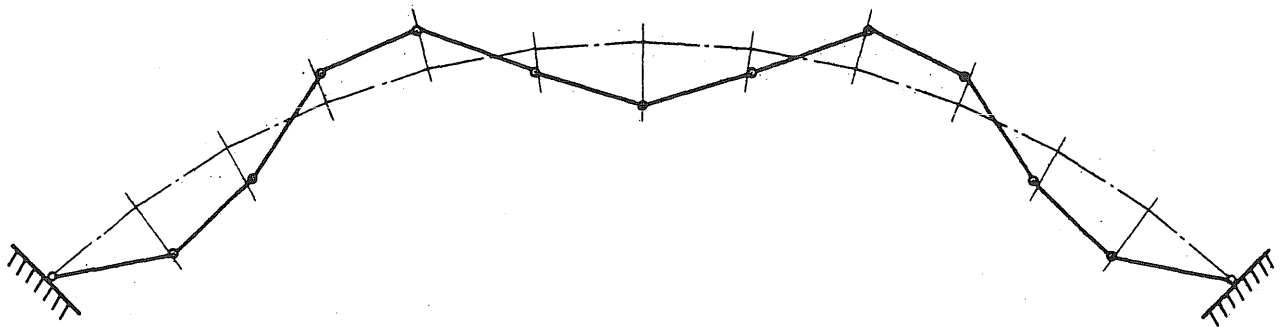
FIG. 4.2 NATURAL MODES OF VIBRATION FOR A TWO-HINGED UNIFORM CIRCULAR ARCH
 $f/L_0 = 0.2$, $L_0/r = 100$, $z = 12$



First Symmetrical Mode, $T = 2.225 T_0$



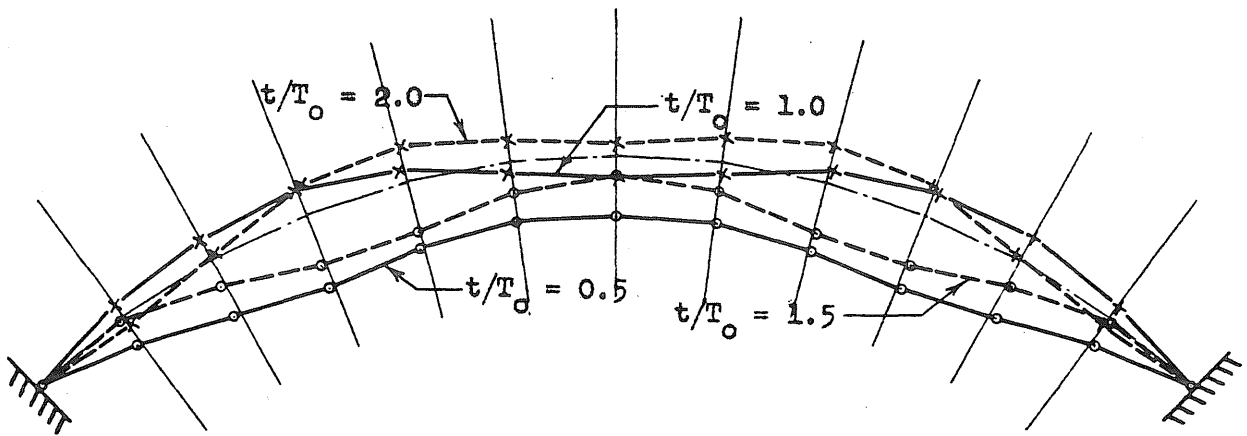
Second Symmetrical Mode, $T = 1.066 T_0$



Third Symmetrical Mode, $T = 0.784 T_0$

(b) Symmetrical Modes

FIG. 4.2 (Continued)



(a) Displacement Configurations

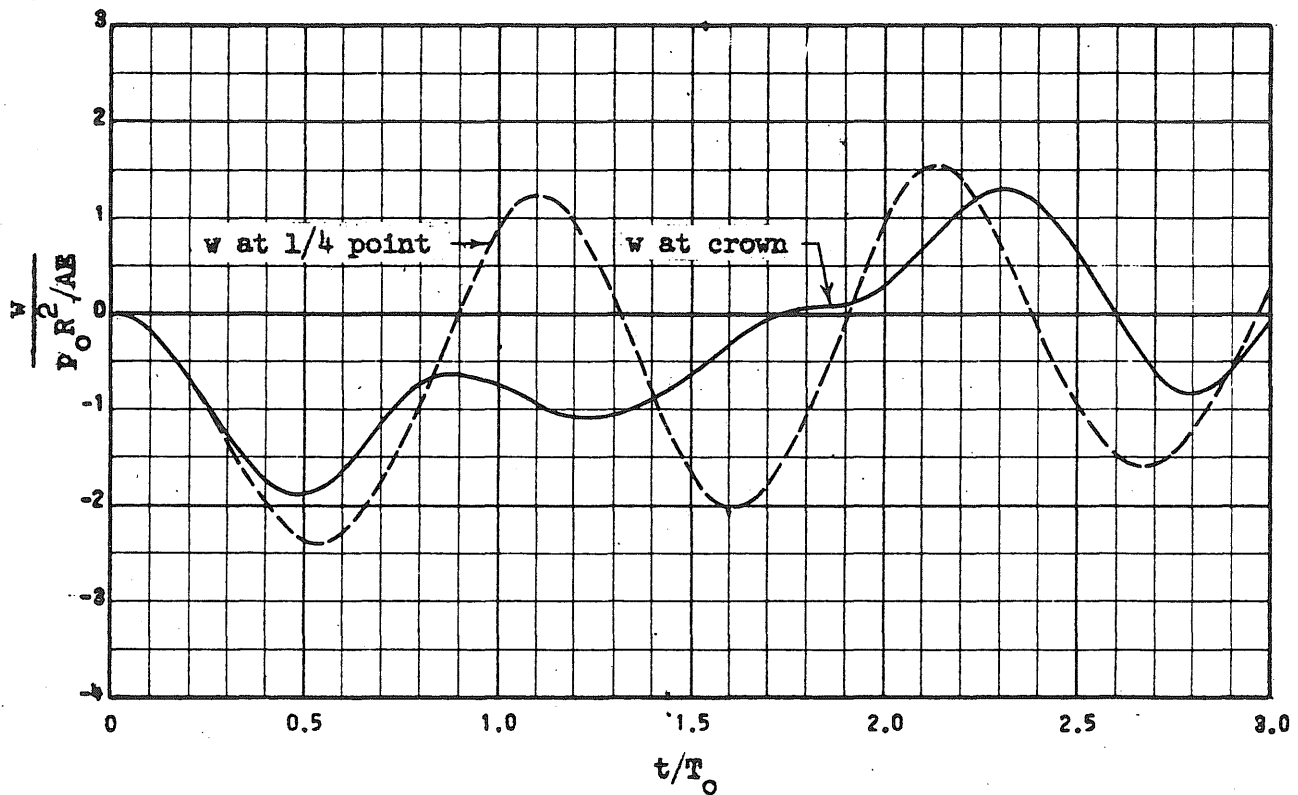
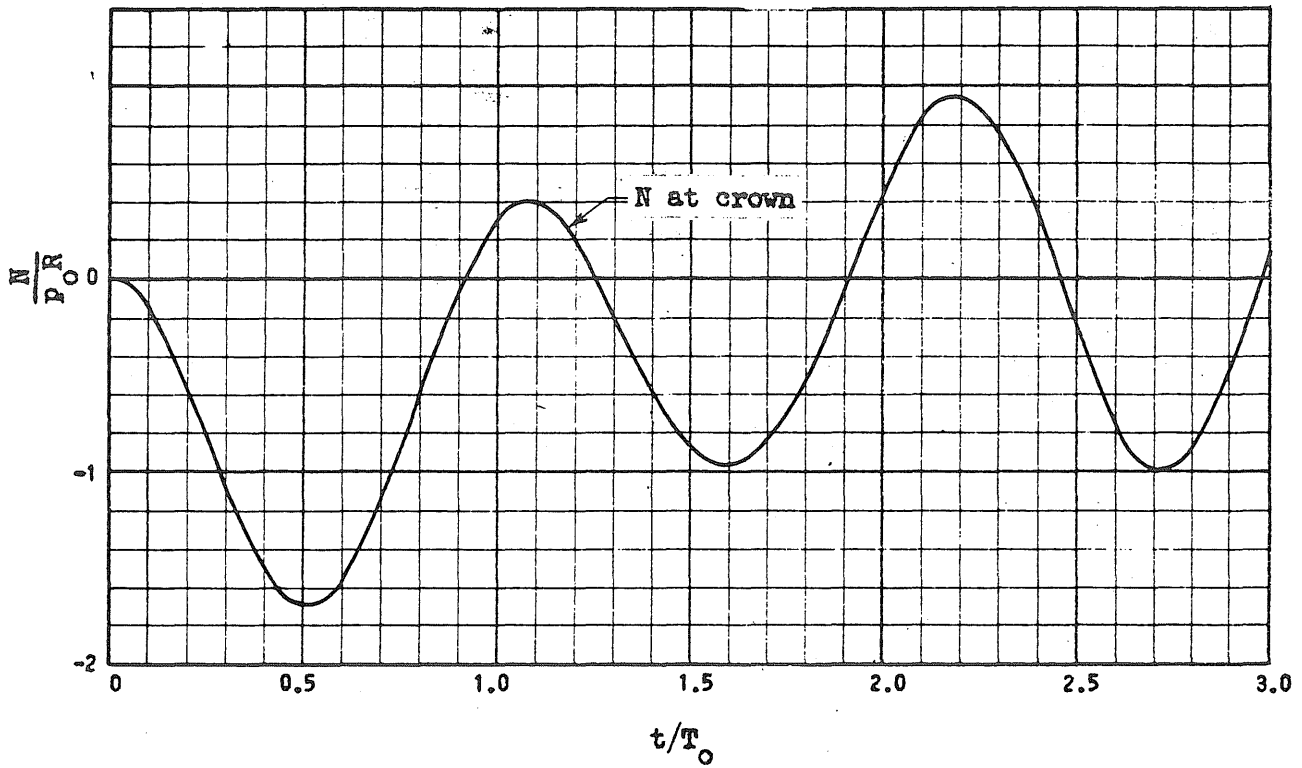
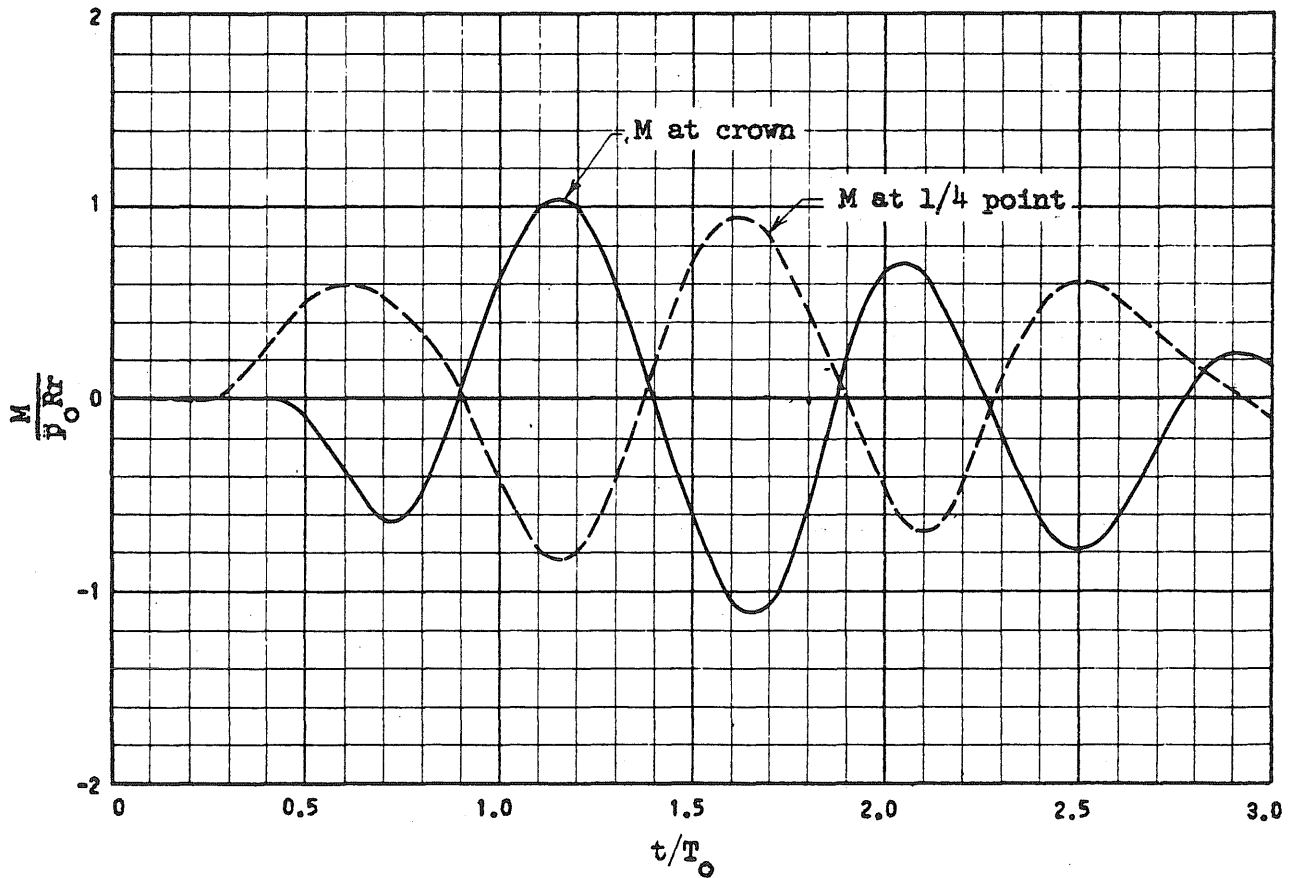
(b) Radial Displacement, w

FIG. 4.3 TYPICAL RESPONSE CURVES FOR AN ARCH UNDER A UNIFORM ALL-AROUND PRESSURE PULSE

$$f/L_0 = 0.2, L_0/r = 100, p_0/p_{cr} = 1.0, t_d/T_0 = 2.0$$



(c) Axial Force, N



(d) Bending Moment, M

FIG. 4.3 (Continued)

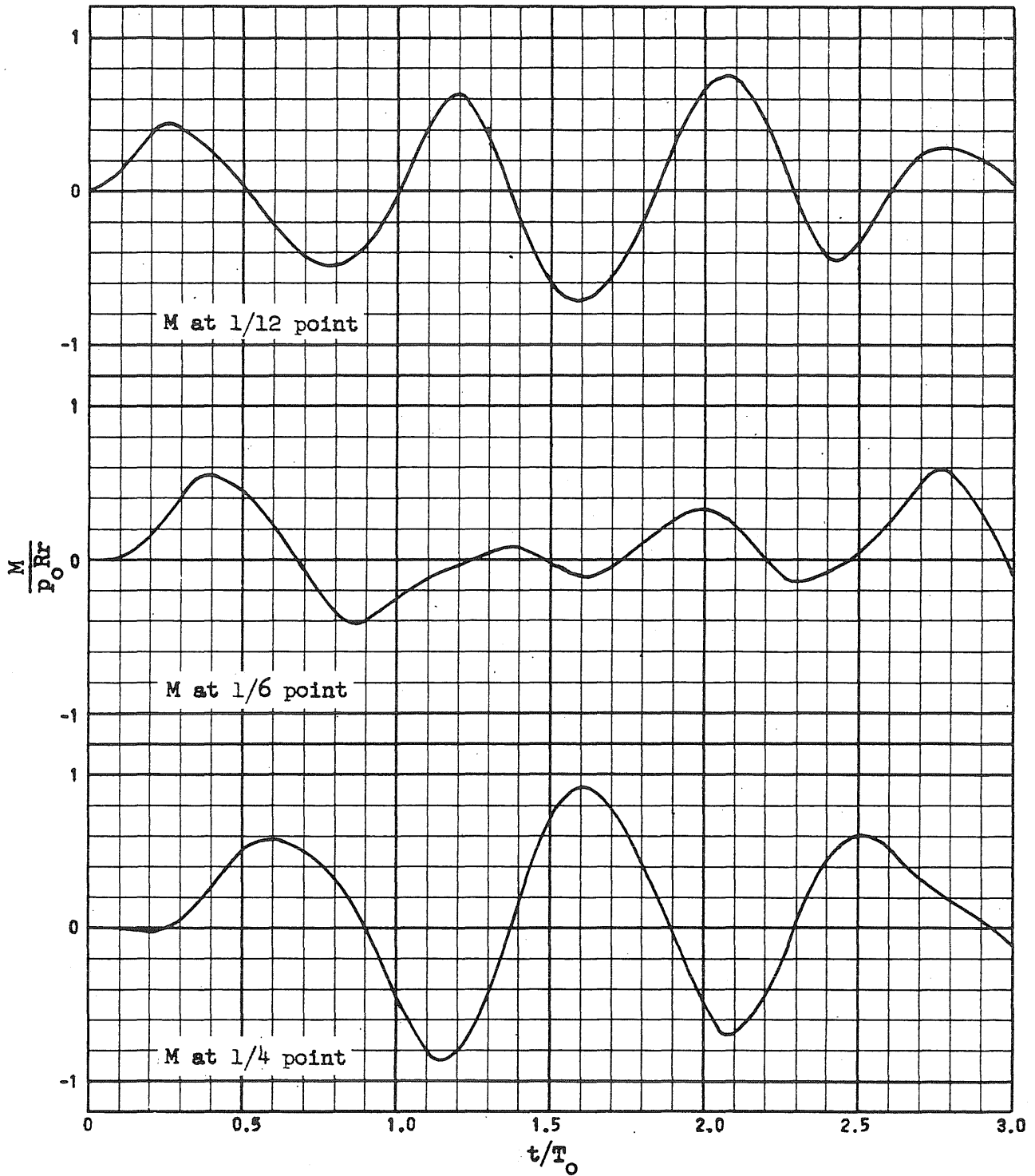


FIG. 4.4 RESPONSE CURVES OF BENDING MOMENT IN AN ARCH FOR A UNIFORM ALL-AROUND PRESSURE PULSE
 $f/L_0 = 0.2$, $L_0/r = 100$, $p_0/p_{cr} = 1.0$, $t_d/T_0 = 2.0$

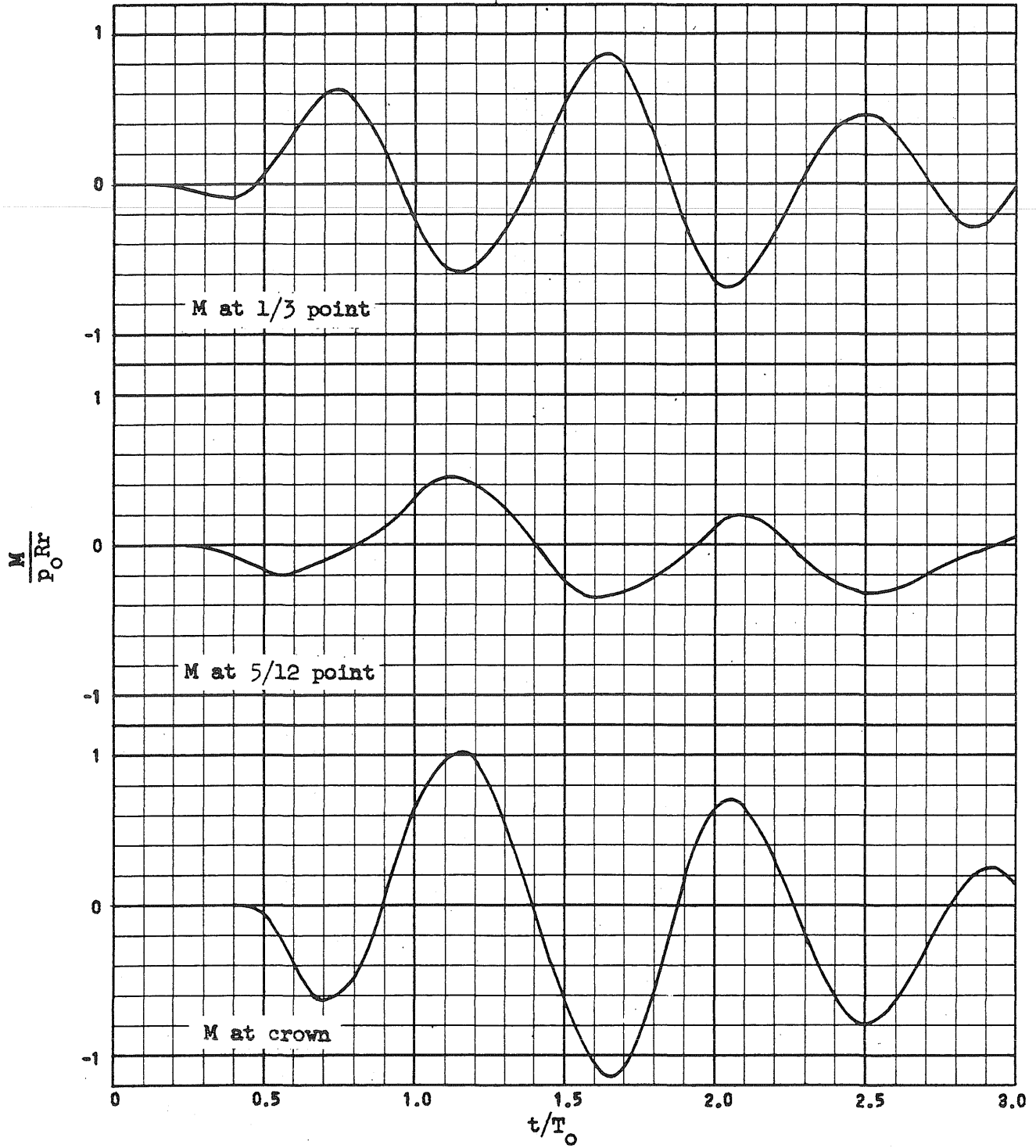


FIG. 4.4 (Continued)

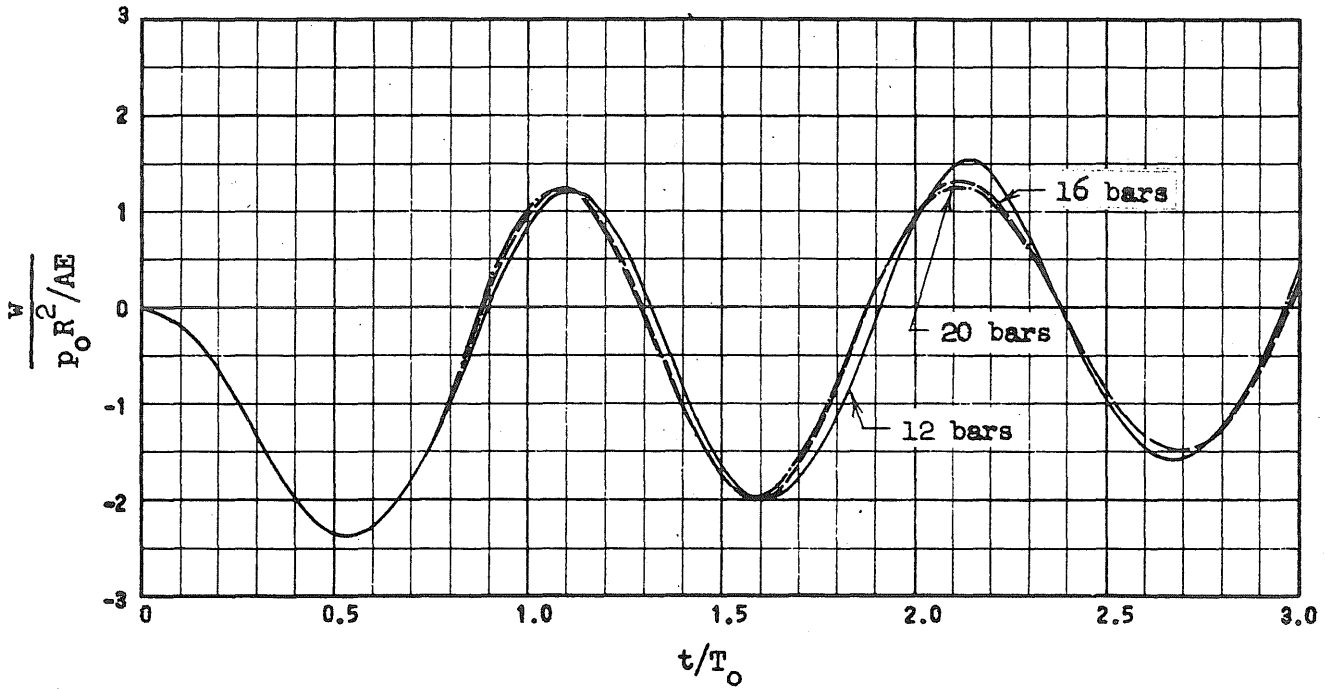
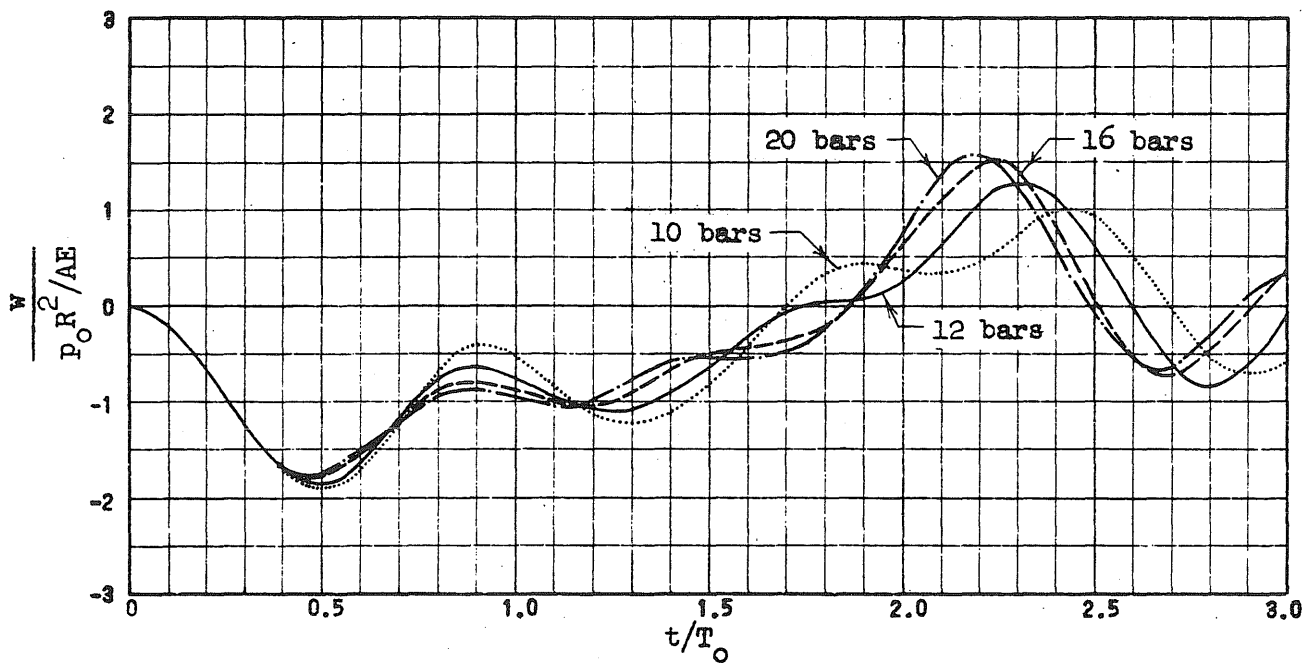
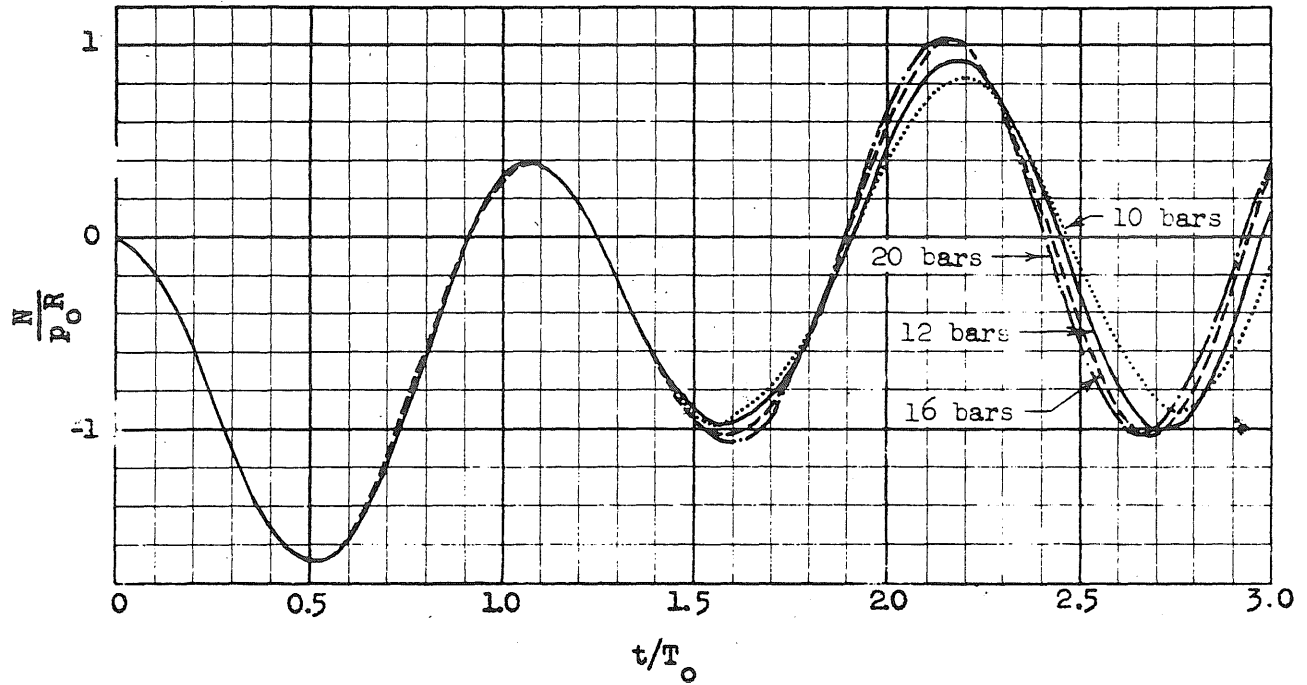
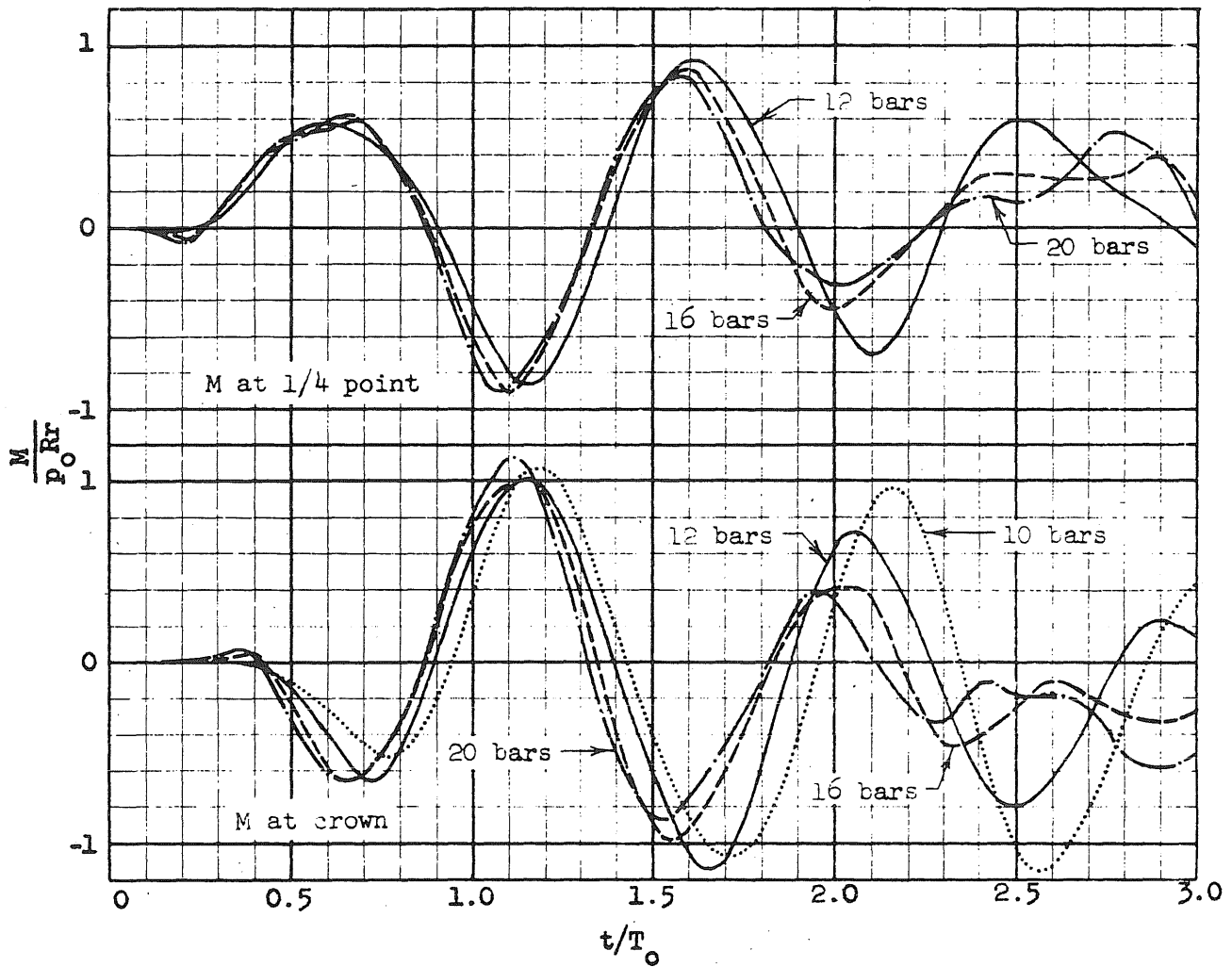
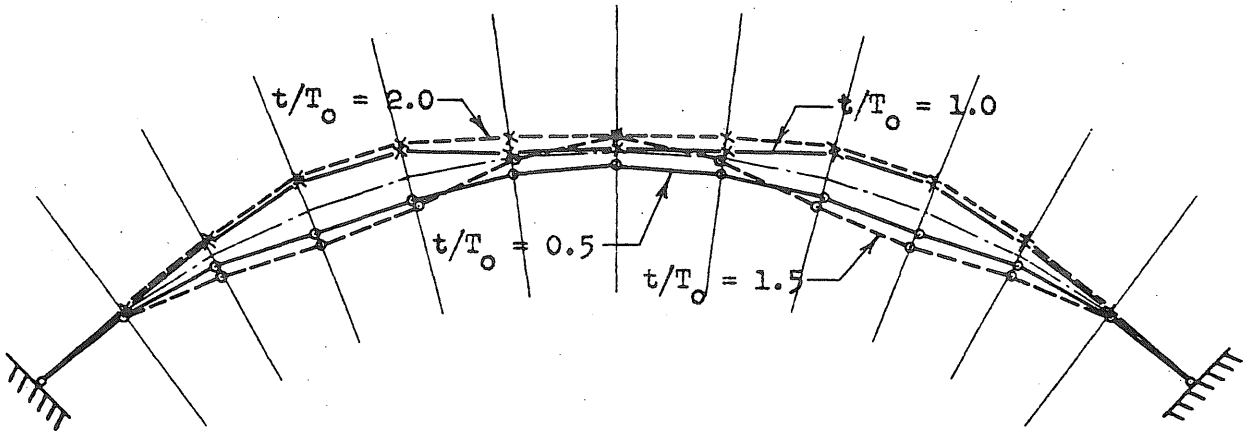
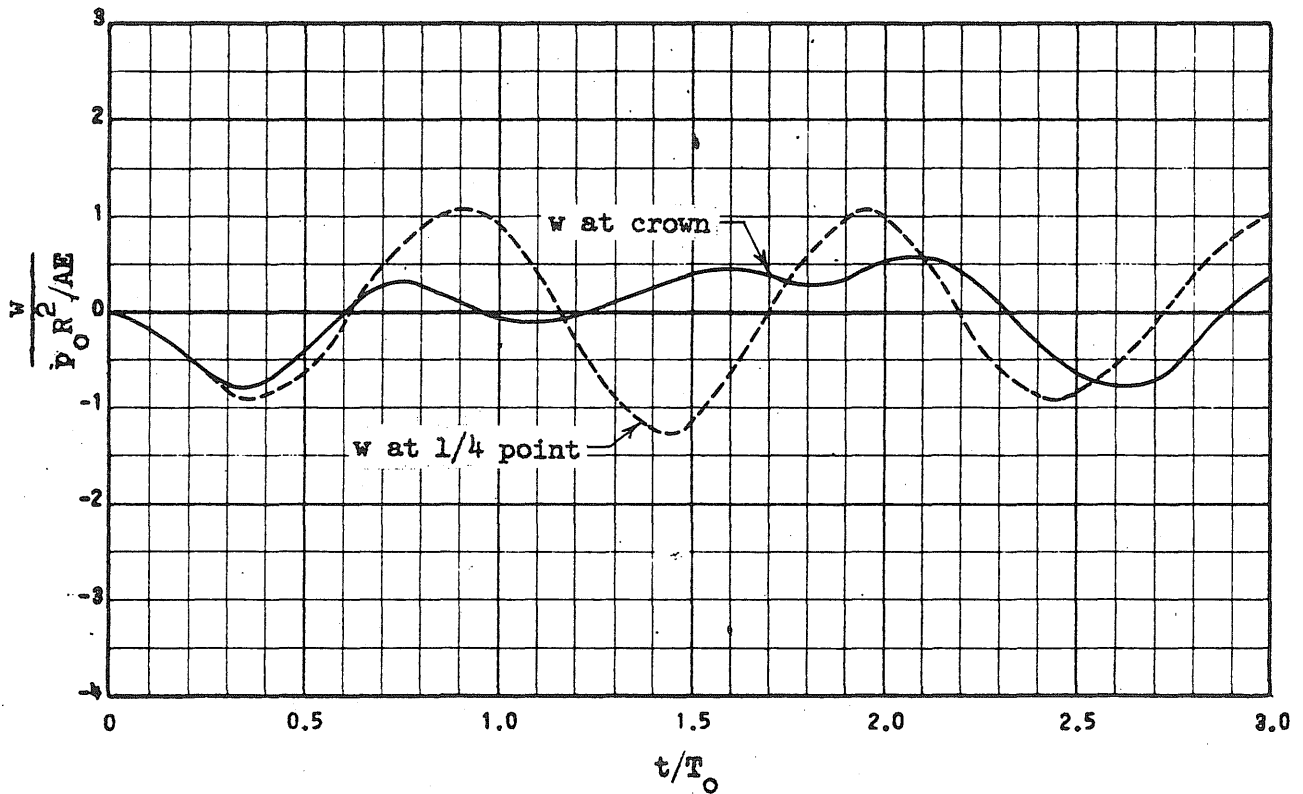
(a) Radial Displacement, w , at 1/4 point(b) Radial Displacement, w , at crown

FIG. 4.5 EFFECT OF NUMBER OF BARS ON RESPONSE
 $f/L_0 = 0.2$, $L_0/r = 100$, $p_0/p_{cr} = 1.0$, $t_d/T_0 = 2.0$

(c) Axial Force, N , at crown(d) Bending Moments, M



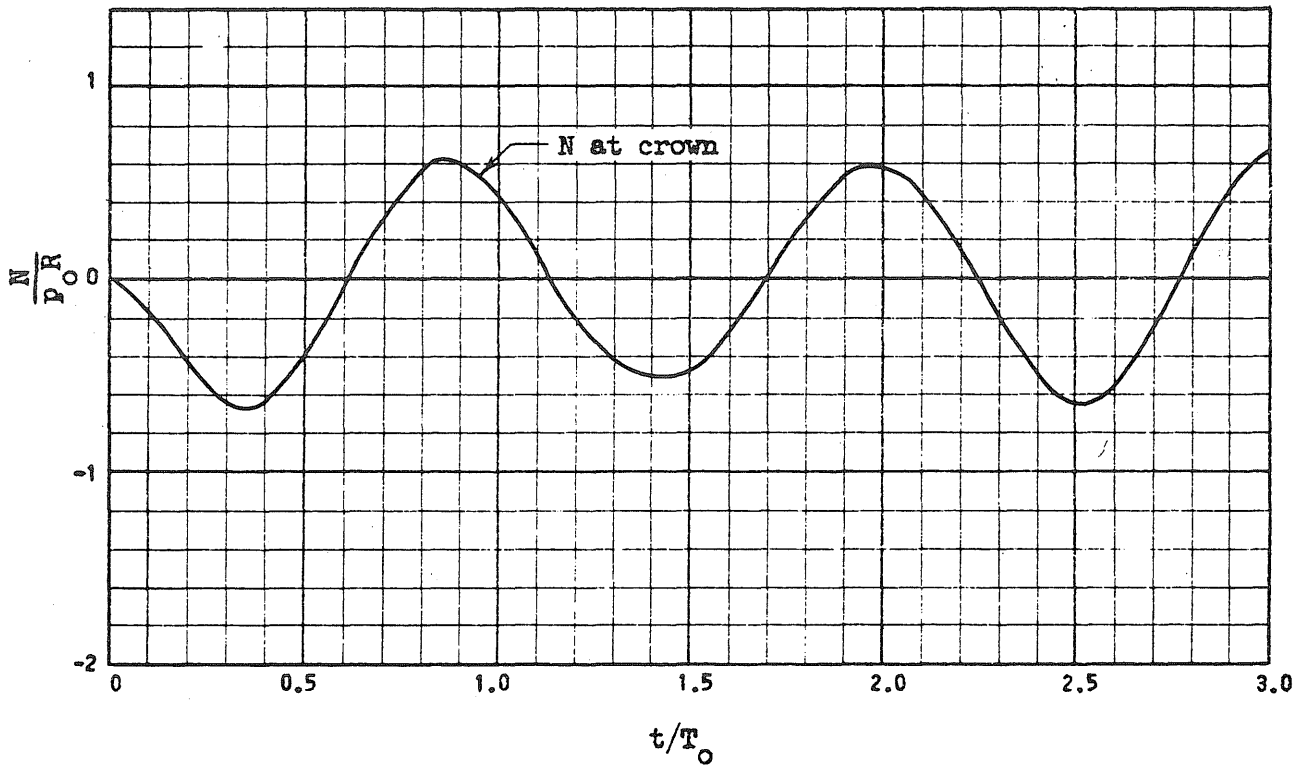
(a) Displacement Configurations



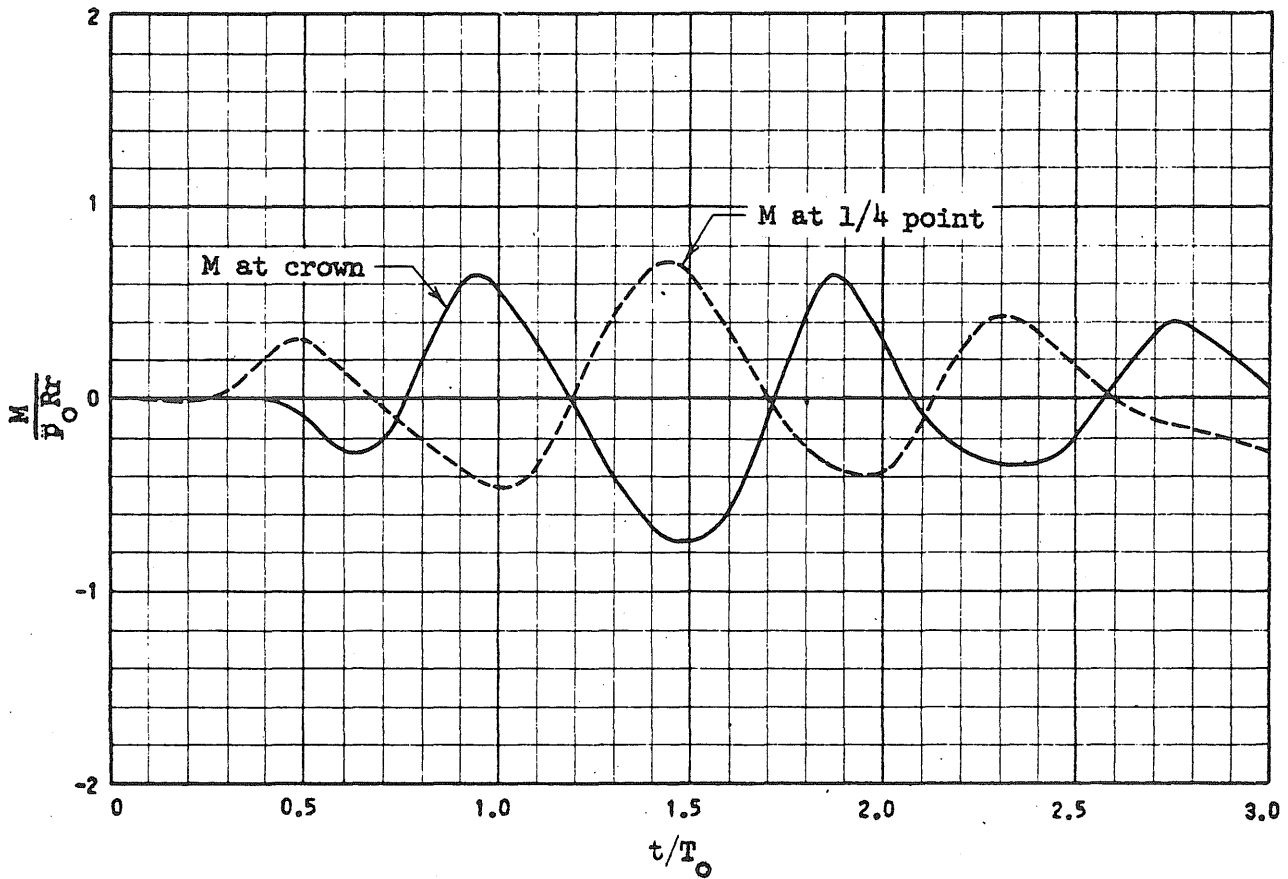
(b) Radial Displacement, w

FIG. 4.6 RESPONSE CURVES FOR AN ARCH UNDER A UNIFORM ALL-AROUND PRESSURE PULSE-- $t_d/T_0 = 0.25$

$$f/L_0 = 0.2, L_0/r = 100, p_0/p_{cr} = 1.0$$

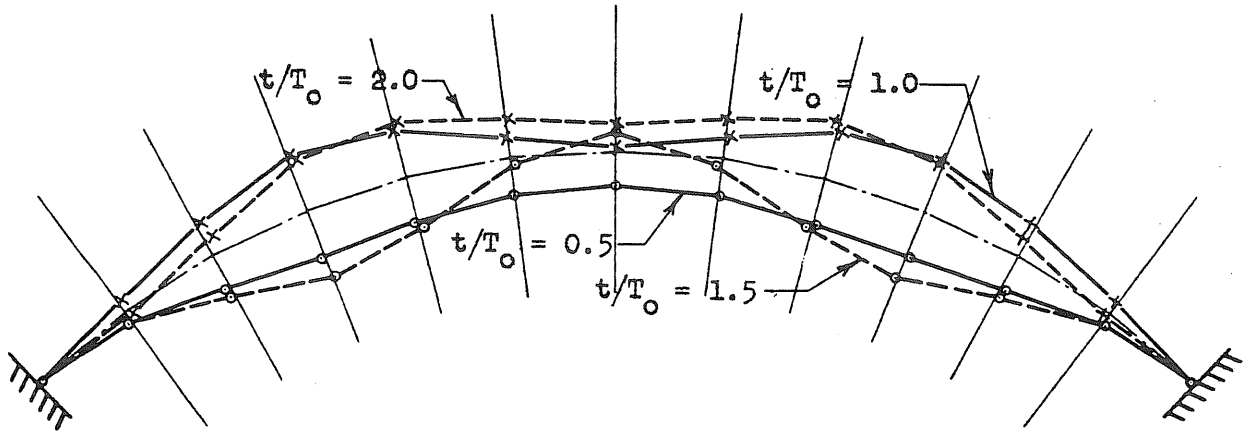


(c) Axial Force, N

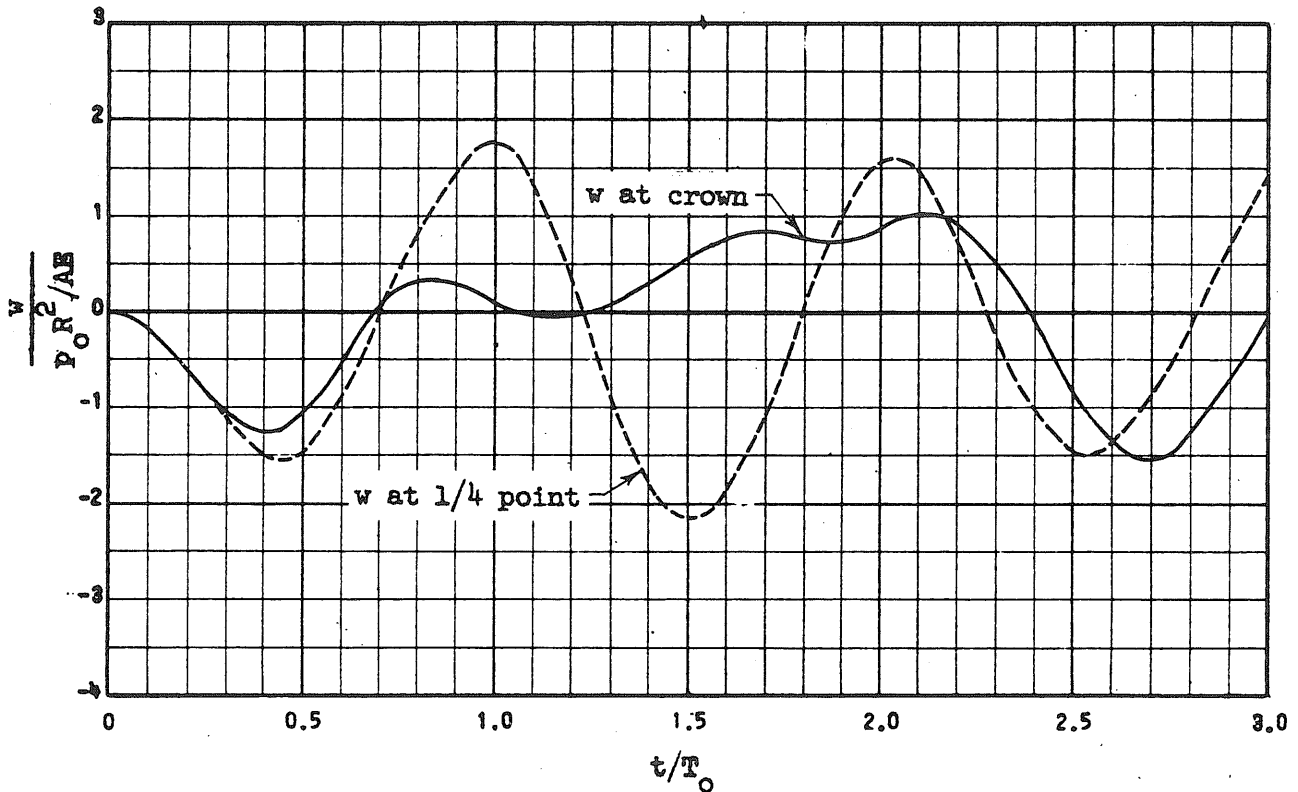


(d) Bending Moment, M

FIG. 4.6 (Continued)

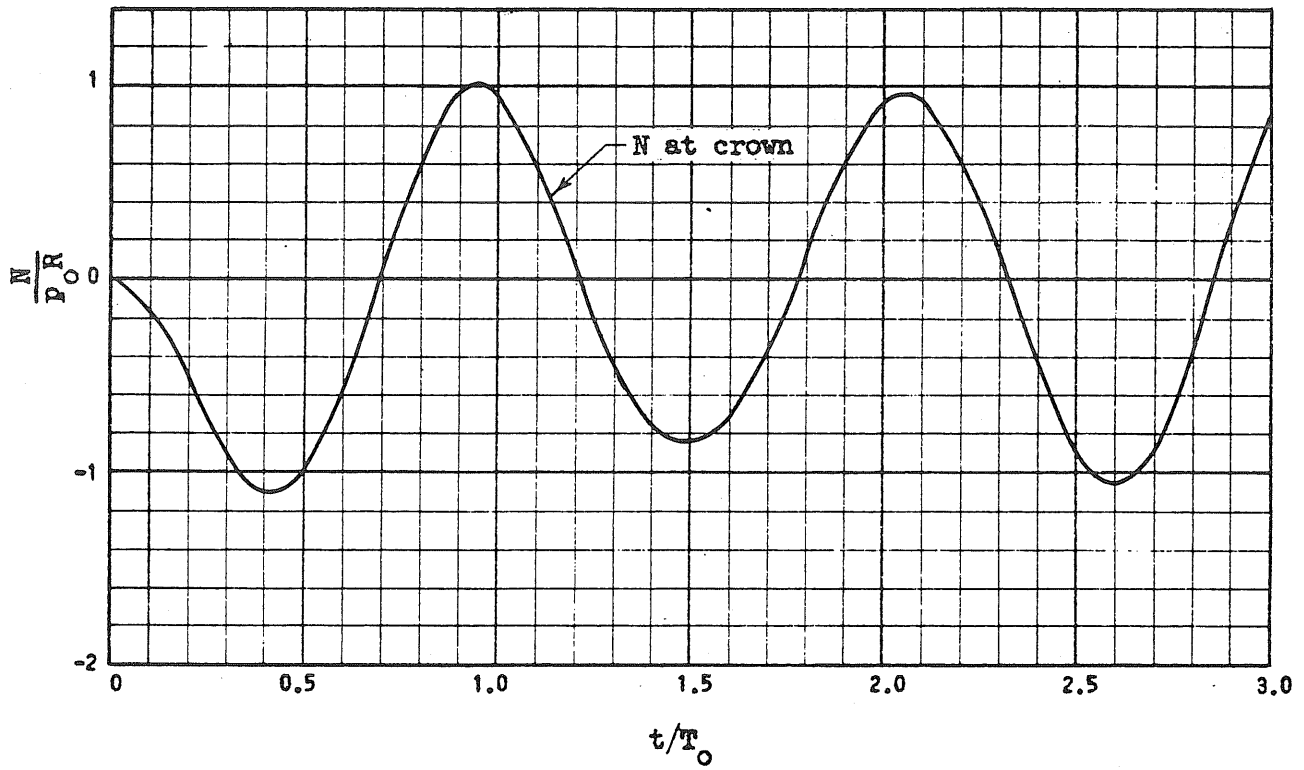


(a) Displacement Configurations

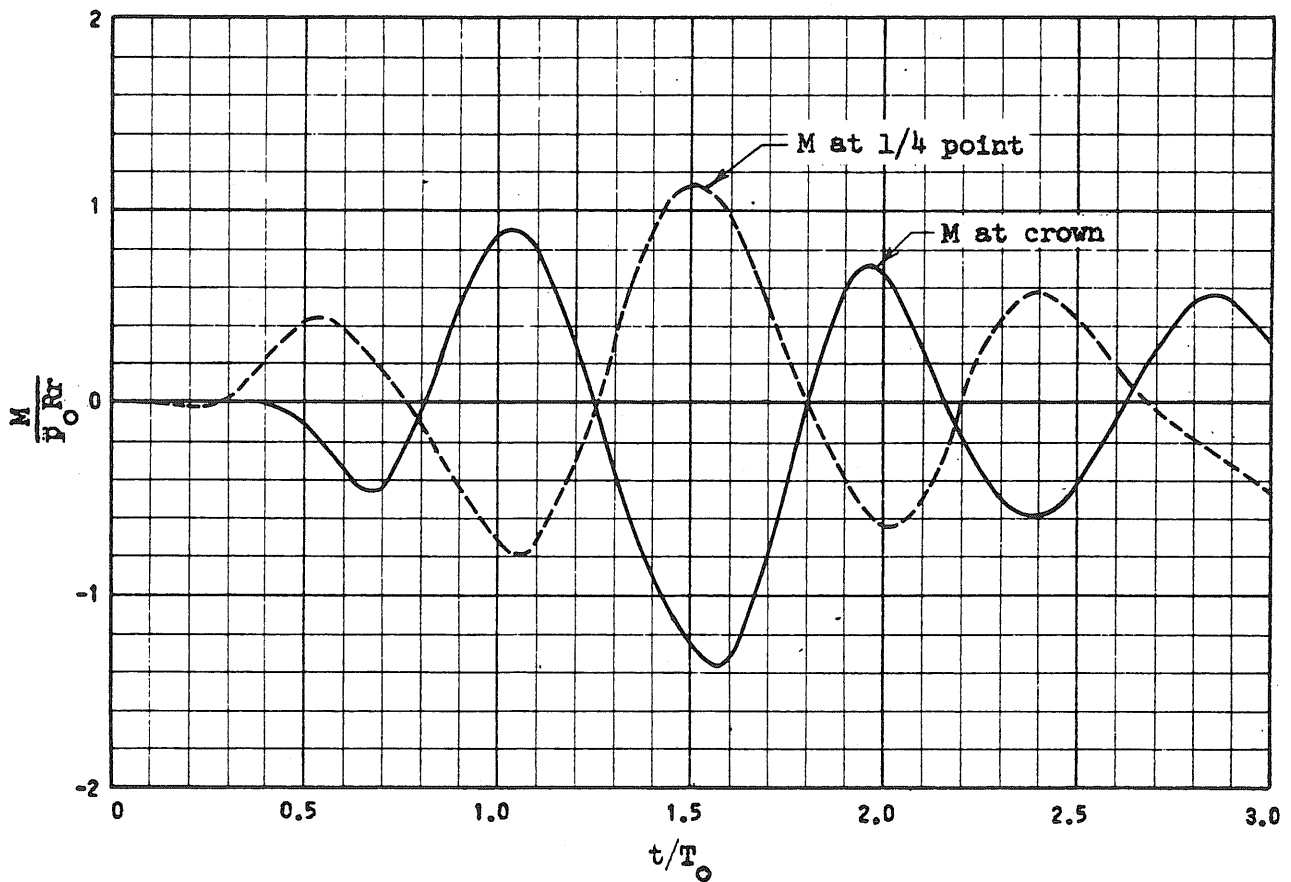


(b) Radial Displacement, w

FIG. 4.7 RESPONSE CURVES FOR AN ARCH UNDER A UNIFORM ALL-AROUND PRESSURE PULSE-- $t_d/T_0 = 0.50$
 $f/L_0 = 0.2, L_0/r = 100, p_0/p_{cr} = 1.0$

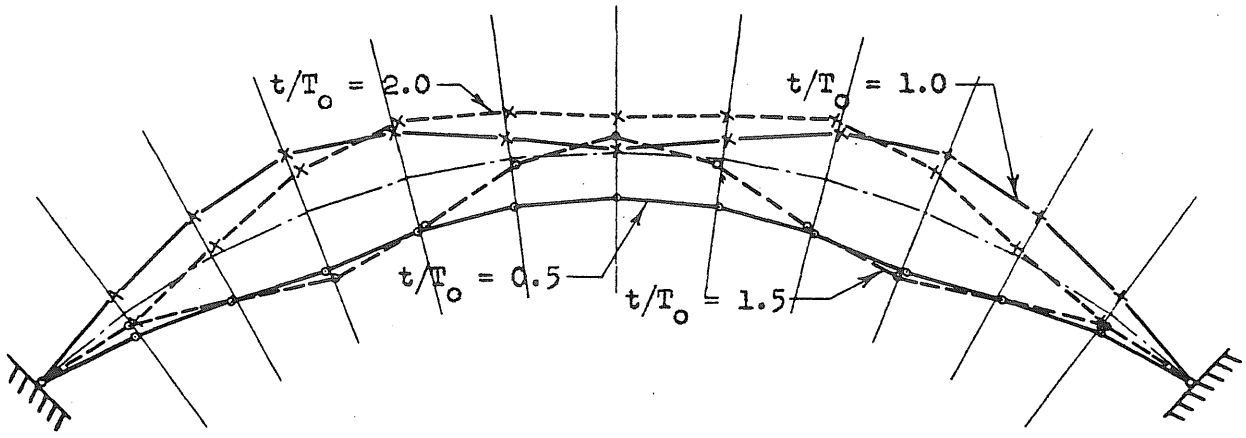


(c) Axial Force, N

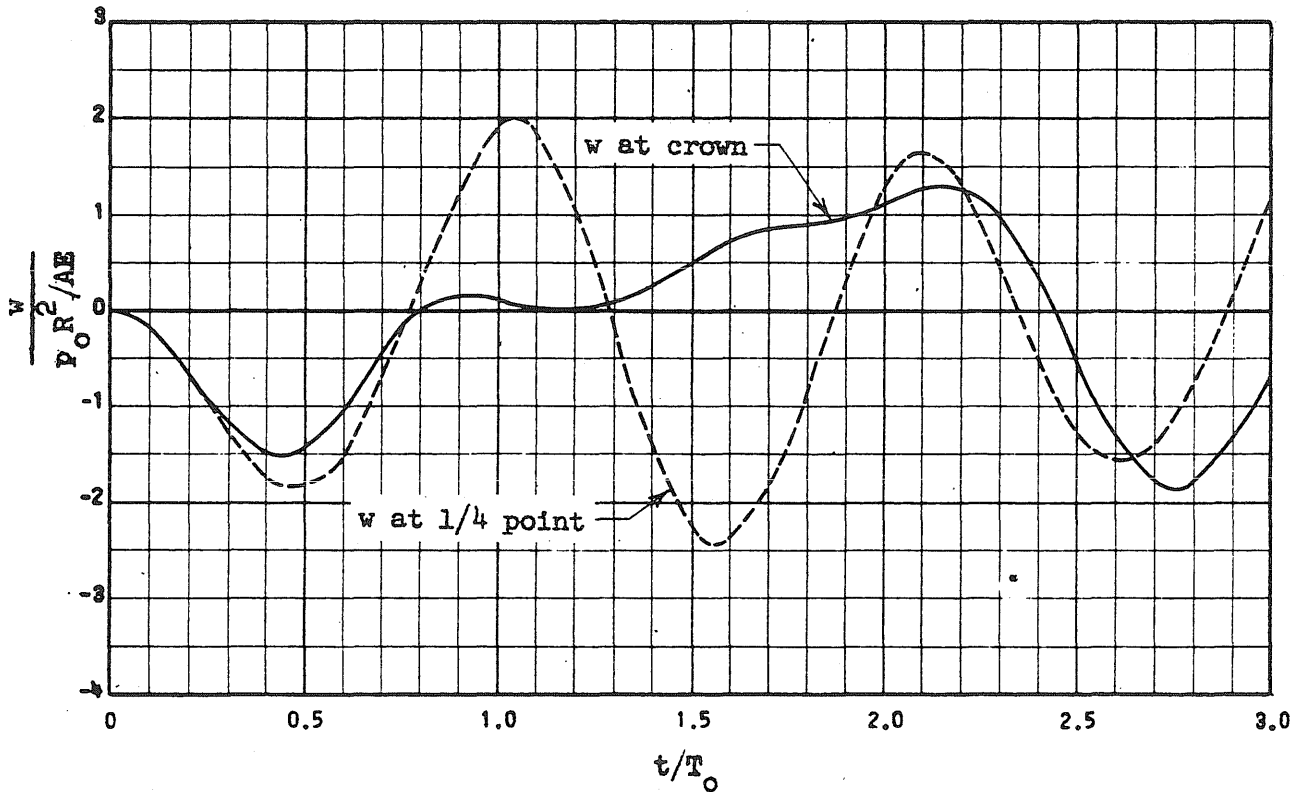


(d) Bending Moment, M

FIG. 4.7 (Continued)

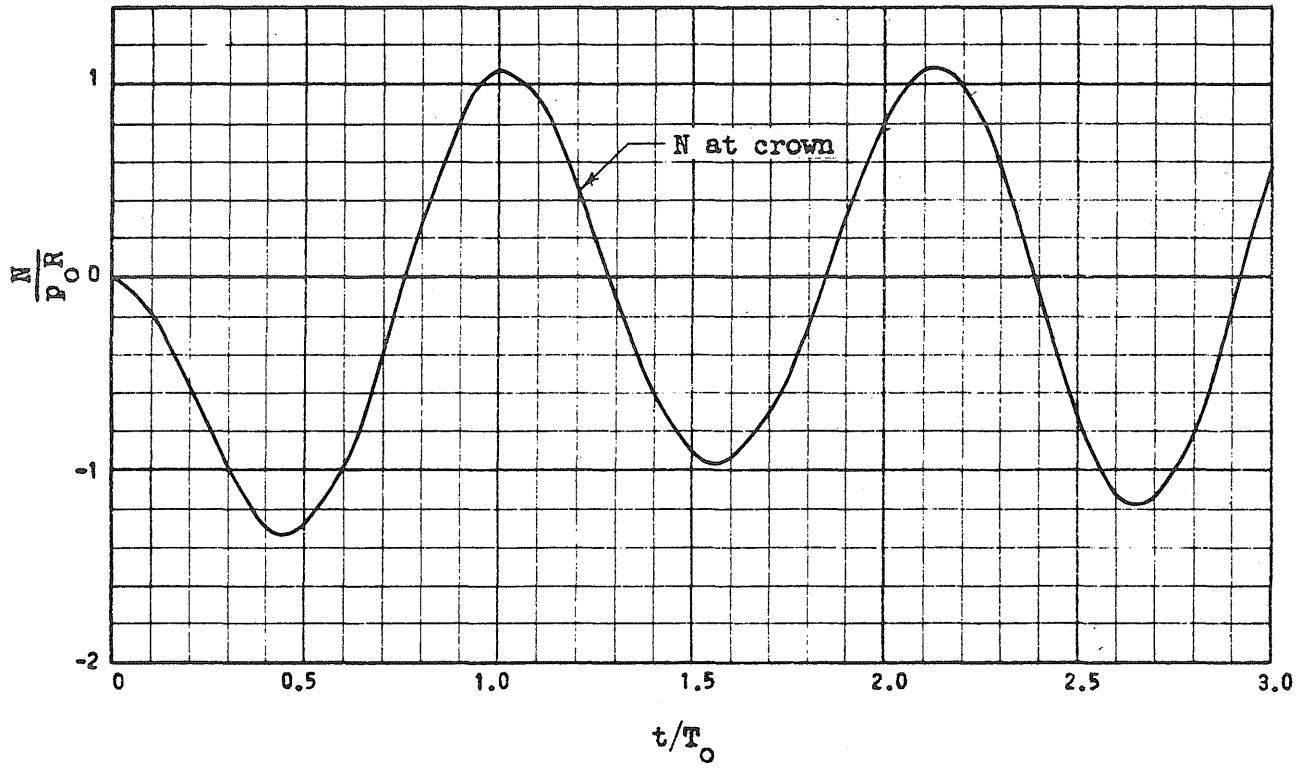


(a) Displacement Configurations

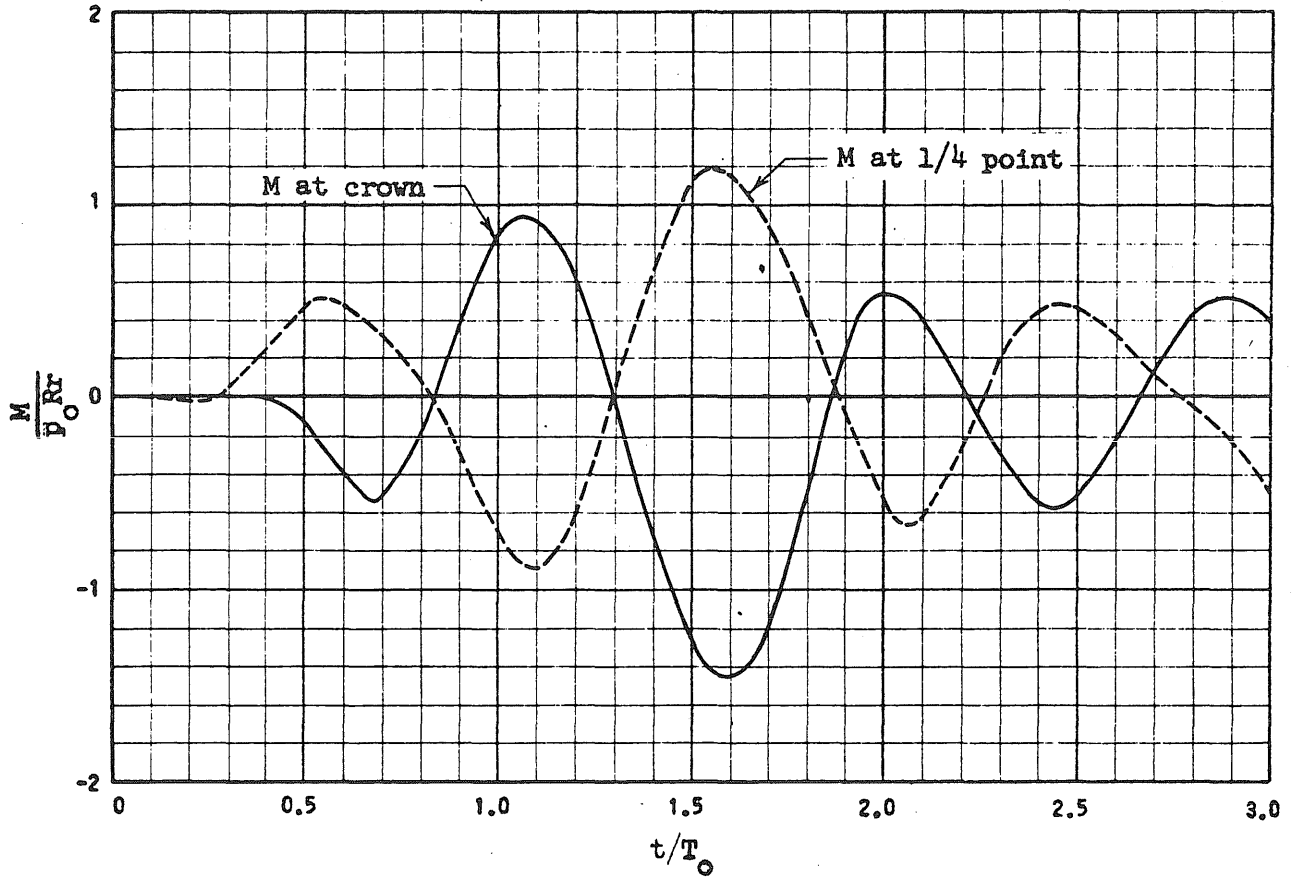


(b) Radial Displacement, w

FIG. 4.8 RESPONSE CURVES FOR AN ARCH UNDER A UNIFORM ALL-AROUND PRESSURE PULSE-- $t_d/T_0 = 0.75$
 $f/L_0 = 0.2, L_0/r = 100, P_0/P_{cr} = 1.0$

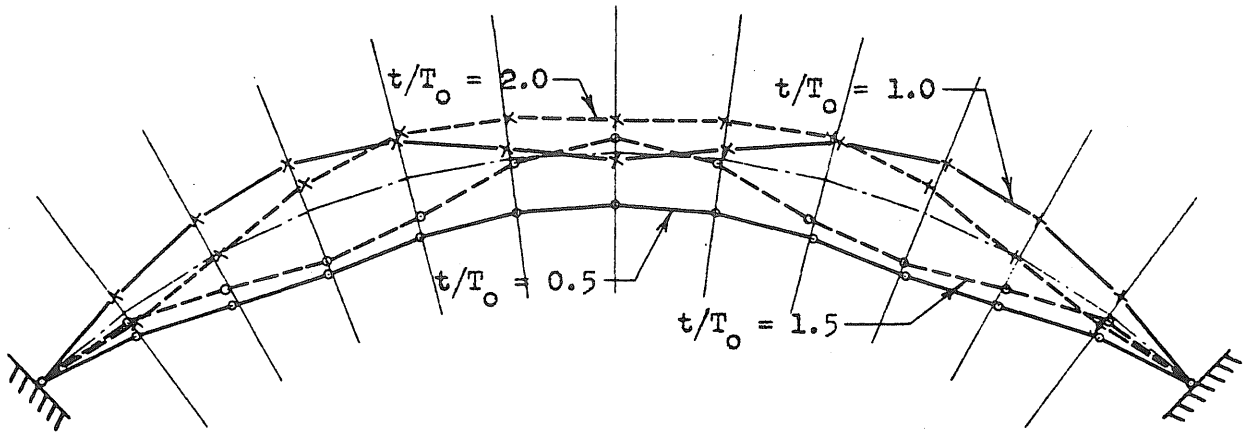


(c) Axial Force, N

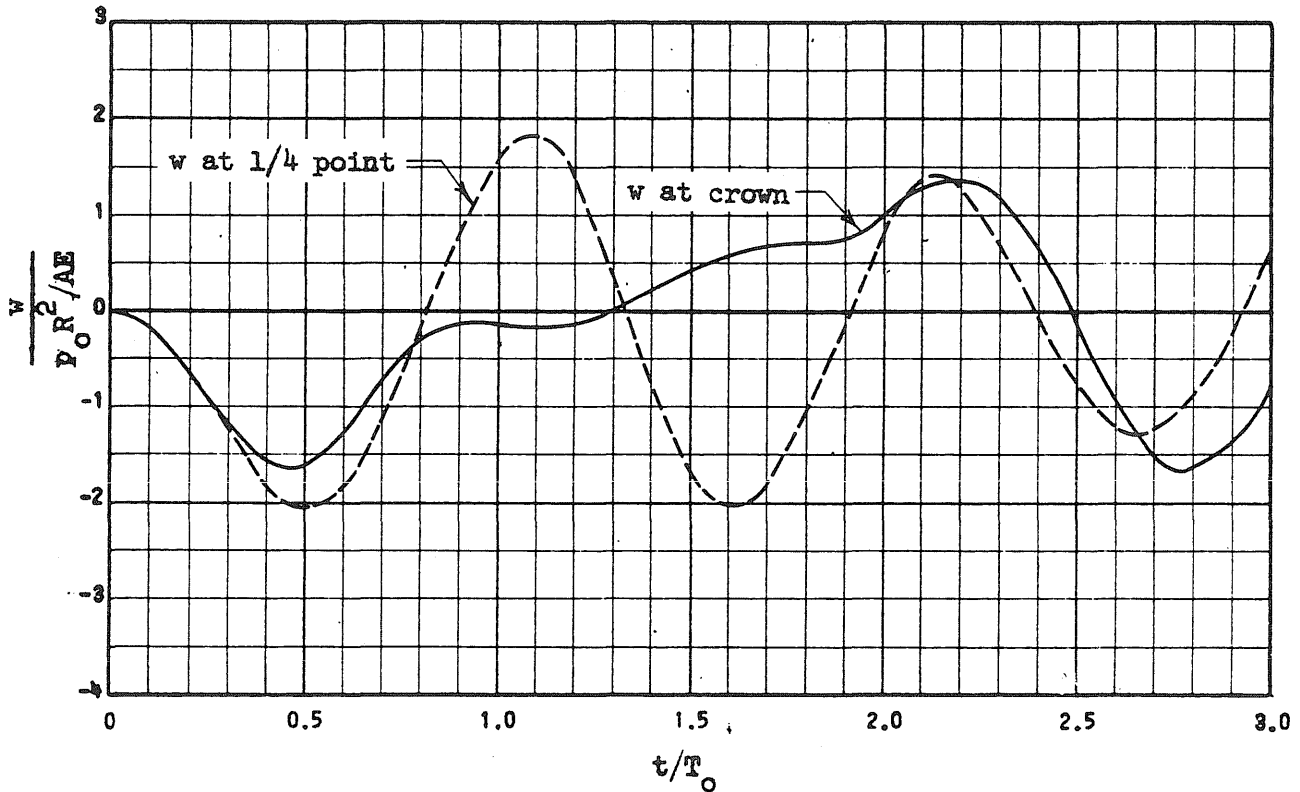


(d) Bending Moment, M

FIG. 4.8 (Continued)

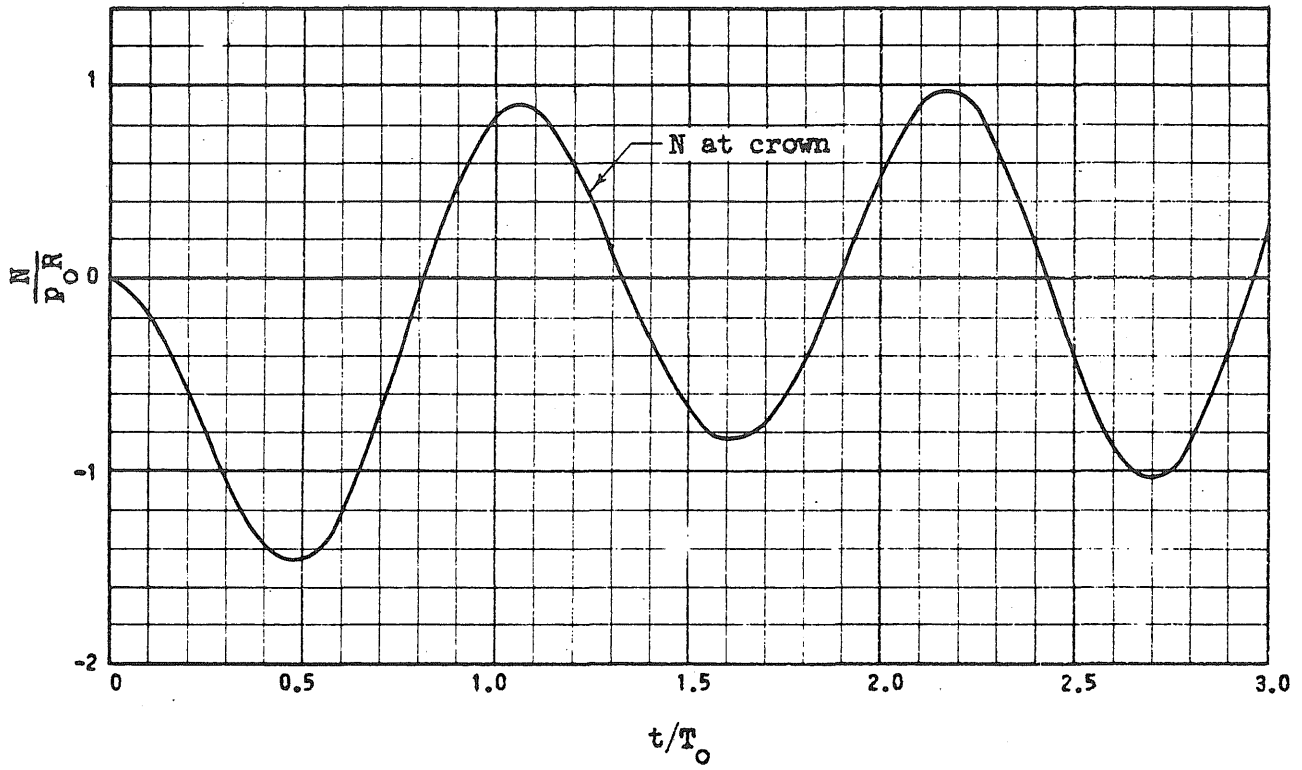


(a) Displacement Configurations

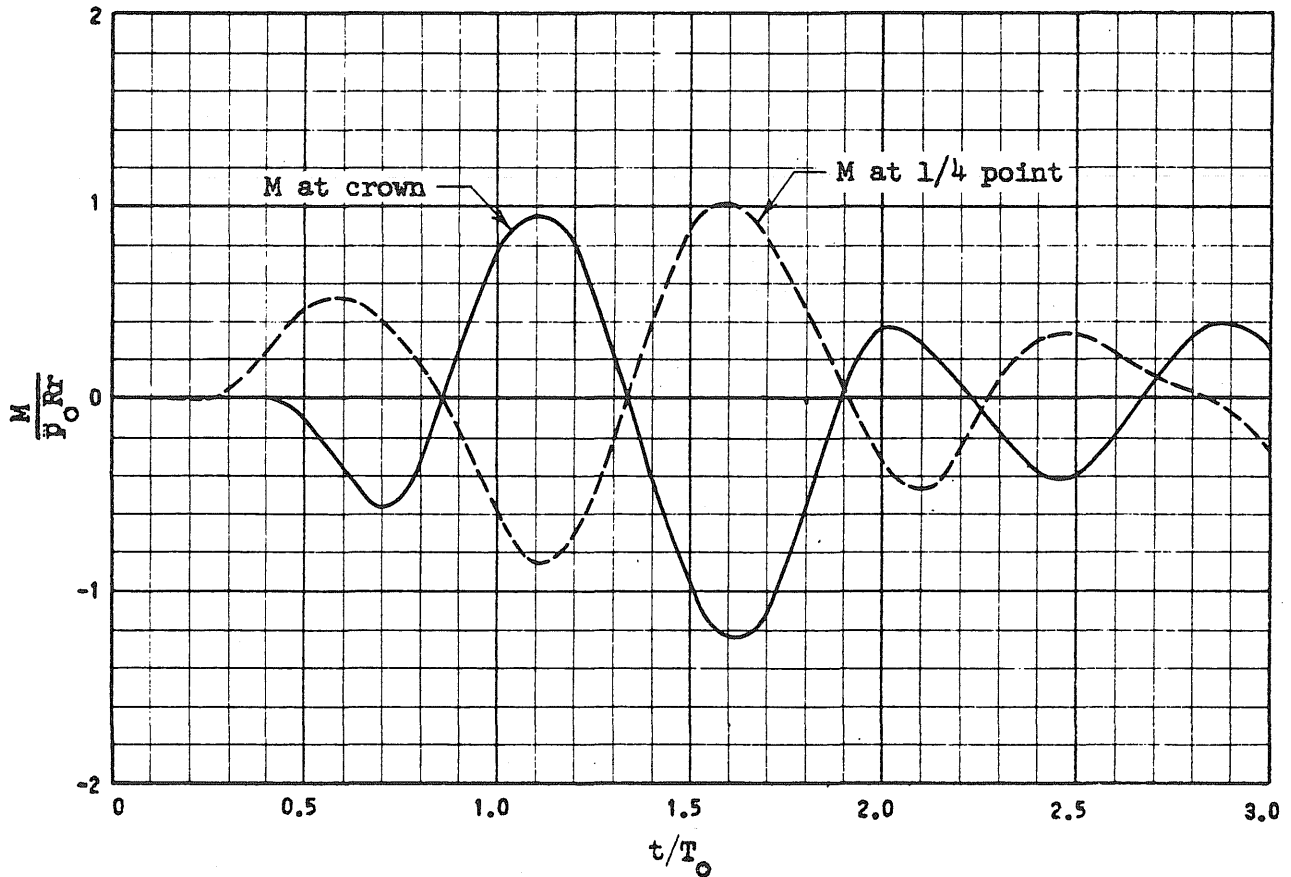


(b) Radial Displacement, w

FIG. 4.9 RESPONSE CURVES FOR AN ARCH UNDER A UNIFORM ALL-AROUND PRESSURE PULSE-- $t_d/T_0 = 1.0$
 $f/L_0 = 0.2, L_0/r = 100, p_0/p_{cr} = 1.0$

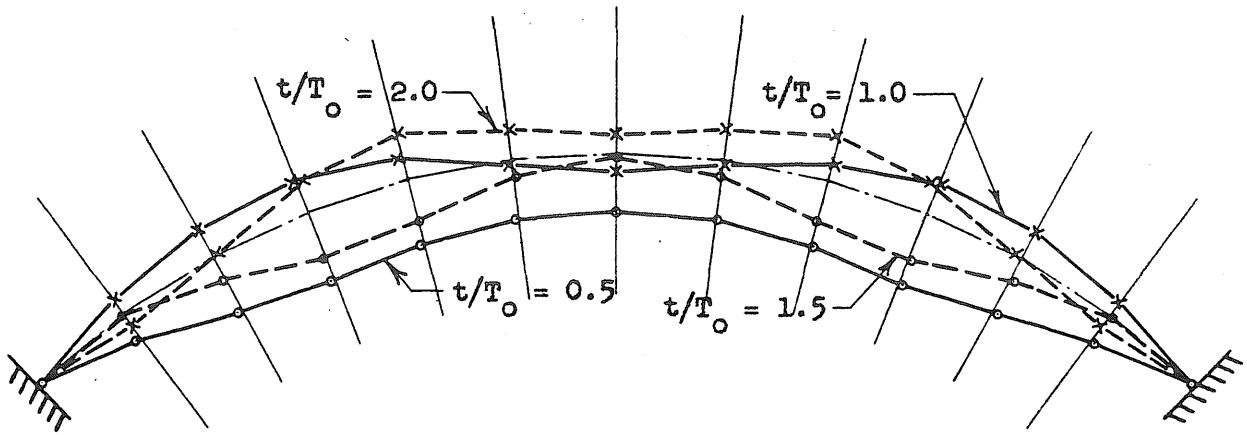


(c) Axial Force, N

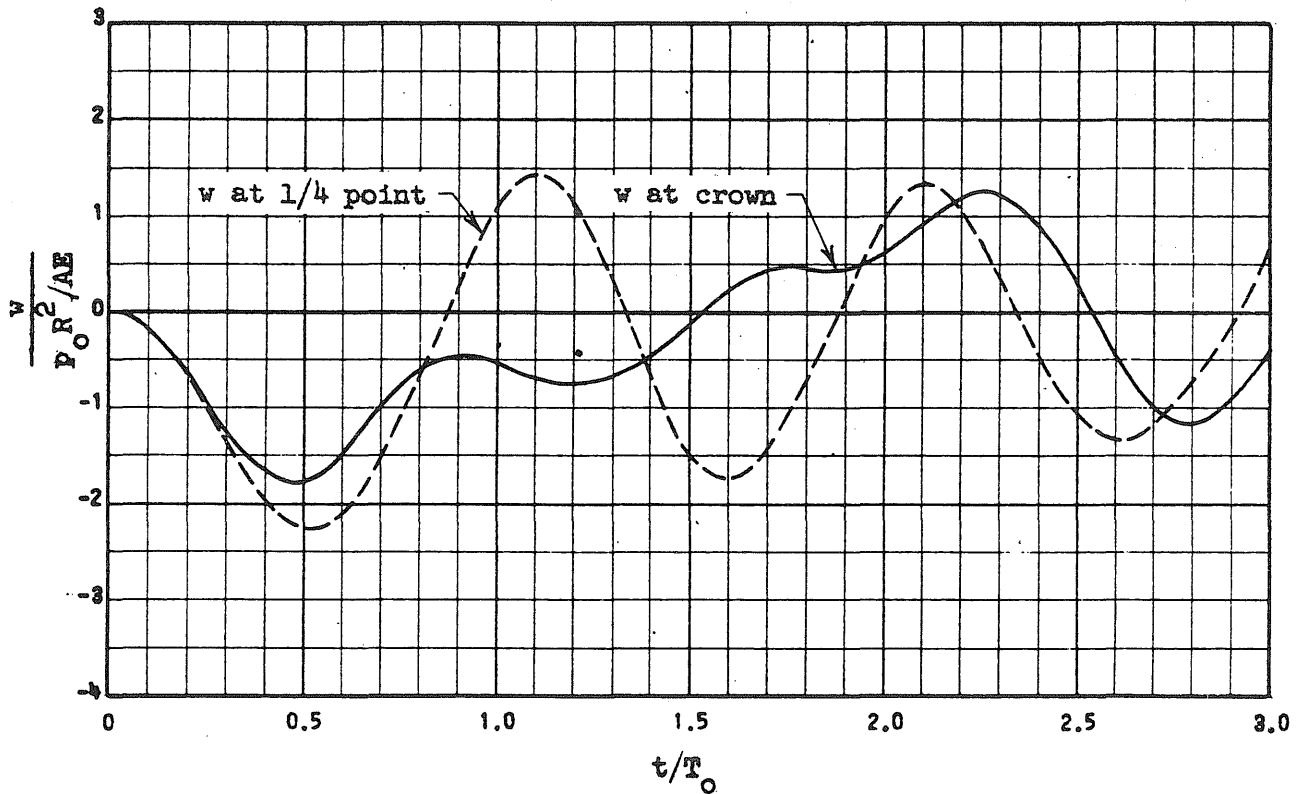


(d) Bending Moment, M

FIG. 4.9 (Continued)



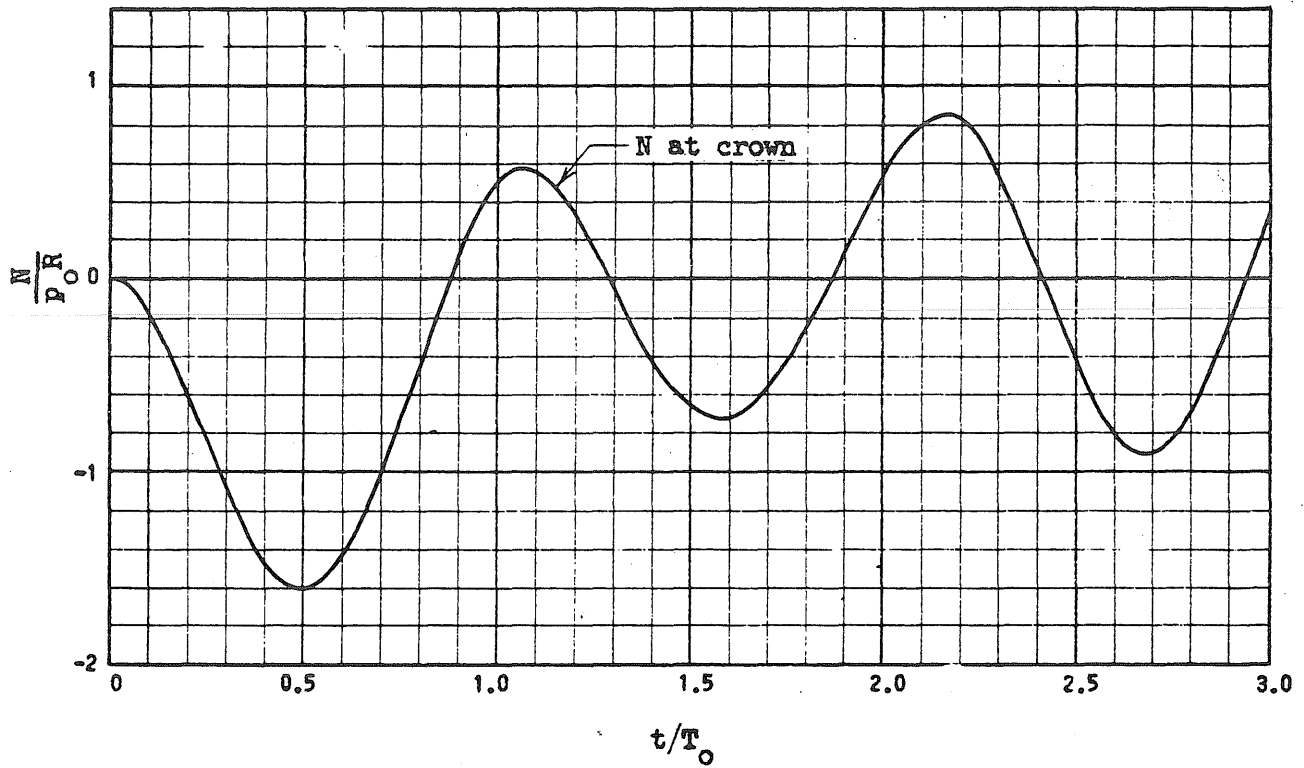
(a) Displacement Configurations



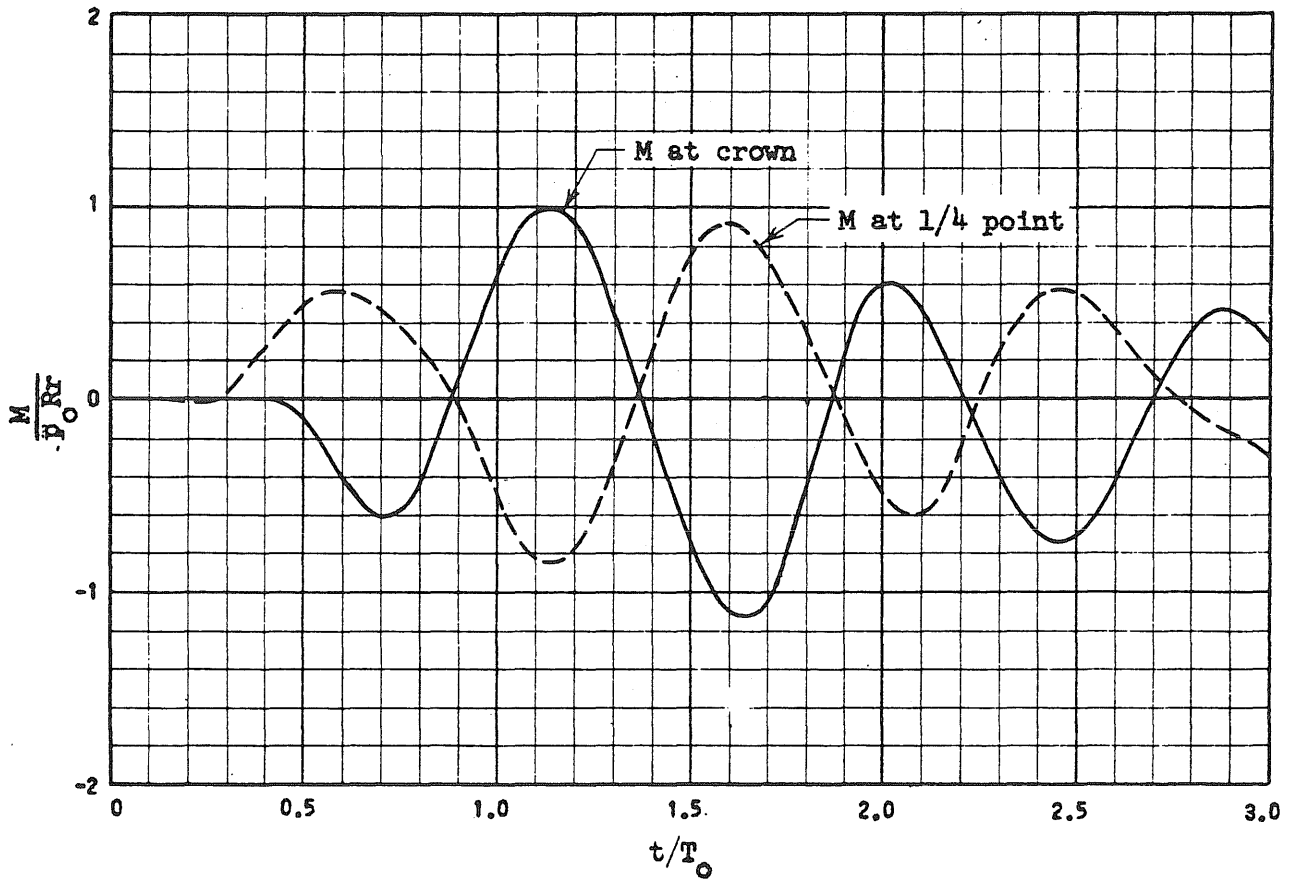
(b) Radial Displacement, w

FIG. 4.10 RESPONSE CURVES FOR AN ARCH UNDER A UNIFORM ALL-AROUND PRESSURE PULSE-- $t_d/T_0 = 1.5$

$f/L_0 = 0.2, L_0/r = 100, p_0/p_{cr} = 1.0$

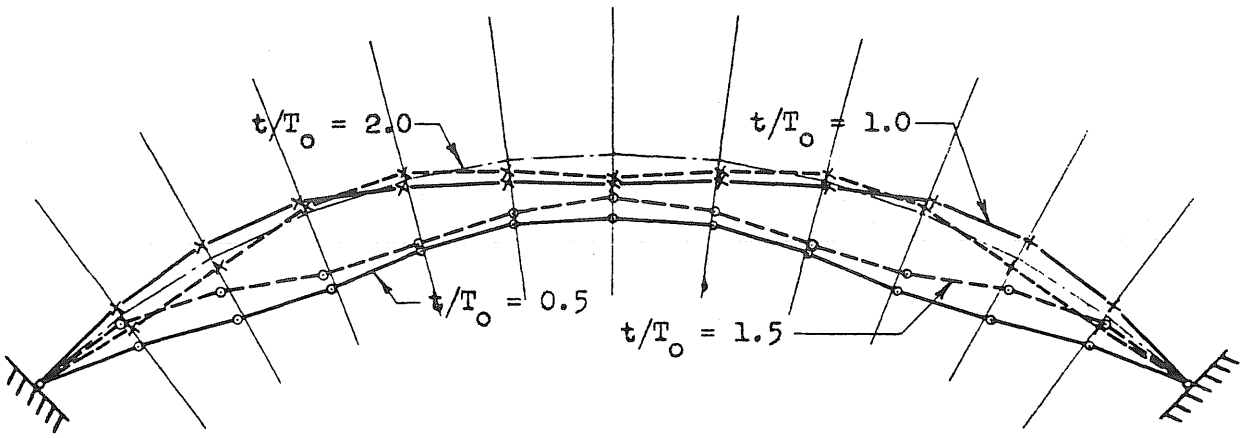


(c) Axial Force, N

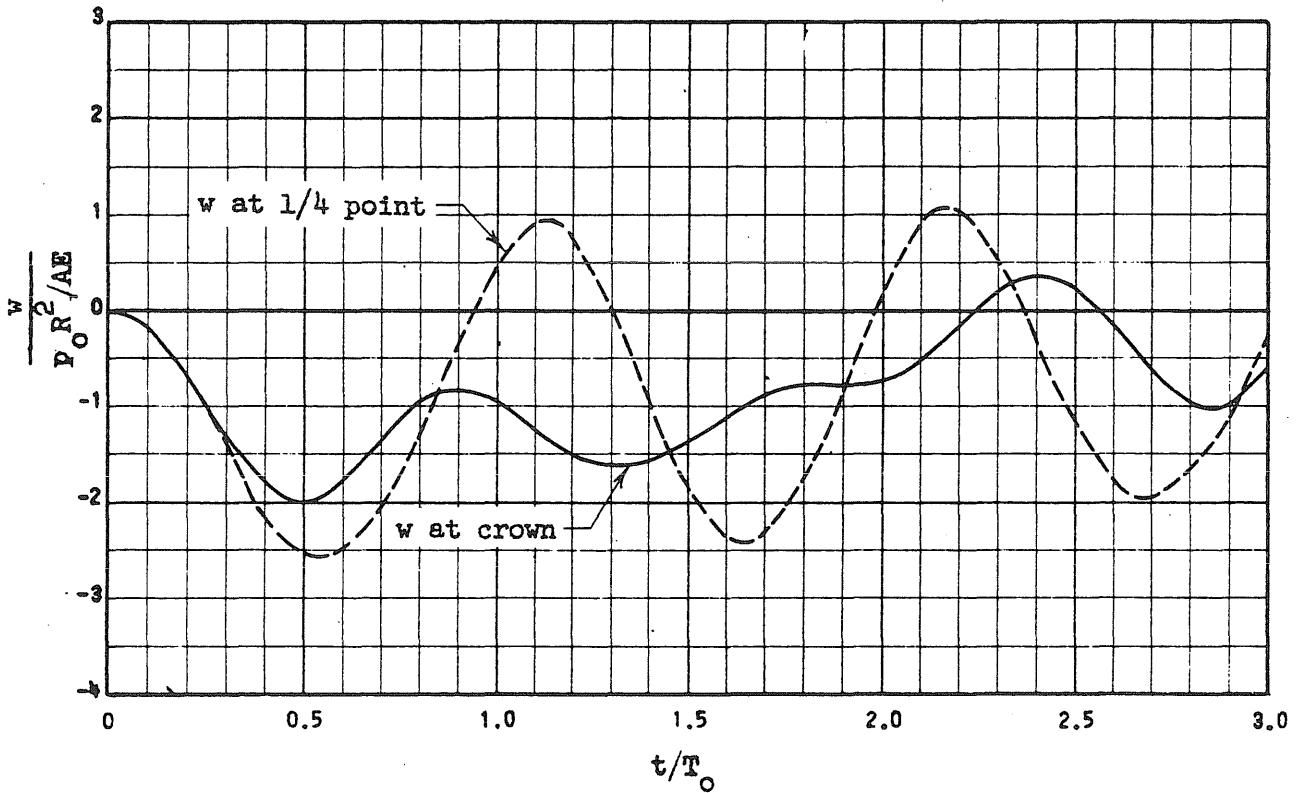


(d) Bending Moment, M

FIG. 4.10 (Continued)

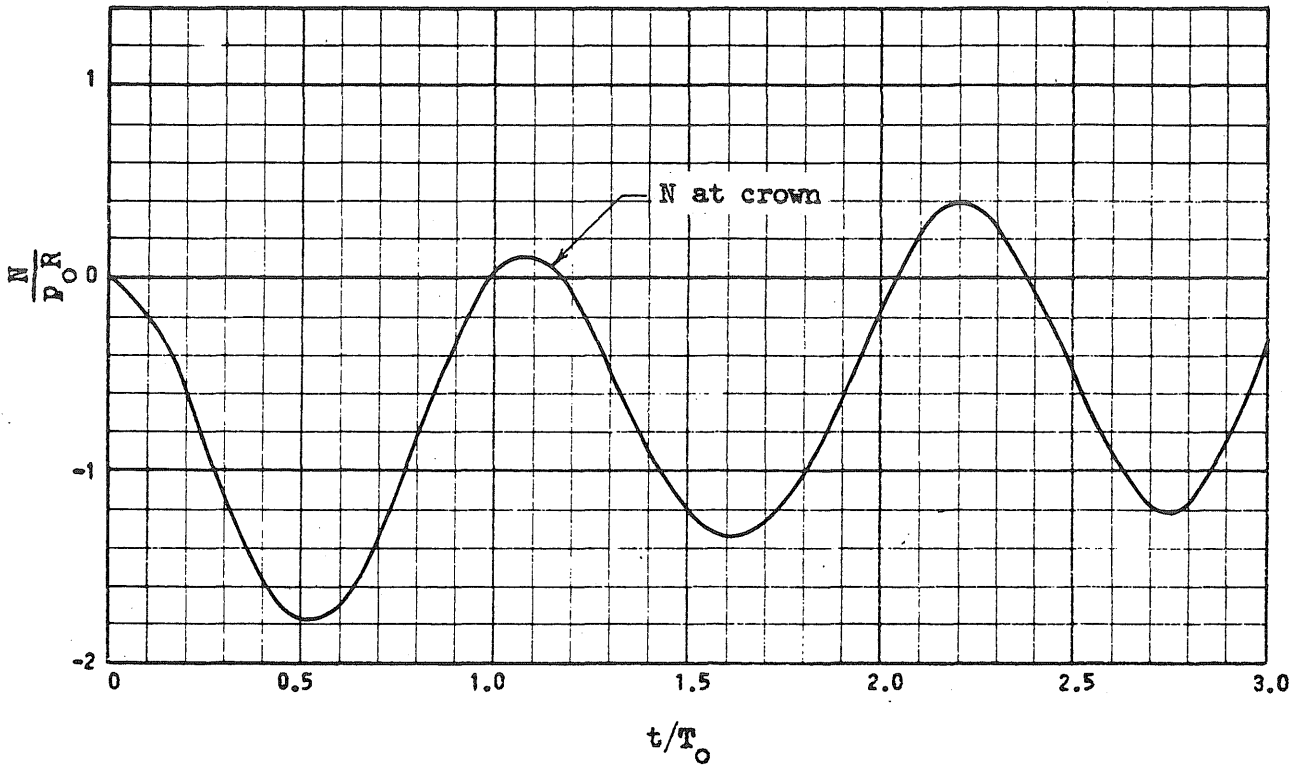


(a) Displacement Configurations

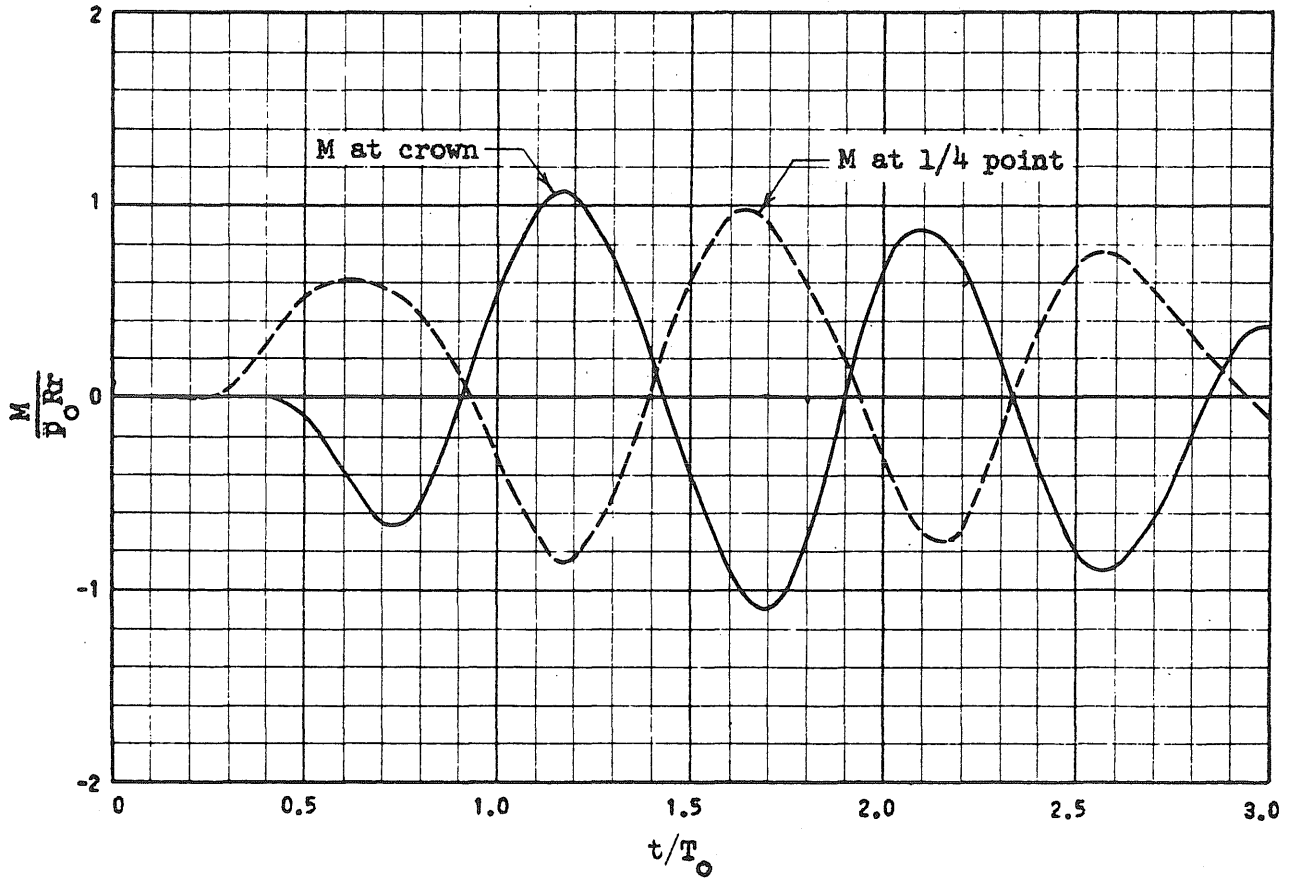


(b) Radial Displacement, w

FIG. 4.11 RESPONSE CURVES FOR AN ARCH UNDER A UNIFORM ALL-AROUND PRESSURE PULSE-- $t_d/T_0 = 4.0$
 $f/L_0 = 0.2, L_0/r = 100, p_0/p_{cr} = 1.0$

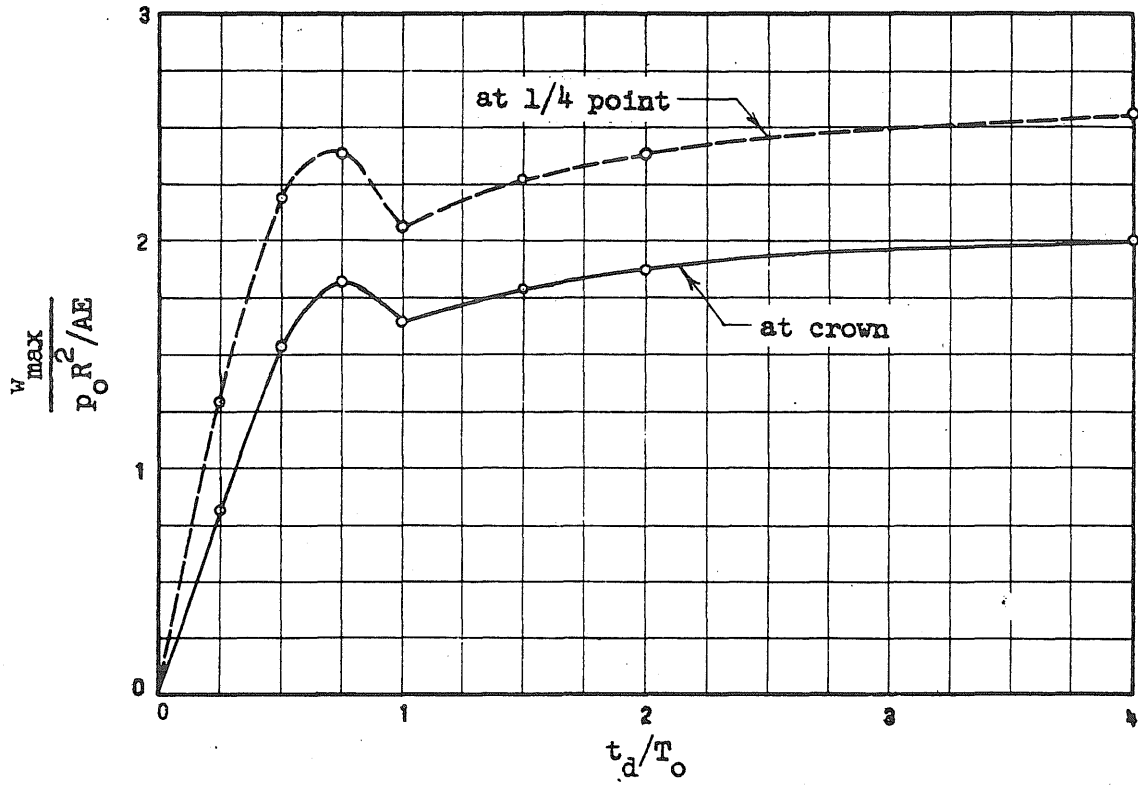


(c) Axial Force, N

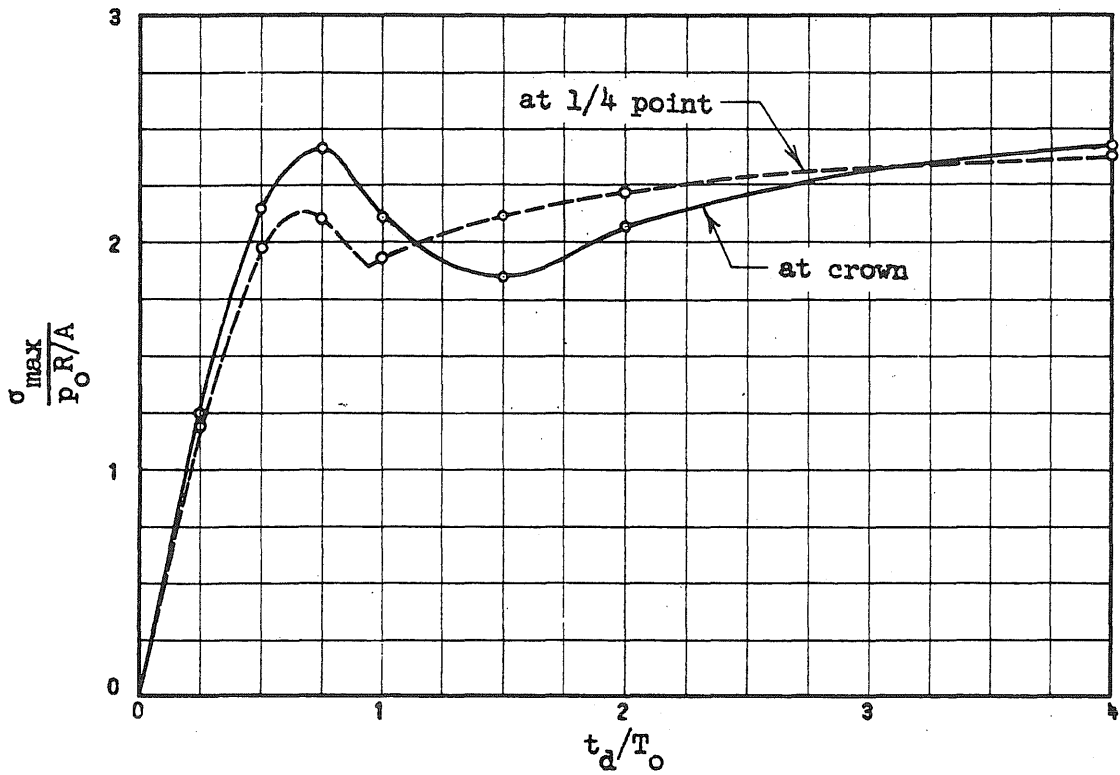


(d) Bending Moment, M

FIG. 4.11 (Continued)



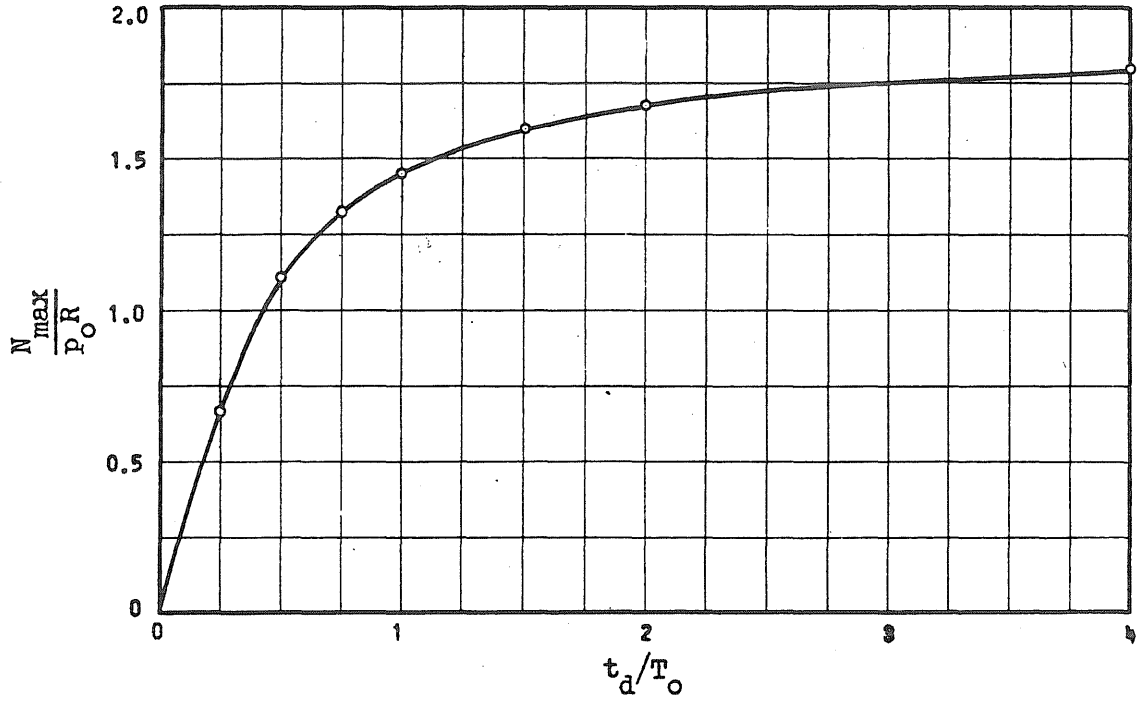
(a) Maximum Radial Displacements, w_{max}



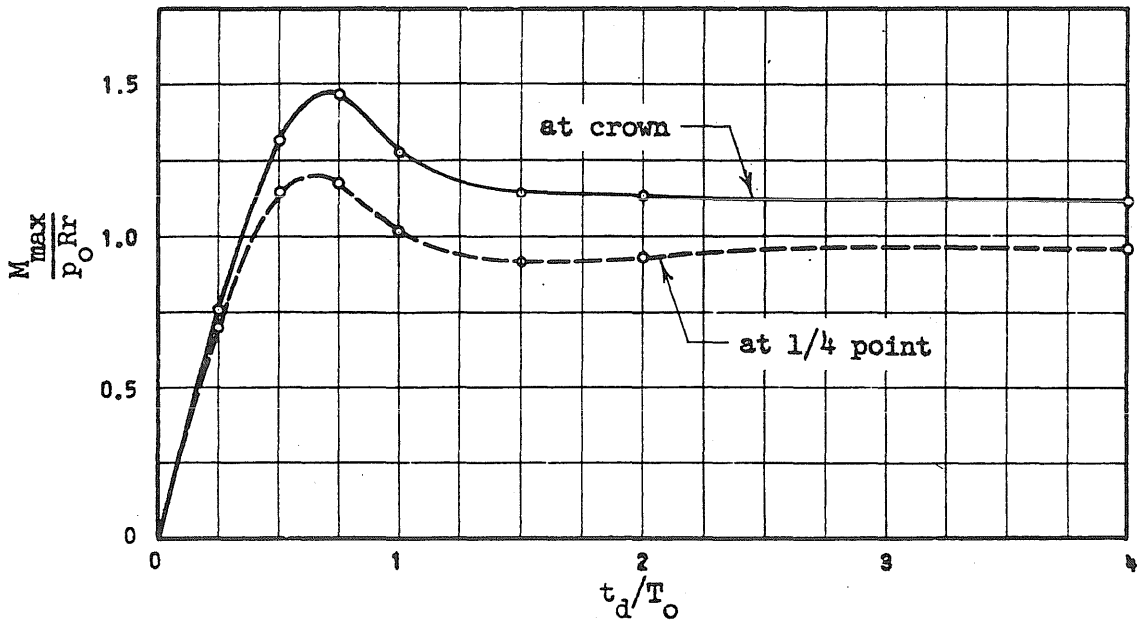
(b) Maximum Stresses, σ_{max} , for $c/r = 1$

FIG. 4.12 RESPONSE SPECTRA FOR AN ARCH UNDER A UNIFORM ALL-AROUND PRESSURE PULSE

$$f/L_0 = 0.2, L_0/r = 100, p_0/p_{cr} = 1.0$$



(c) Maximum Axial Force, N_{max} , at crown



(d) Maximum Moments, M_{max}

FIG. 4.12 (Continued)

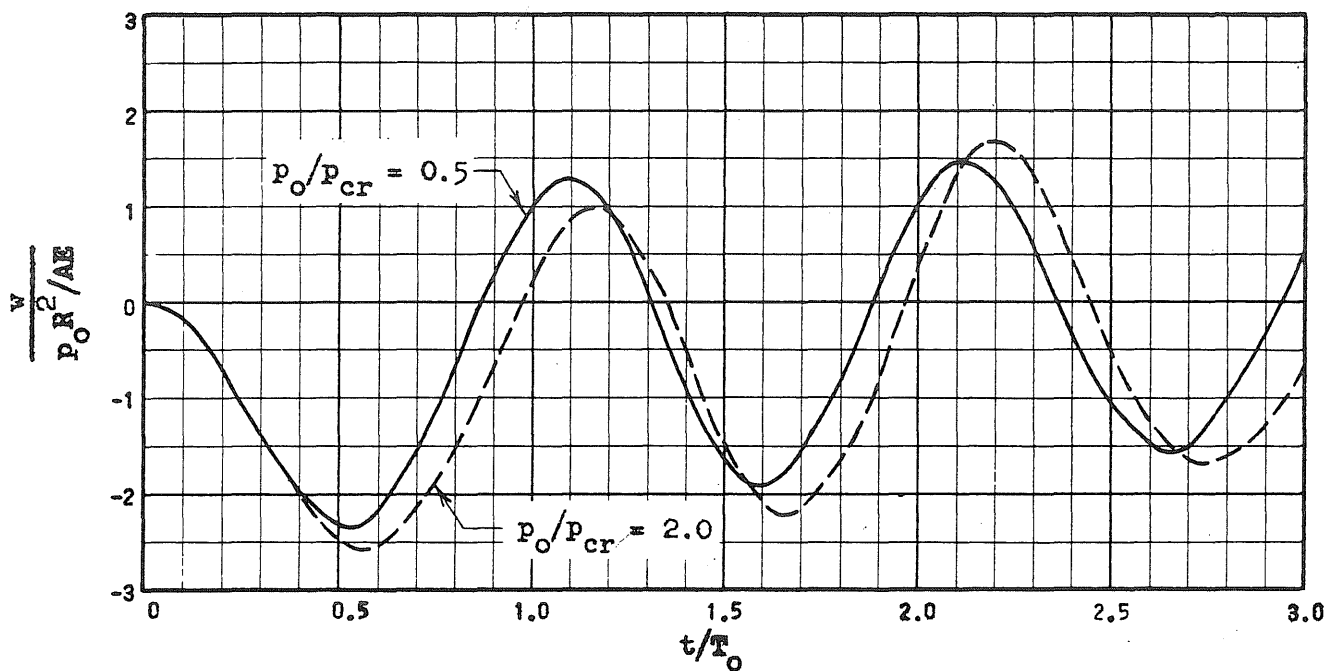
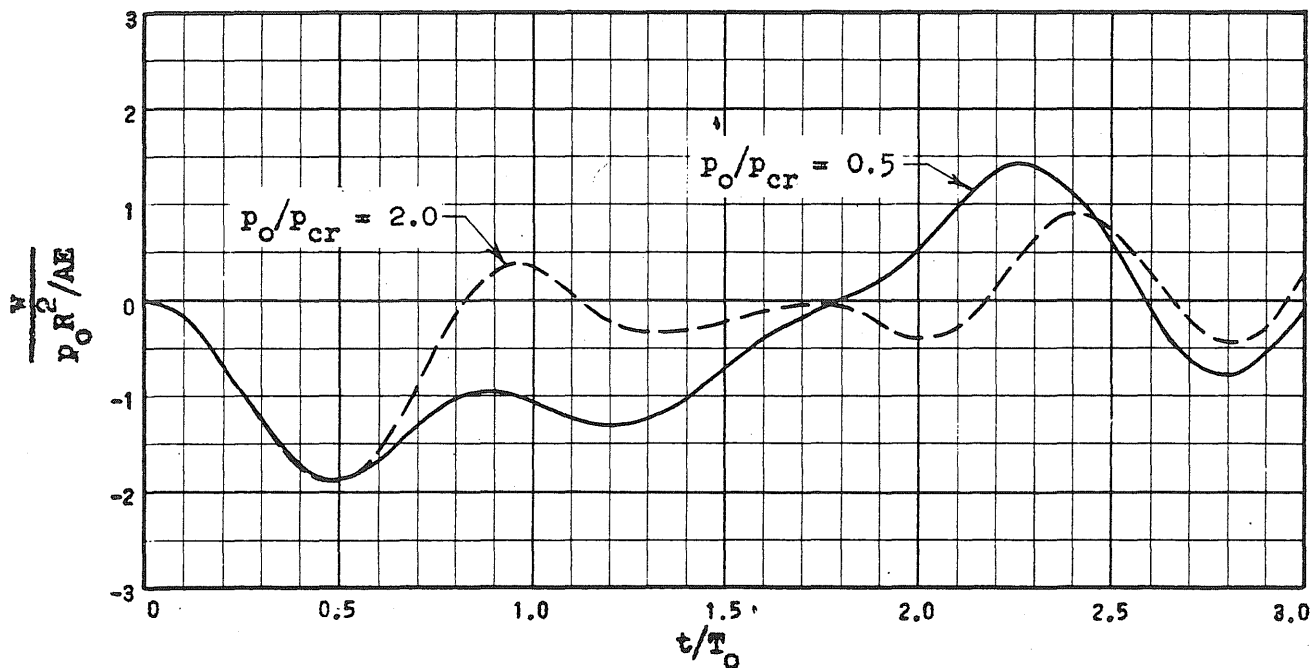
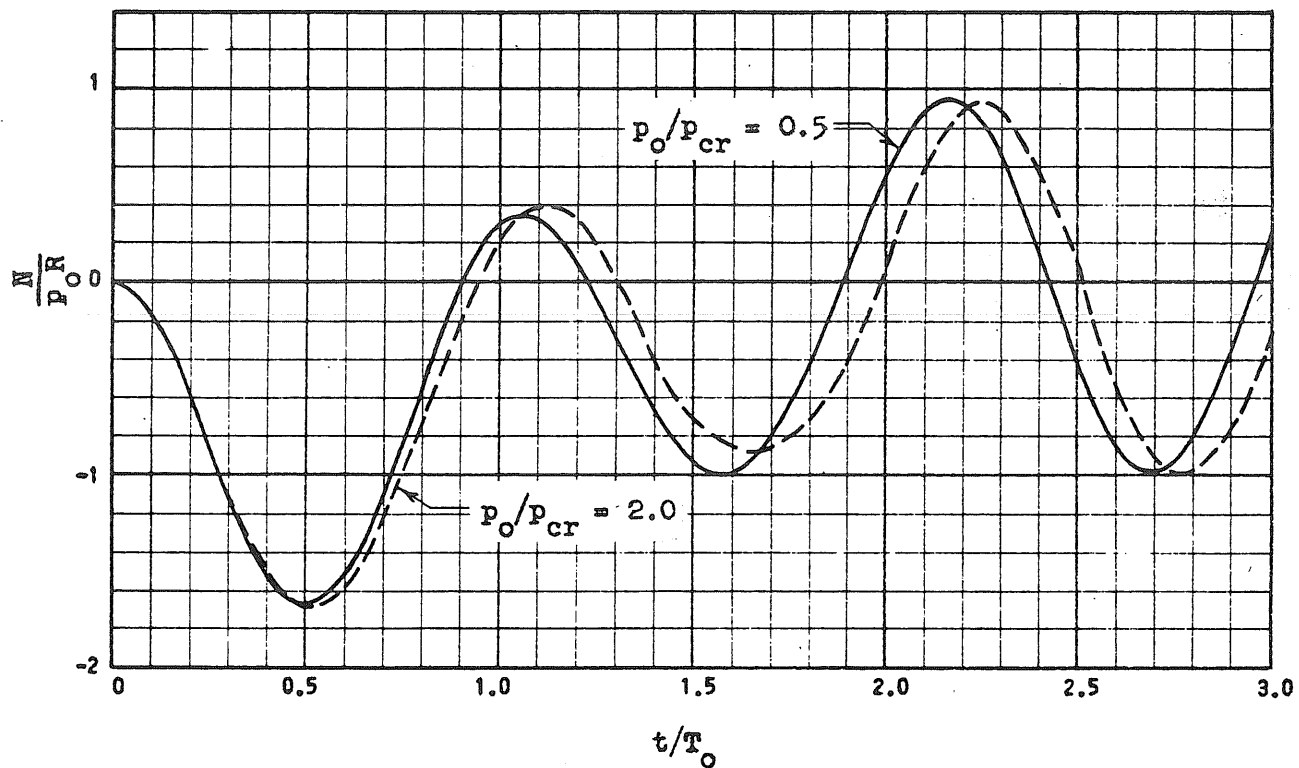
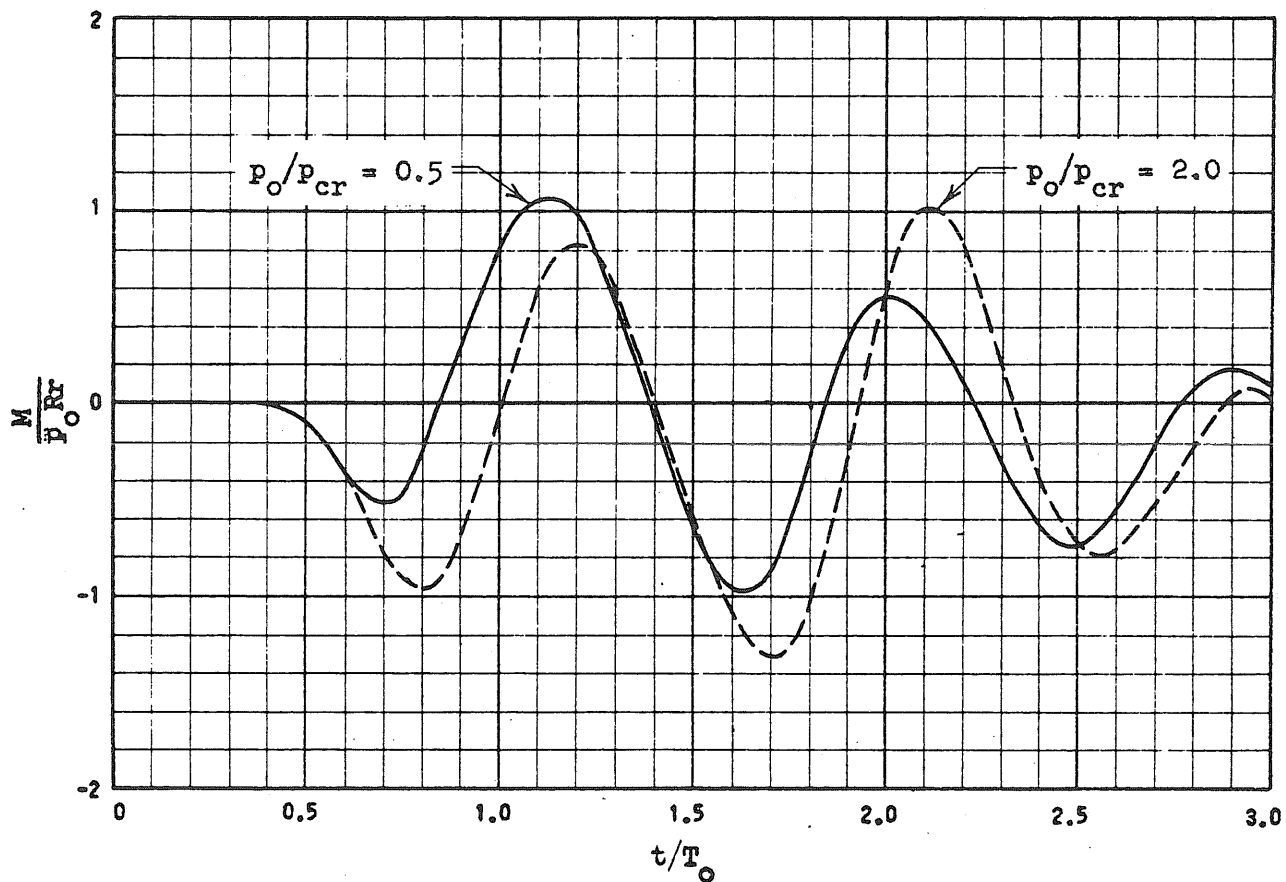
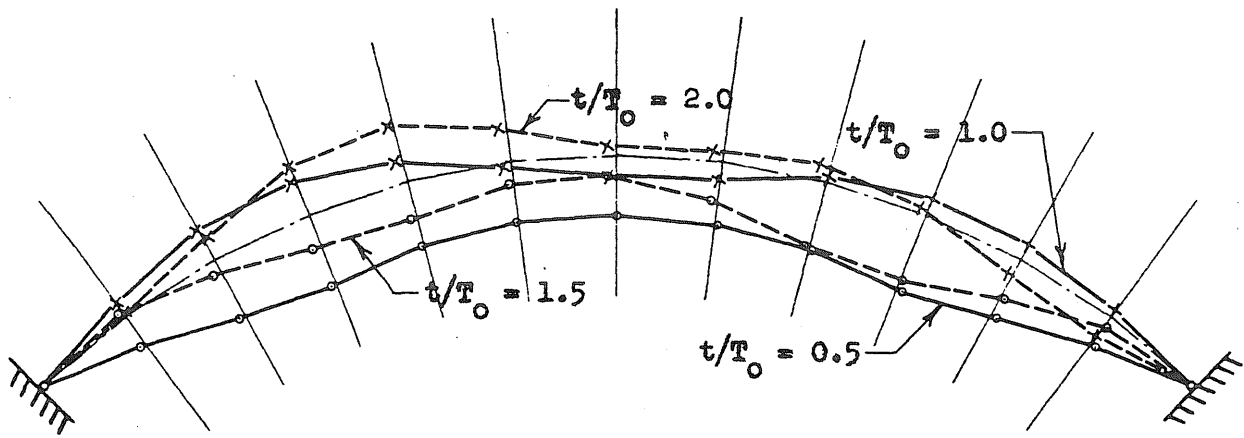
(a) Radial Displacement, w , at $1/4$ point(b) Radial Displacement, w , at crown

FIG. 4.13 EFFECT OF PEAK PRESSURE ON RESPONSE FOR A UNIFORM ALL-AROUND PRESSURE PULSE

$$f/L_0 = 0.2, L_0/r = 100, t_d/T_0 = 2.0$$

(c) Axial Force, N , at crown(d) Bending Moment, M , at crown



(a) Displacement Configurations

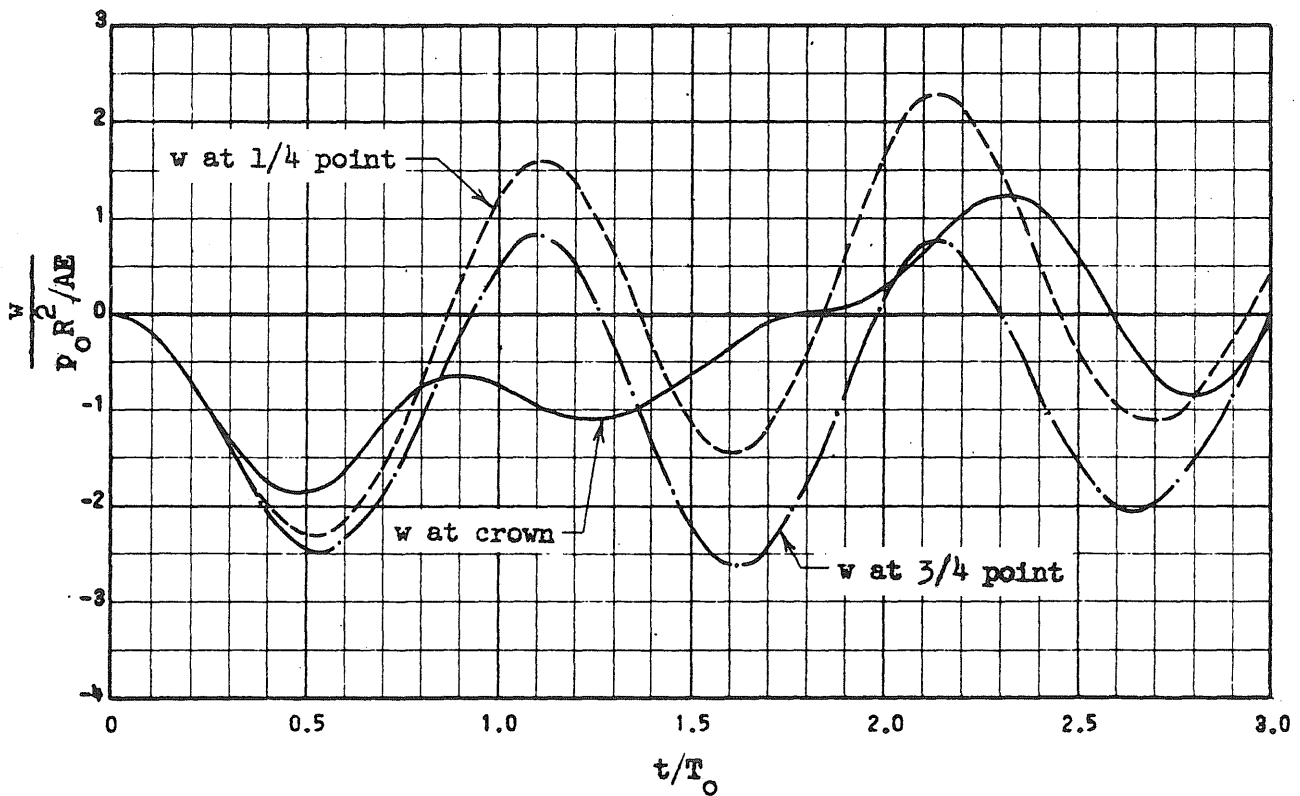
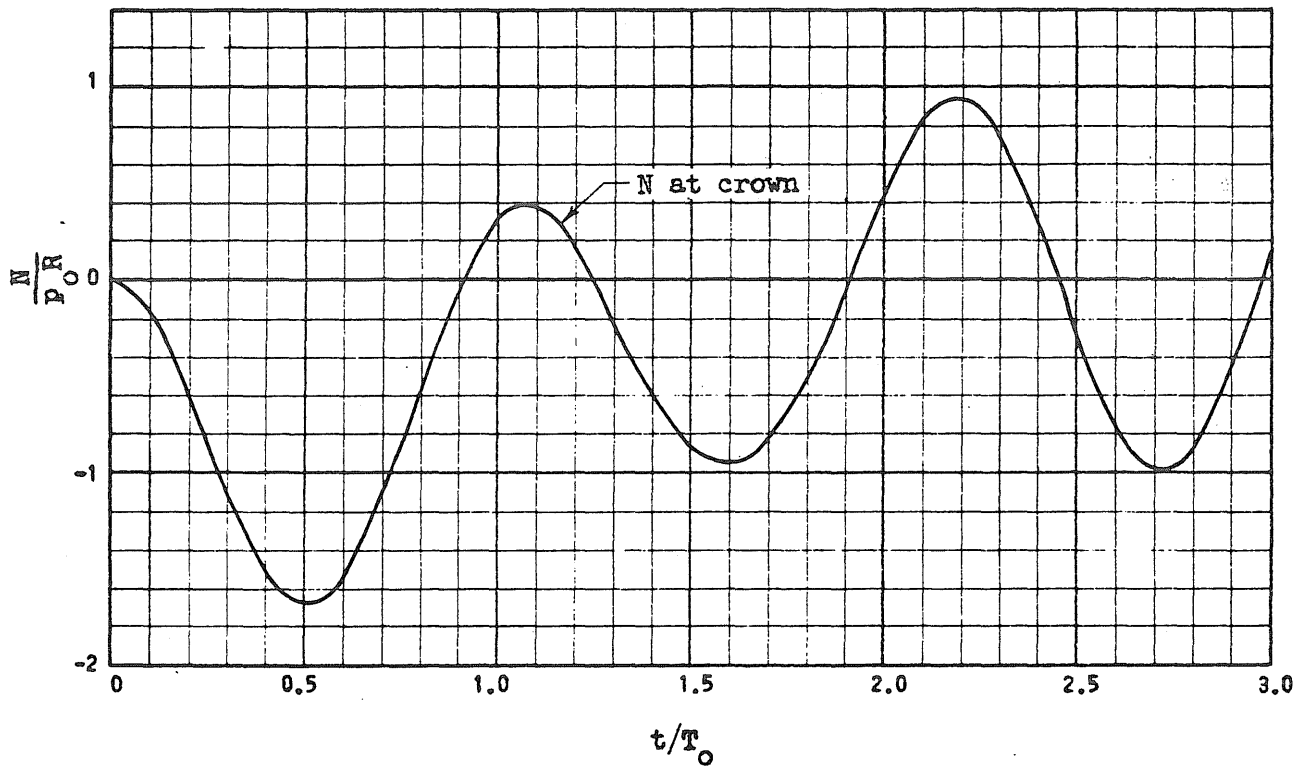
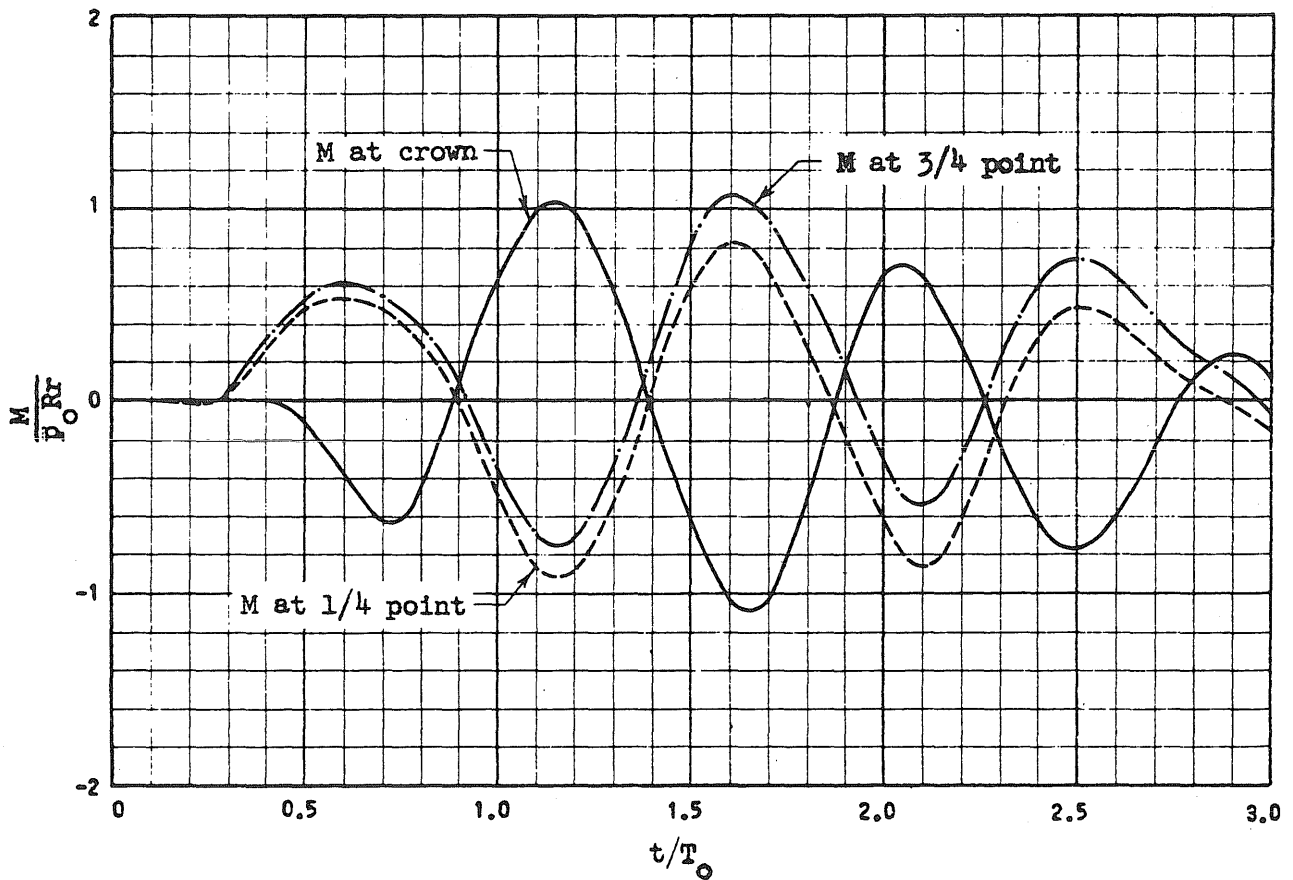
(b) Radial Displacement, w

FIG. 4.14 EFFECT OF INITIAL OUT-OF-ROUNDNESS ON RESPONSE FOR A UNIFORM ALL-AROUND PRESSURE PULSE

$$f/L_0 = 0.2, L_0/r = 100, p_0/p_{cr} = 1.0, t_d/T_0 = 2.0, \bar{w}_m/L_0 = 0.001$$

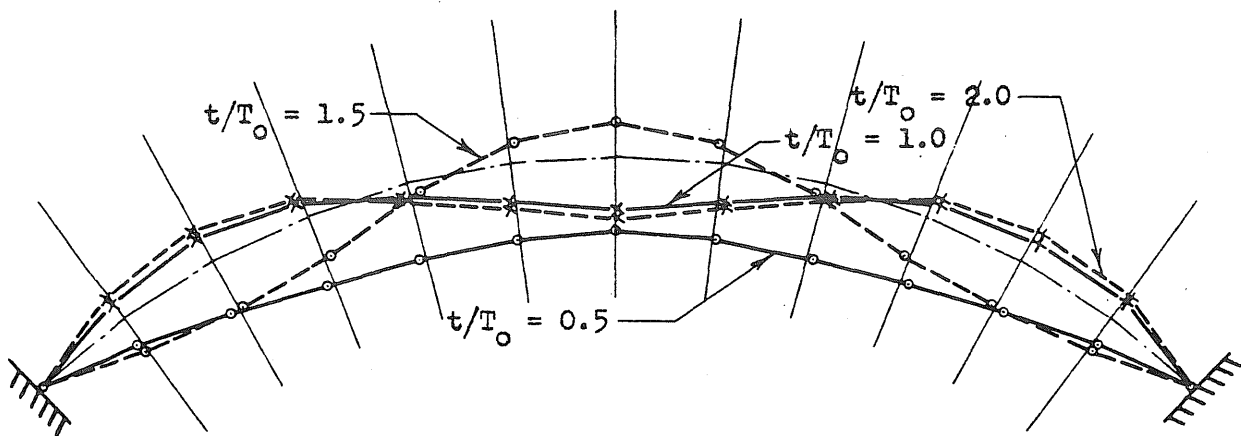


(c) Axial Force, N

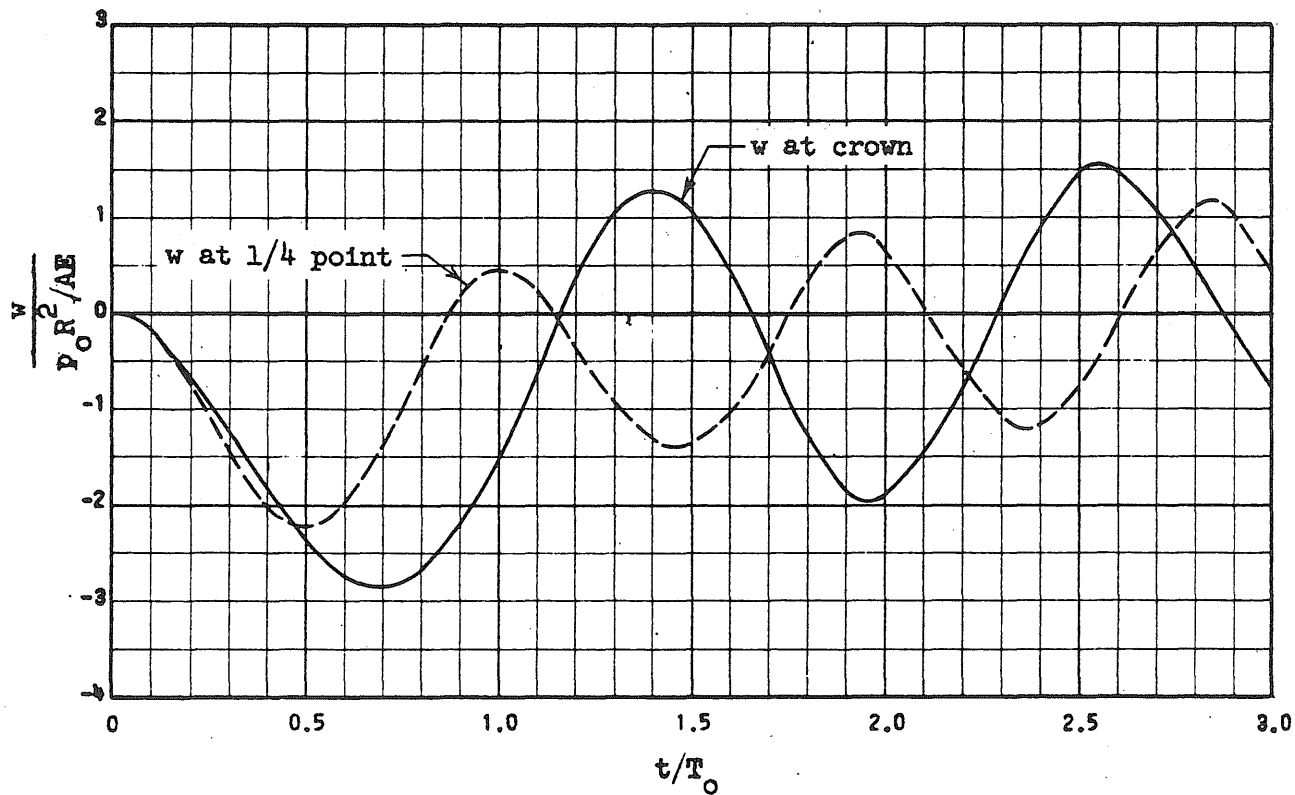


(d) Bending Moment, M

FIG. 4.14 (Continued)



(a) Displacement Configurations



(b) Radial Displacement, w

FIG. 4.15 RESPONSE CURVES FOR AN ARCH UNDER A UNIFORM ALL-AROUND PRESSURE PULSE-- $L_0/r = 50$

$$f/L_0 = 0.2, p_0/p_{cr} = 1.0, t_d/T_0 = 2.0$$

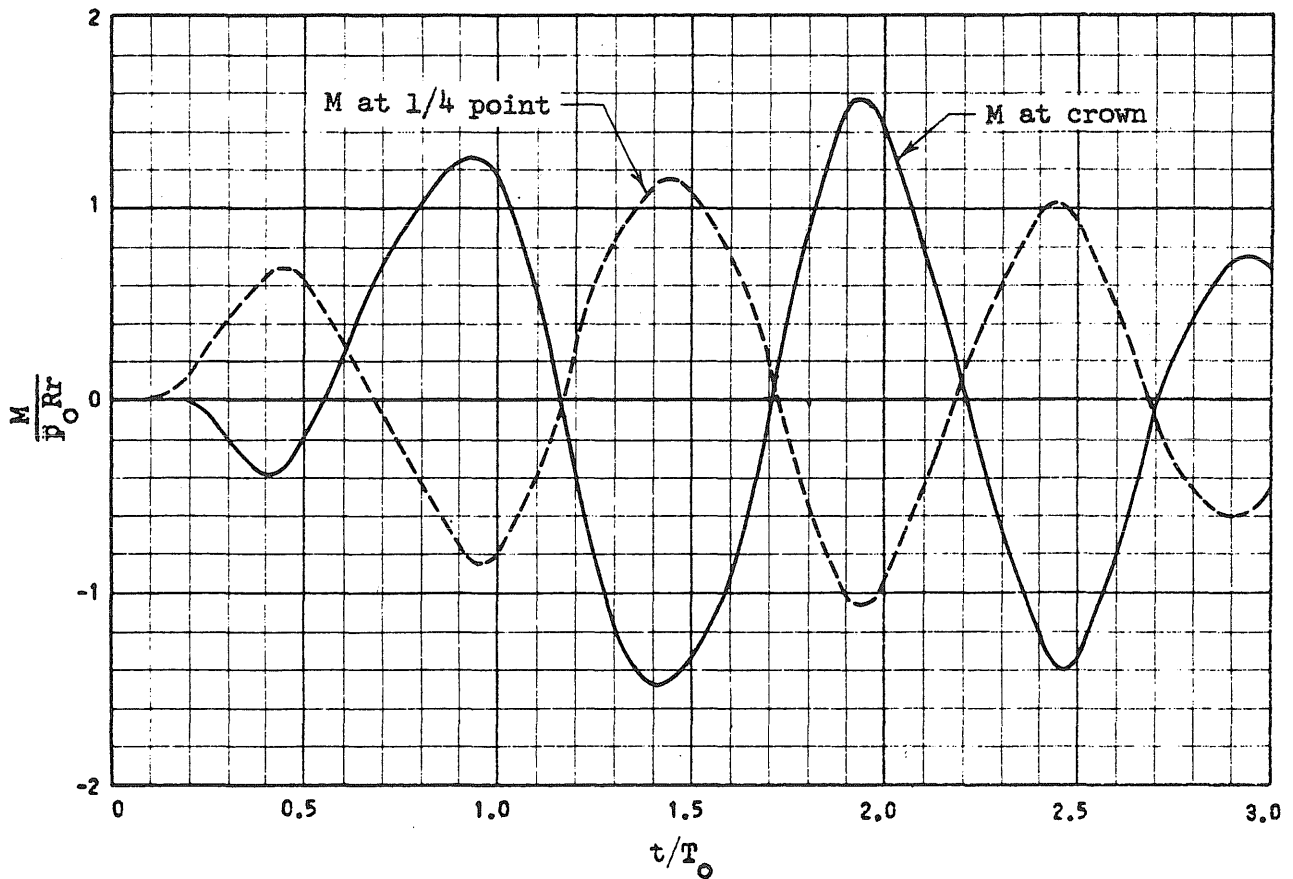
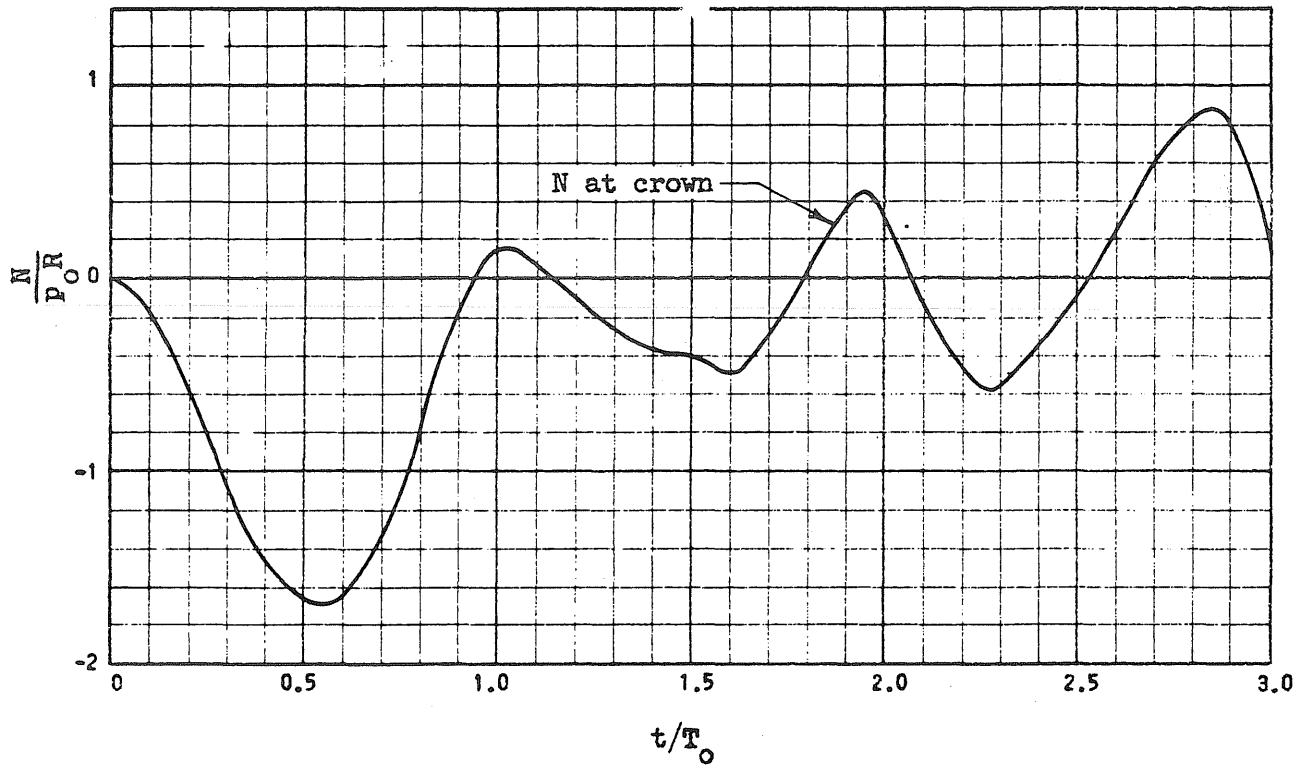
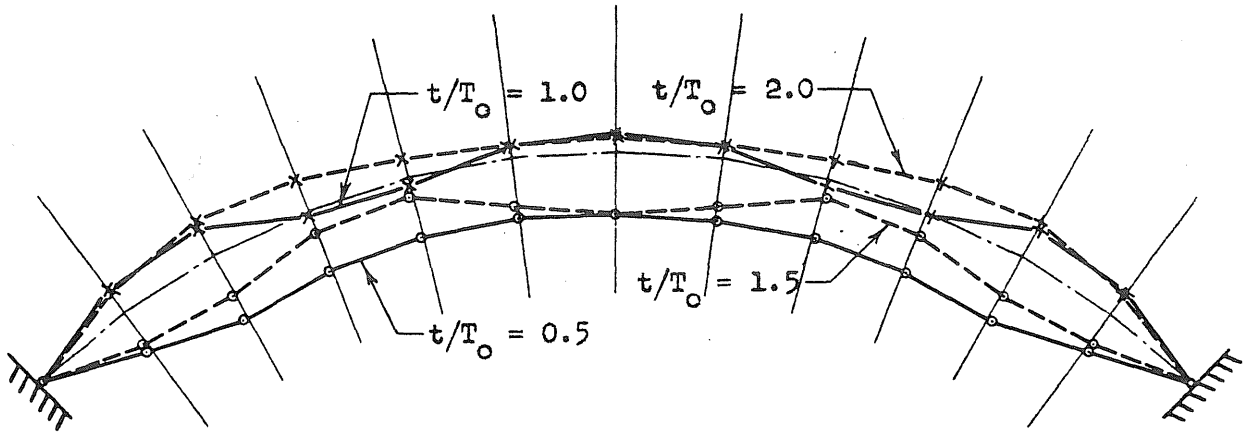
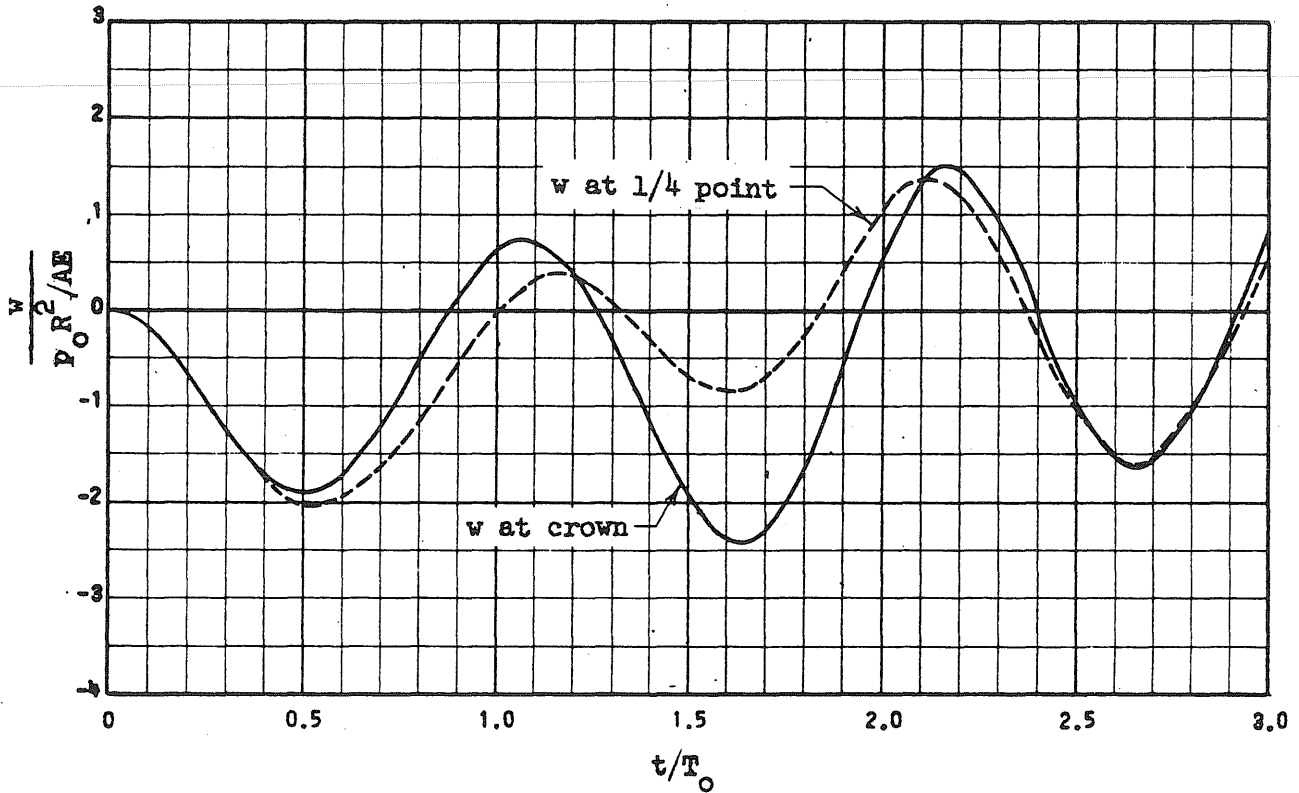


FIG. 4.15 (Continued)



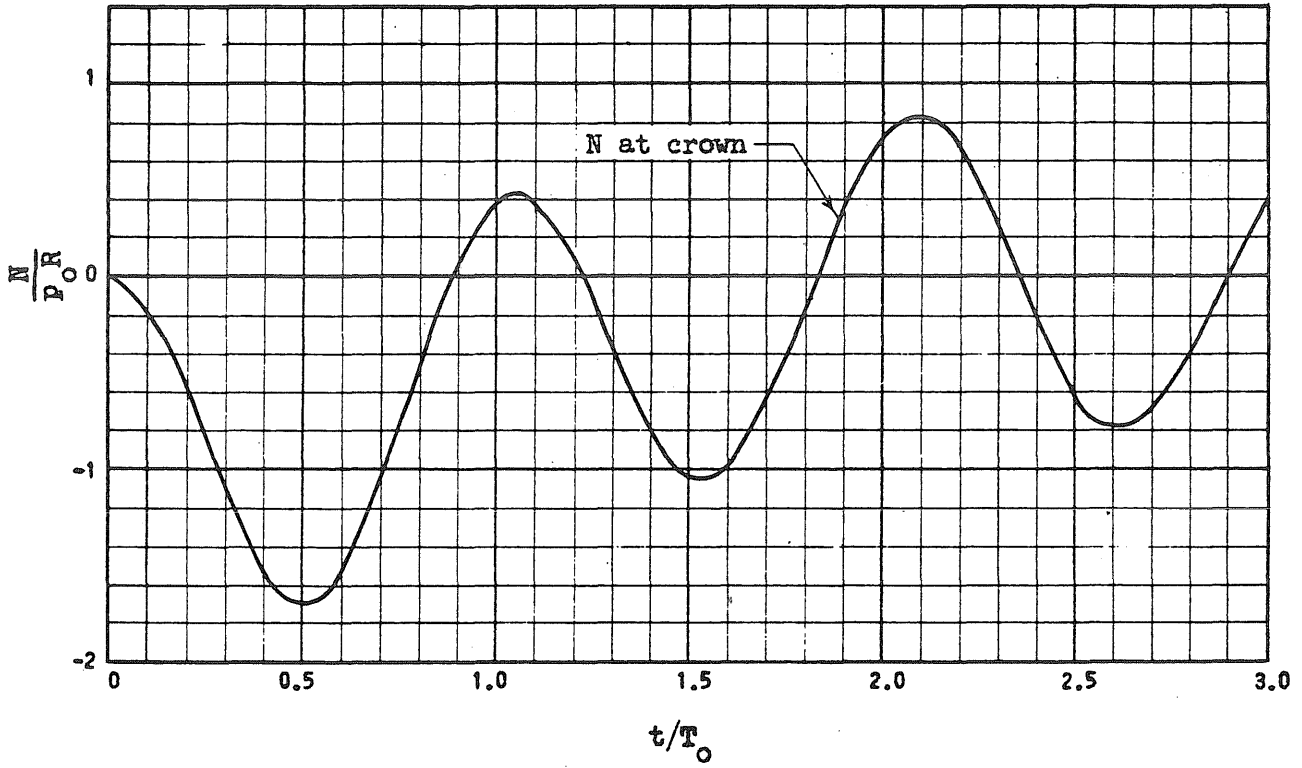
(a) Displacement Configurations



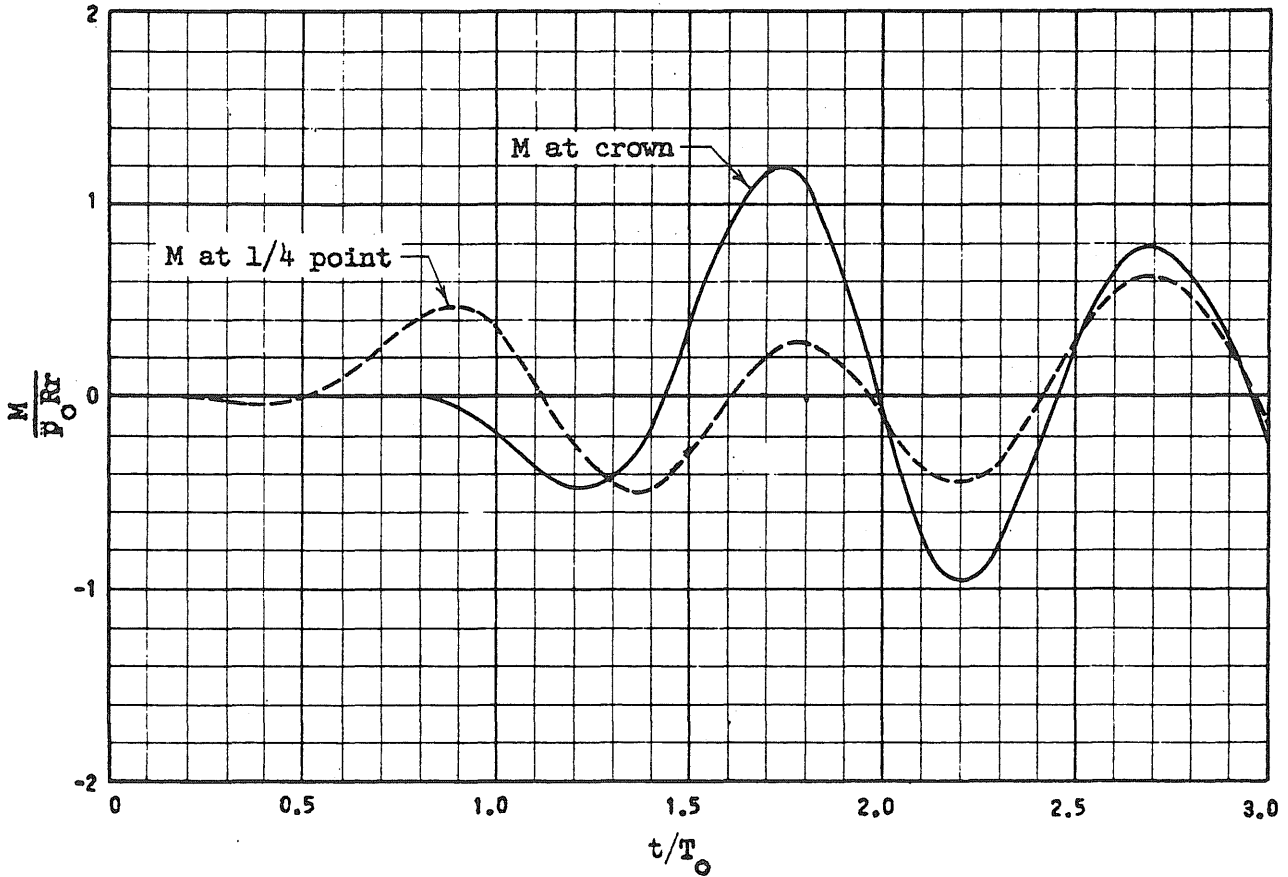
(b) Radial Displacement, w

FIG. 4.16 RESPONSE CURVES FOR AN ARCH UNDER A UNIFORM ALL-AROUND PRESSURE PULSE-- $L_0/r = 200$

$$f/L_0 = 0.2, p_0/p_{cr} = 1.0, t_d/T_0 = 2.0$$

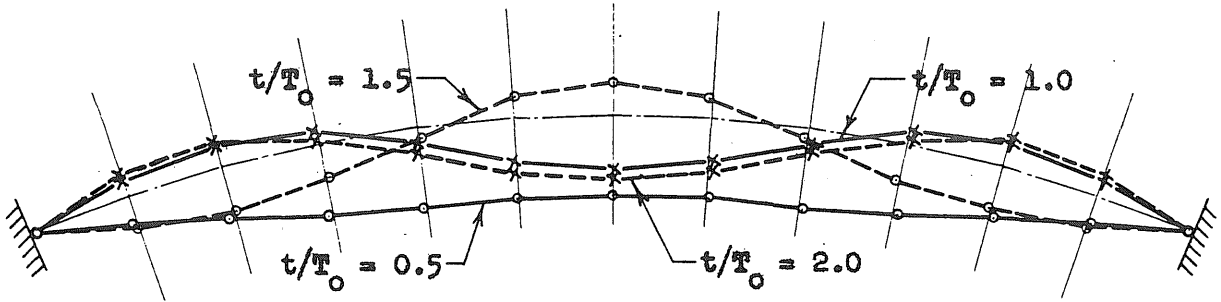


(c) Axial Force, N

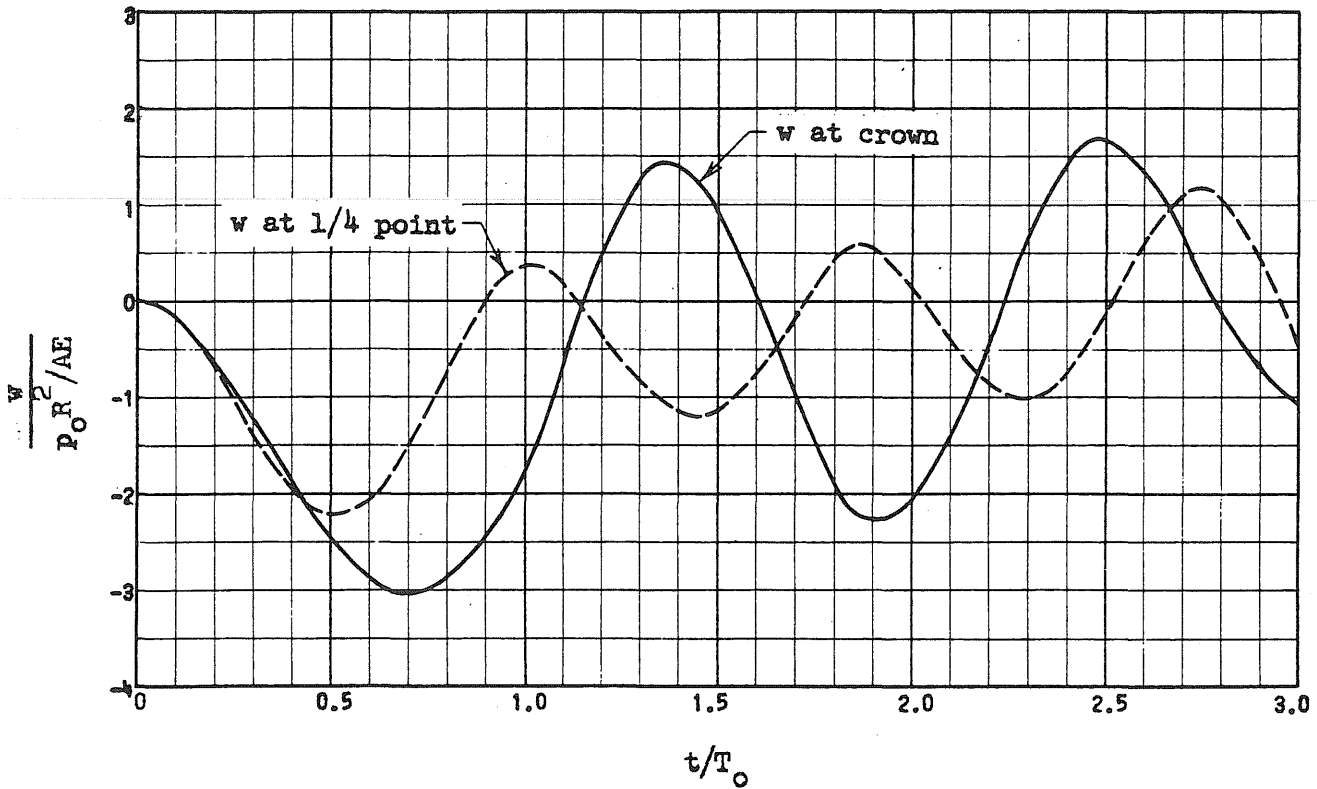


(d) Bending Moment, M

FIG. 4.16 (Continued)

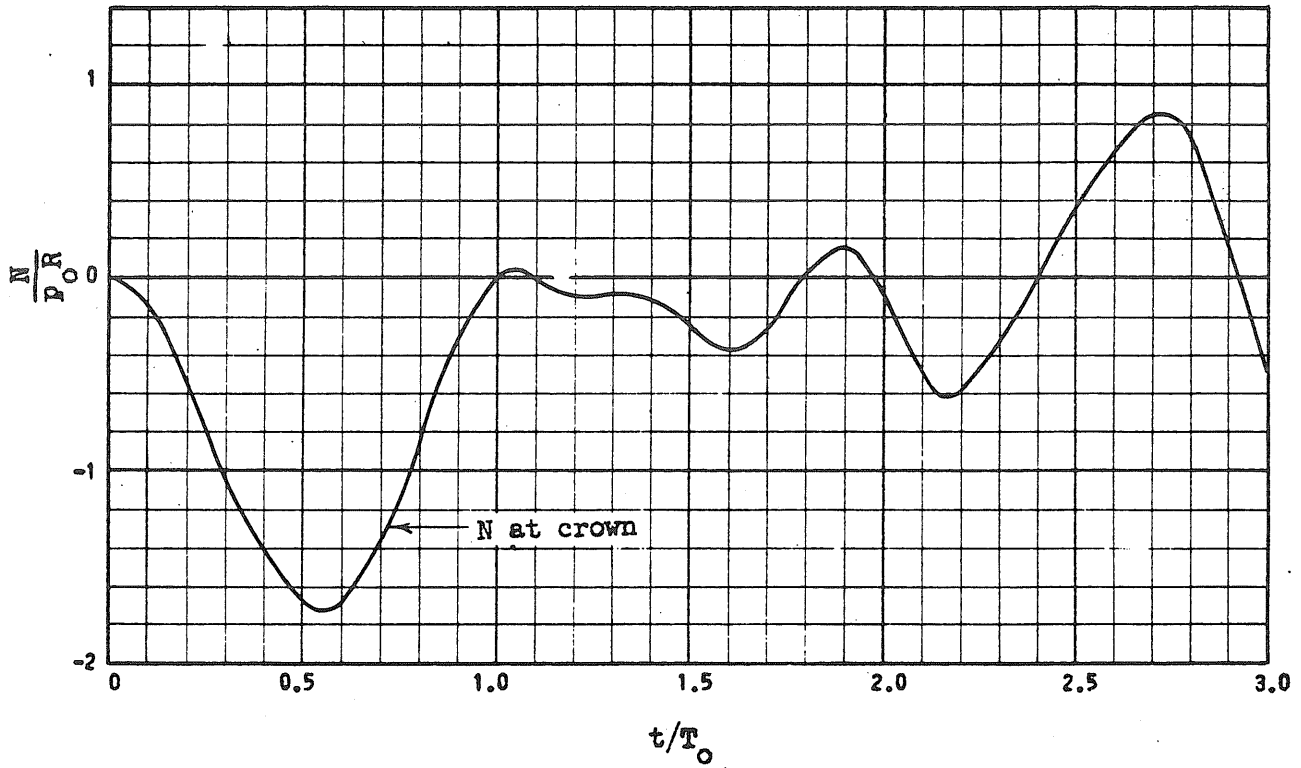


(a) Displacement Configurations

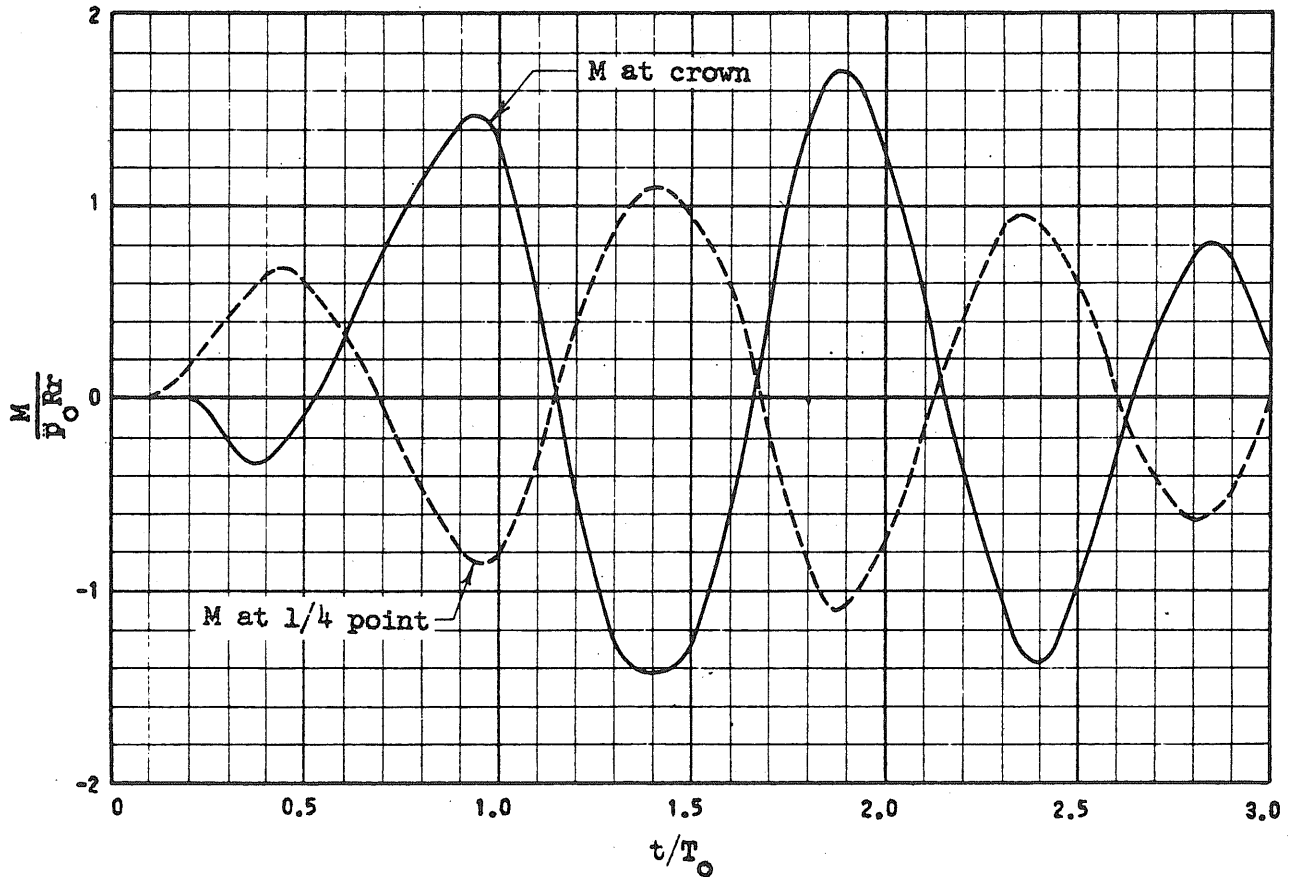


(b) Radial Displacement, w

FIG. 4.17 RESPONSE CURVES FOR AN ARCH UNDER A UNIFORM ALL-AROUND PRESSURE PULSE-- $f/L_0 = 0.1$
 $L_0/r = 100, P_0/P_{cr} = 1.0, t_d/T_0 = 2.0$



(c) Axial Force, N



(d) Bending Moment, M

FIG. 4.17 (Continued)

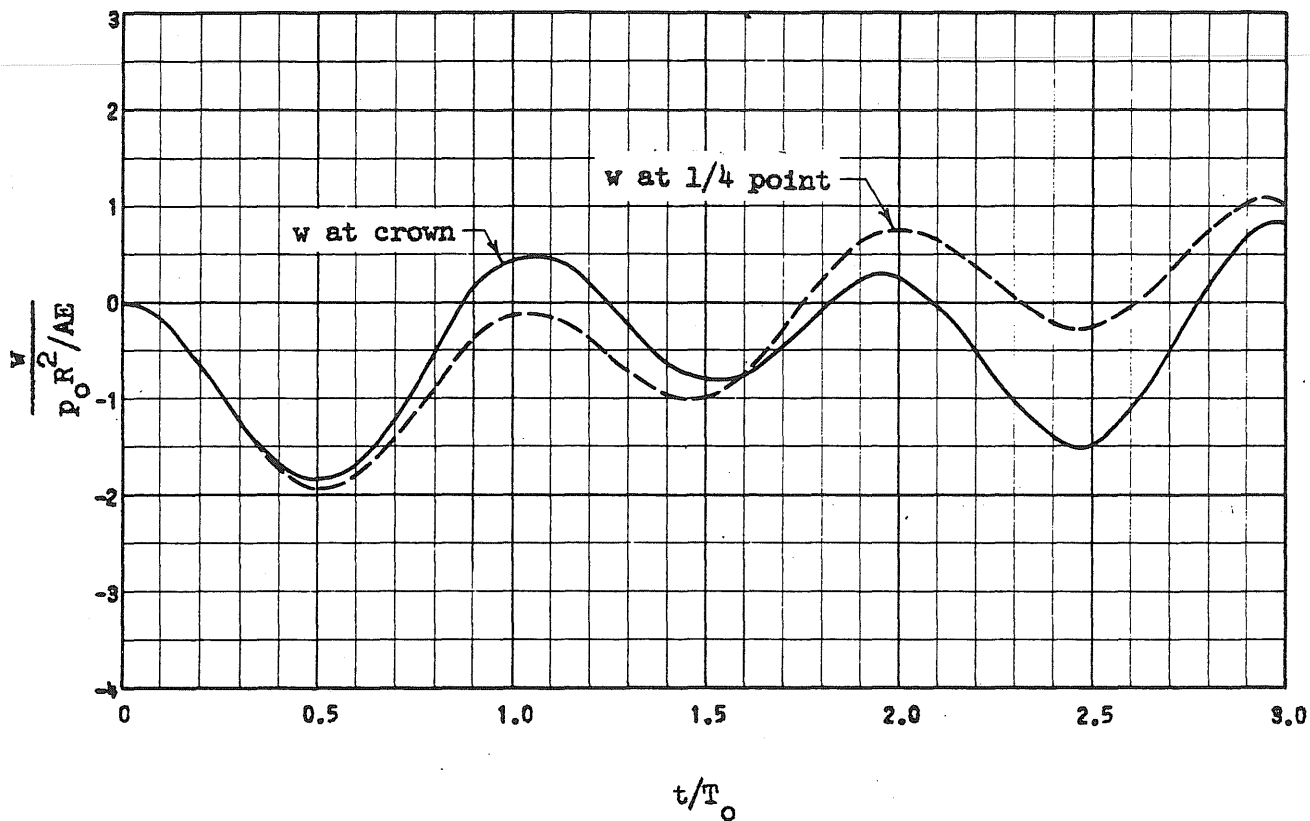
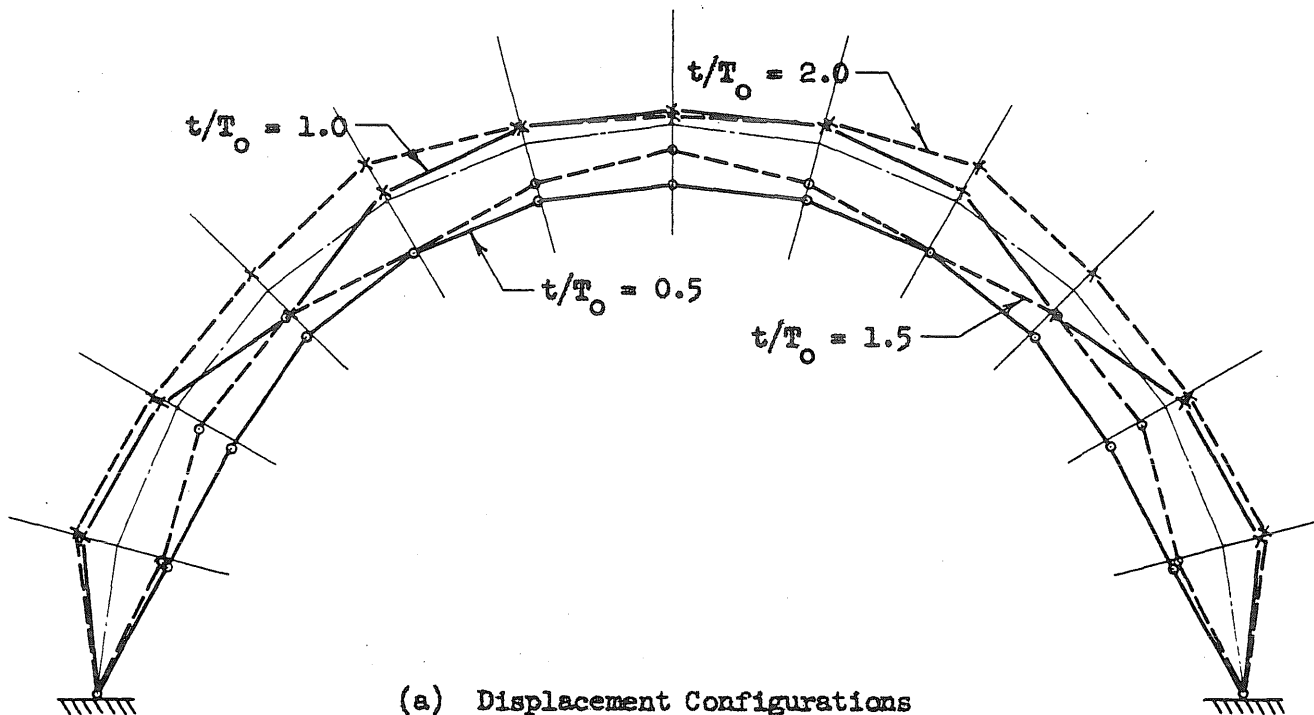
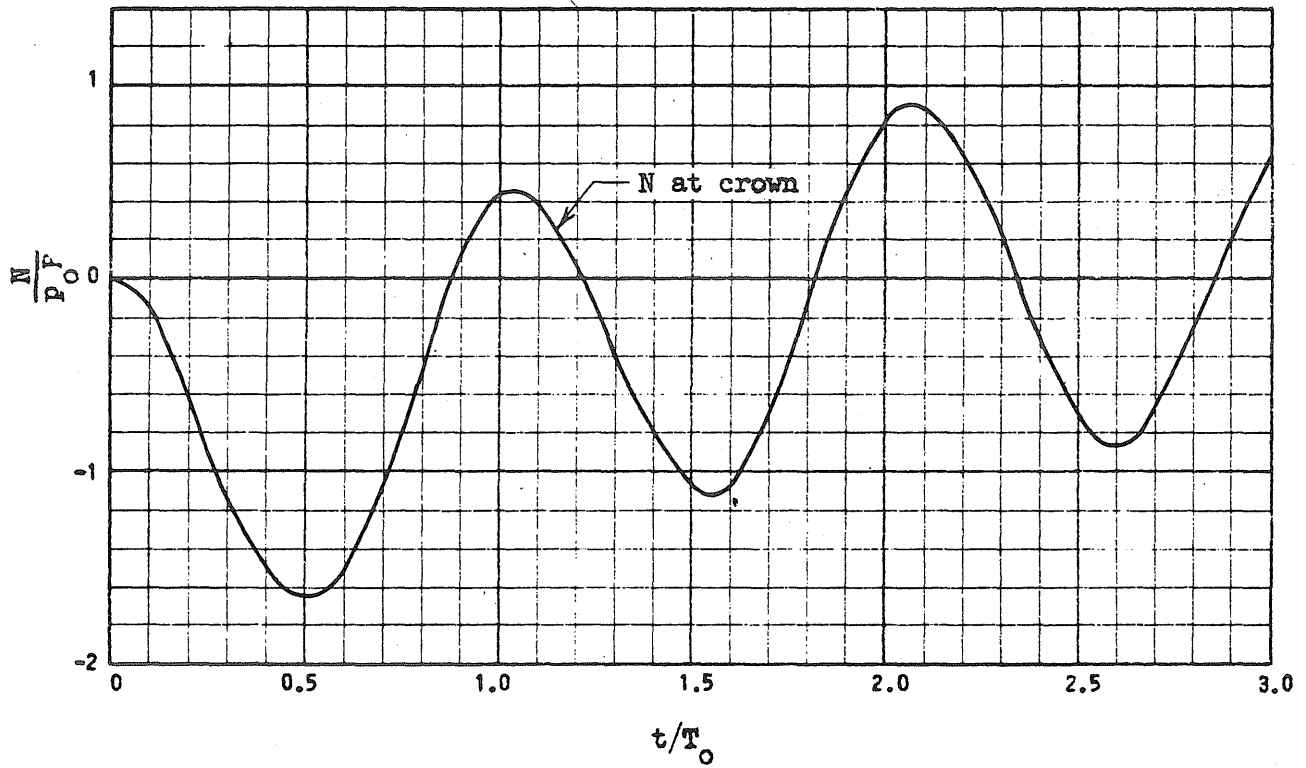
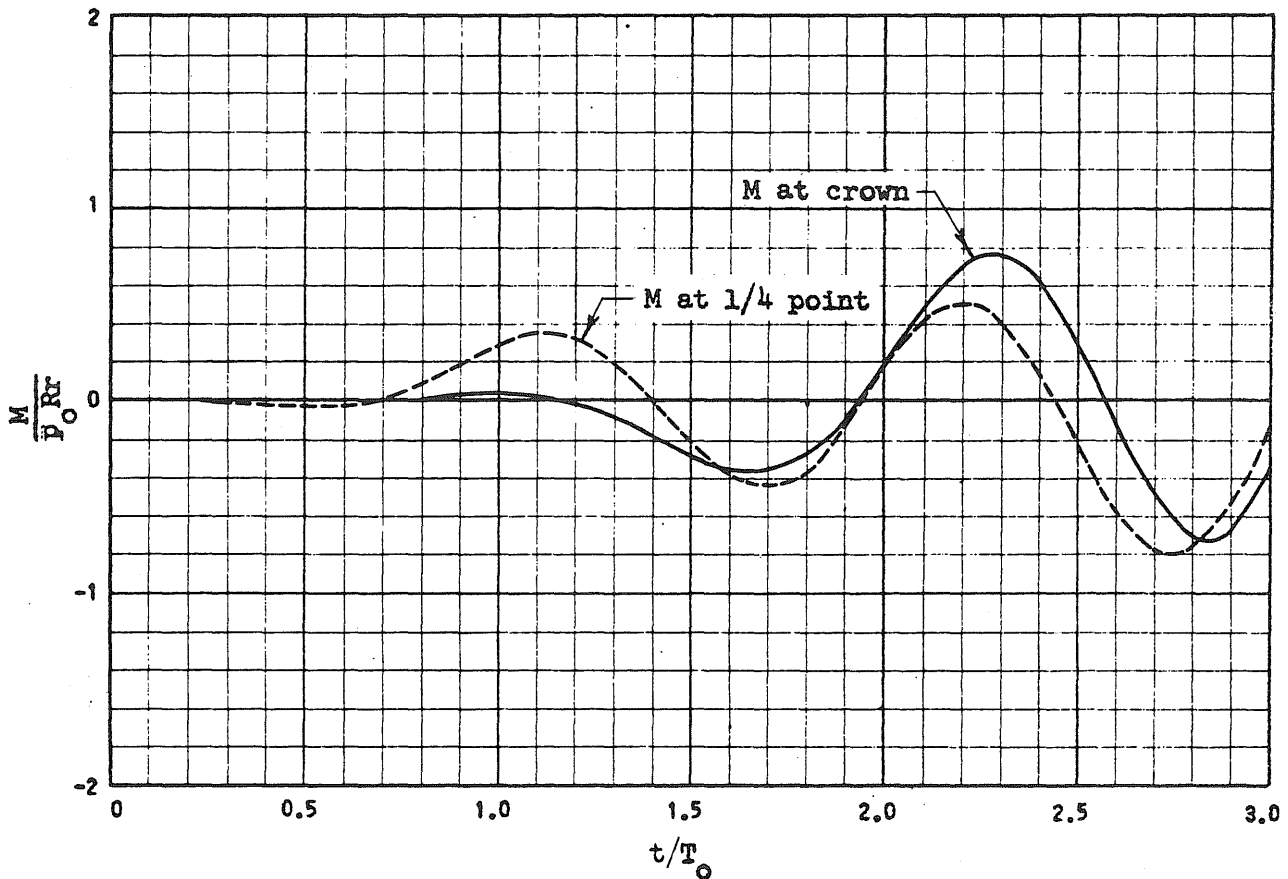


FIG. 4.18 RESPONSE CURVES FOR AN ARCH UNDER A UNIFORM ALL-AROUND PRESSURE PULSE-- $f/L_0 = 0.5$

$$L_0/r = 100, p_0/p_{cr} = 1.0, t_d/T_0 = 2.0$$

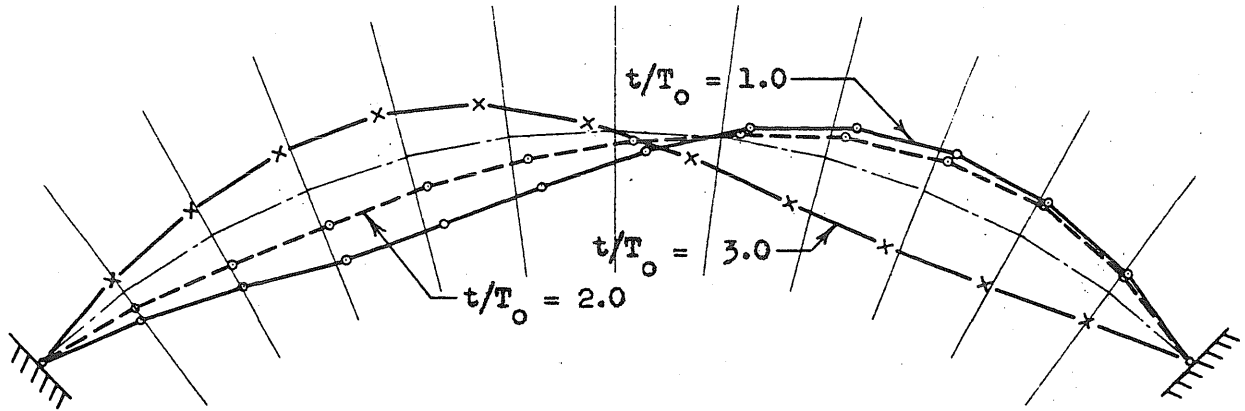
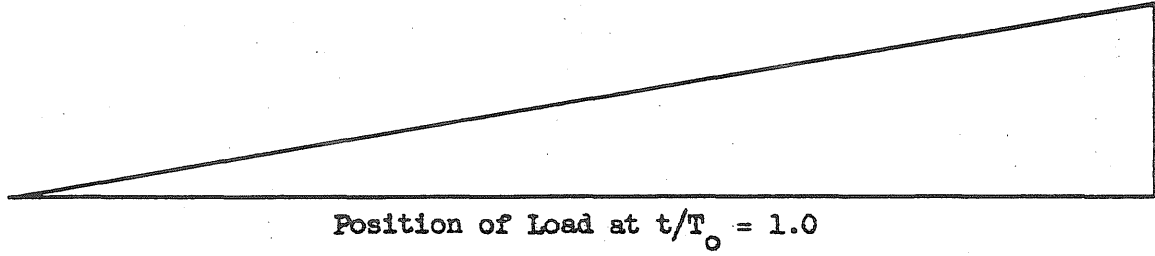


(c) Axial Force, N

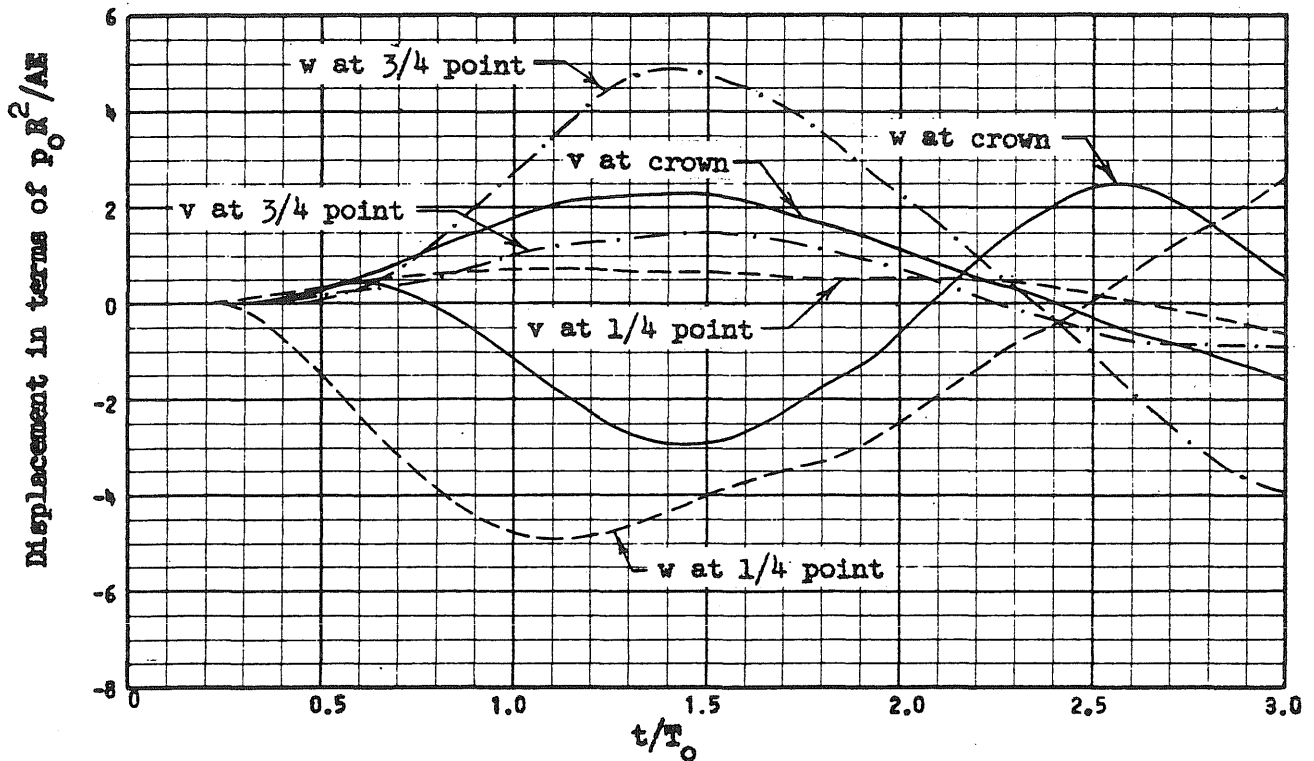


(d) Bending Moment, M

FIG. 4.18 (Continued)



(a) Displacement Configurations



(b) Radial and Tangential Displacements, w and v

FIG. 5.1 TYPICAL RESPONSE CURVES FOR AN ARCH SUBJECTED TO A TRIANGULAR MOVING PRESSURE

$f/L_0 = 0.2, L_0/r = 100, p_0/p_{cr} = 1.0, t_t/T_0 = 1.0, t_d/t_t = 1.0$

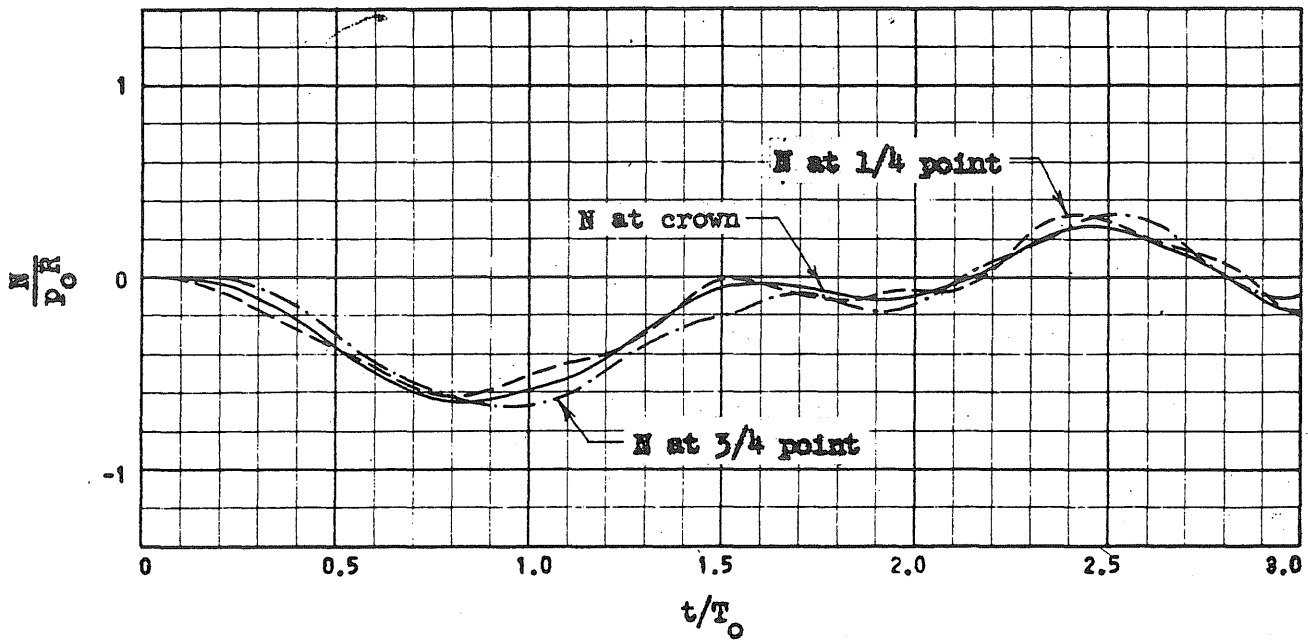
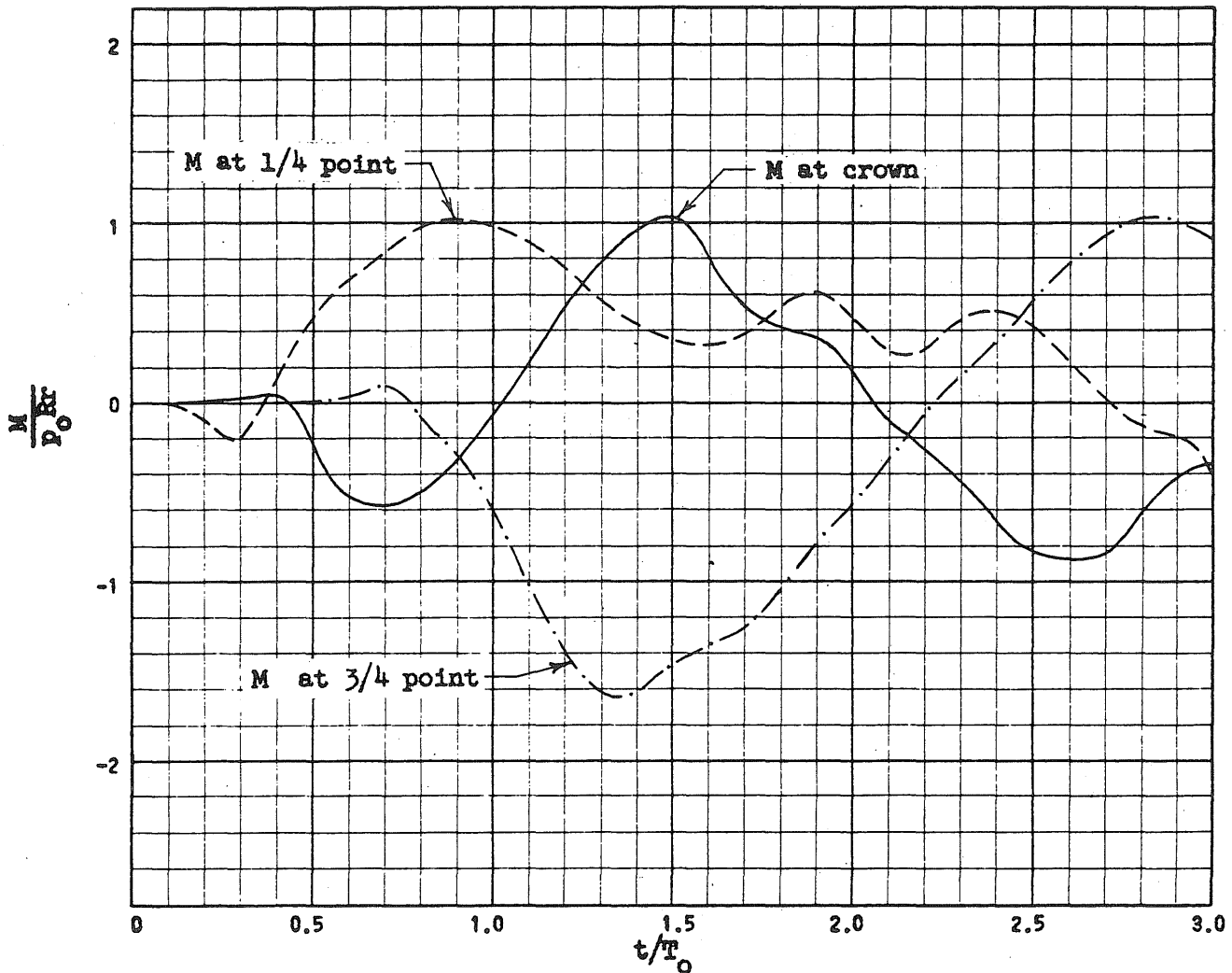
(c) Axial Force, N (d) Bending Moment, M

FIG. 5.1 (Continued)

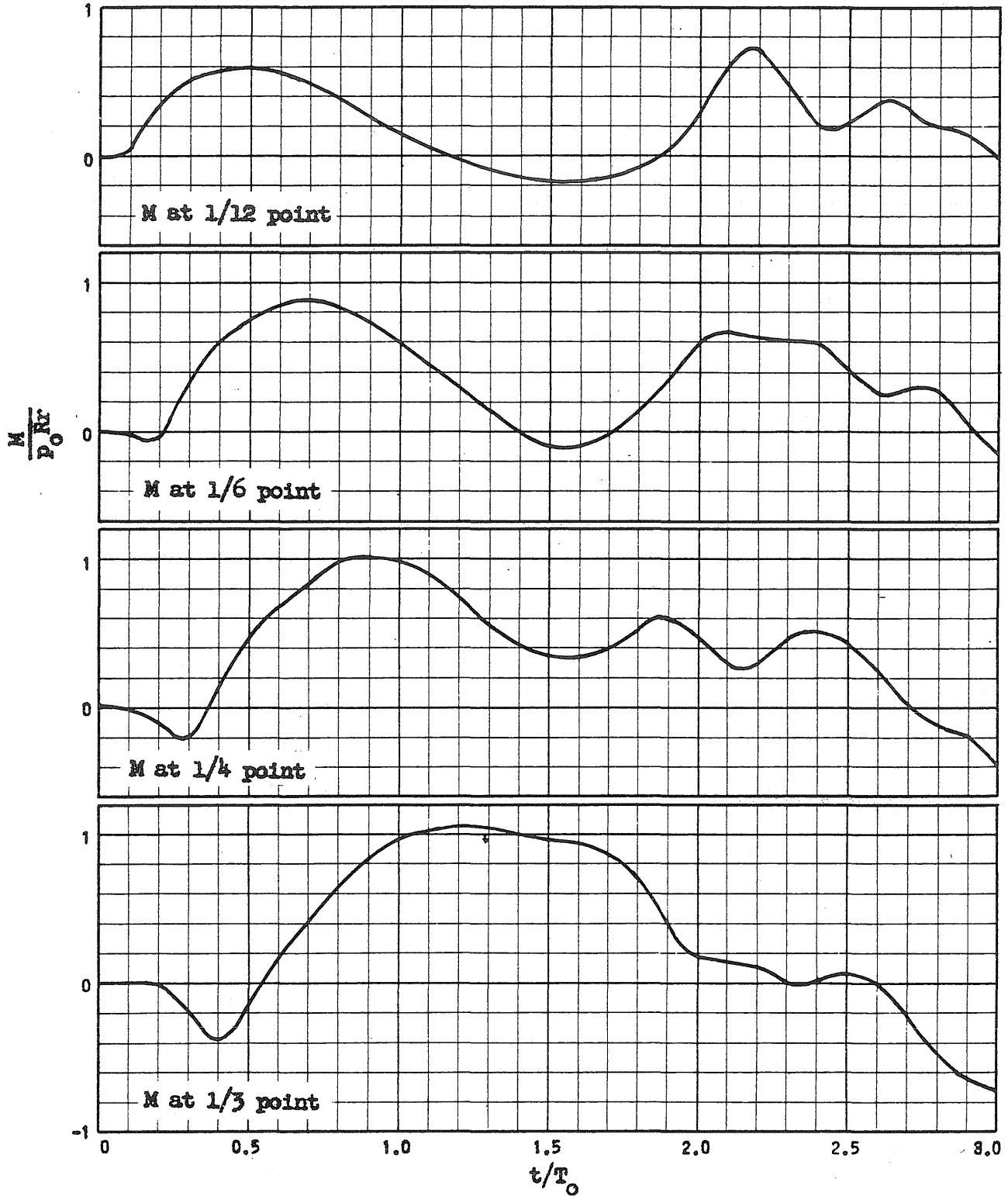


FIG. 5.2 RESPONSE CURVES OF BENDING MOMENT IN AN ARCH
FOR A TRIANGULAR MOVING PRESSURE

$$f/L_0 = 0.2, L_0/r = 100, p_0/p_{cr} = 1.0, t_d/T_0 = 1.0, t_d/t_t = 1.0$$

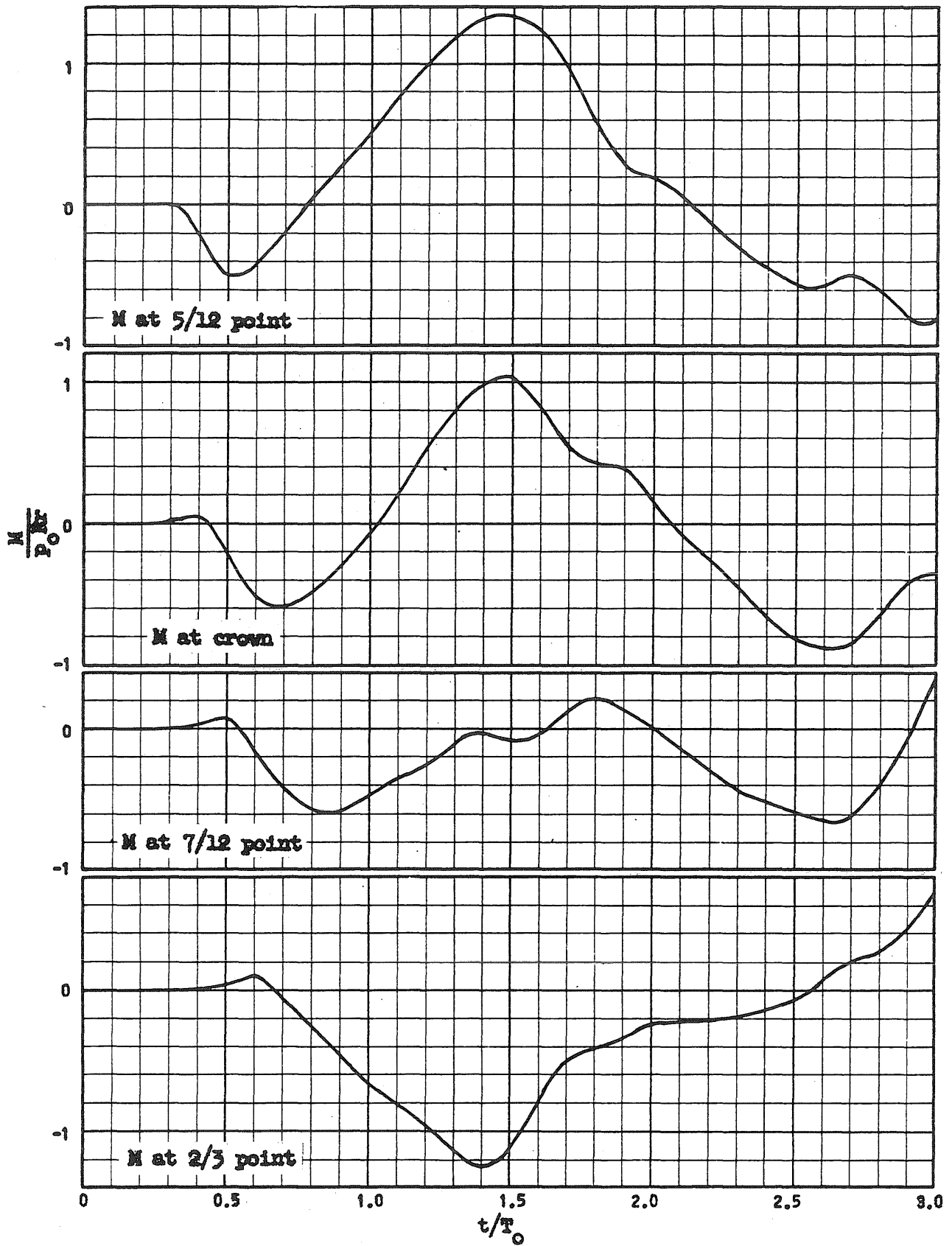


FIG. 5.2 (Continued)

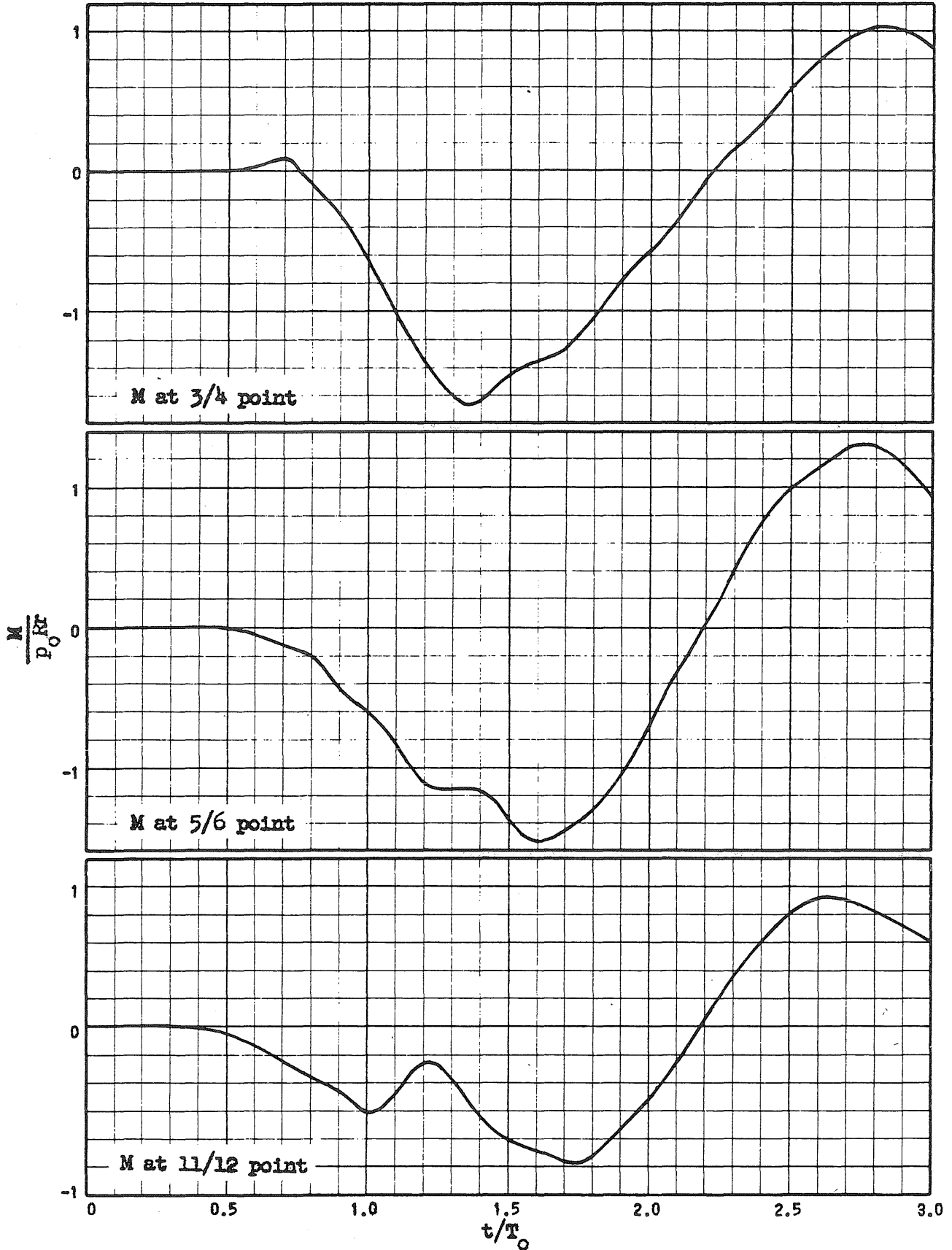
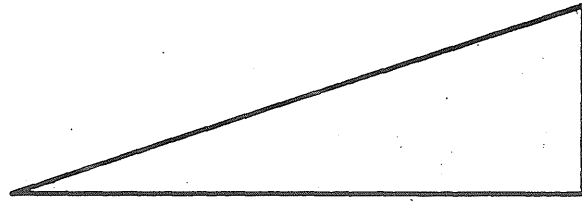
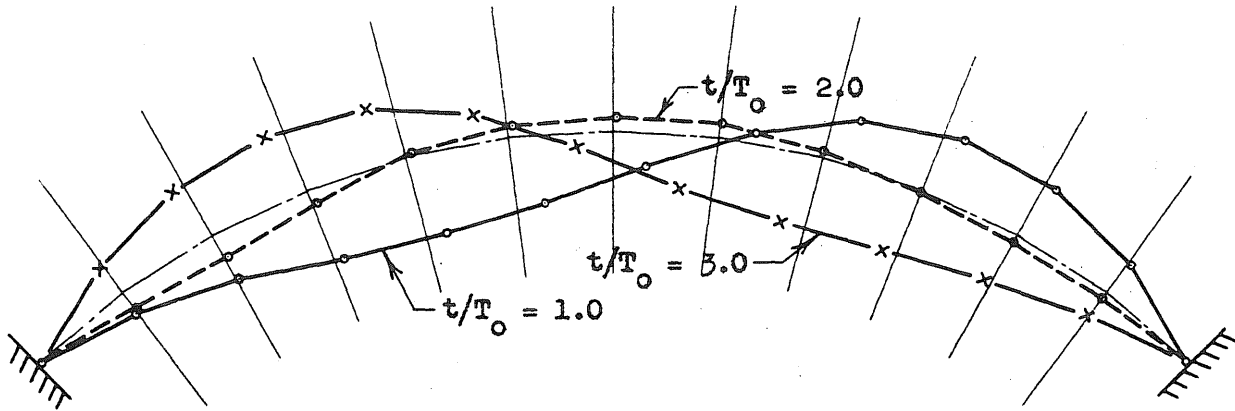


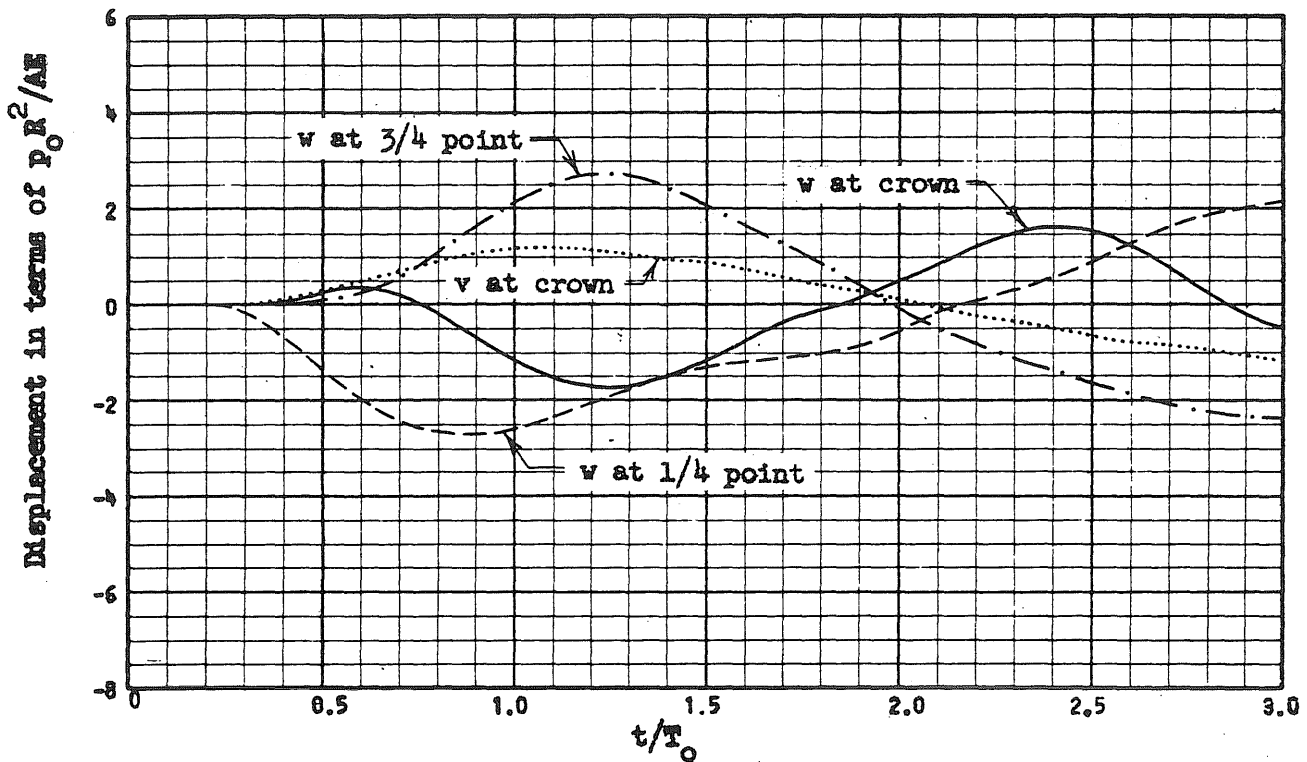
FIG. 5.2 (Continued)



Position of Load at $t/T_0 = 1.0$



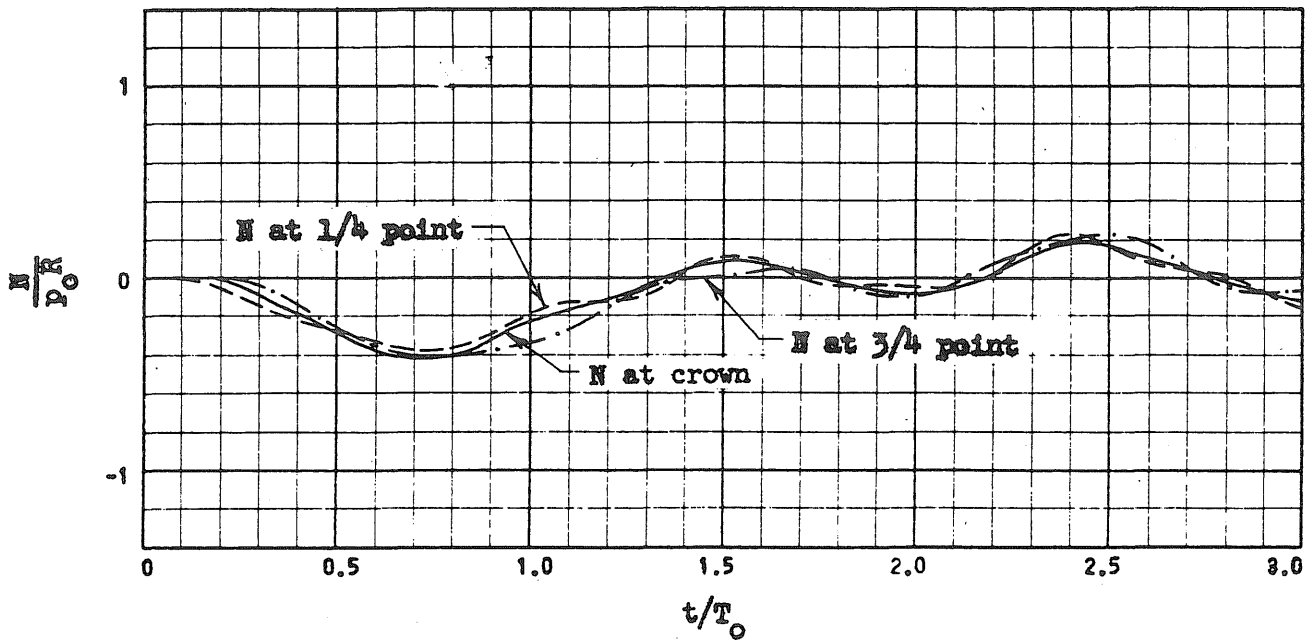
(a) Displacement Configurations



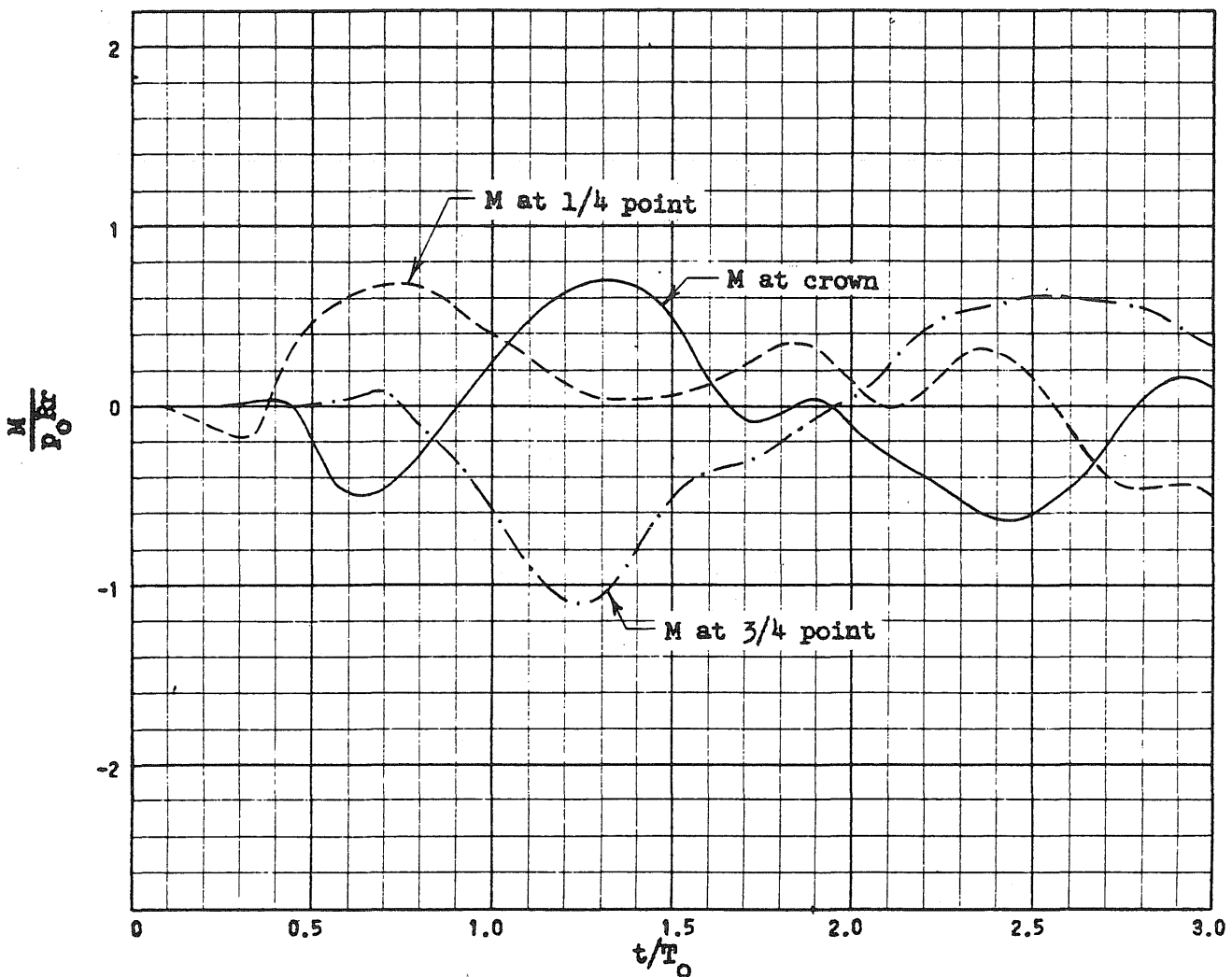
(b) Radial and Tangential Displacements, w and v

FIG. 5.3 RESPONSE CURVES FOR AN ARCH SUBJECTED TO A TRIANGULAR MOVING PRESSURE-- $t_d/t_t = 0.5$

$f/L_0 = 0.2, L_0/r = 100, p_0/p_{cr} = 1.0, t_t/T_0 = 1.0$

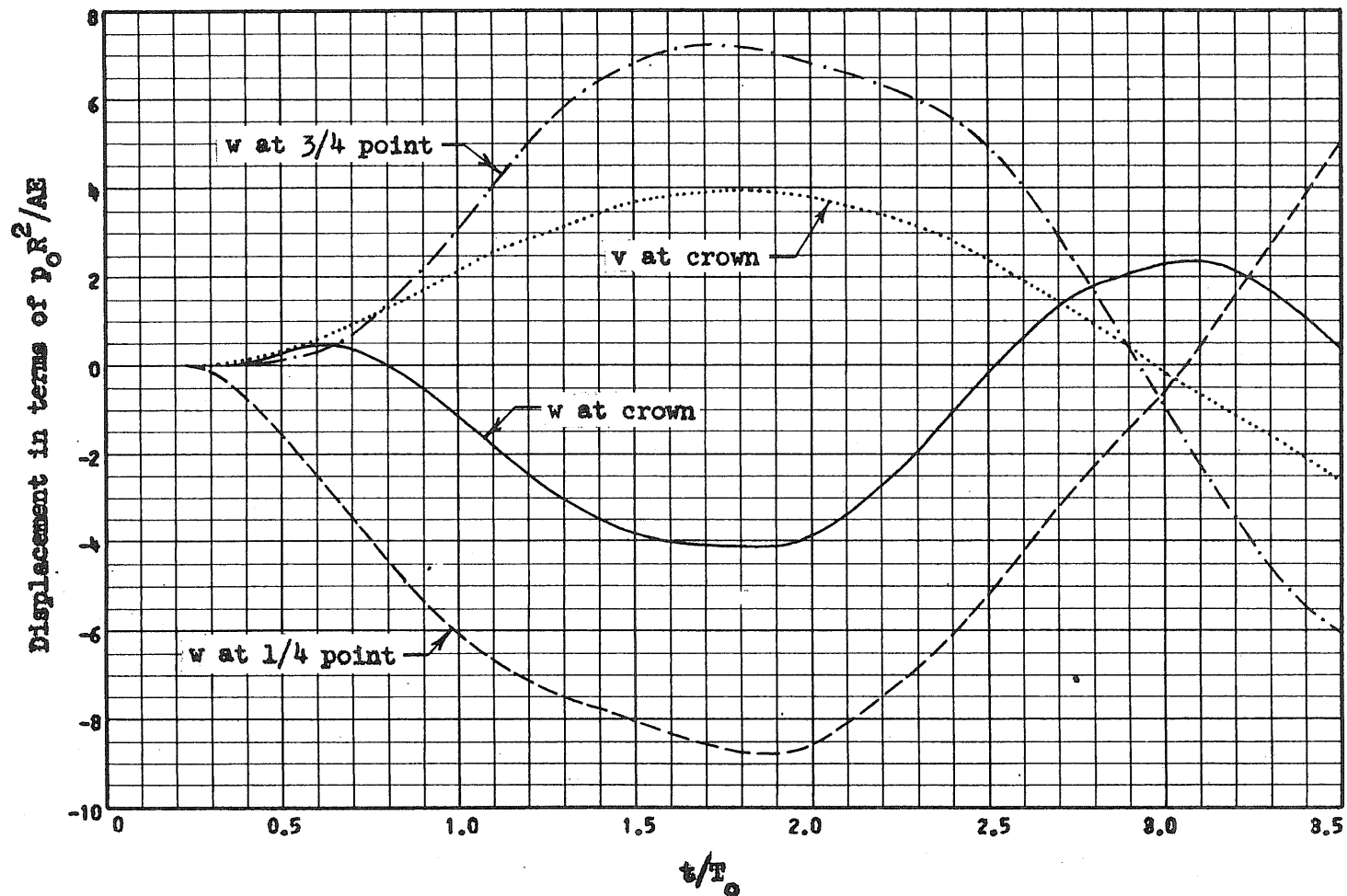


(c) Axial Force, N



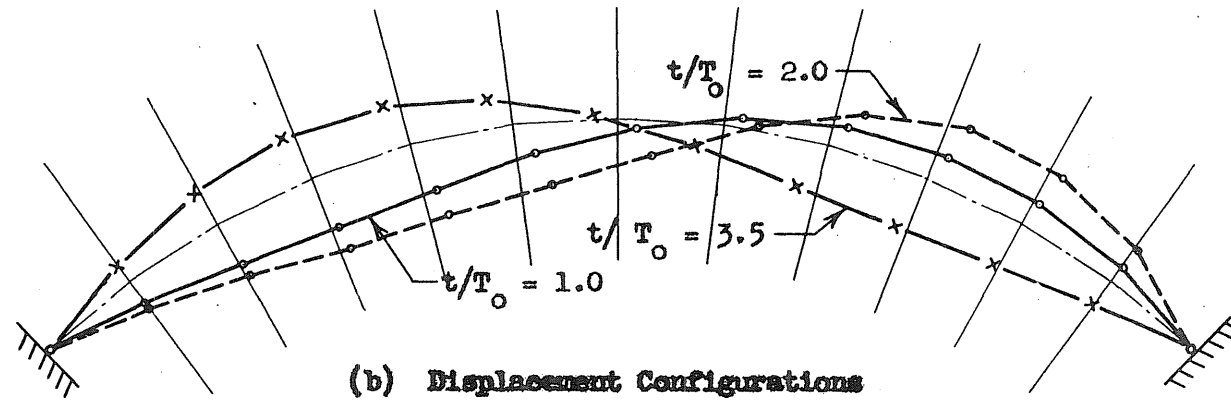
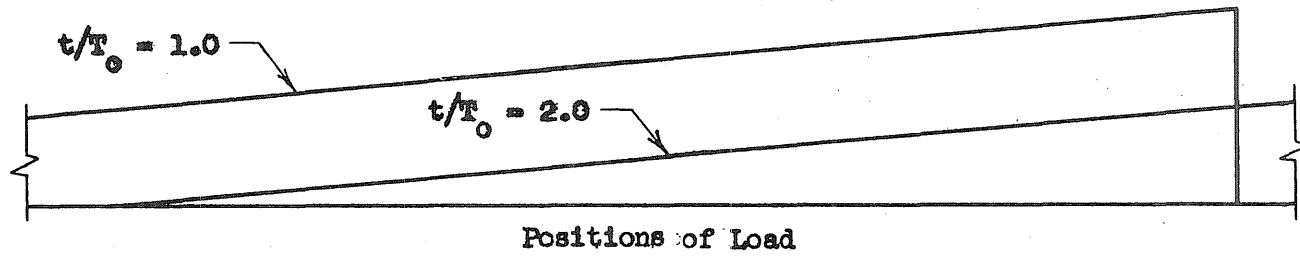
(d) Bending Moment, M

FIG. 5.3 (Continued)

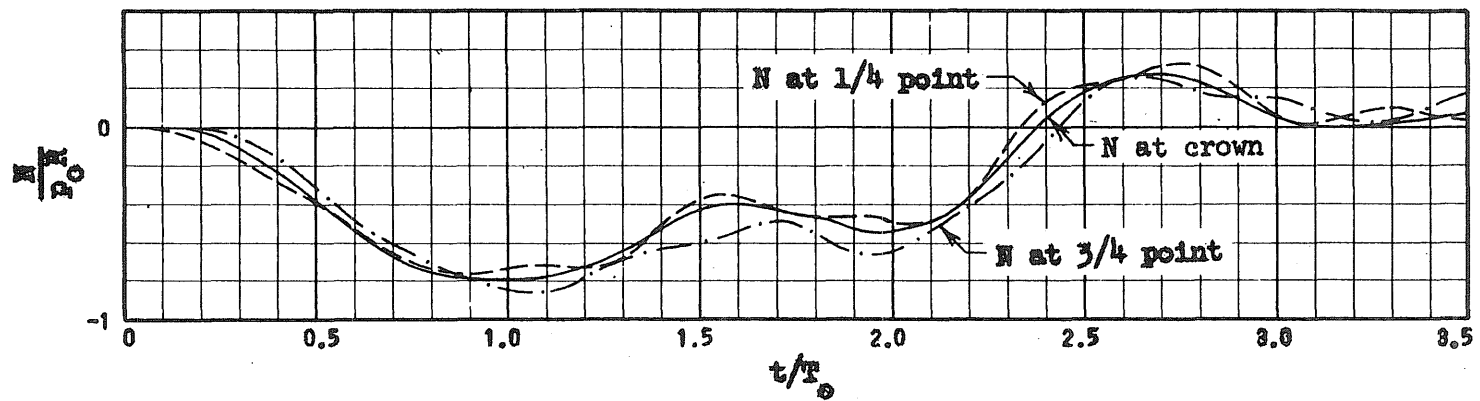


(a) Radial and Tangential Displacements, w and v

FIG. 5.4 RESPONSE CURVES FOR AN ARCH SUBJECTED TO A TRIANGULAR MOVING PRESSURE-- $t_d/t_t = 2.0$
 $f/L_0 = 0.2$, $L_0/r = 100$, $p_0/p_{cr} = 1.0$, $t_t/T_0 = 1.0$

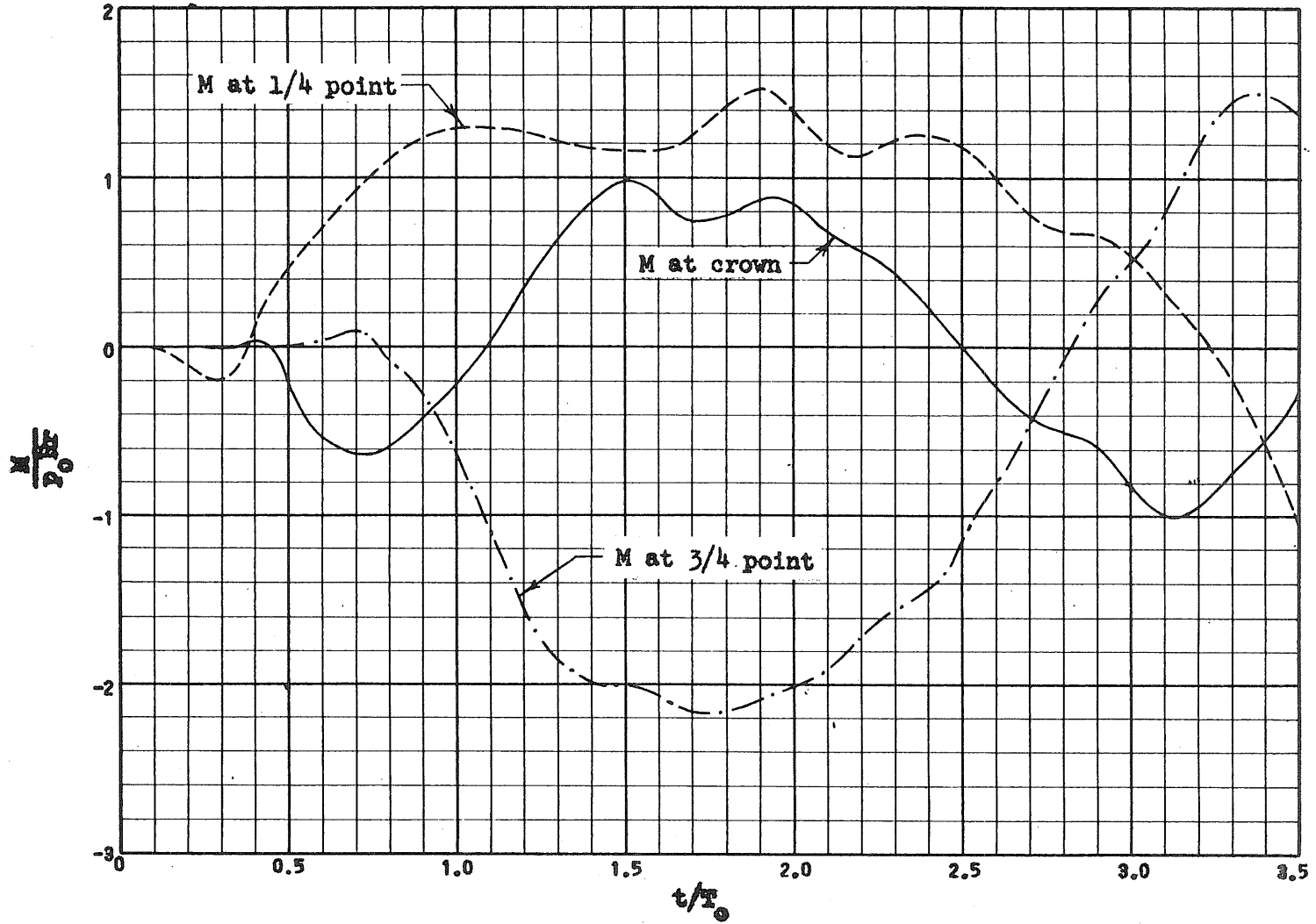


(b) Displacement Configurations



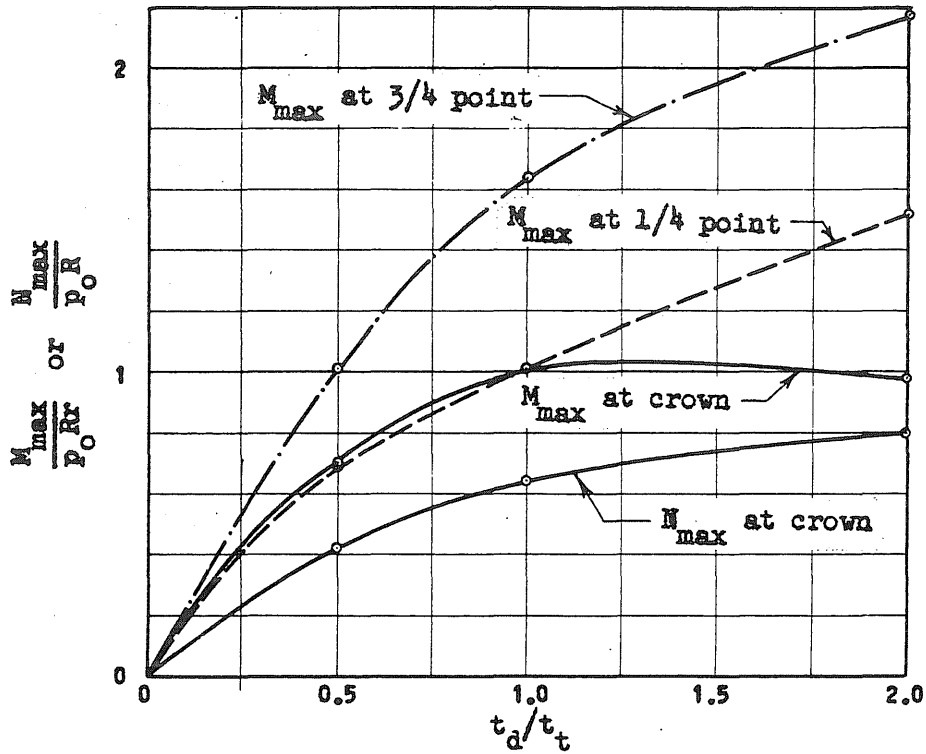
(c) Axial Force, N

FIG. 5.4 (Continued)

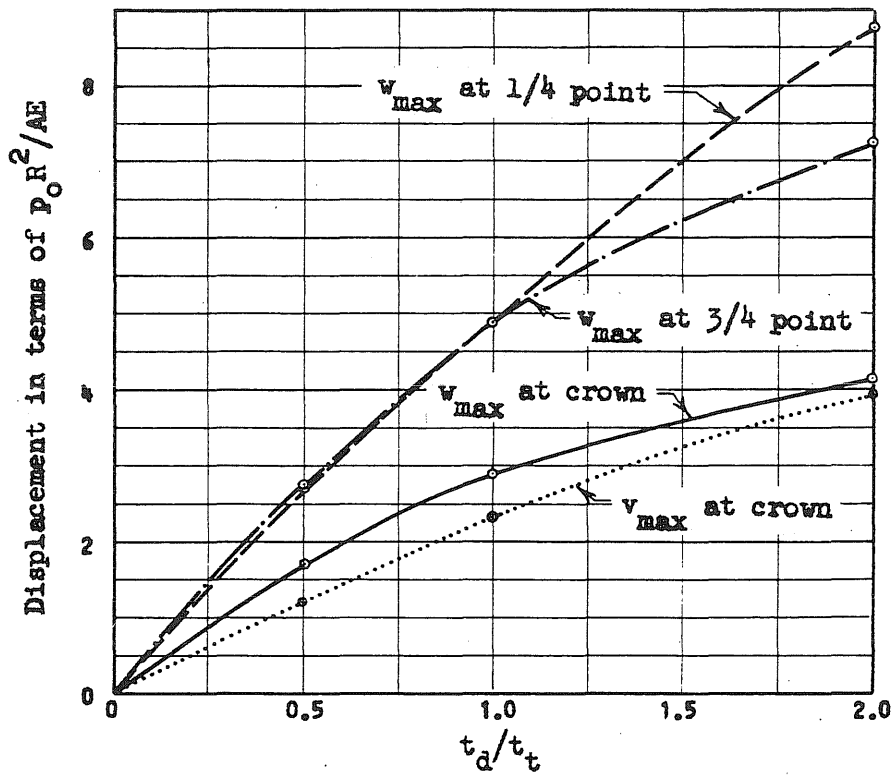


(d) Bending Moment, M

FIG. 5.4 (Continued)



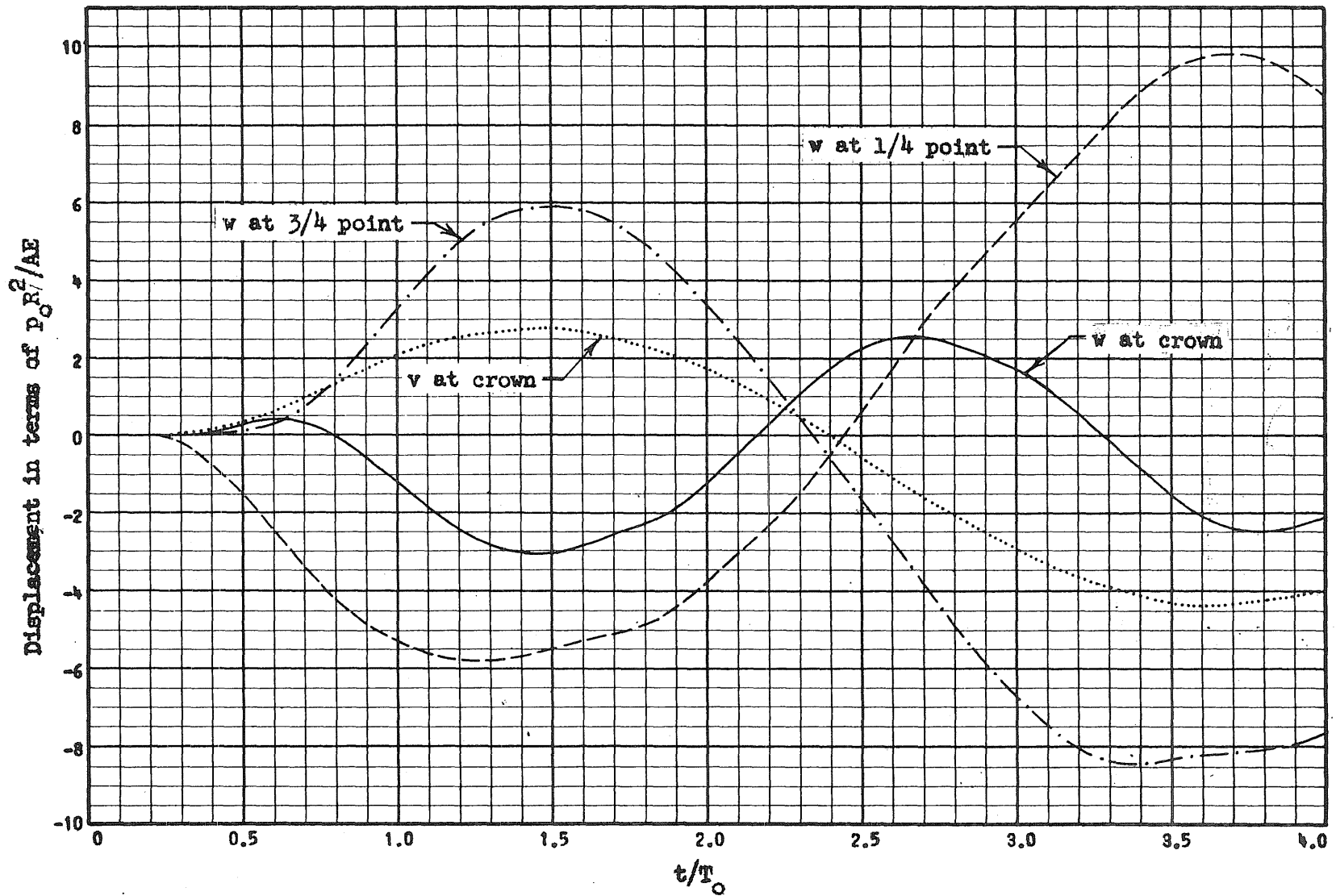
(a) Maximum Moment, M_{max} , and Maximum Axial Force, N_{max}



(b) Maximum Radial and Tangential Displacements, w_{max} and v_{max}

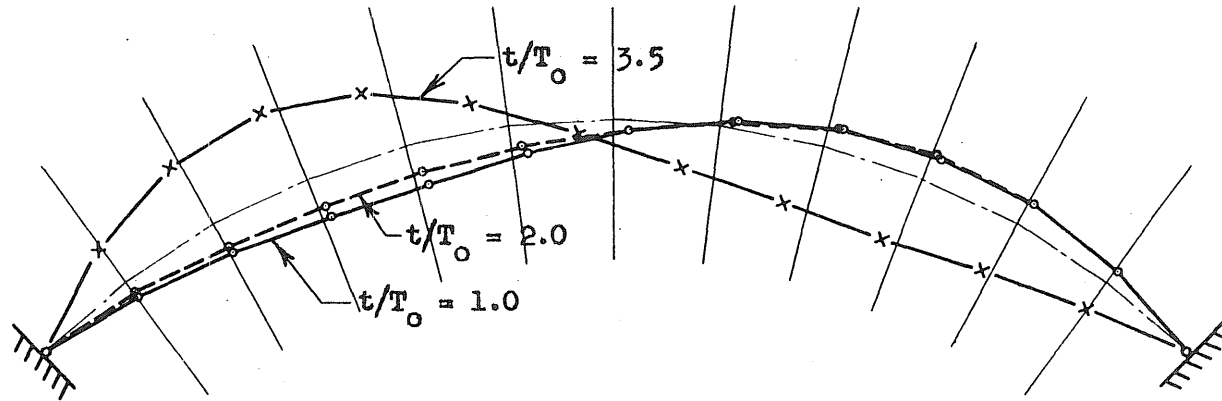
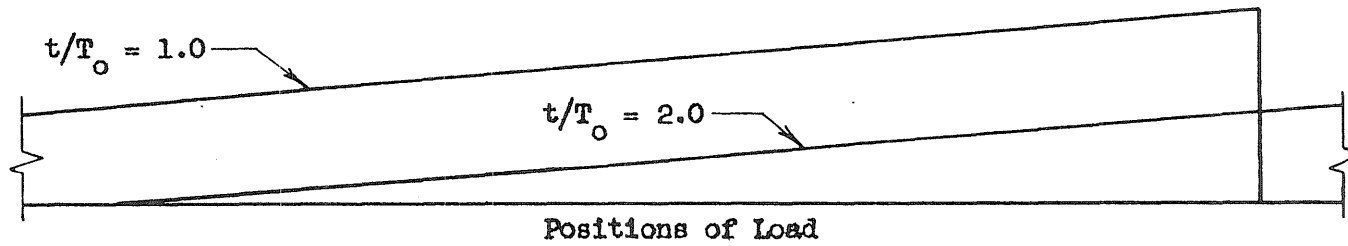
FIG. 5.5 RESPONSE SPECTRA FOR AN ARCH SUBJECTED TO A TRIANGULAR MOVING PRESSURE

$f/L_0 = 0.2, L_0/r = 100, p_0/p_{cr} = 1.0, t_t/T_0 = 1.0$

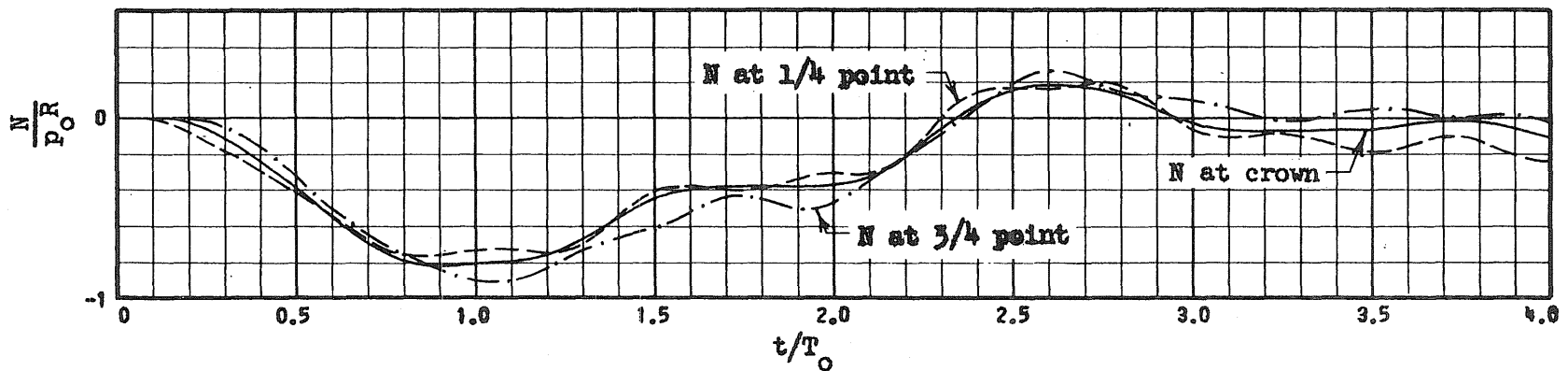


(a) Radial and Tangential Displacements, w and v

FIG. 5.6 RESPONSE CURVES FOR AN ARCH SUBJECTED TO A TRIANGULAR MOVING PRESSURE-- $p_0/p_{cr} = 0.001$
 $f/L_0 = 0.2$, $L_0/r = 100$, $t_t/T_0 = 1.0$, $t_d/t_t = 2.0$

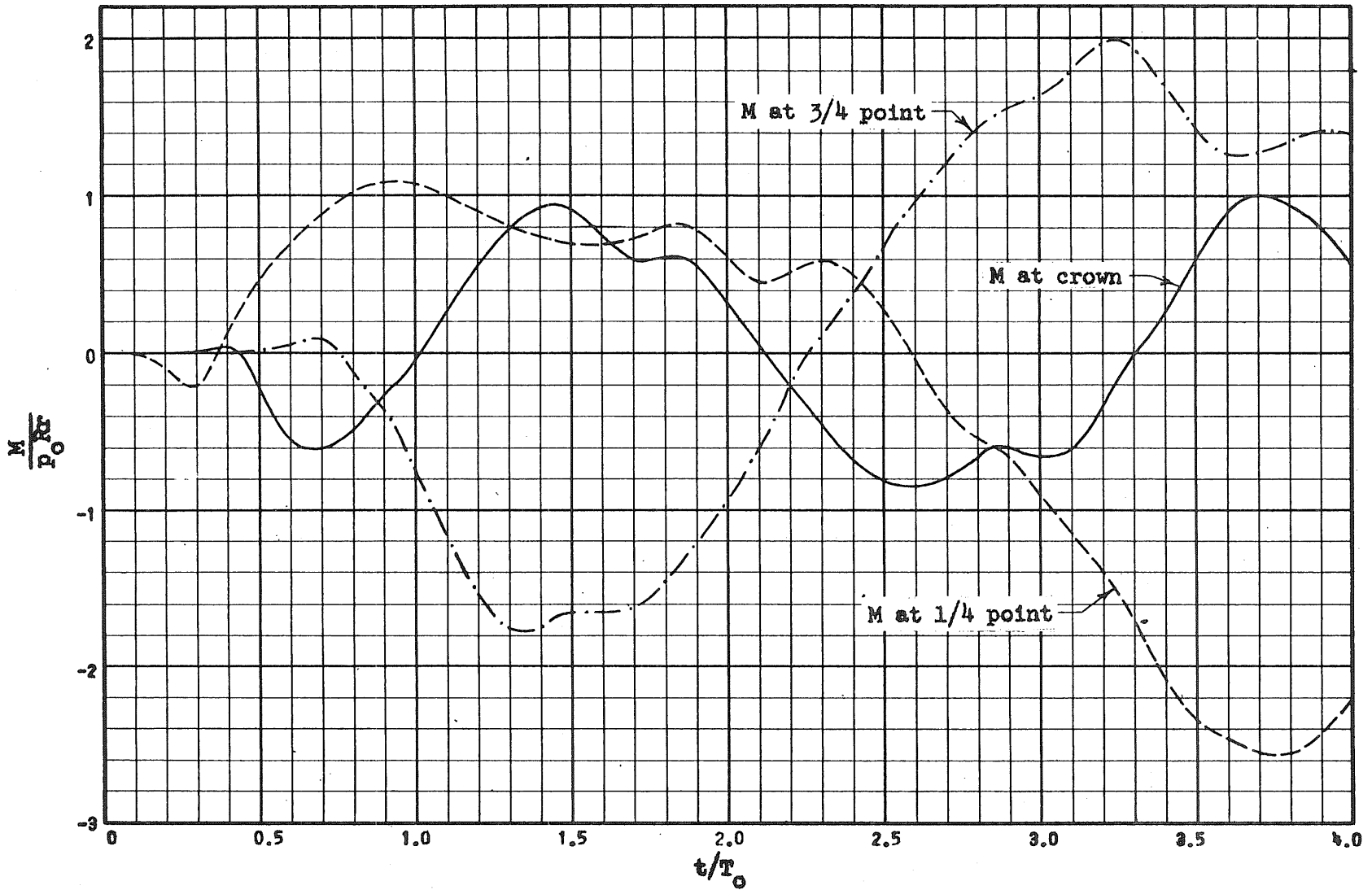


(b) Displacement Configurations



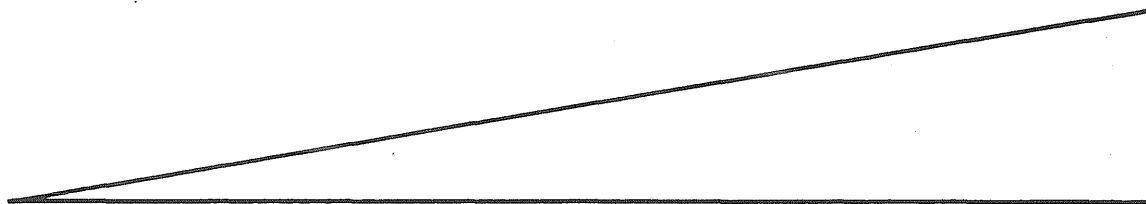
(c) Axial Force, N

FIG. 5.6 (Continued)

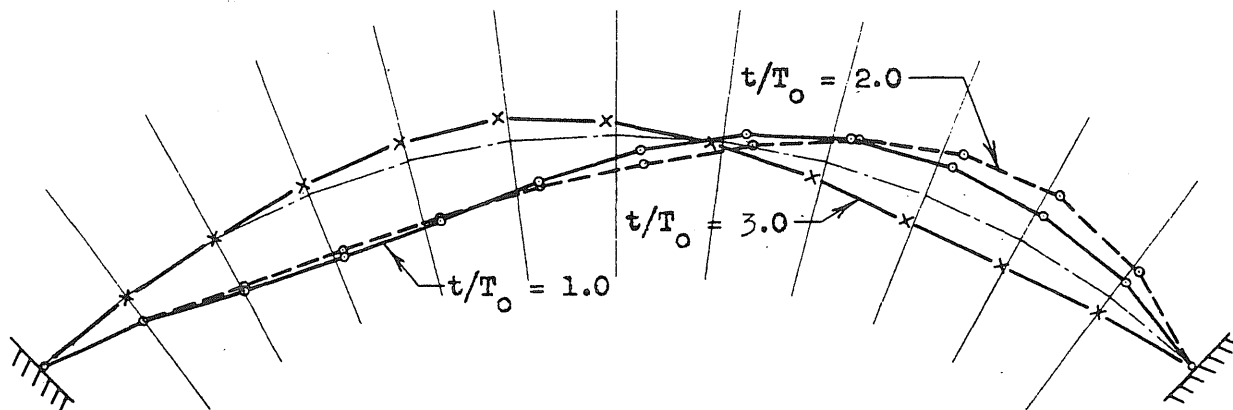


(d) Bending Moment, M

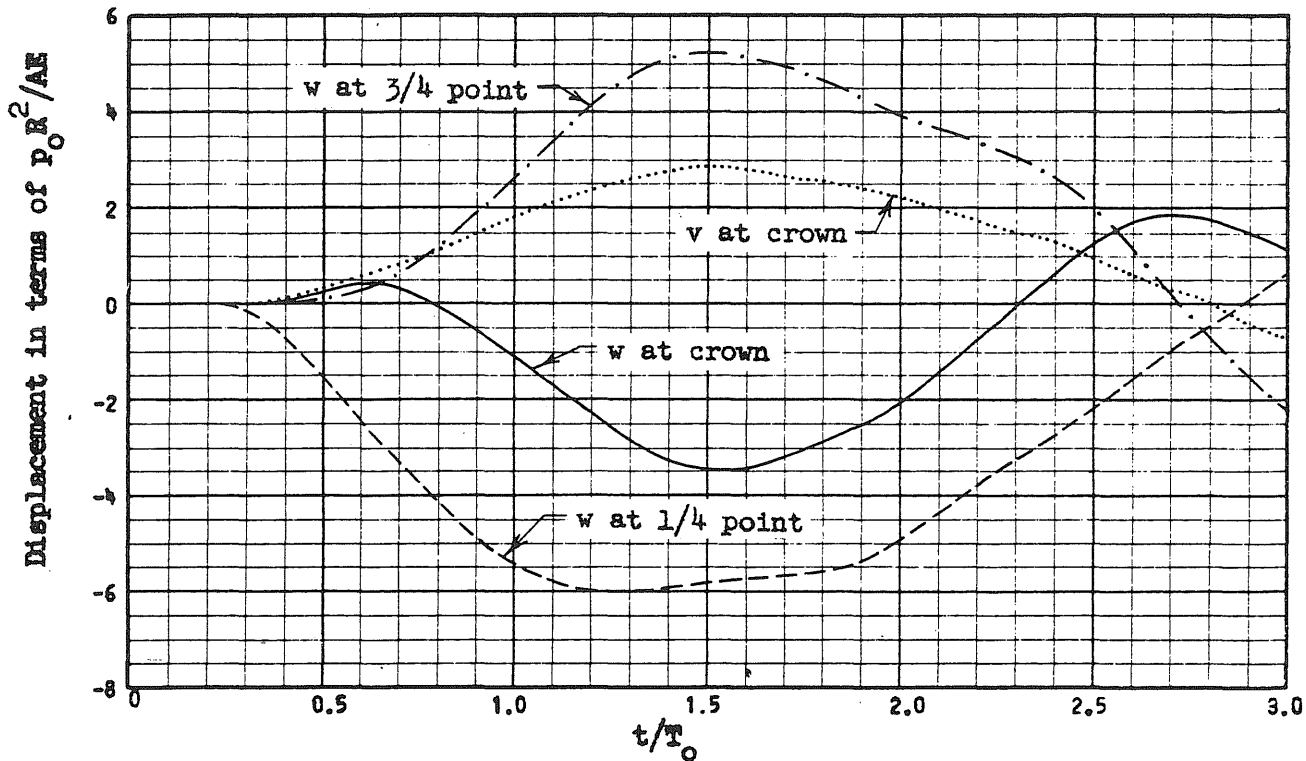
FIG. 5.6 (Continued)



Position of Load at $t/T_0 = 1.0$



(a) Displacement Configurations



(b) Radial and Tangential Displacements, w and v

FIG. 5.7 RESPONSE CURVES FOR AN ARCH SUBJECTED TO A TRIANGULAR MOVING PRESSURE-- $p_0/p_{cr} = 2.0$

$f/L_0 = 0.2, L_0/r = 100, t_t/T_0 = 1.0, t_d/t_t = 1.0$

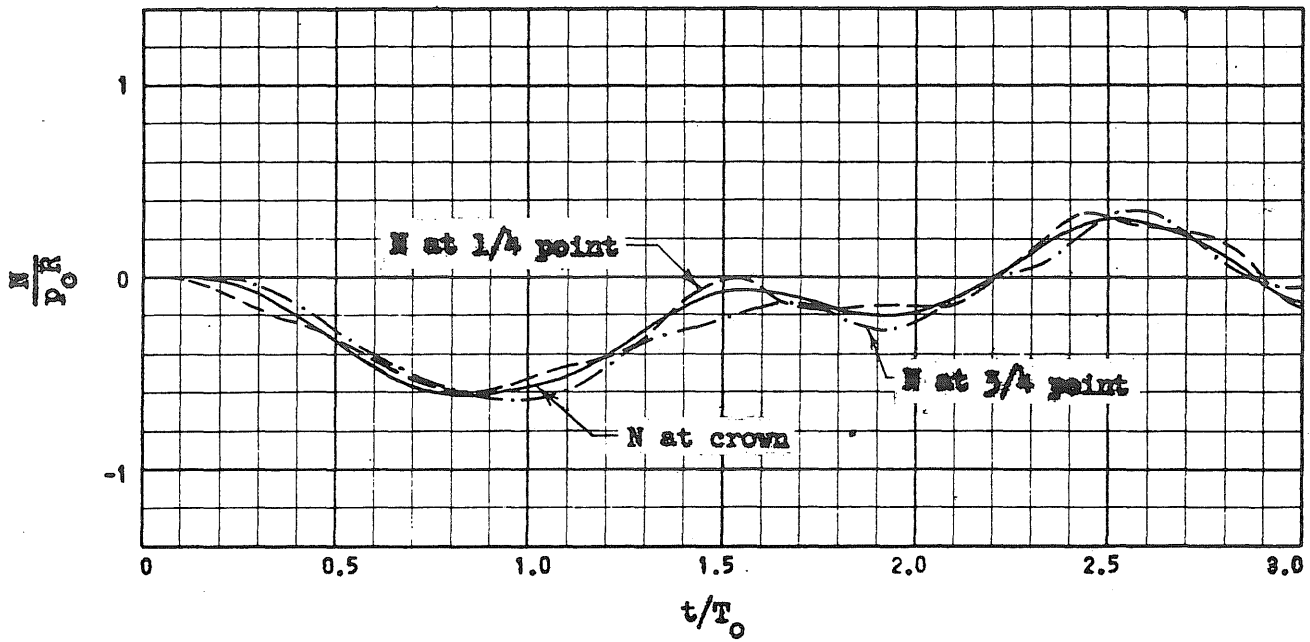
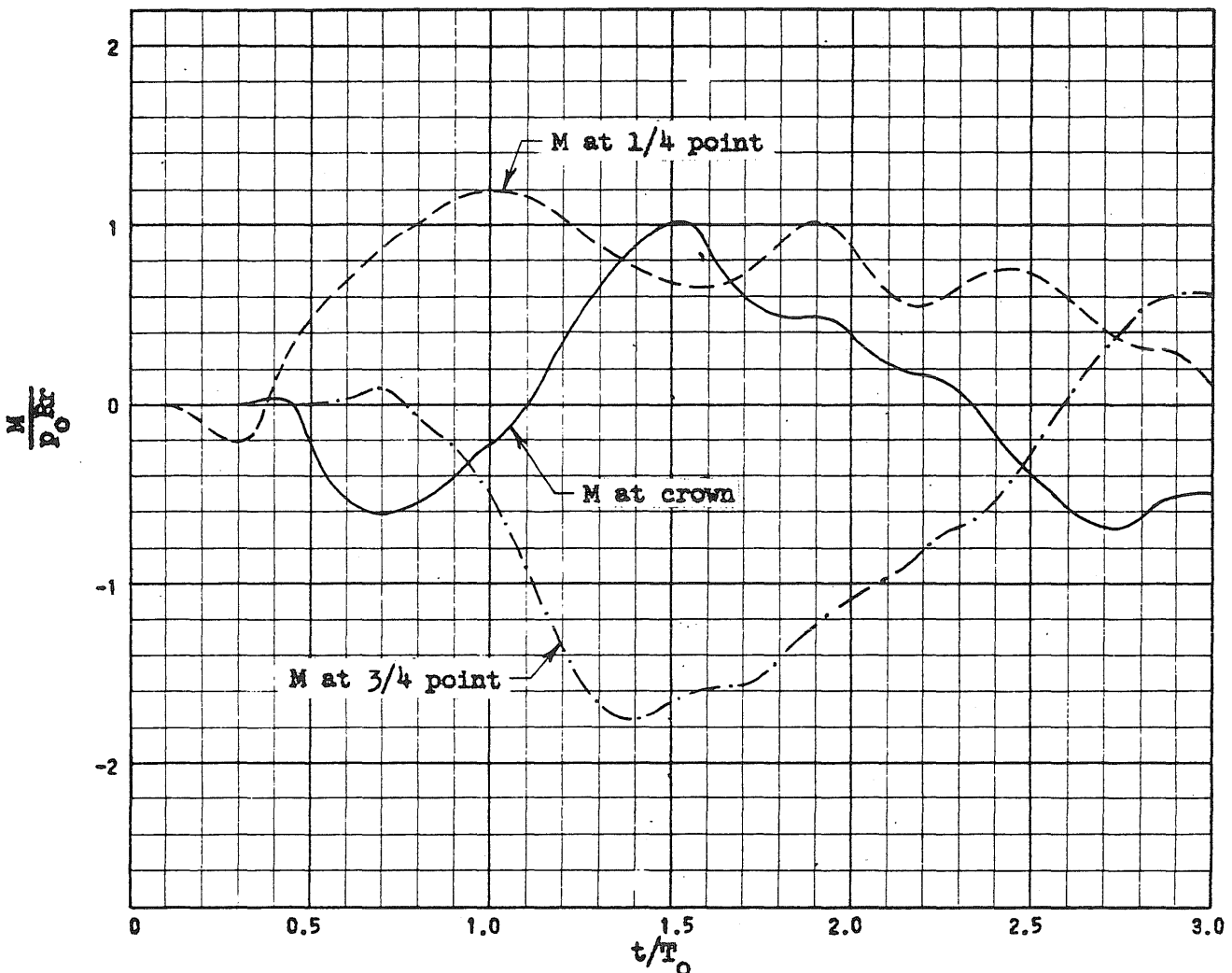
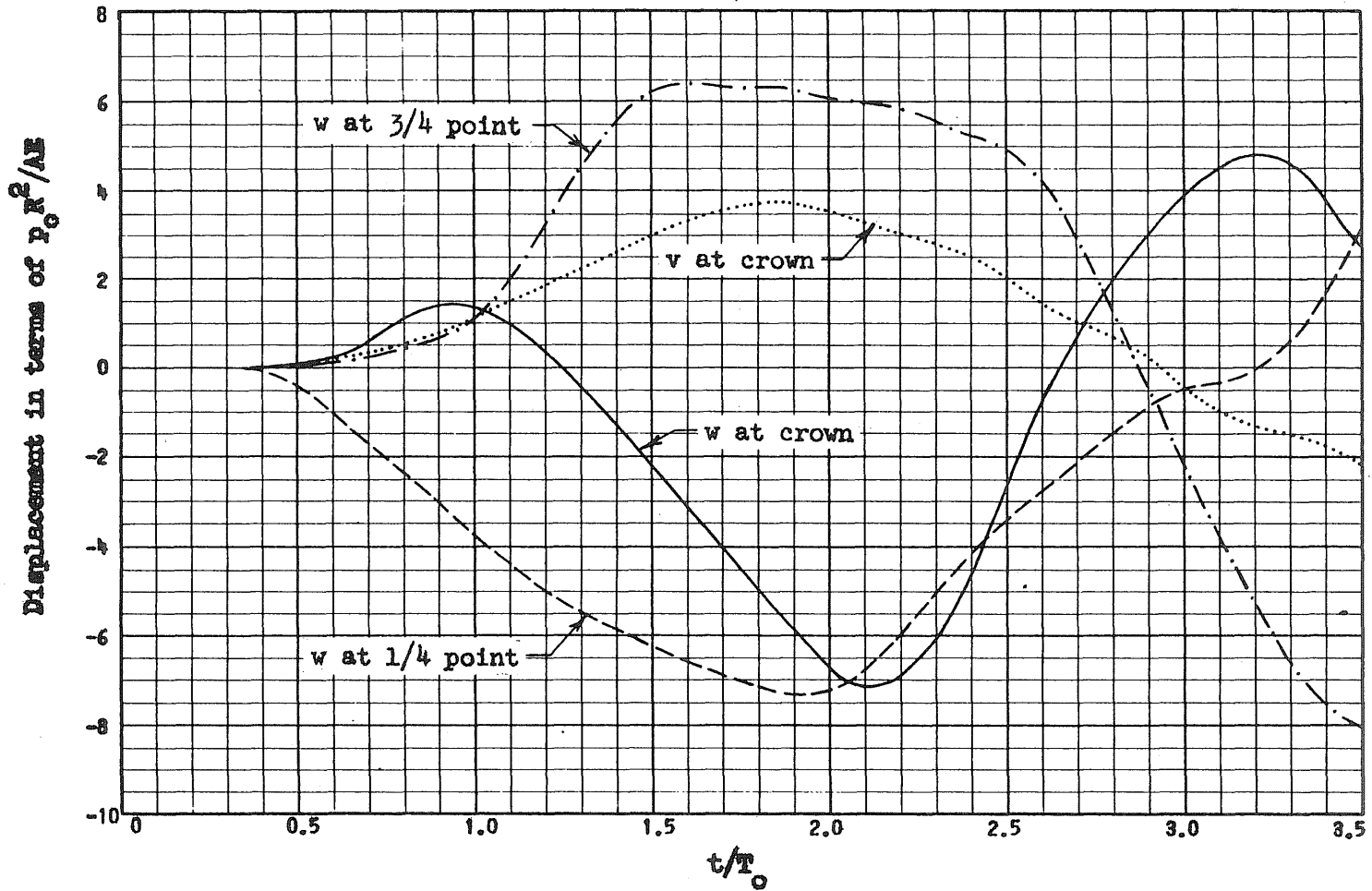
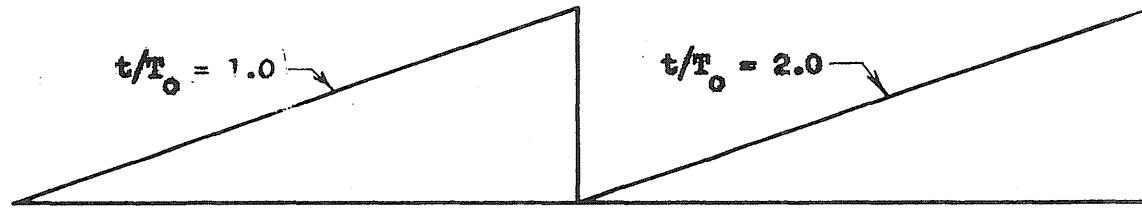
(c) Axial Force, N (d) Bending Moment, M

FIG. 5.7 (Continued)

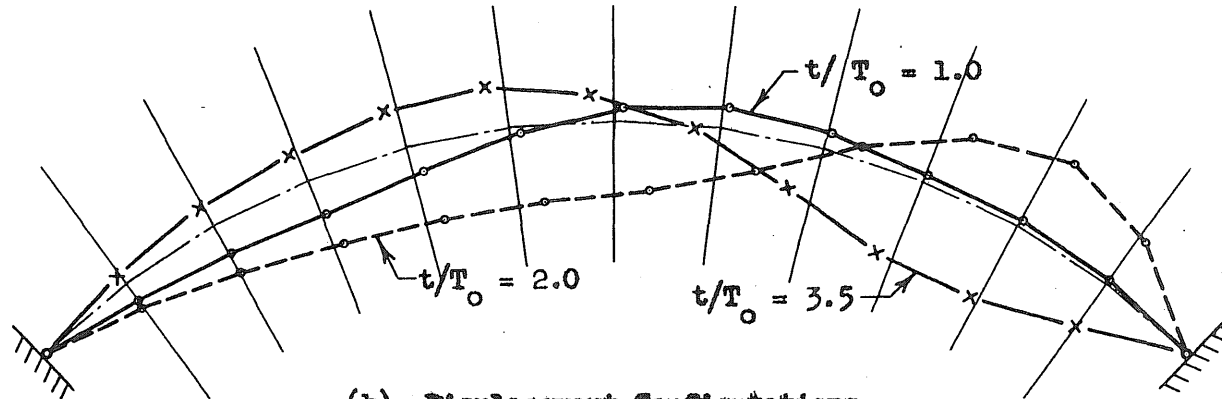


(a) Radial and Tangential Displacements, w and v

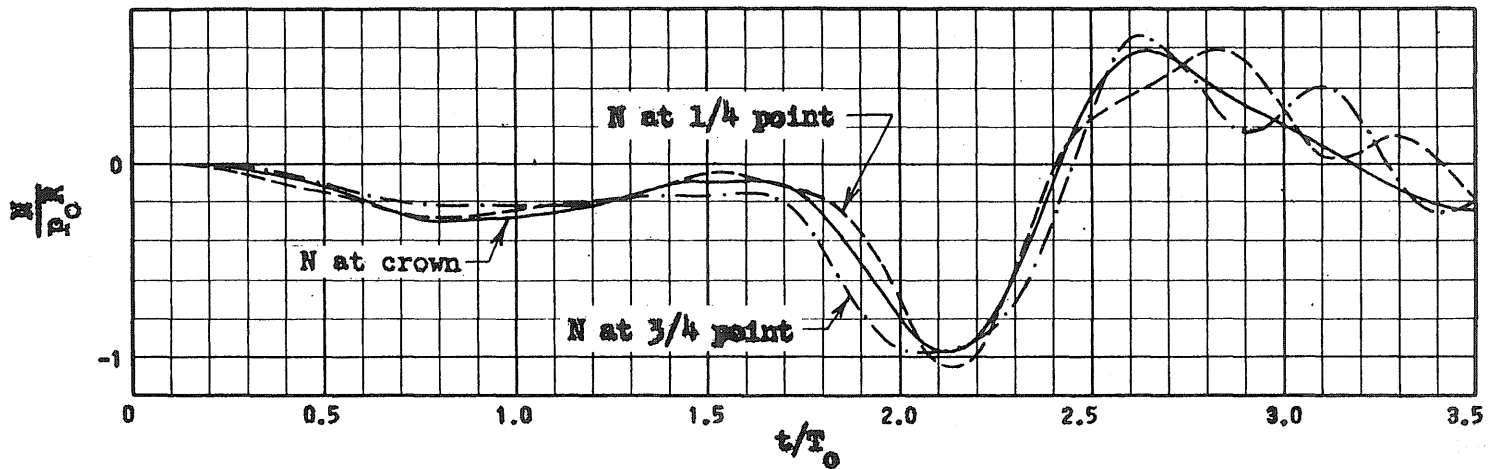
FIG. 5.8 RESPONSE CURVES FOR AN ARCH SUBJECTED TO A TRIANGULAR MOVING PRESSURE-- $t_t/T_0 = 2.0$
 $f/L_0 = 0.2$, $L_0/r = 100$, $p_0/p_{cr} = 1.0$, $t_d/t_t = 0.5$



Positions of Load

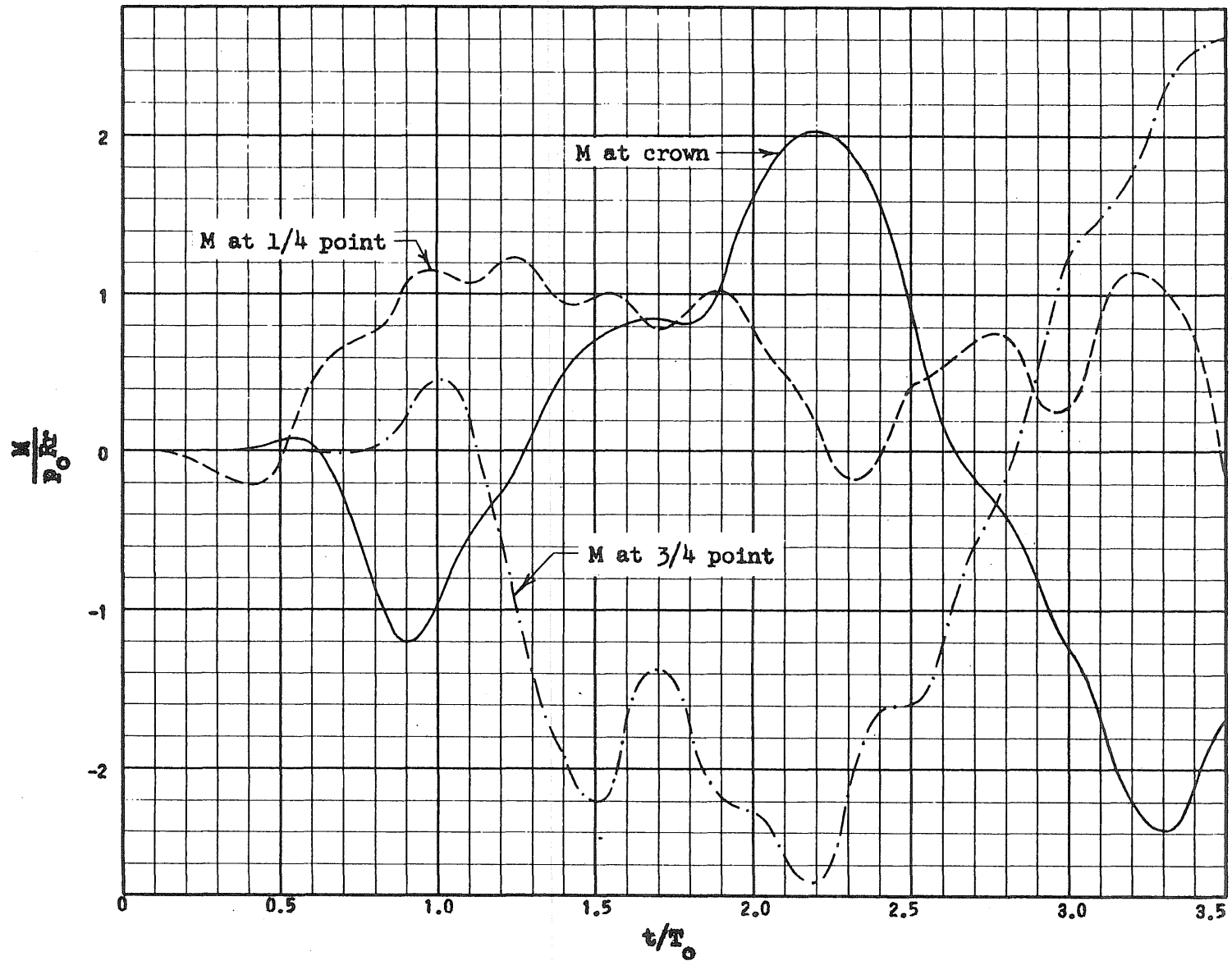


(b) Displacement Configurations



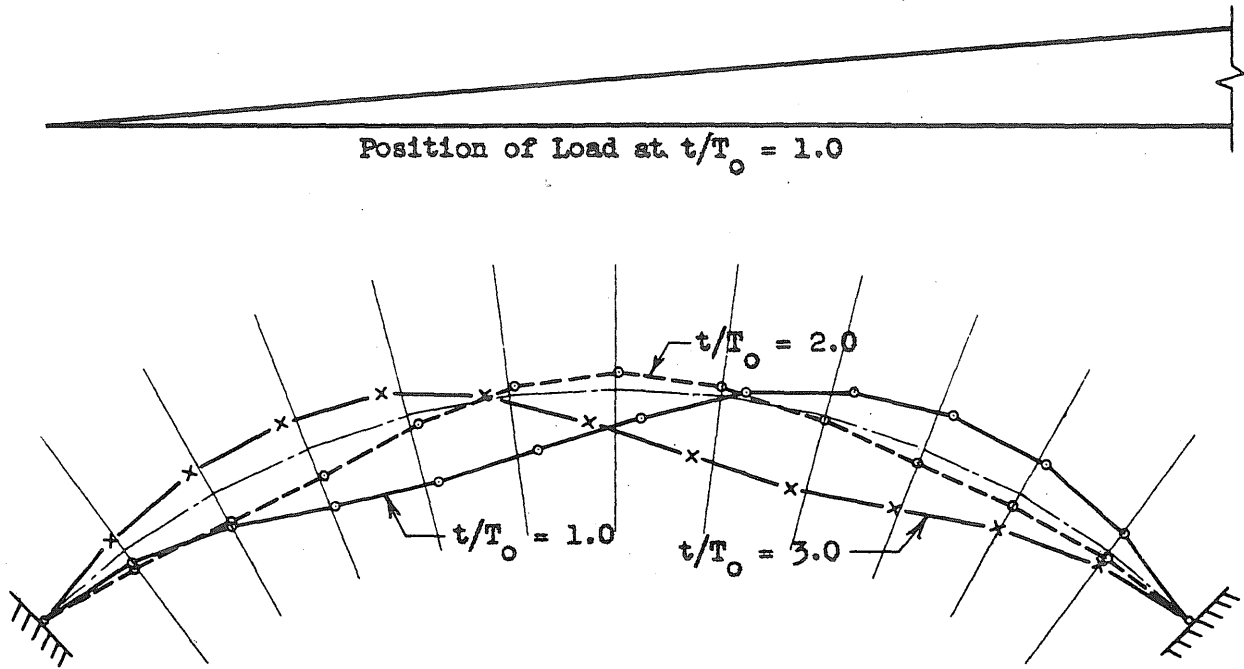
(c) Axial Force, N

FIG. 5.8 (Continued)

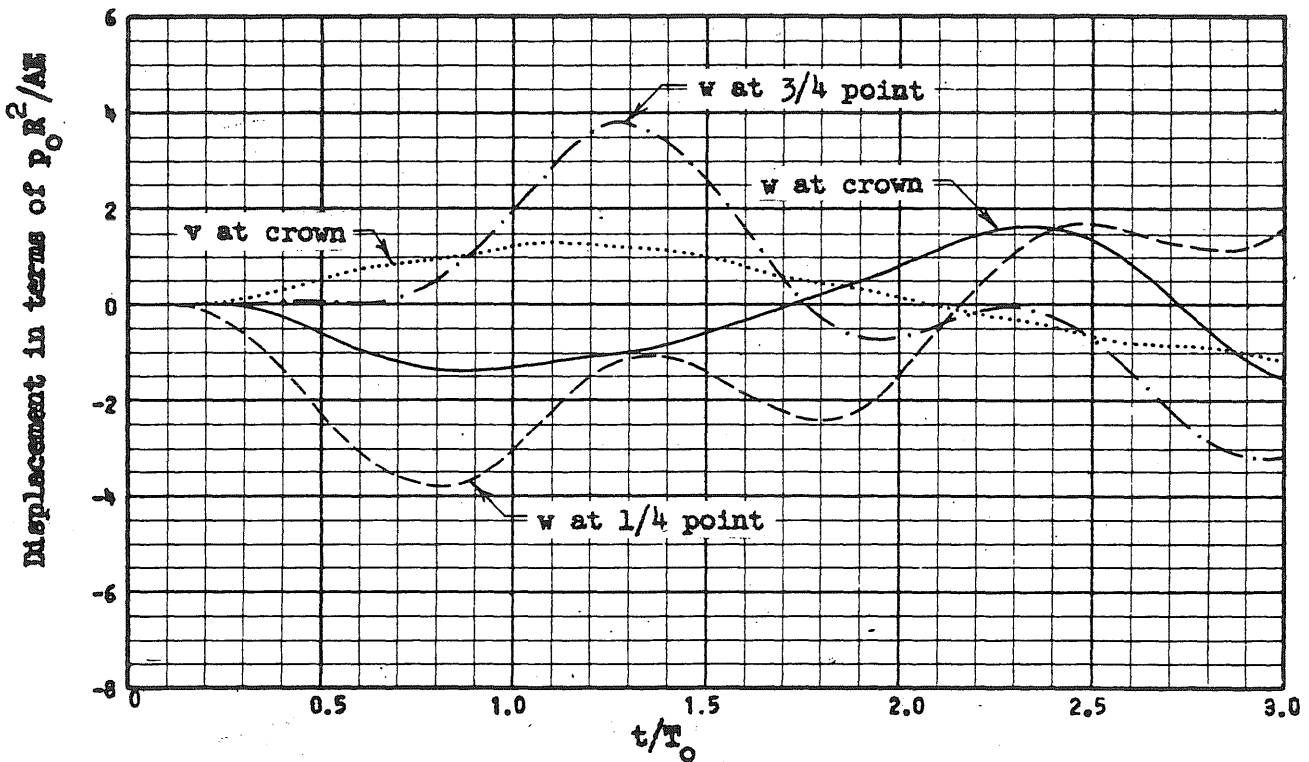


(d) Bending Moment, M

FIG. 5.8 (Continued)

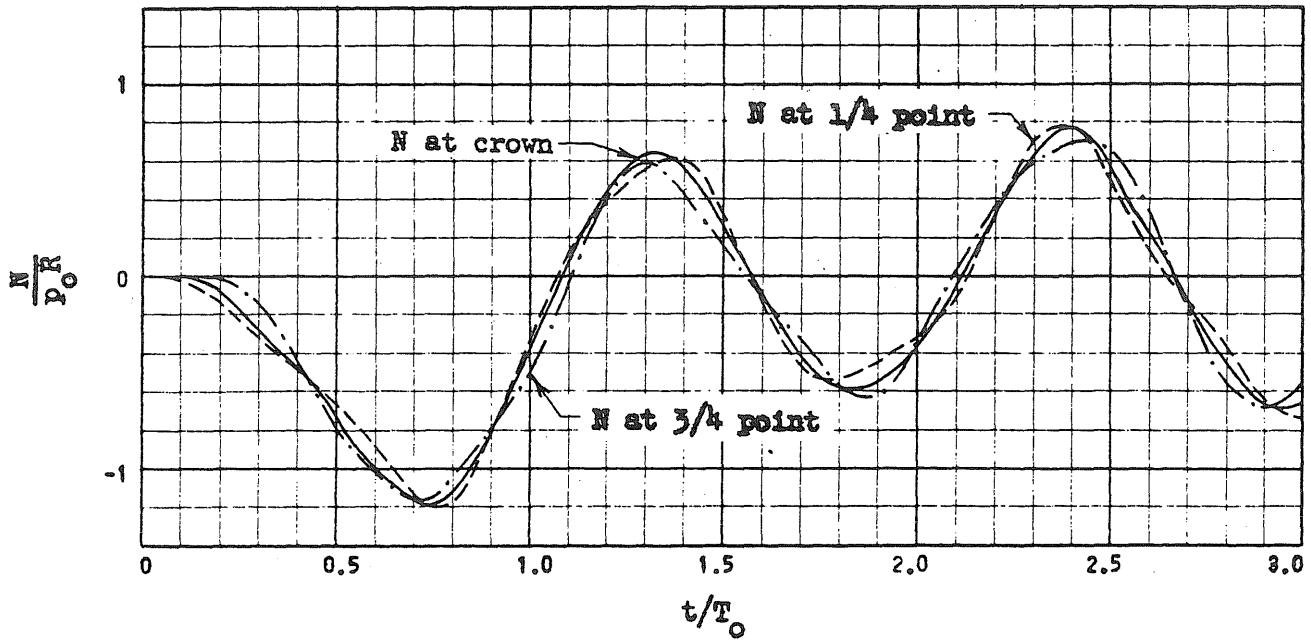
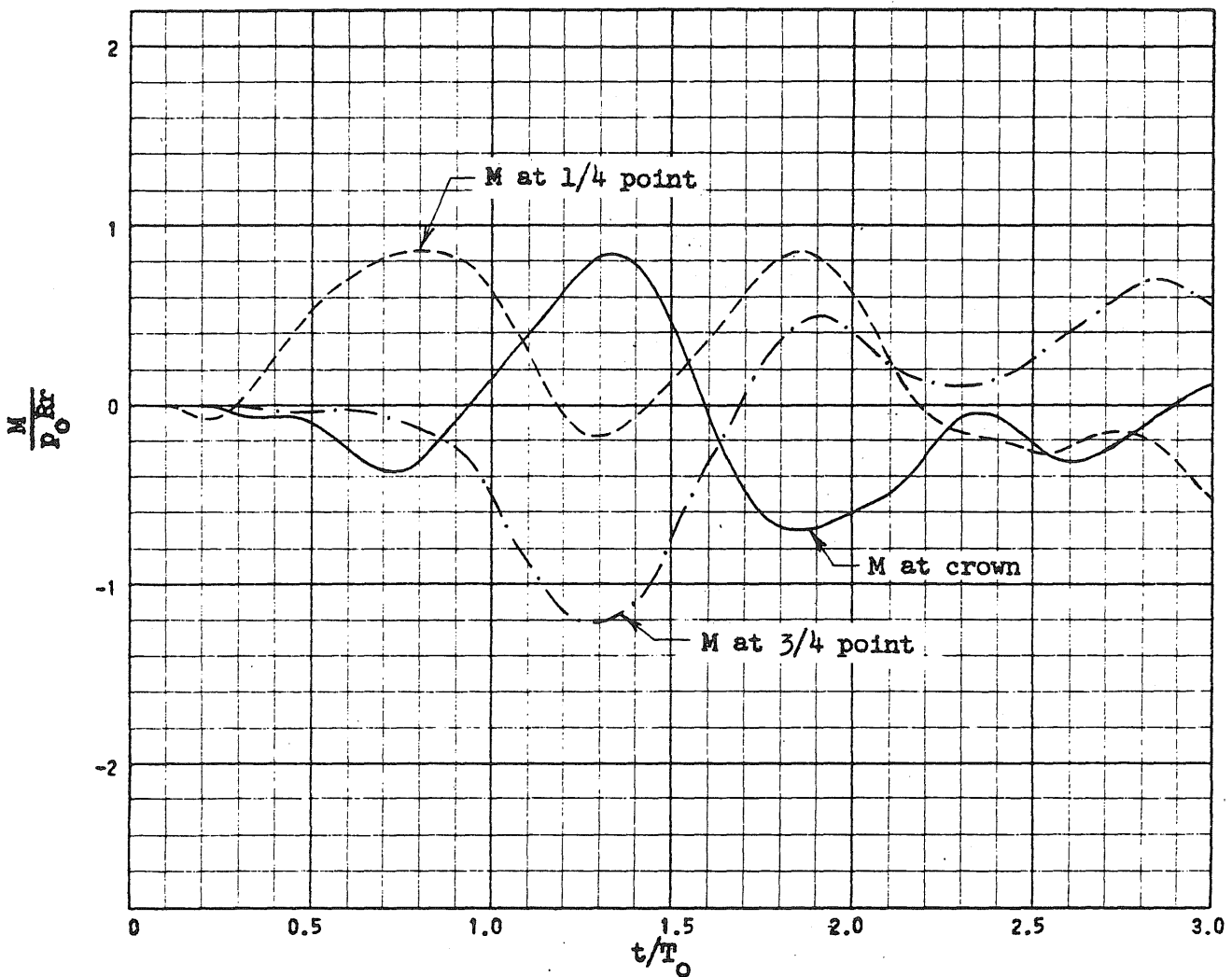


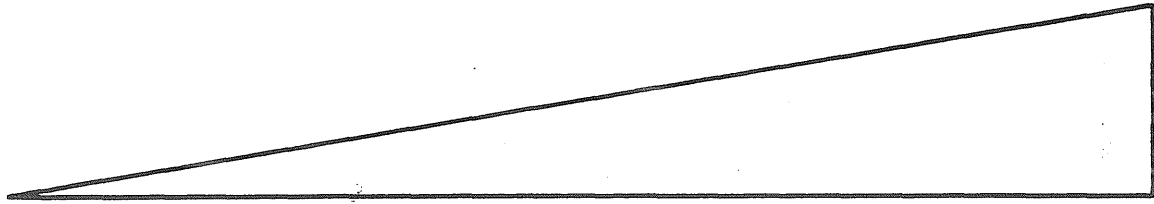
(a) Displacement Configurations



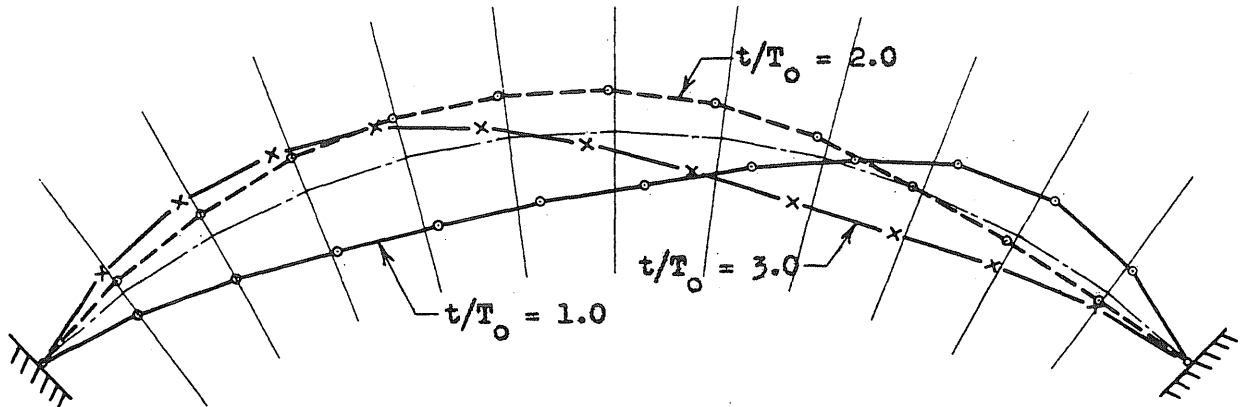
(b) Radial and Tangential Displacements, w and v

FIG. 5.9 RESPONSE CURVES FOR AN ARCH SUBJECTED TO A TRIANGULAR MOVING PRESSURE-- $t_t/T_0 = 0.5$
 $f/L_0 = 0.2$, $L_0/r = 100$, $p_0/p_{cr} = 1.0$, $t_d/t_t = 2.0$

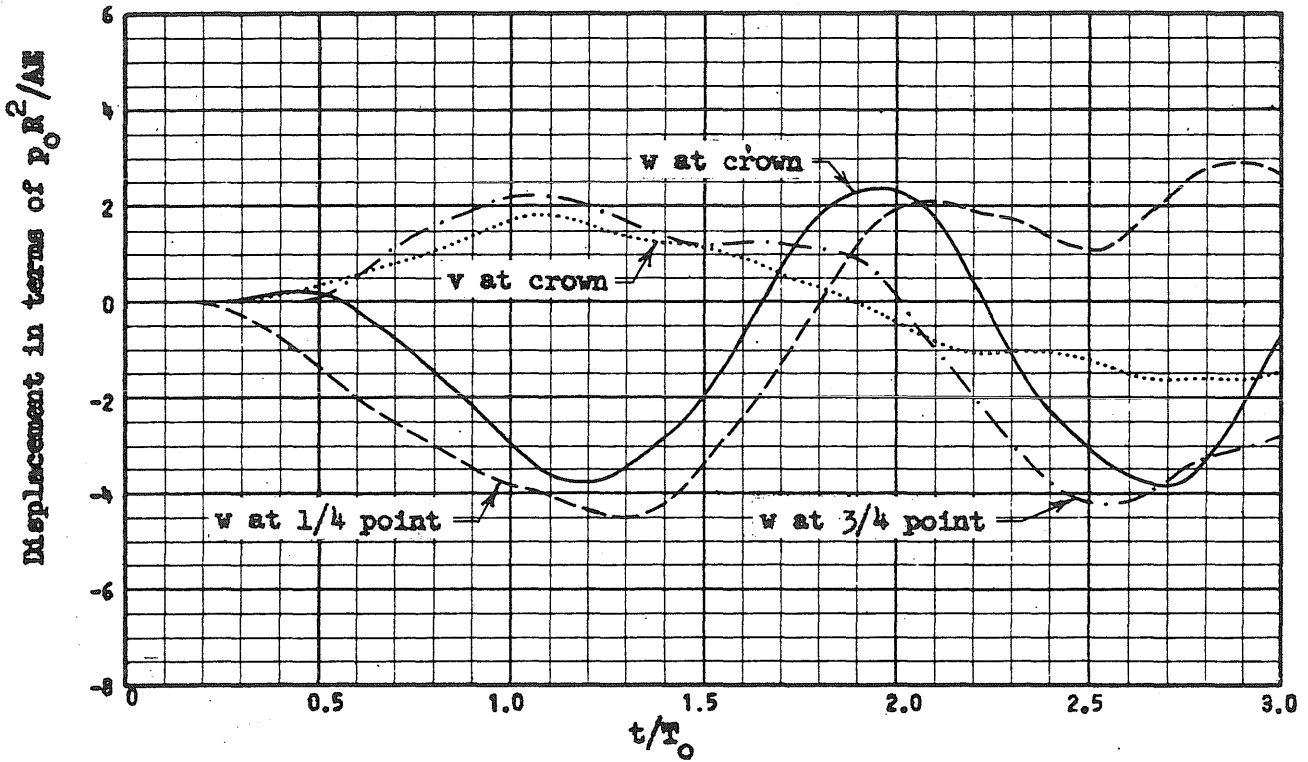
(c) Axial Force, N (d) Bending Moment, M



Position of Load at $t/T_0 = 1.0$



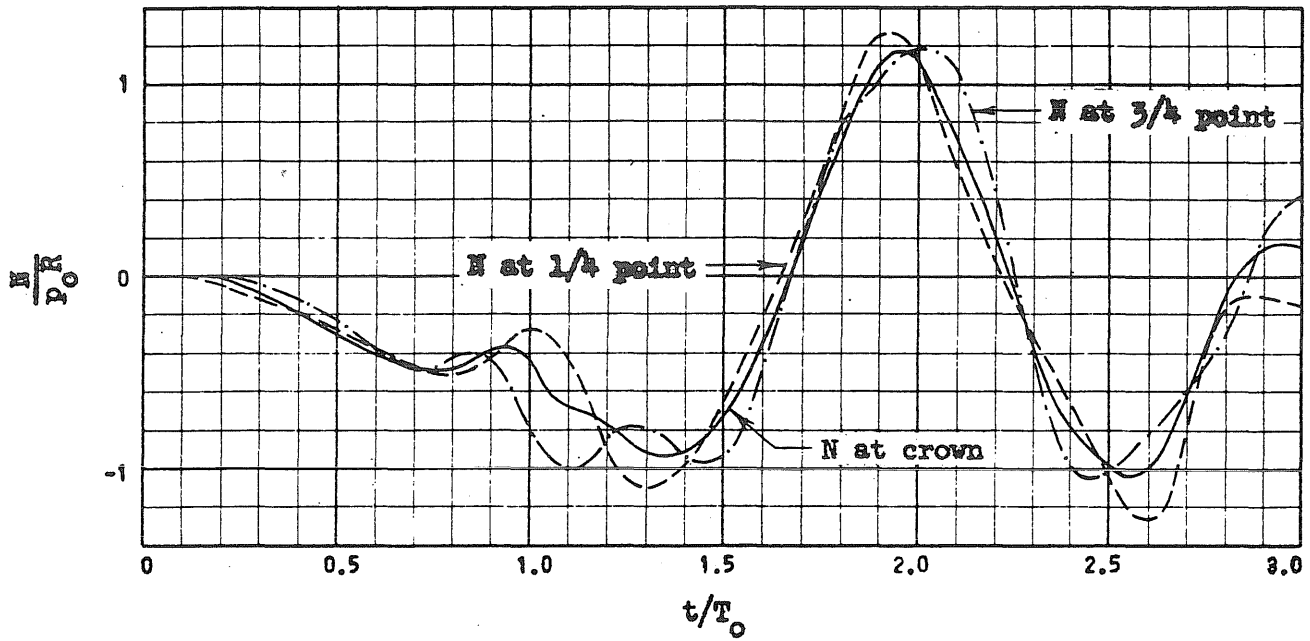
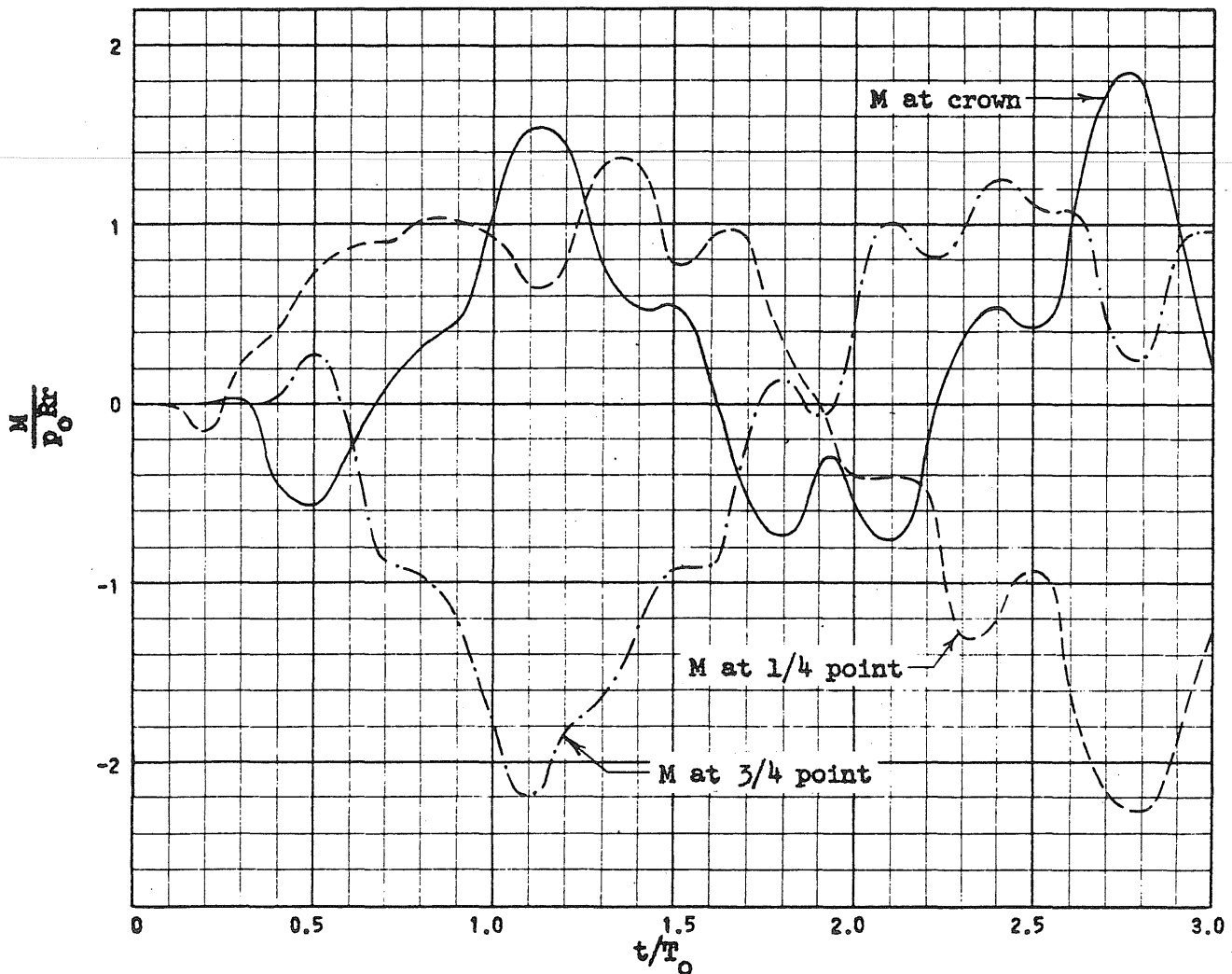
(a) Displacement Configurations

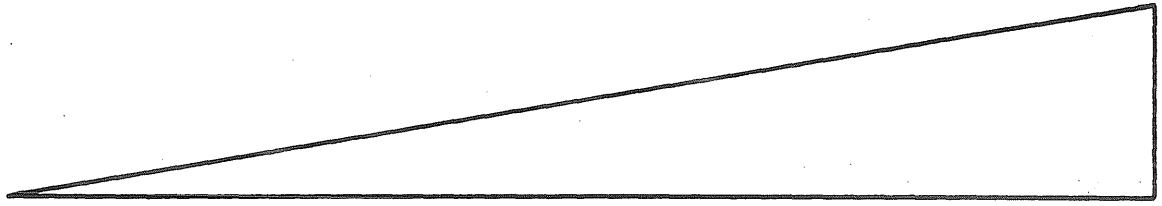


(b) Radial and Tangential Displacements, w and v

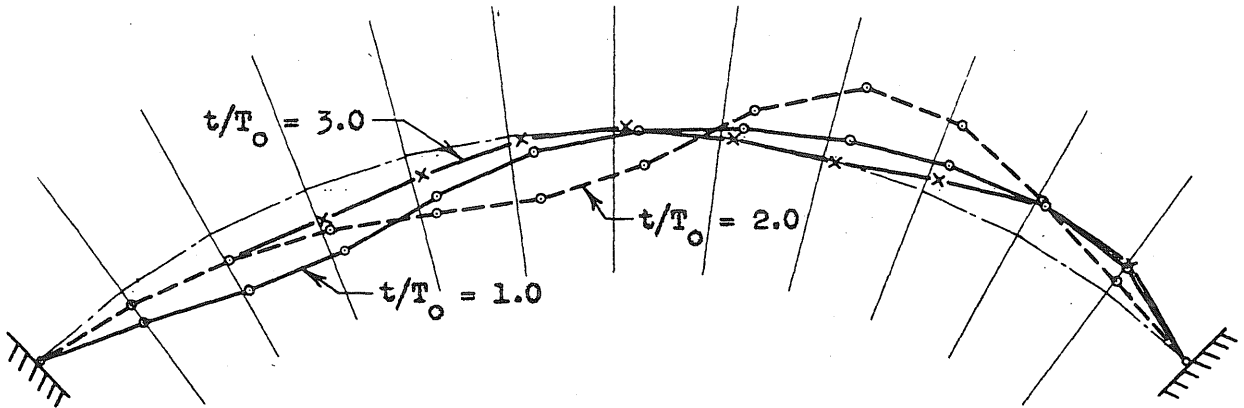
FIG. 5.10 RESPONSE CURVES FOR AN ARCH SUBJECTED TO A TRIANGULAR MOVING PRESSURE-- $L_0/r = 50$

$f/L_0 = 0.2, p_0/p_{cr} = 1.0, t_t/T_0 = 1.0, t_d/t_t = 1.0$

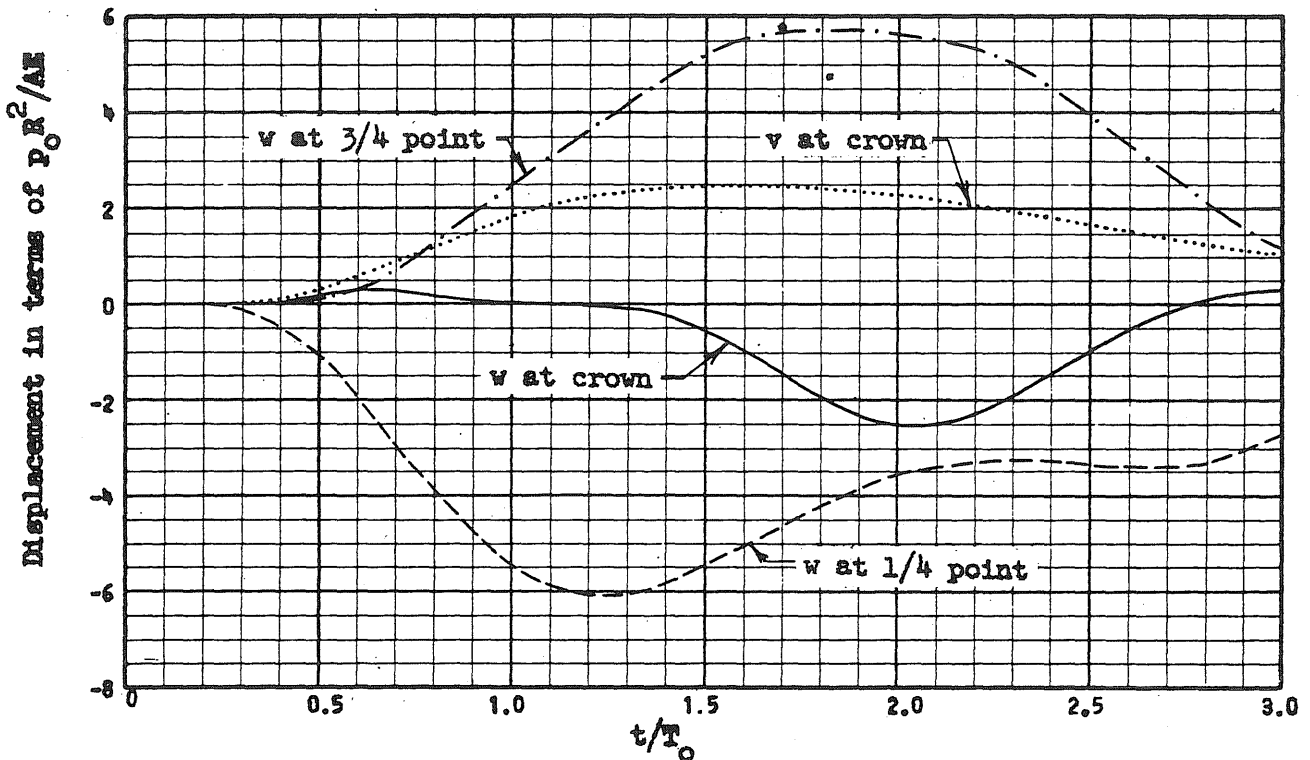
(c) Axial Force, N (d) Bending Moment, M



Position of Load at $t/T_0 = 1.0$



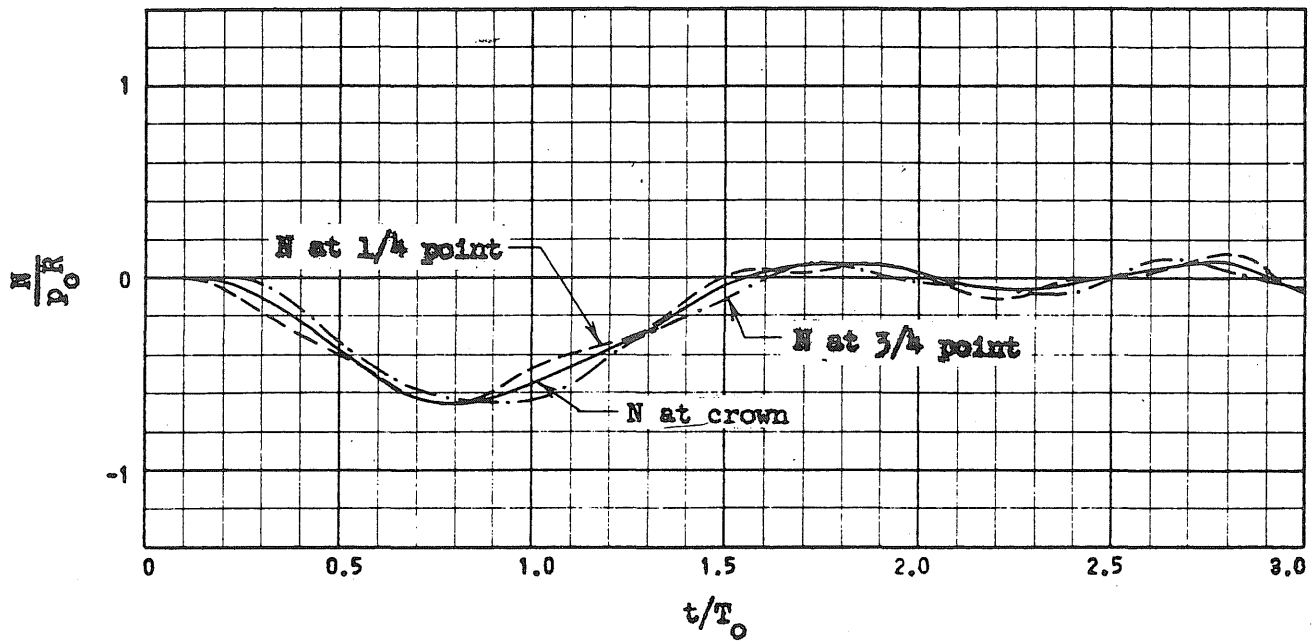
(a) Displacement Configurations



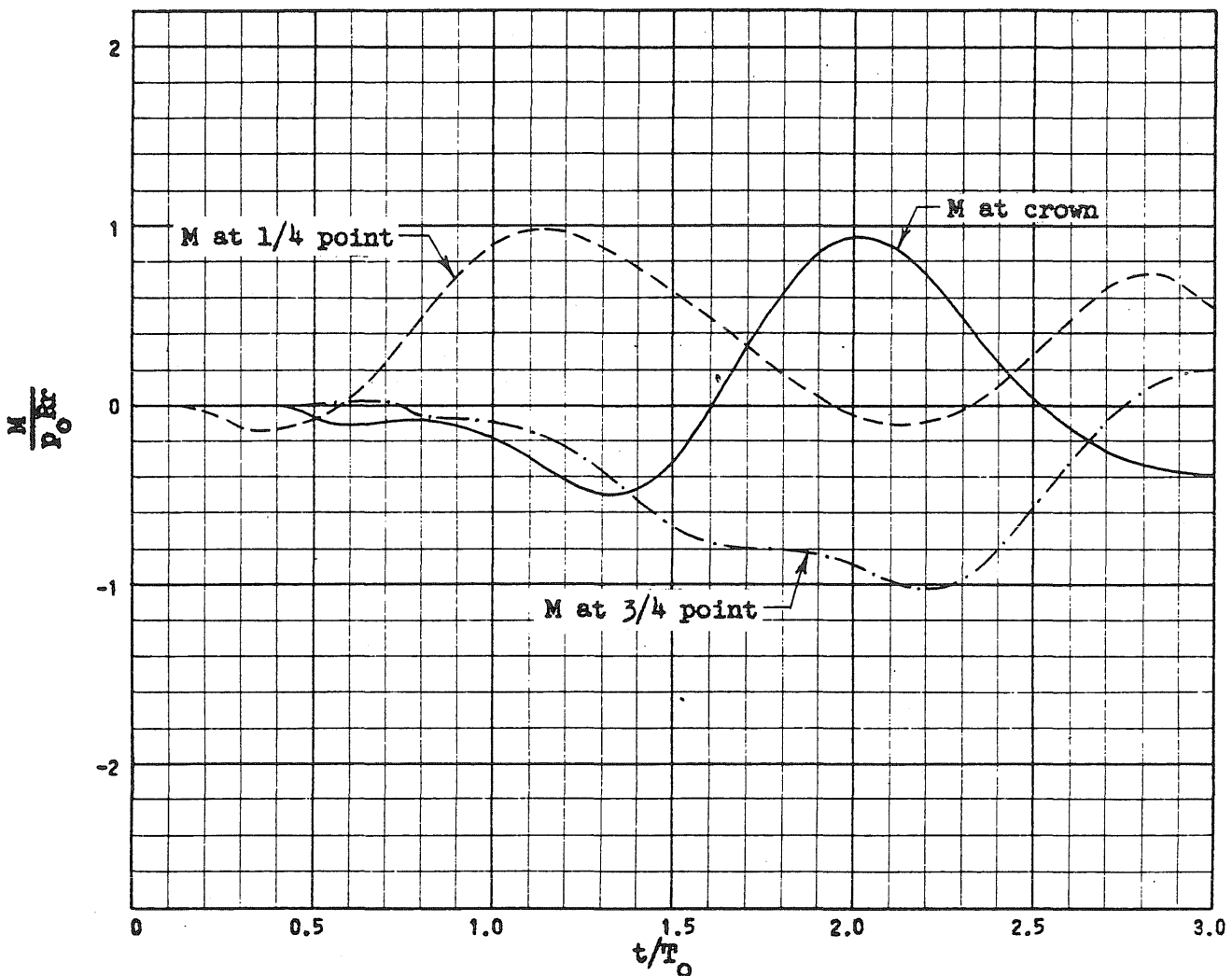
(b) Radial and Tangential Displacements, w and v

FIG. 5.11 RESPONSE CURVES FOR AN ARCH SUBJECTED TO A TRIANGULAR MOVING PRESSURE-- $L/r = 200$

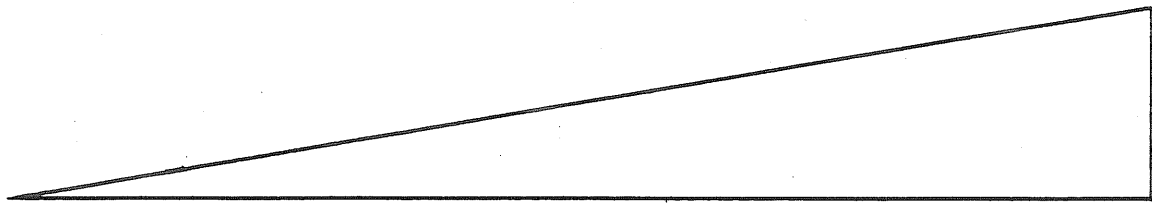
$f/L_0 = 0.2, p_0/p_{cr} = 1.0, t_t/T_0 = 1.0, t_d/t_t = 1.0$



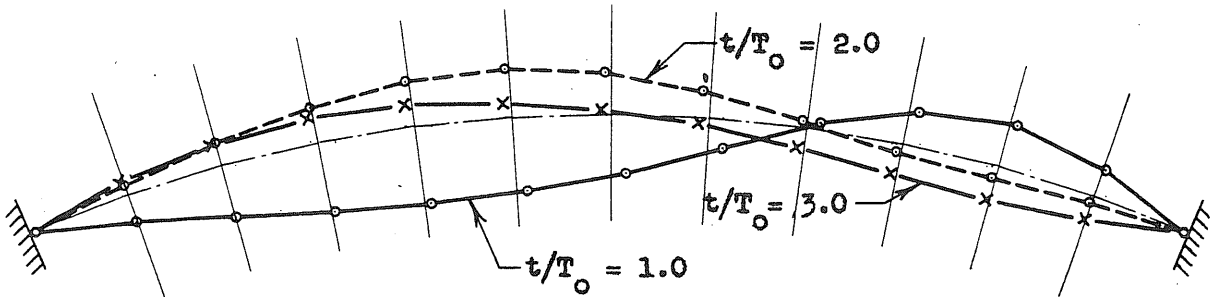
(c) Axial Force, N



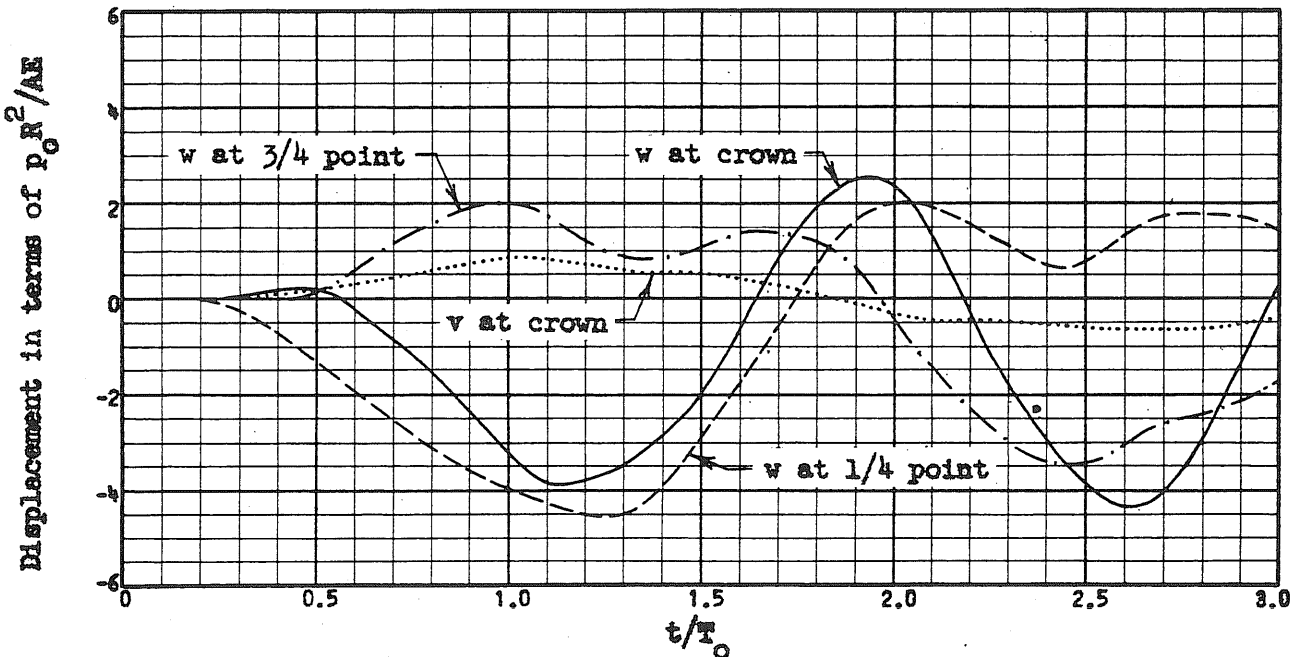
(d) Bending Moment, M



Position of Load at $t/T_0 = 1.0$



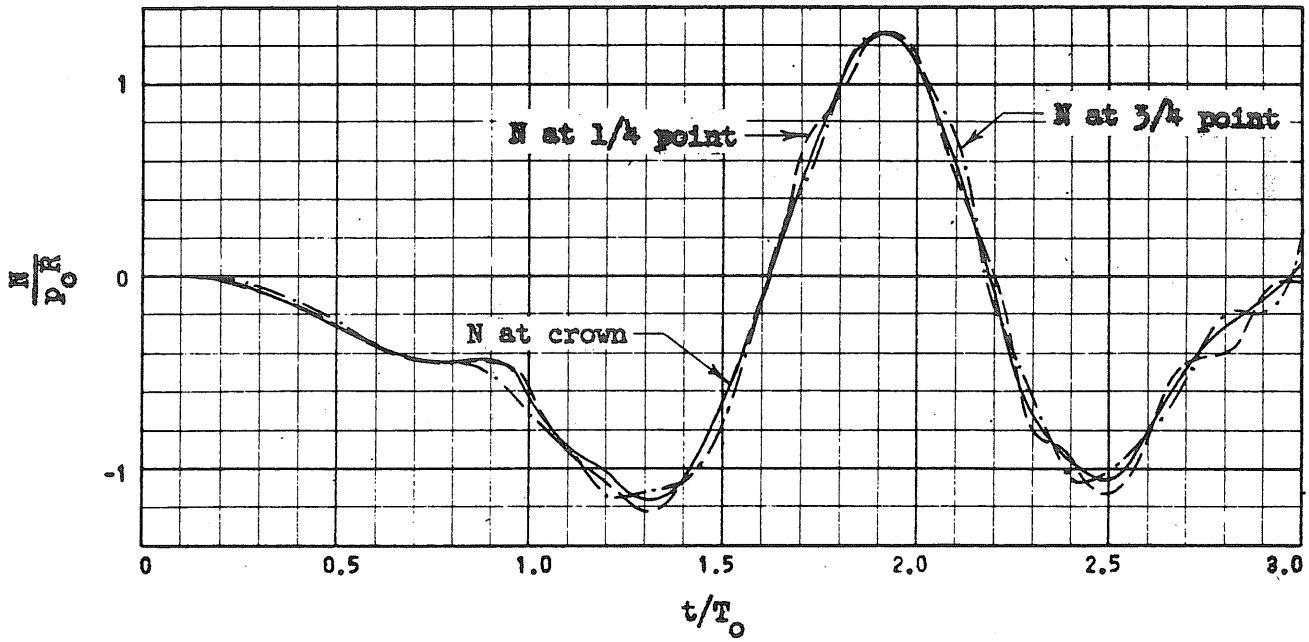
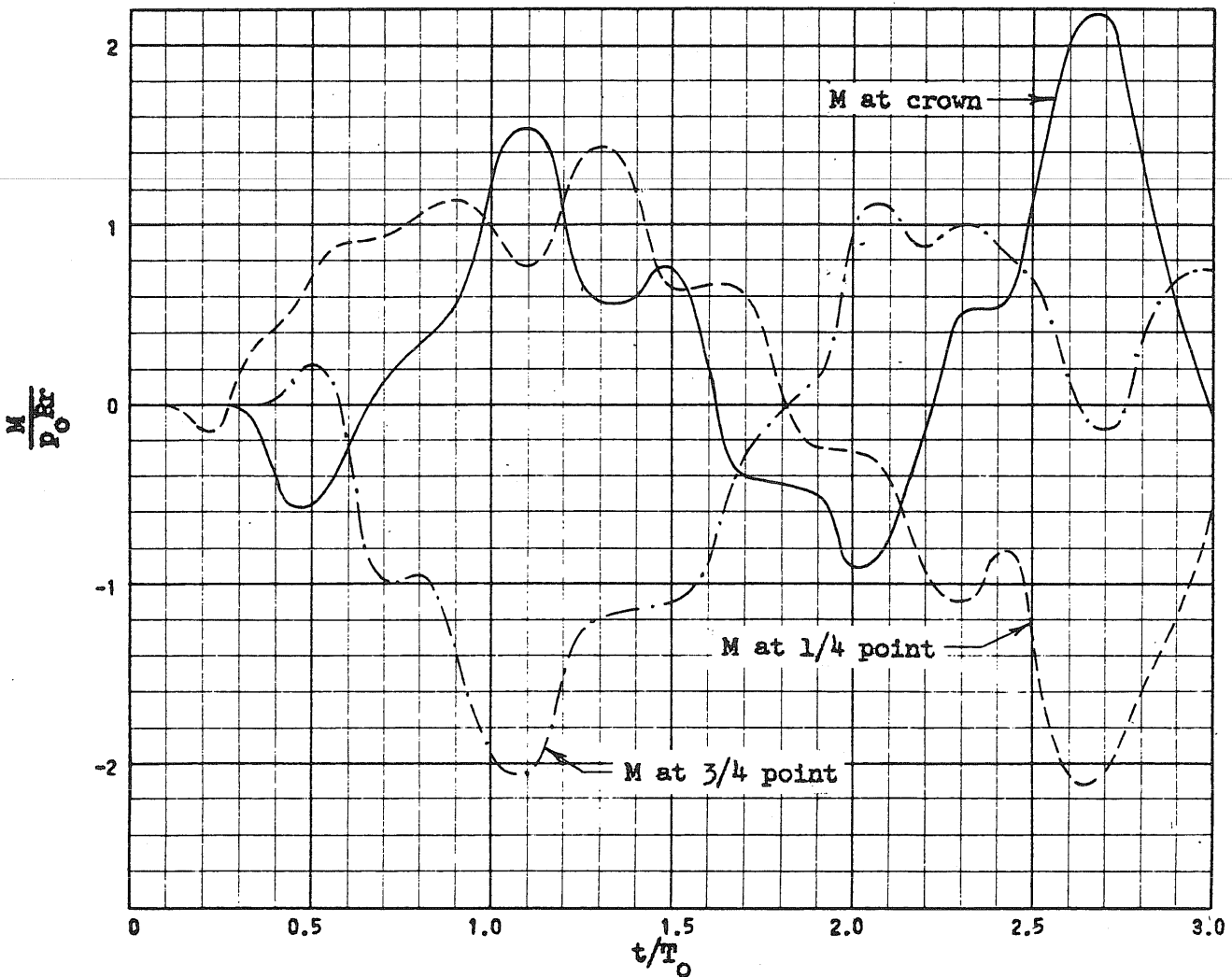
(a) Displacement Configurations

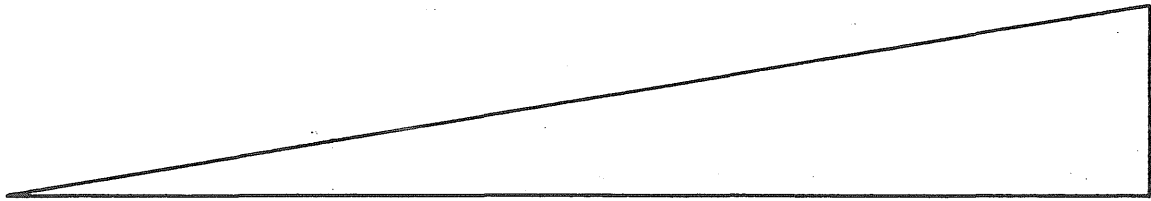


(b) Radial and Tangential Displacements, w and v

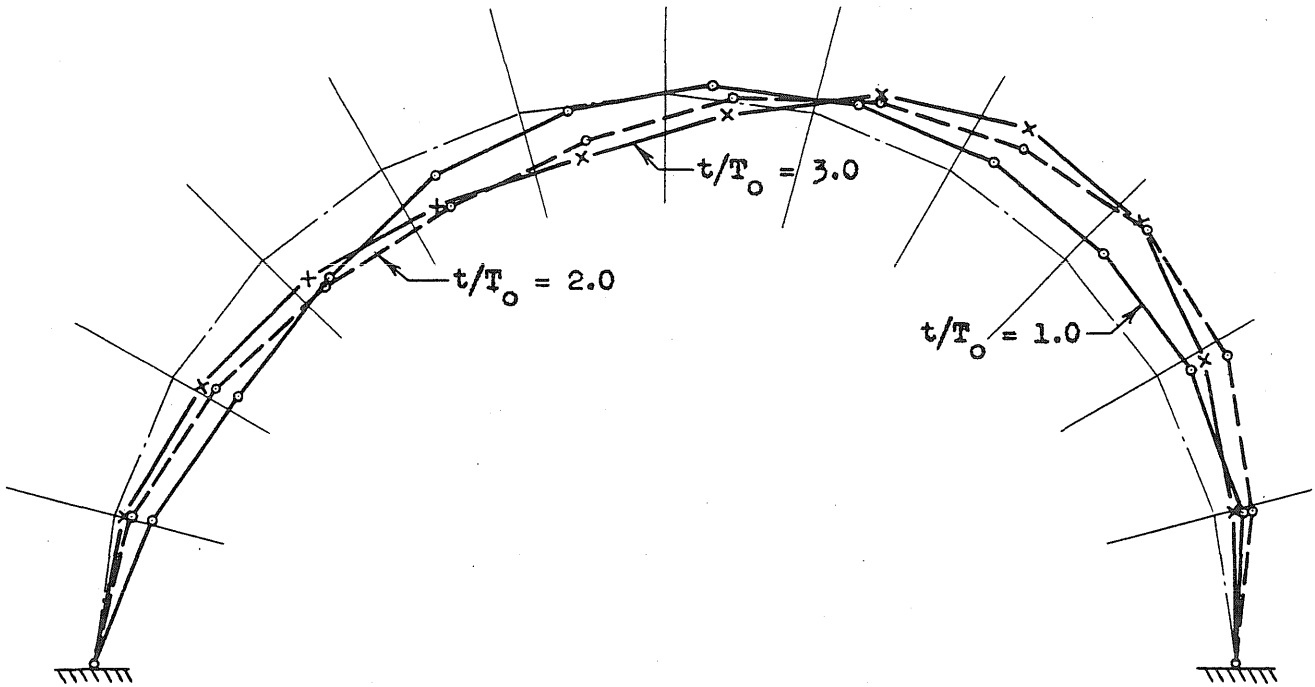
FIG. 5.12 RESPONSE CURVES FOR AN ARCH SUBJECTED TO A TRIANGULAR MOVING PRESSURE-- $f/L_0 = 0.1$

$L_0/r = 100, p_0/p_{cr} = 1.0, t_t/T_0 = 1.0, t_d/t_t = 1.0$

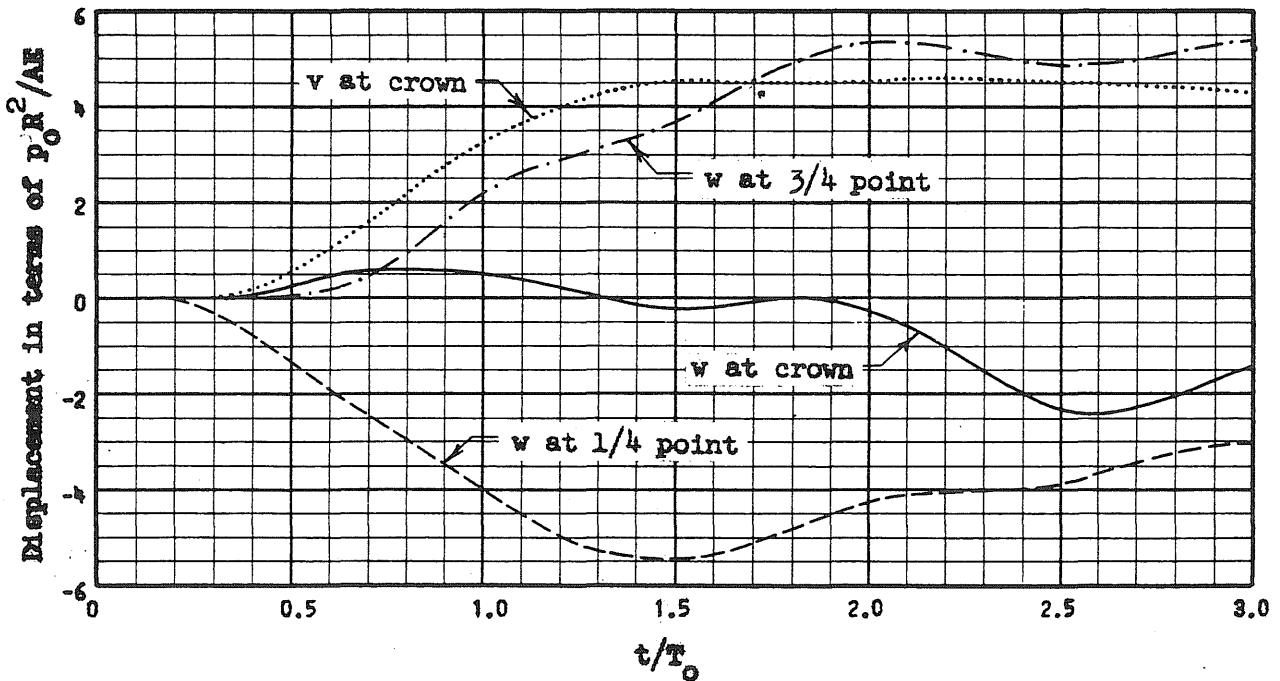
(c) Axial Force, N (d) Bending Moment, M



Position of Load at $t/T_0 = 1.0$



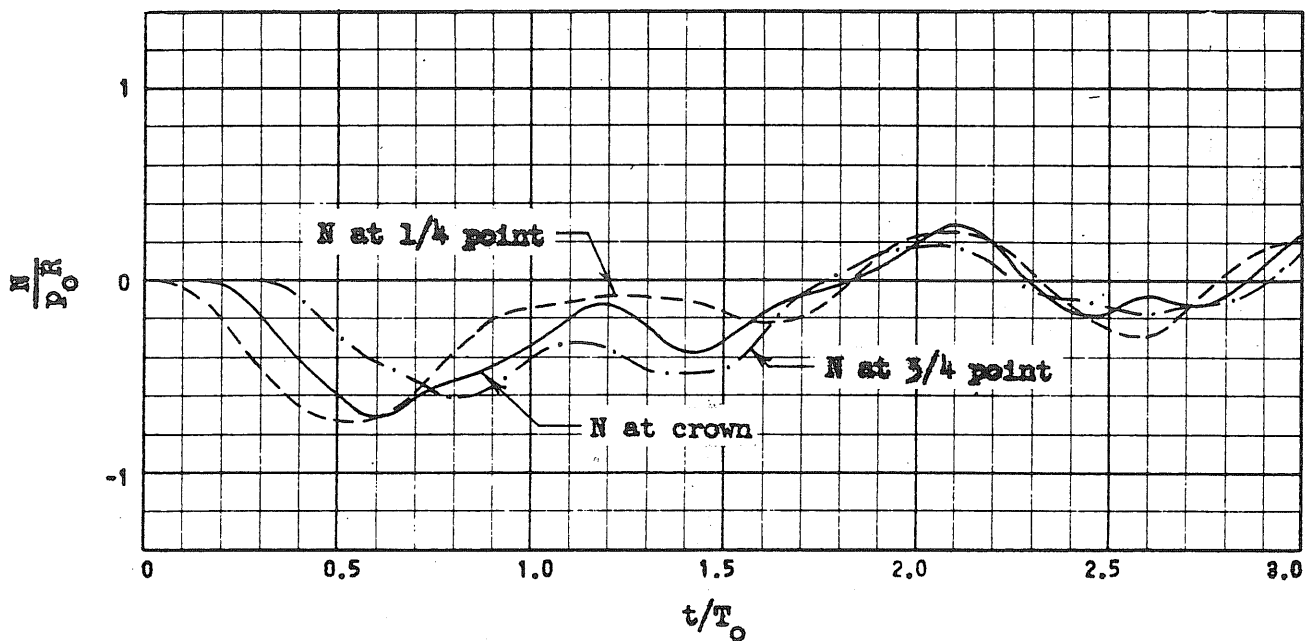
(a) Displacement Configurations



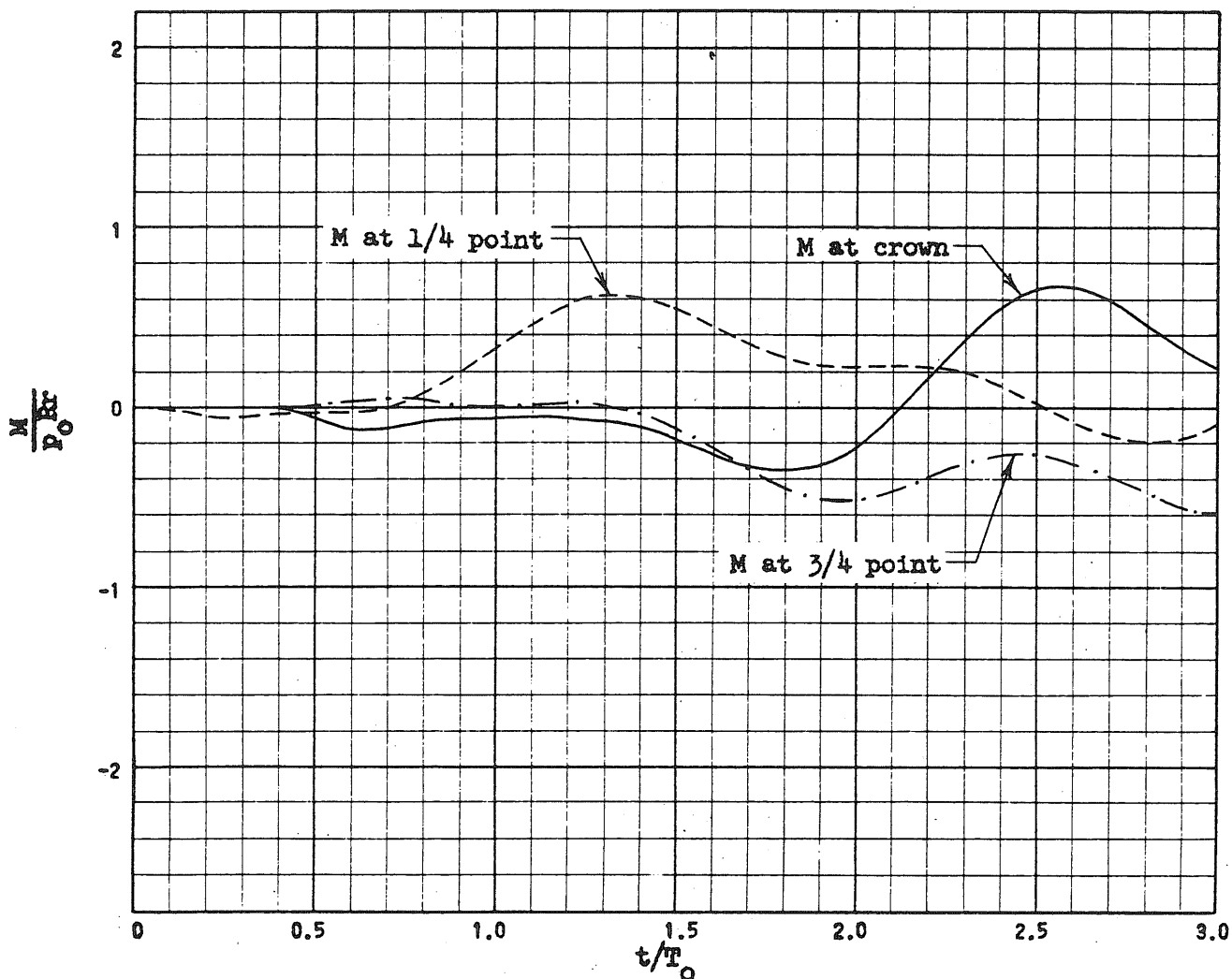
(b) Radial and Tangential Displacements, w and v

FIG. 5.13 RESPONSE CURVES FOR AN ARCH SUBJECTED TO A TRIANGULAR MOVING PRESSURE-- $f/L_0 = 0.5$

$L/r_0 = 100$, $p_0/p_{cr} = 1.0$, $t_t/T_0 = 1.0$, $t_d/t_t = 1.0$



(c) Axial Force, N



(d) Bending Moment, M

FIG. 5.13 (Continued)

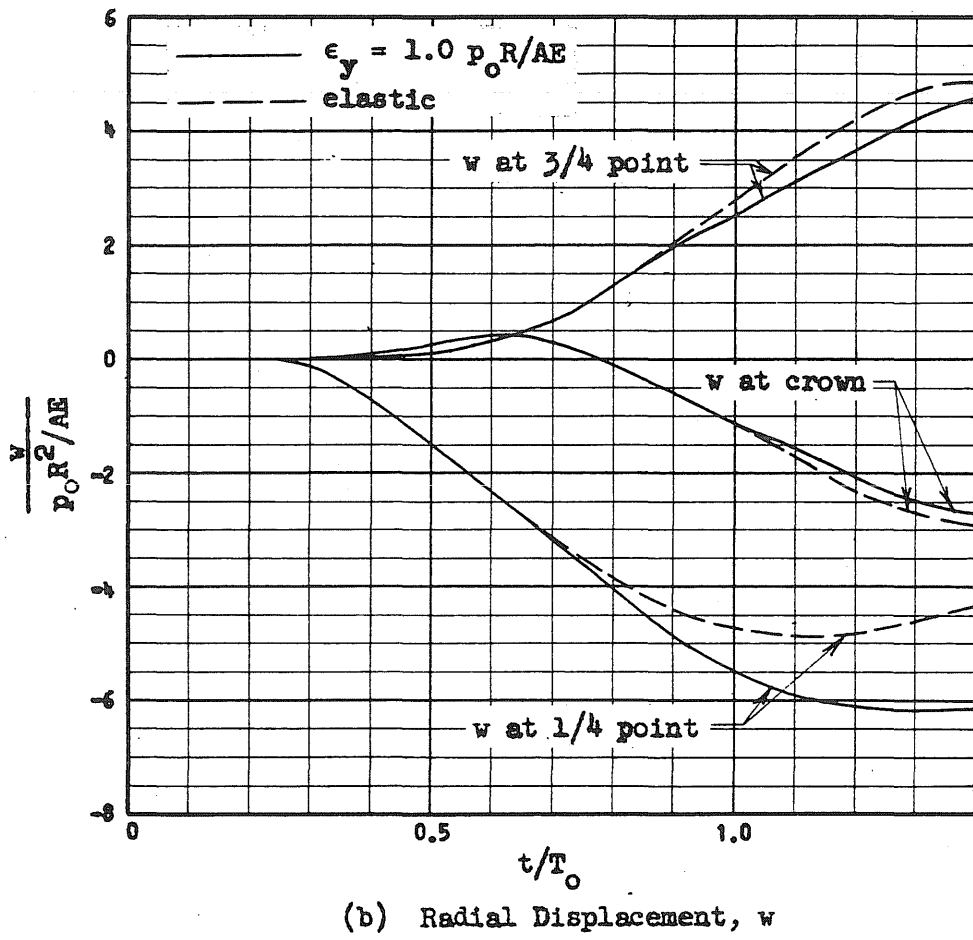
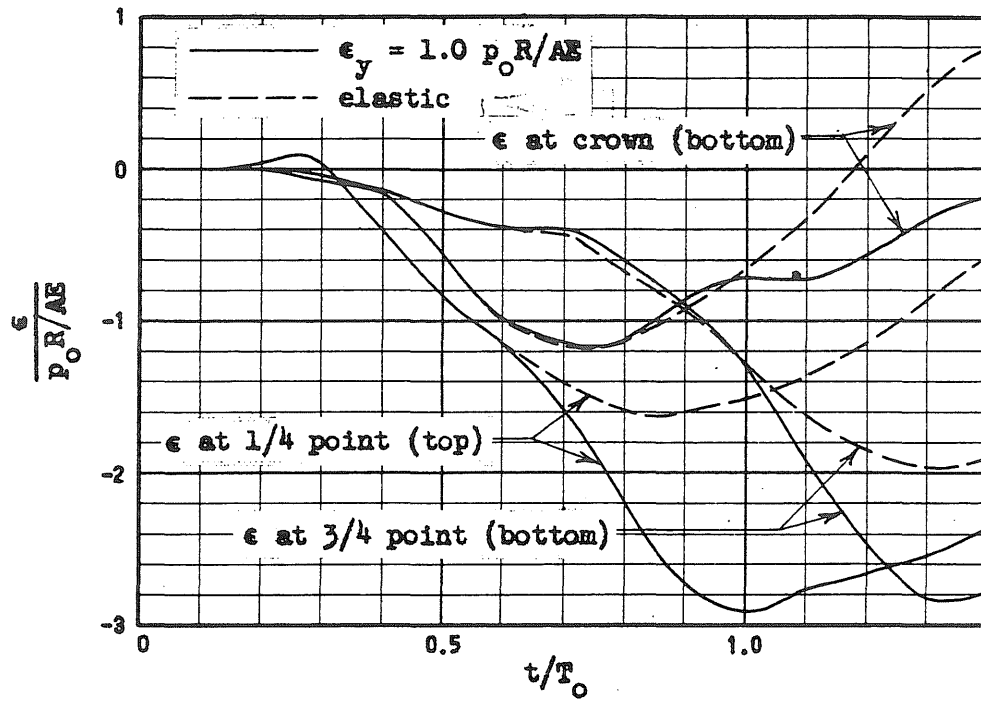
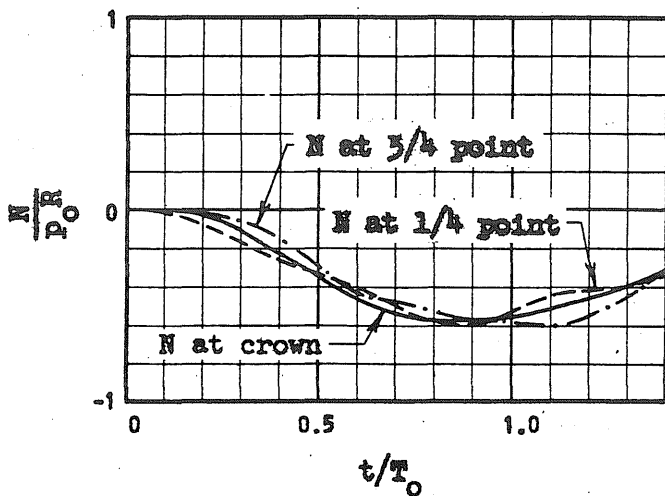
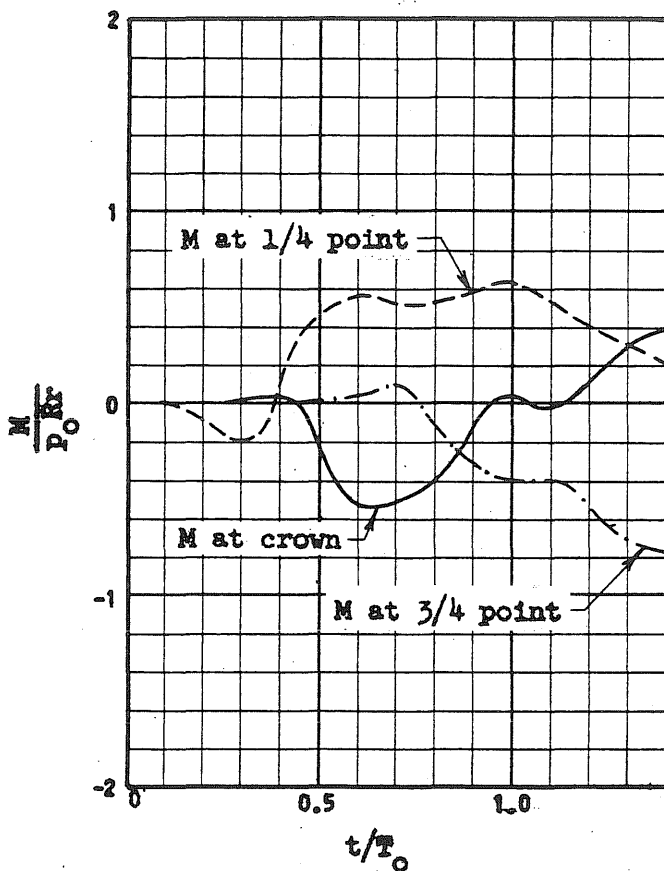


FIG. 5.14 CURVES FOR INELASTIC RESPONSE OF AN ARCH SUBJECTED TO A TRIANGULAR MOVING PRESSURE-- $\epsilon_y = 1.0 p_0 R/AE$
 $f/L_0 = 0.2, L_0/r = 100, p_0/p_{cr} = 1.0, t_t/T_0 = 1.0, t_d/t_t = 1.0$



(c) Axial Force, N



(d) Bending Moment, M

FIG. 5.14 (Continued)

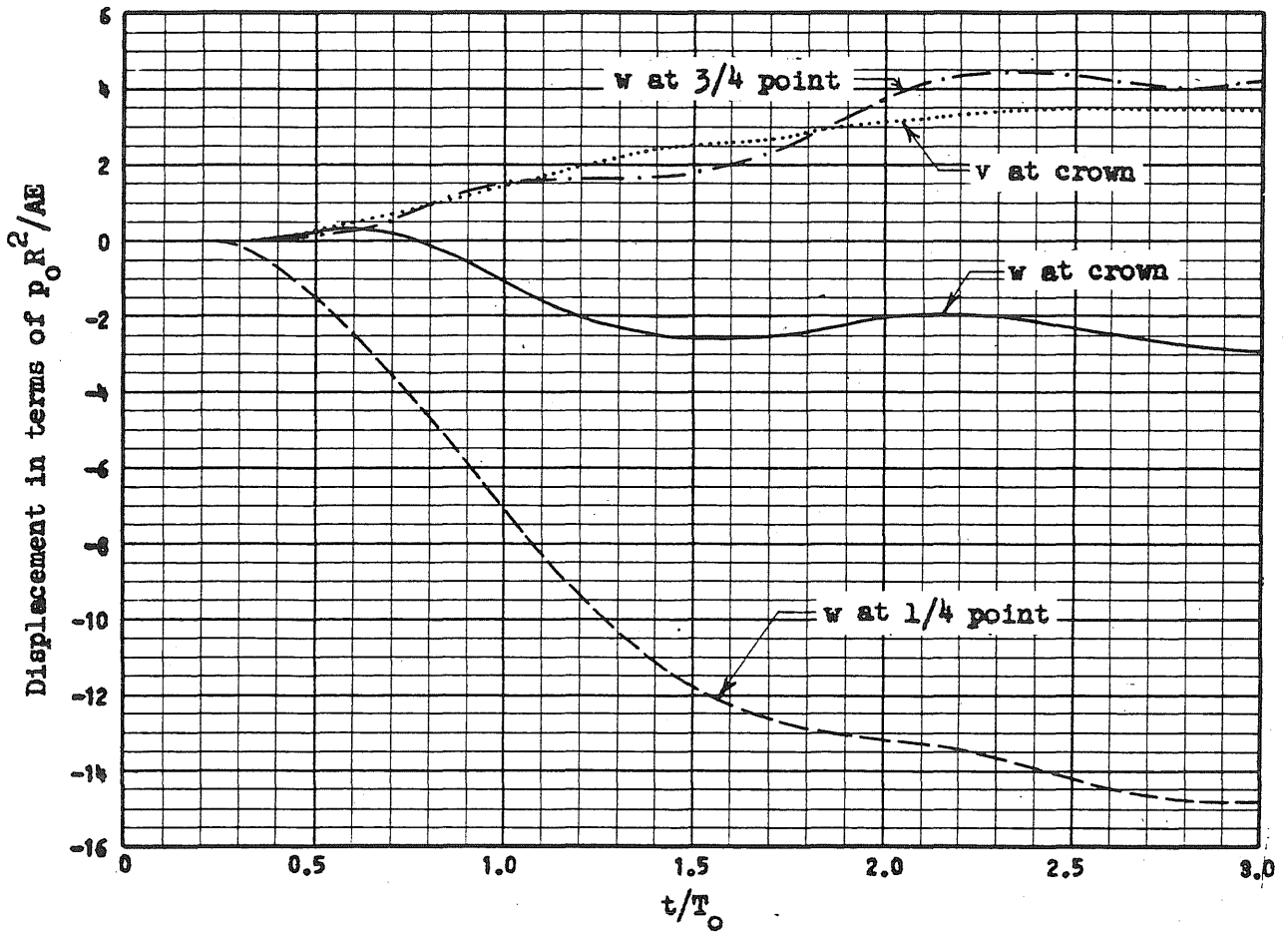
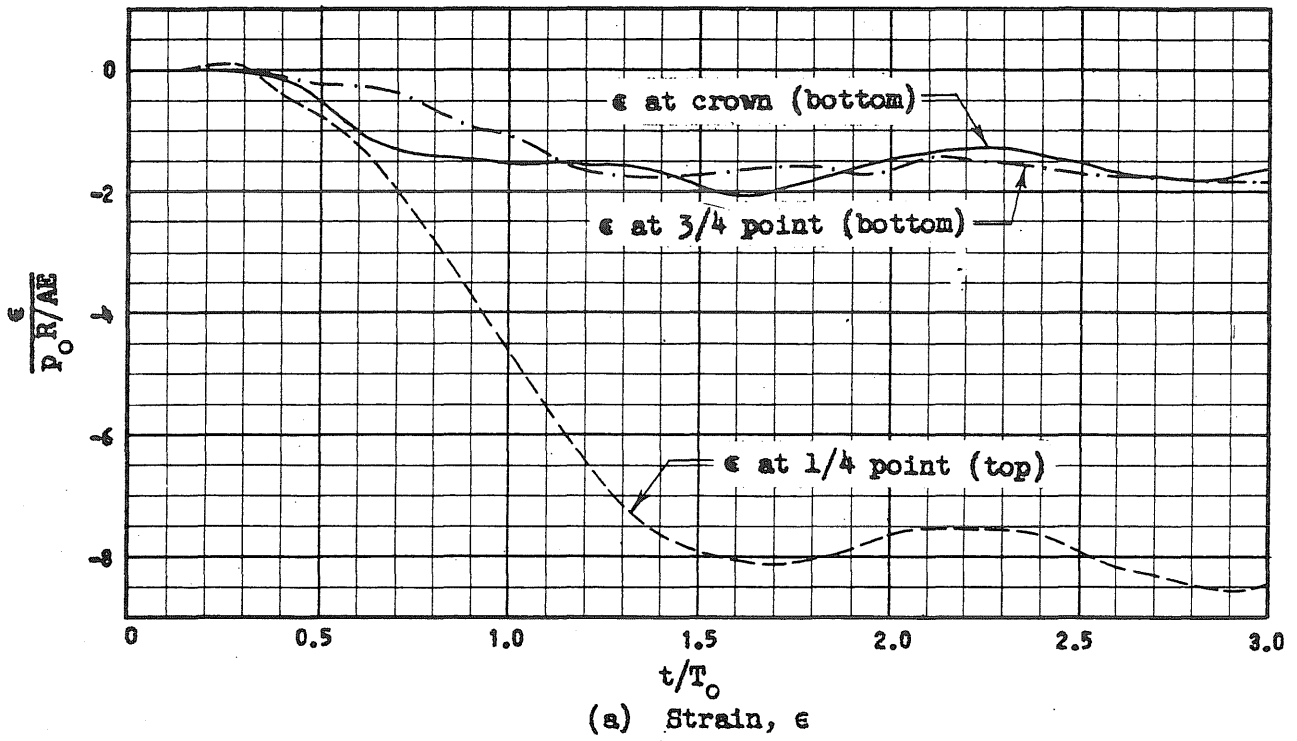
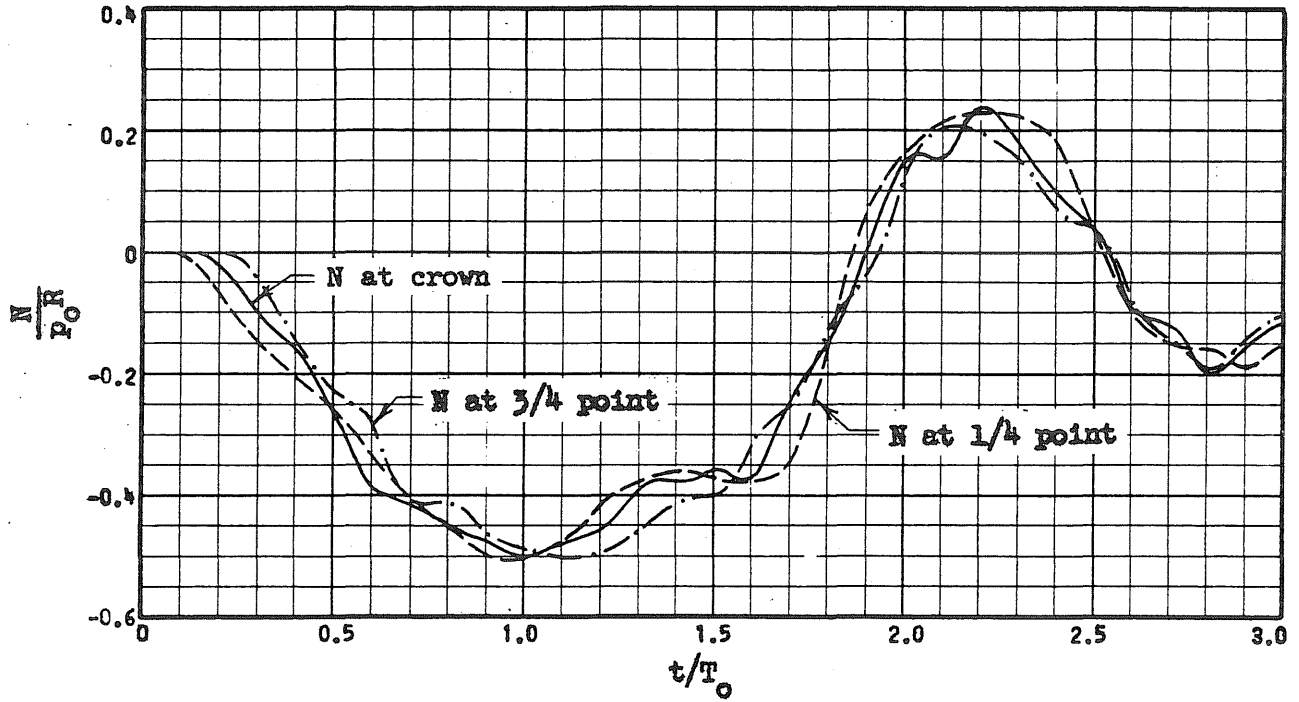
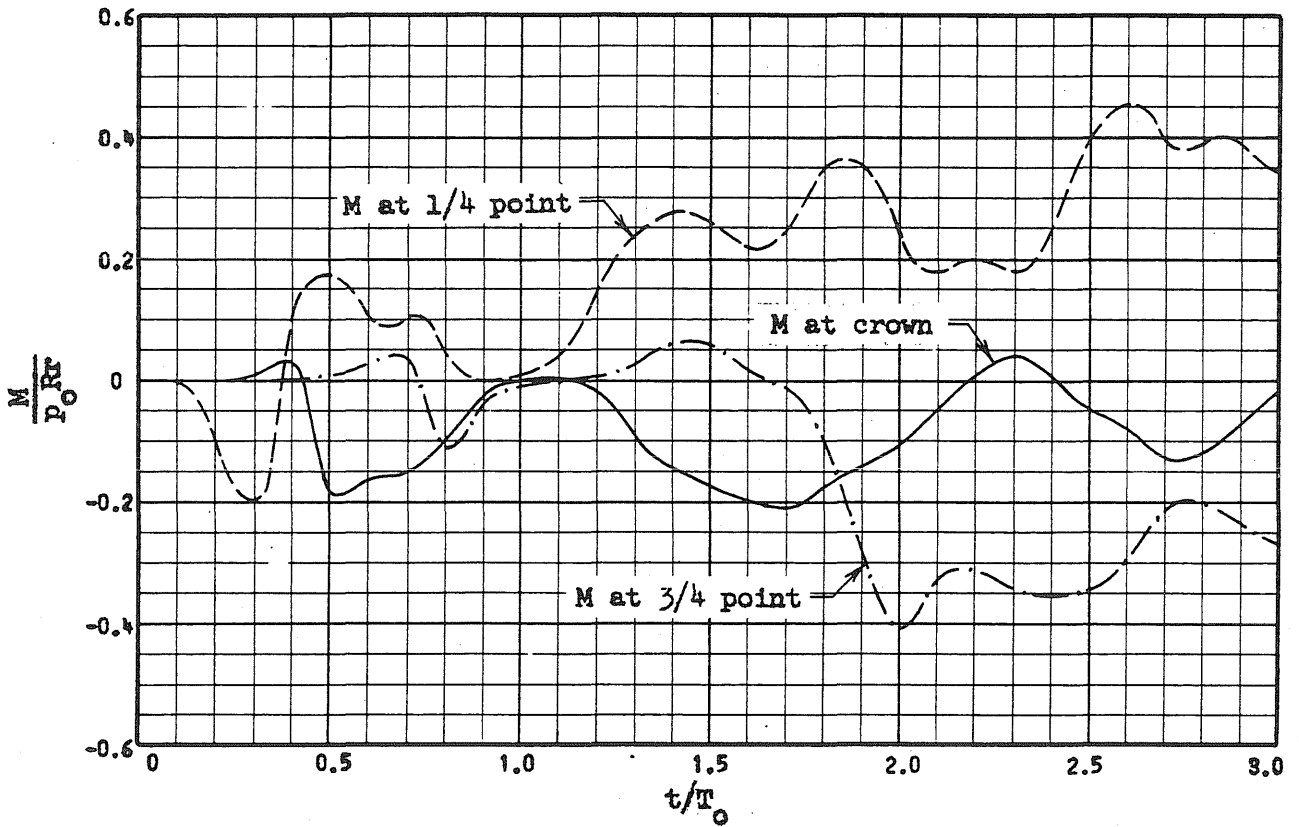


FIG. 5.15 CURVES FOR INELASTIC RESPONSE OF AN ARCH SUBJECTED TO A TRIANGULAR MOVING PRESSURE -- $\epsilon_y = 0.5 p_0 R/AE$

$f/L_0 = 0.2, L_0/r = 100, p_0/p_{cr} = 1.0, t_d/T_0 = 1.0, t_d/t_t = 1.0$



(c) Axial Force, N



(d) Bending Moment, M

FIG. 5.15 (Continued)

DISTRIBUTION

No. Cys

HEADQUARTERS USAF

1 Hq USAF (AFDDC), Wash 25, DC
 1 Hq USAF (AFOOA), Wash 25, DC
 1 Hq USAF (AFOIE), Wash 25, DC
 1 Hq USAF (AFDRT), Wash 25, DC
 1 Hq USAF (AFCIN), Wash 25, DC
 1 USAF Dep IG for Insp (AFCDI-B-3), Norton AFB, Calif

MAJOR AIR COMMANDS

ARDC, Andrews AFB, Wash 25, DC
 1 (RDRW)
 1 (RDZ)
 1 AFBMD (WDAT), AF Unit Post Office, Los Angeles 45, Calif
 1 SAC (DINC), Offutt AFB, Nebr
 1 TAC (TDA), Langley AFB, Va
 1 AMC (MCW7), Wright-Patterson AFB, Ohio
 1 ADC (Ops Anlys), Ent AFB, Colorado Springs, Colo
 1 AUL, Maxwell AFB, Ala
 1 USAFA, United States Air Force Academy, Colo

ARDC CENTERS

WADD, Wright-Patterson AFB, Ohio
 1 (Dir of Sys Mgt)
 1 (WWAD)
 1 (Structures Branch, Aircraft Laboratory)
 1 AF Research Division (Technical Library), Bldg T-Y, Wash 25, DC

KIRTLAND AFB

AFSWC, Kirtland AFB, NMex
 1 (SWNH)
 5 (SWOI)
 3 (SWRS)

DISTRIBUTION (cont'd)

No. Cys

OTHER AIR FORCE AGENCIES

Los Angeles Air Procurement District, ATTN: Administrative Contracting Officer, 1700 Main Street, Santa Monica, Calif

1 For (RAND Nuclear Energy Division)

ARMY ACTIVITIES

1 Chief of Research and Development, Department of the Army, ATTN: Special Weapons and Air Defense Division, Wash 25, DC

1 Director, Ballistic Research Laboratories, ATTN: Library, Aberdeen Proving Ground, Md

1 Commanding Officer, US Army Engineers, Research and Development Laboratories, Ft Belvoir, Va

1 Office of the Chief, Corps of Engineers, US Army, ATTN: Protective Construction Branch, Wash 25, DC

NAVY ACTIVITIES

1 Commanding Officer and Director, Naval Civil Engineering Laboratory, Port Hueneme, Calif

1 Chief, Bureau of Yards and Docks, Department of the Navy, Wash 25, DC

OTHER DOD ACTIVITIES

1 Chief, Defense Atomic Support Agency, ATTN: Document Library Branch, Wash 25, DC

1 Commander, Field Command, Defense Atomic Support Agency, ATTN: FCAG3, Sandia Base, NMex

6 ASTIA (TIPDR), Arlington Hall Sta, Arlington 12, Va

1 Director, Advanced Research Projects Agency, Department of Defense, The Pentagon, Wash 25, DC

OTHER

1 American Machine and Foundry Company, ATTN: Mr. T. G. Morrison, 1104 South Wabash Avenue, Chicago 5, Ill

1 University of Massachusetts, ATTN: Dr. Merit P. White, Dept of Civil Engineering, Amherst, Mass

1 Massachusetts Institute of Technology, Dept of Civil and Sanitary Engineering, ATTN: Dr. Robert J. Hansen, 77 Massachusetts Ave., Cambridge 39, Mass

DISTRIBUTION (cont'd)

No. Cys

- 1 E. H. Plesset Associates, Inc., ATTN: Mr. Marc Peter, Jr.,
6399 Wilshire Blvd., Los Angeles 48, Calif
- 1 Armour Research Foundation, Illinois Institute of Technology,
ATTN: Mr. Ray Sauer, 3422 South Dearborn Street,
Chicago 16, Ill
- 1 Stanford Research Institute, Menlo Park, Calif

